A solvent-free alternative for green liquid-liquid biphasic oxidations

Bishopp, Simon

Award date:
2014

Awarding institution:
University of Bath

A solvent-free alternative for green liquid-liquid biphasic oxidations

Simon David Bishopp

A thesis submitted for the degree of Doctor of Philosophy

University of Bath

Centre for Sustainable Chemical Technology

Department of Chemical Engineering

June 2014

Table of Contents

Table of Figures, Tables and Schemes

Acknowledgements

I would like to acknowledge the EPSRC for funding my research in the Centre for Doctoral Training in Sustainable Chemical Technologies.

I would like to thank my supervisors, Dr Laura Torrente-Murciano and Dr Janet Scott for their tireless efforts over the last 3 years. I very much appreciate the guidance you have offered and your patience. Laura, I think I learnt to multi-task to some extent, wouldn't you say?

To the members of my group, Rebecca Bamford, Alex Gilbank and Alf Hill, I truly couldn't have done it without you, so, thank you for listening to me whine for 3 years. To all my colleagues and friends in both Chemical Engineering and Chemistry whom I haven't mentioned by name, thank you for making my time in Bath so much fun.

In particular I would like to thank the technical staff in both the Department of Chemical Engineering and the Department of Chemistry for their assistance during the course of this research. In both the analytical side and day-to-day concerns you all helped contribute to some extent.

Finally, thank you to my family for their financial support and just always being there. Sorry I haven't seen you as much I should have.

Abstract

The work contained within this thesis presents a multidisciplinary method for the integrated reaction and separation of a liquid-liquid biphasic system. The area of multiphase liquid reactions is traditionally addressed through use of a solvent system to achieved mutual dissolution. However, the removal of such solvents in downstream processing often entails a high energy cost. This research investigated the potential to perform these reactions, specifically between oil and aqueous phases, without a solvent, thereby negating the downstream removal cost.

The method presented in this thesis proposes the rate limiting step of the liquid-liquid reaction be determined, specifically the relationship between interfacial surface area and rate of reaction. The use of high shear homogenisation, microfluidic and capillary based droplet creation methods enabled a range ($3.9 – 9.6x10^{-4}$ $m^2.g^{-1}$) of oil-aqueous interfacial areas to be formulated. The rate limiting step of a model reaction, the epoxidation of sunflower seed oil with an aqueous solution of hydrogen peroxide, sodium tungstate and a carboxylic acid, was dependent on the interfacial surface area, but only when less than 0.25 $m^2.g^{-1}$. At oil-aqueous areas in excess of this the reaction system was rate limited by the aqueous phase formation of active catalyst species, a peroxotungstate.

The design and construction of a continuous membrane reactor based on the rate of reaction information was carried out. By operating under conditions such that an interfacial surface area in excess of 0.25 m^2g^{-1} was maintained, the biphasic system was successfully reacted on large scale (5 L), and critically the inherent immiscibility of the oil-aqueous system allowed for the facile downstream separation of phases. Therefore this research presents an approach to achieve the non-mass transfer limited reaction and downstream separation of a liquid-liquid biphasic system without the use of solvents.

Nomenclature

All units are SI units, unless stated otherwise in text

Term	Description
A	Membrane surface area
ΔA	Interfacial area change on dispersion
A_t	Total surface area
a_s	Surfactant activity
Ca	Capillary number
C_i	Molar concentration of i
d	Critical diameter
D	Membrane tube diameter
D_{AB}, D_i	Diffusivity of A through B, i
D[3,2]	Sauter mean diameter
d_c	Channel diameter
d_d	Droplet diameter
d_i	Geometric mean diameter
d_h	upper class boundary diameter
d_l	lower class boundary diameter
d_m	Membrane diameter
d_o	Outlet tubing diameter
d_p	Average pore diameter
E_a	Activation energy
f	Fanning friction factor
ΔG_d	Free energy change on dispersion
h	Height of cap

J_d	Dispersed phase flux
k_c	Mass transfer coefficient
k_r	Reaction rate constant
k_t	Thermal conductivity
L	Membrane thickness
l	Film thickness
l_c	Critical hydrophobic tail length
L_p	Membrane permeability
M_d	Mass flow rate
M_r	Molar mass
n	number of plugs
n_i	Number distribution
P_c	Continuous phase pressure
P_d	Dispersed phase pressure
Pr	Prandtl number
ΔP_{tm}	Transmembrane pressure
Q_c	Continuous phase flow rate
Q_d	Dispersed phase flow rate
r	Radius
r_i	Rate of reaction with respect to component i
R	Ideal gas constant
Re	Reynolds number
r_i	Rate of reaction with respect to component *i*
R_{jet}	Radius of jet
SA_p	Surface area per plug
Sc	Schmidt number
Sh	Sherwood number
T	Temperature
U,u	Fluid velocity
v	Kinematic viscosity
v_d	Dispersed phase volume in reactor
v_p	Partial molar volume
V	Droplet volume
V_i	Relative volume in class
V_r	Volume of reactor
V_t	Total volume

V_{ax}	Axial fluid velocity
W	Channel width
We	Weber number
X_t	Conversion

Greek Symbol	**Description**
α	Droplet size constant
Γ_s	Surface excess
ΔS	Entropic force change
$\mu_{c/d}$	Fluid viscosity. Subscript relate to dispersed (d), continuous (c) phase
Π	Surface pressure
$\rho_{d/c}$	Fluid density. Subscript relate to dispersed (d), continuous (c) phase
θ	Angle
θ_c	Contact angle
τ	Residence time
τ_w	Wall shear stress
φ	Flow rate ratio, Q_d / Q_c

Abbreviation	**Description**
CPP	Critical packing parameter
CTAB,CTAC	Hexadecyltrimethylammonium halides
DoE	Design of Experiments
HLB	Hydrophile-lipophile balance
PEEK	Polyether ether ketone
PTFE	Polytetrafluoroethylene
SANS	Small angle neutron scattering
SAXS	Small angle X-ray scattering
SSA	Specific Surface Area

1 Introduction

Preparative organic chemistry is often subject to certain physical limitations when dealing with the huge range of substrates, reagents, solvents and additional materials often required to achieve a synthesis. Associated with this vast array of ingredients is the added complication of phase incompatibility. Frequently a synthesis will require the use of material in one, two, three or even (when dealing with supercritical media) more states. In order for a synthesis to be successful, the issue of inter- and intraphase mass transfer of the reacting species must be considered, and potentially, overcome.

In a real-world situation, successful laboratory synthesis by no means guarantees market viability. Not only must the chemistry be scalable, but the chemical engineering aspects must be feasible, of which the issue of interphase mass transfer is not trivial. Understanding and harnessing the fundamental relationships between phase transfer and reactivity is critical for the adoption of a process.

To illustrate the concepts above, one can envisage a biphasic system containing two immiscible components. For example, a lipophilic, hydrophobic organic molecule is required to react with a hydrophilic organic molecule, or in a more extreme situation, with an inorganic salt insoluble in most organic media. In this situation one would typically

approach the problem with the use of a solvent able to dissolve all the components. Standard solvent systems (small organic molecules, often halogenated) can, and indeed are, used in many industrial situations, however with the issues of toxicity, expense and separation problems their use is far from ideal. Another, arguably more important, area of concern (since the onset of the green chemistry movement just prior the turn of the millennium) is the environmental impacts of solvent use, particularly halogenated solvents. In fact one of the Green Chemistry principles as laid out by Anastas and Warner (2000) in their seminal work, is:

> *"The use of auxiliary substances should be made unnecessary whenever possible and innocuous when used."*

With the development of novel solvents such as ionic liquids and supercritical fluids a solution can often be found to match any requirements. Where these solutions fall down is when the focus shifts to larger scale operations. Ionic liquids are currently very expensive and often particularly toxic in aquatic ecosystems. Similar issues arise with supercritical fluids with extremely robust equipment required on even a small scale. In many cases the use of such fluids becomes unfeasible on larger scales or requires installation of a new plant.

Clearly the research and development of practices which can relieve the need for solvent dependence and ease the concerns associated with interphase mass transfer are important. In fact, embracing the principles above would suggest the ideal situation would be to achieve the same outcome, say product synthesis and reaction rates without the need for any solvent.

If one approaches the problem holistically in terms of bench chemistry through to larger scale engineering, the use of a liquid-liquid system can actually be beneficial in some unit operations. Considering the above situation of phase immiscibility, whilst problematic from a reaction aspect, can significantly simplify downstream separation and purification processes. Unfortunately separation alone is not useful if the components are unable to react successfully. However, a solution can be found for liquid-liquid systems by acknowledging that the extent of a mass transfer limited, biphasic reaction can theoretically be controlled by the size of the interfacial area. That is to say for a fast reaction the interphase diffusion limitation can be overcome through adjustment of the surface area.

A method to achieve this control is by defining the size of droplets of one phase dispersed in another. Obviously there is now a balance which needs to be weighed, between the size of droplet, the rate of reaction, and the ease of separation. Small droplets may lead to rapid reaction, but may also be problematic in the separation stage. Another important aspect,

from a commercial viewpoint is that of energy expenditure as increasing the surface area will typically incur a higher energy cost. When attempting to optimise a system such as this, the critical question to be answered is therefore,

"What is the *minimum* energy input required to create the interface area necessary to effectively *negate interface mass transfer* limitation, whilst *maintaining* expedient *separation*?"

To answer the above question of course the necessary interface area has first to be determined. The study of the dispersion of one liquid in another is the realm of emulsification. In this field, stability, in terms of longevity of dispersion, is often desirable and as such surface active molecules (surfactants) are commonly used. This extended time in which a defined interface area exists in such stabilised systems can be exploited to perform liquid-liquid reactions. Indeed by altering the definable interface areas and observing the resultant biphasic rate of reaction the point of mass transfer independence can be revealed. I.e. the minimum surface area to negate mass transfer limitation.

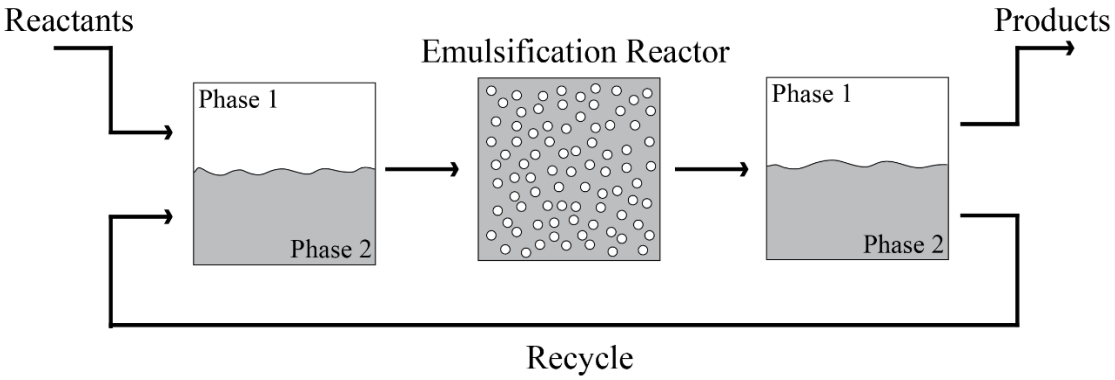

Figure 1.1 - Biphasic reaction utilising transient emulsification with integrated separation and recycle

By formulating a dispersion with the aforementioned minimum area but now without using stabilising agents such that the dispersion exists only transiently, the entire process of reaction and separation can be realised. This was the goal of this research, summarised in Figure 1.1.

1.1 Research scope

The overarching theme of this project was the development of engineering alternatives to avoid the use of solvents in liquid-liquid systems whilst integrating the reaction and separation steps in a process.

To achieve the aim of this project a series of objectives along with associated tasks were devised:

- Obtain a model biphasic system which was suitable for both dispersion and reaction by ensuring that,
    - The reactive components were mutually immiscible, such that they formed a biphase
    - That measureable levels of conversion are obtained in practical time scales
- Reliably and reproducibly obtain dispersions over a range of quantifiable interface areas through understanding the relationships between droplet size and
    - Surfactant, oil and aqueous phase volumes
    - Power input in the form of speed and duration of high shear homogenisation
    - Flow rate ratios for a range of microfluidic device geometries
- Obtain comprehensive kinetic data assessing rate of reaction with respect to
    - The droplet size
    - The individual components of the reaction
- To assess the above, develop rigorous analytical methods for droplet sizing and extent of reaction;
- Utilise kinetic data to integrate reaction and separation in non-surfactant stabilised systems
    - Implementation of a continuous microfluidic reactor
    - Scale up the overall concept and implement using a tubular membrane reactor

The specific nature of the chemical transformation of the reaction is not currently under investigation, it used as a model system. Therefore aspects such as catalyst development will not be considered. However the reaction considered within this report, the epoxidation of vegetable oils, is commercially relevant. This investigation will consider the use of biphasic systems, of which one phase is aqueous. Due to this the reaction scope is temperature limited to less than 100 °C (without use of pressure equipment).

This research was conducted in the Centre for Sustainable Chemical Technologies (CSCT) at the University of Bath. This multidisciplinary centre sits at the interface between chemical engineering and chemistry, and as such this research embodies the ethos of the centre marrying the aspects of chemical transformation, chemical reaction engineering and process integration.

1.2 Knowledge dissemination

The research contained herein has been presented orally and as a poster at a number of international events namely the 2012 Green Chemistry Gordon's Research Seminar and Research Conference and the 6th International Conference on Green and Sustainable Chemistry where the work was acknowledged through special commendation by the organising committee. In addition to the above, presentation of the work, again both orally and in poster form were given as part of annual international showcases of the CSCT. Work contained in Chapter 5 has been published in Green Chemistry (Bishopp *et al.*, 2014), manuscript in Appendix 3.

In keeping with the ethos of the CSCT knowledge dissemination in the wider context in the form of public outreach was undertaken through presentation of fundamental chemistry and engineering principles at science fairs in the UK, namely Cheltenham and Bath.

1.3 Thesis structure

The remaining chapters contained within this thesis are listed below along with a brief description of their contents to put it into context with the project goals.

2. Literature Review and Theory

   Reviews the current literature pertaining to methods of dispersion formulation along with relevant reactions performed in such media, highlighting the need for the research reported here. Also contained in this chapter are the relevant theoretical considerations important for discussion of the following results chapters.

3. Experimental Procedures

   Outlines the methods used to achieve the results contained within the thesis.

4. Controlling the Liquid-Liquid Interface

   Results and discussion relating to the formulation of a range of surface areas using a combination of methodologies, such as high shear homogenisation and microfluidic droplet generation.

5. Analysis of a Liquid-Liquid Chemical Process

   Results and discussion relating to analysis of the steps of the epoxidation of vegetable oils, to determine the rate limiting step of the reaction.

6. Process Integration: Reaction and Separation

   Utilisation of the previous chapter results in the integration of continuous reaction and separation in the epoxidation of vegetable oil through the implementation of a membrane reactor.

7. Overall Conclusions

   Draws together the outcomes of all of the results sections, placing them in context with the aims and literature gaps. Following this, proposals for areas to continue this research as well as interesting new research routes based off some of the areas briefly studied herein are presented.

2 Literature Review and Theory

This review is arranged such that it complements the structure of the following results chapters in this thesis. As such, the following topics are covered:-

- The formulation of oil in water dispersions with a range of interfacial areas by:
    - traditional emulsification methods
    - microfluidic based technologies
    - membrane based technologies
- Aspects of emulsion stability and characterisation techniques
- The use of biphasic and dispersed systems as reaction media, focusing on:
    - basic stirred tank systems
    - general emulsion media
    - microfluidic systems
    - membrane systems

In addition, some space is given to a review of literature relating to oxidative reactions conducted in biphasic systems, reflecting the reaction system used in this investigation.

Finally, a reminder of key chemical engineering concepts of reaction rate and interfacial mass transfer are also included, owing to their importance in the discussion in the following chapters.

2.1 Interfacial area control

In liquid-liquid biphasic reaction systems, which rely upon the interaction, or interchange, of molecules contained within the different phases, the control of interfacial phenomena and indeed the nature and extent of the interface is paramount. In the simplest sense, the total area which makes up the boundary, which can be seen as two dimensional for the purposes of this explanation, is critical from a basic dimensional analysis of a diffusion led process. The diffusion of components is commonly expressed in terms of a flux, defined as a function of area.

$$Flux = \frac{Moles}{Area \cdot Time} = \frac{mol}{m^2 \cdot s} \qquad 2.1$$

Of course, the interfacial environment, and the processes which predominate therein, are far more complicated than this simplistic view suggest, however for the purposes of this introduction, this is secondary to the point that diffusive flux is defined per unit area. As such this section is focussed on the techniques and investigations into the alteration of and, crucially, to maintenance of the interfacial area of two phase liquid-liquid systems.

More specifically, the research area dedicated to the science and technology of interfaces, including liquid-liquid, is that of emulsification. This review starts with a broad introduction to emulsion terminology.

2.1.1 Dispersion terminology

The IUPAC (International Union of Pure and Applied Chemistry) defines a dispersion thus,

> *"Material comprising more than one phase where at least one of the phases consists of finely divided phase domains, often in the colloidal size range, dispersed throughout a continuous phase"(Broze, 1999)*

In addition, the terminology used in the literature is dependent on the particular combination of phases and states that are under investigation, summarised in Table 2.1. Of particular relevance to the work contained within this thesis are liquid-liquid dispersions.

Table 2.1 - Dispersion terminology (Kissa, 1999)

Dispersion medium	Disperse phase	Description
Gas	Liquid	Mist (Aerosol)
Gas	Solid	Smoke (Aerosol)

Liquid	Gas	Foam
Liquid	Liquid	Emulsion
Liquid	Solid	Dispersion
		Suspension
Solid	Gas	Solid foam
Solid	Liquid	Solid emulsion
Solid	Solid	Solid suspension

When one discusses ternary liquid phase dispersive systems, the majority can be encompassed under the terms: emulsion, microemulsion, nanoemulsion or micelle. To help put the contents of the thesis into context these concepts are briefly described here.

First to be considered are emulsions. These systems are comprised of two or more liquid phases which are each insoluble with respect to the others. Clayton (1943), almost 70 years ago, proffered the following, but by no means the first, definition of an emulsion:

> *"An emulsion is a system containing two liquid phases, one of which is dispersed as globules in the other."*

In fact, Clayton proceeds further and defines some of the terminology now in common parlance in the numerous disciplines to which dispersions are common place:

> *"That liquid which is broken up into globules is termed the dispersed phase, whilst the liquid surrounding the globules is known as the continuous phase or dispersing medium."*

Emulsions can be of two forms. If a simple binary system is considered whereby one phase consists of a common hydrocarbon, the oil, and the other pure water, two separate outcomes can occur. Where water is the continuous phase and the oil the dispersed phase, the emulsion is known as an oil-in-water system (O/W) and *vice versa* when the oil is taken as the continuous phase and water the dispersed phase: a water-in-oil system (W/O). Systems known collectively as multiple emulsions exist where by droplets of additional, different dispersed phases are contained within one another. These will not be covered within this review, however dedicated literature is available (Aserin, 2008).

It is useful to define an approximate size range when dealing with dispersed systems, therefore the definition that shall be used here, taken from Prince (1977), suggests that an emulsion droplet will lie approximately in the micrometre domain, that is from 1 μm to 200-

300 μm. Emulsions with droplet sizes above these are not commonly encountered due to their susceptibility to emulsion breakdown processes.

To allow for comparison between other dispersed systems, it is worth noting at this point that a standard emulsion is characterised by a lack of thermodynamic stability. That is to say that upon standing an emulsion will eventually separate out into its constituent phases.

Whilst the above distinctions actually hold true for all the other commonly encountered dispersions, contrary to the assigned prefixes the exact classification of microemulsion is not based only upon the magnitude of the dispersed phase's droplet dimension.

The term microemulsion was first coined by Schulman *et al.* (1959), however it is commonly perceived that this was not the start of the field. In fact Prince (1977) suggests that the concept had already been commercially applied in the generation of floor waxes in the late 1920s, albeit without particular scientific reasoning. Academic endeavour is first attributed to the work described by Hoar and Schulman (1943) in their study of colloidal dispersions. It is worth adding that alongside Schulman and co-worker's studies in the area of microemulsions in the 1950s, Winsor (1954) is also credited with the fundamental discovery and definition of the term.

The definition of the term microemulsion has taken many years to reach common acceptance, with much debate spurring on fundamental research into the area of characterisation. Microemulsions are now almost universally regarded as being macroscopically homogeneous in that they resemble a single phase system whilst being truly microscopically heterogeneous. They are thermodynamically stable and are, at least, ternary systems containing aqueous, oily and amphiphilic (often multiple) components. This has been summarised eloquently by Kumar and Mittal (1999) in their compendium of the area:

> *"Microemulsions are thermodynamically stable isotropic dispersions of oil and water containing domains of nanometer dimensions stabilized by the interfacial film of surface active agents."*

Again, as with standard emulsions, the exact dimensions of the droplets belie their name. Frustratingly no two publications seem to share the same exact size ranges, however, for the purposes of this report, microemulsions shall be defined as containing dispersed phase droplet sizes of 10 nm to 100 nm.

It is worth including a brief mention in this review about the grey areas that surround the borders of microemulsion nomenclature. Micellar, 'swollen' micelle, and micellular dispersions are all terms encountered in the literature used to describe oil/water/surfactant

systems. The term micelle pertains to self-assembled surfactant microstructures. In this context the 'swollen' micelle or micellular dispersion imply that they are filled with dispersed phase. Investigators in this area urge that a difference exists and that the term microemulsion should be used when a dispersed phase contains droplets large enough that the physical properties of the pure dispersed component are identifiable. This proposal implies that microemulsions have a minimum droplet size irrespective of their above definition related to thermodynamic stability. For the sake of simplicity, this distinction will not be made within this report and both systems will be included under the term microemulsion.

Another classification which arises is that of a nanoemulsion. This can be thought of as a standard emulsion, but with nanometre scale dispersed phase domains. The similarity between normal emulsions and nanoemulsions is that both are thermodynamically unstable. Confusion arises due to the apparent lengthy kinetic stability exhibited by nanoemulsions, leading to similar properties (in the short term) of optical transparency and low viscosity often exhibited by microemulsions (Tadros *et al.*, 2004). One important distinction, and that which is directly related to the length of kinetic stability, is that nanoemulsion formation requires a large energy input using methods such as high pressure homogenisation or ultrasonication (Torchilin, 2006), whereas microemulsification is often spontaneous (Becher, 1983).

As stated in the discussion above, thermodynamic stability is an important defining property of dispersed systems. This topic will be discussed in greater detail in section 2.1.2.1.

A summary of various dispersed systems is provided in Table 2.2 along with approximate droplet sizes for reference. It is worth noting that the droplet dimensions included in Table 2.2 should only be taken as a rough guide, since, as discussed above, ambiguity exists as to the exact values.

Table 2.2 - Comparison of the defining characteristics of colloidal systems (Stubenrauch, 2009)

	Microemulsions	Micelles	Emulsions	Nanoemulsions
Spontaneity of formation	Yes	Yes	No	No
Thermodynamic stability	Yes	Yes	No	Approaching thermodynamic stability
Size range	~50 nm	< 10 nm	0.5 – 50 μm	20 – 200 nm
Surfactant content	> 10 %	< 5 %	1 - 20 %	< 10 %
Appearance	Transparent	Transparent	Turbid	Translucent

For simplicity in discussing the concepts and results contained herein the distinction between an emulsion and a liquid-liquid dispersion is that the emulsion contains a surface active stabilising agent and the other does not. That is to say that when the term emulsion is used, the use of a surface stabilising agent is implied.

2.1.1.1 Components of an emulsion

The minimum number of separate components in an emulsion formulation, in the simplest stabilised system, is three. For the sake of simplicity, and following the large majority of cases across the various fields of emulsion technology, one of the phases will be aqueous. The second phase, often referred to as 'the oil', is a substance insoluble in the aqueous phase. The third component is commonly an amphiphile, usually a surfactant with hydrophilic head groups and lipophilic chains. As a brief aside, the use of solid colloidal particulates with an intermediate hydrophobicity can also be used, resulting in what is termed a 'Pickering' emulsion (Pickering, 1907). In addition it is often the case that additional components can be present dissolved in either the oil or aqueous phases. Figure 2.1 shows the three simplest systems which can exist. The lowest volume fraction of each emulsion is at first glance assumed to be the dispersed phase; however this is not always the case. Indeed systems can arise when both O/W and W/O are present in the same vessel, potentially separated by a bicontinuous region.

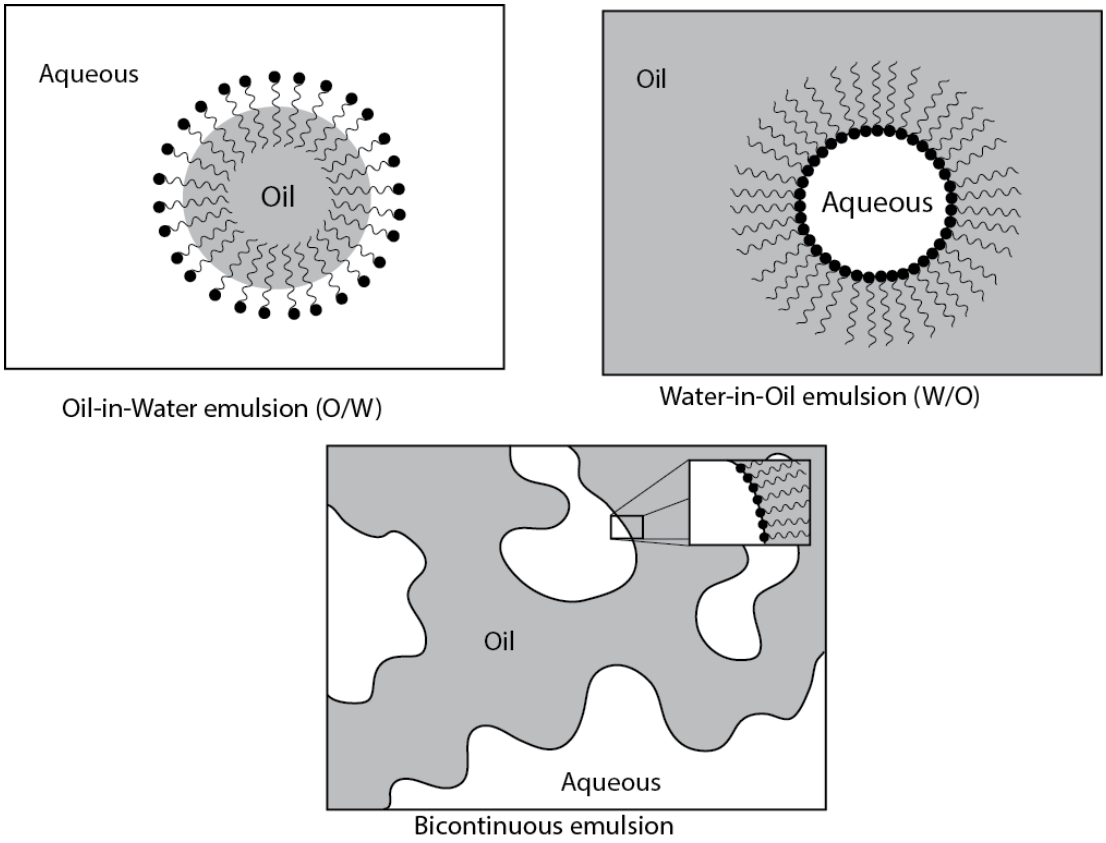

Figure 2.1 – A diagrammatic representation of the three commonly encountered emulsions structures. Top-left clockwise: oil-in-water, water-in-oil, and bicontinuous.

In addition to the three basic forms given above, a series of distinct intermediate situations have been identified. Termed the Winsor systems, they are used to categorise situations in which emulsion phases can exist in tandem with other phases. When the volume fraction of oil is sufficiently large an O/W emulsion sits below the excess oil phase, this is known as the Winsor I or $\underline{2}$. When there are both excess oil and water phases (usually through lack of surfactant) a three phase system exists where a bicontinuous emulsion exists between an upper oil phase and lower water phase. This is termed Winsor III or 3. When there is an excess water phase which sits underneath an W/O emulsion, the system is referred to as Winsor II or$\overline{2}$. The single phase homogenous emulsion (either W/O or O/W) is commonly referred to as Winsor IV (Mittal and Kumar, 1999). Illustrations of the 4 typical systems are presented in Figure 2.2.

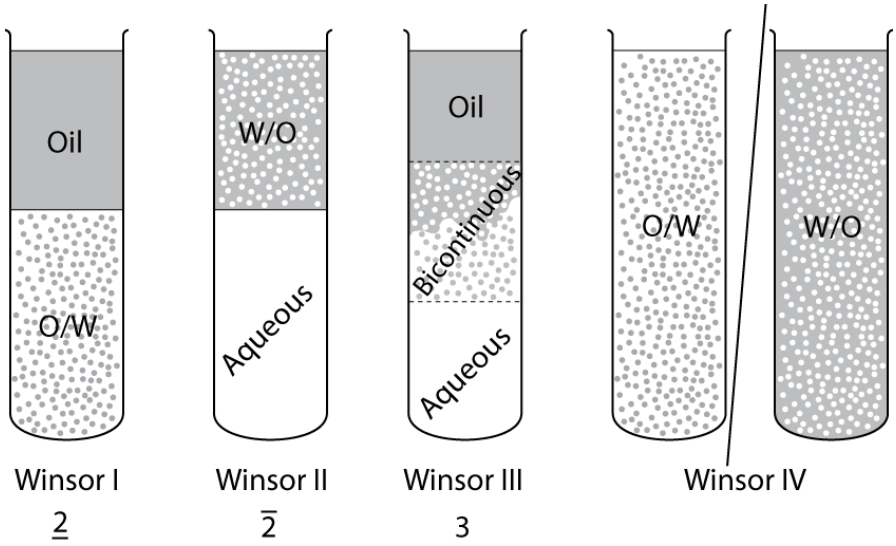

Figure 2.2 - The Winsor Systems. Where O/W, W/O, and bicontinuous refer to the emulsion composition.

For a simple ternary system phase diagrams such as that in Figure 2.3 can be used to map the phase regions as functions of concentration of the different components. Such triangular phase diagrams can also be useful for quaternary (or higher) systems if one (or more) of the corners can be taken as fixed mixtures of components.

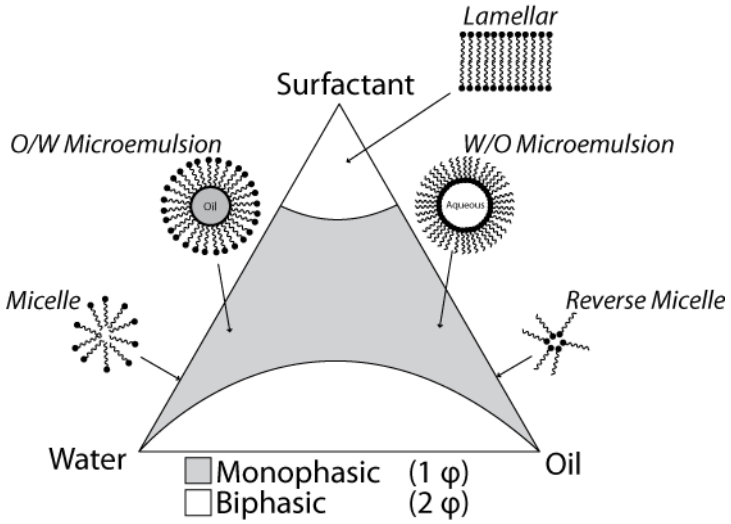

Figure 2.3 - Hypothetical ternary diagram showing expected regional microstructures. Each corner represents 100% of the indicated component

2.1.2 Chemical stabilisation of emulsion

The stabilisation of a liquid-liquid interface is often a primary goal for many formulation scientists in, for example, the pharmaceutical, food and consumer products industries. For the sake of academic endeavour the ability to quantify an interface area in existence for an appreciable length of time is extremely useful. In this section briefly the fundamental

science behind stabilisation is summarised and surface active agents used to effect stabilisation reviewed.

2.1.2.1 Thermodynamics of emulsion stability

Thermodynamic theory dictates that the minimisation of free energy is the driving force for changes occurring in a system. A simplified view of this can be applied to dispersed systems. For a dispersion of two mutually immiscible components the change in free energy is equal to a balance between the product of interfacial surface tension and the interfacial area and the product of temperature and entropic forces acting in the system, Equation 2.2.

$$\Delta G_d = \gamma \Delta A - T\Delta S \qquad 2.2$$

Where ΔG_d is the free energy change on formation of a dispersion; γ is the interfacial tension; ΔA is the interfacial area change on formation; T is temperature and ΔS is the combination of the entropic forces (Lawrence and Rees, 2000).

In order to achieve minimisation of the free energy, the product of the first two terms (γ and ΔA) needs to be minimised and the product of the second two (T and ΔS), maximised. Since a simple biphasic system will have an interface tension in the range 30-50 $mN.m^{-1}$ (Stubenrauch, 2009), a change in the overall interface area typically results in a larger change for the first product than for the second in terms of entropic increase. As such, when immiscible phases are combined, a high energy state exists which is minimised by a minimisation of surface area, i.e., the coalescence of droplets and loss of the dispersion.

In order to maintain the dispersion, a negative free energy change is required which can be achieved by a combination of an extremely low interfacial tension (although still positive) coupled with sufficient entropic contribution. That contribution is attributed to the increase in disorder by segregation of a single phase into a multitude of smaller sized dispersed domains in addition to other small factors, such as the influence of the interface curvature and interfacial surfactant diffusion (Binks, 1998).

In order to effect a change, additives must be introduced into the system to modify the environment present at the interface between the two immiscible phases. These additives are known as surfactants, a contraction of ‘surface active agents’.

As is evident from Equation 2.2, a significant reduction in the interfacial tension is the controlling factor in obtaining the required negative free energy change for a system to exist in a new low energy state. By analysis of a discreet region of interface between two

immiscible phases, the free energy change can now be written as a function of the change in interfacial tension.

$$\Delta G = \Delta\gamma A - T\Delta S \qquad 2.3$$

A change in interfacial tension between clean, γ_o, and modified, γ, interface can be written in terms of the surface pressure, Π (Equation 2.3).

$$\Pi \equiv \gamma_o - \gamma \qquad 2.4$$

The surface pressure is, in addition, a function of the area per molecule absorbed at the surface and can be equated to other system parameters via the Gibbs isotherm equation, as in Equation 2.5:

$$d\Pi = -d\gamma = RT\Gamma_s d\ln a_s \qquad 2.5$$

Where Γ_s is the surface excess, i.e., moles of surfactant absorbed per unit surface area of interface; and a_s is the surfactant activity of the surfactant in solution; and *R* is the ideal gas constant. The above relationship only holds for a system at equilibrium and for a single nonionic surfactant.

The surface excess and activity terms, given in Equation 2.5, are a function of the bulk surfactant concentration and as such the equation can be used to determine the minimum amount of surfactant required to reach the lowest possible interfacial tension. Assuming a system at equilibrium: as the concentration of bulk surfactant increases there is an increase in interface concentration and hence surface excess. A corresponding increase in surface pressure and hence a reduction in interfacial tension results. This holds true up to the point at which the activity of the surfactant molecules at the interface is equivalent to the activity of the surfactants arranged in micelles. This point equates to the minimum surface tension obtainable for the given system and the surfactant concentration to which this corresponds is known as the critical micelle concentration, CMC. This is represented pictorially in Figure 2.4.

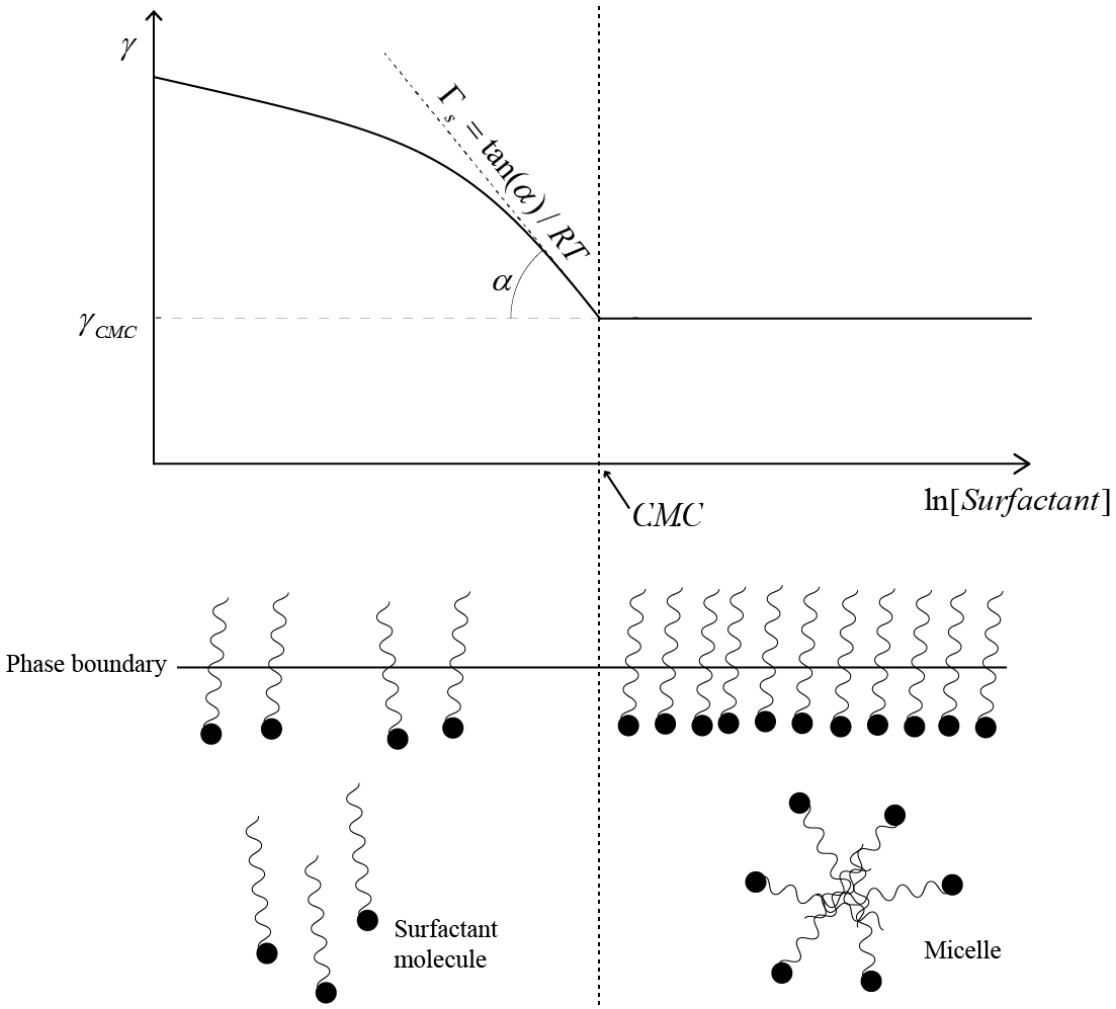

Figure 2.4 – The change in interfacial tension response across the critical micelle concentration of a non-ionic surfactant in a solution. The surface excess can be calculated from the tangent of the interfacial tension-surfactant concentration curve at the CMC. The bottom diagram depicts the behaviour of the surfactant molecules at the interface and in the bulk before and after the CMC (Binks, 1998).

2.1.2.2 Surfactants

The amphiphilic stabilising components of an emulsion, known commonly as surfactants, can be classified into four major groupings according to the nature of the surfactant molecule:

1. Non-ionic
2. Zwitterionic
3. Cationic
4. Anionic

There are theoretically an infinite number of surfactants available. Commonly known non-ionic surfactants include polyoxyethylene based molecules found in polysorbates (TWEEN®) or sorbiton alkyl esters (Span®). Ionic surfactants make up the rest of the categories, possessing anionic, cationic, or both, groups. One of the most commonly

encountered anionic surfactants is sodium bis-2-ethylhexylsulfosuccinate otherwise known as AOT (Lawrence and Rees, 2000). Quaternary ammonium salts form the majority of the well-known cationic surfactants with hexadecyltrimethylammonium halides (CTAB, CTAC) and didodecylammonium halides (DDAB, DDAC) amongst the most prevalent. Zwitterionic surfactants in the form of phospholipids (Attwood *et al.*, 1992) or amino acids (Faustino *et al.*, 2010) are also known. These and some additional chemical classes known for their surfactant properties are presented in Table 2.3.

Table 2.3 - Examples of common surfactant molecules, along with classification

Chemical Class	**Type**	**Example**
Glycerol alkyl esters	Non-ionic	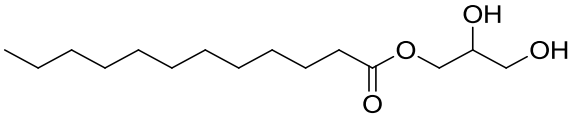
Glucoside alkyl ethers	Non-ionic	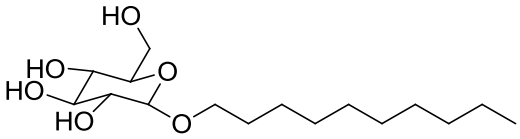
Polyoxyethylene glycol sorbitan alkyl esters	Non-ionic	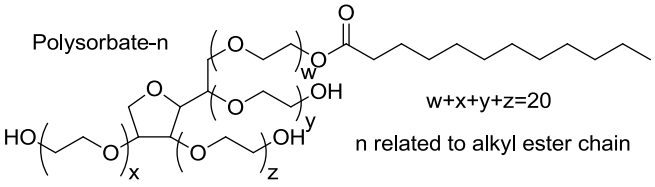
Alkyl sulfates	Anionic	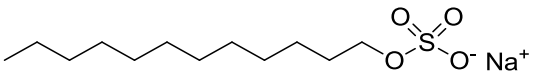
Carboxylates	Anionic	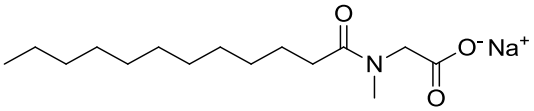
Quaternary ammoniums	Cationic	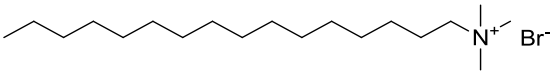
pH dependant amines	Cationic	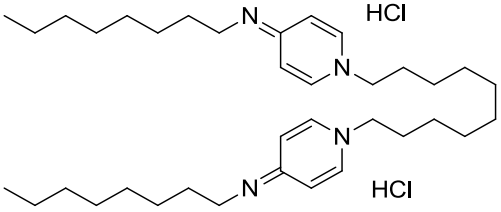

Sulfonates	Zwitterionic	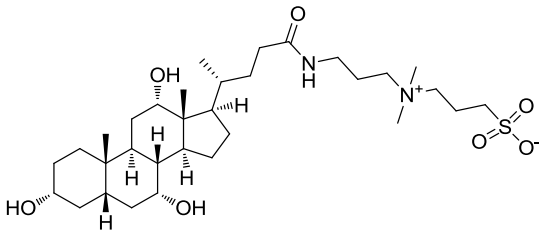

In practice, combinations of the above types are often used to tune the characteristics required for a given dispersion system.

Rationalisation of surfactant choice has been attempted, but it is however still based largely on empirical observations. The hydrophilic-lipophilic balance (HLB) indicates the contribution from the hydrophilic or lipophilic fragments of the surfactant molecule. A low HLB (2-5) favours the formation of W/O systems and, conversely, a high HLB (6-18) will favour the formation of an O/W dispersion.

Other measures such as the critical packing parameter (CPP) relate to the ability of the surfactant to form certain geometries (Israelachvili *et al.*, 1976). Mathematically this can be represented by:

$$CPP = \frac{v}{al_c} \qquad 2.6$$

Where v_p is the partial molar volume of the surfactant's hydrophobic group; a is the optimal head group area and l_c is the critical hydrophobic tail length (assumed to be 70-80% of the fully extended length).

2.1.3 Traditional methods of emulsion formation

The traditional methods for the creation of dispersions will briefly be summarised here. These methods rely upon direct force to divide the dispersed phase up into smaller droplets. They can be broadly categorised into three main groups defined by the equipment used, the liquid mixer, the high shear rotor stator mill, and the high pressure homogeniser (Sherman, 1968).

The technique of liquid mixing, when applied to droplet formation, is a direct adaptation of the well-known chemical engineering unit operation. The adjustment of the tank geometry and baffling, as well as choice and geometry of the impeller, are all known to affect the final droplet sizes.

The rotor-stator colloid mill operates by forcing the liquids into a region of high shear between a rotating section and a stationary wall. The rotational speed is typically adjustable

from 5000 to upwards of 20000 revolutions per minute. Again the geometries and configuration of the rotor and the stator are able to influence the final droplet sizes.

Finally, the use of high pressure homogenisation acts by forcing the crude liquid mixture through a fine orifice at elevated pressures. Typical operating pressures can reach of the order hundreds of bar.

Many variations of the above have been proposed. For a comparison between these and additional methods of emulsification see Becher (1983) and Perry and Green (2008) however the key point is that they are all energy intensive processes.

2.1.4 Microfluidic methods of emulsion formation

Recently the area of microfluidics has received great attention in a diverse range of scientific and technological areas (Whitesides, 2006). Microfluidic devices can generally be defined as an arrangement of sealed flow channels of lengths in the micrometre domain. Typically they are manufactured from optically clear materials such as glass or a polymer to aid visualisation. Indeed, the use of microfluidic devices in the generation of discrete droplets offers an alternative over the more conventional methods of emulsion formation. The uniformity of droplet size, i.e., the monodispersity (Link *et al.*, 2004), of emulsions produced in such a way is often seen as a major advantage in areas such as consumer care products (Pardeike *et al.*, 2009), food additives (Gouin, 2004), nano-material templating (Chan *et al.*, 2005, Hung *et al.*, 2006, Shestopalov *et al.*, 2004), and importantly for the nature of this research, chemical reactions (Song *et al.*, 2006) to name but a few.

Many channel geometries have been previously investigated, but what follows briefly is a review of the three most commonly used in droplet creation, namely, coaxial, flow focused and T-junction microchannels (respectively (a), b) and c) in Figure 2.5) and the relationships used to predict droplet size scaling.

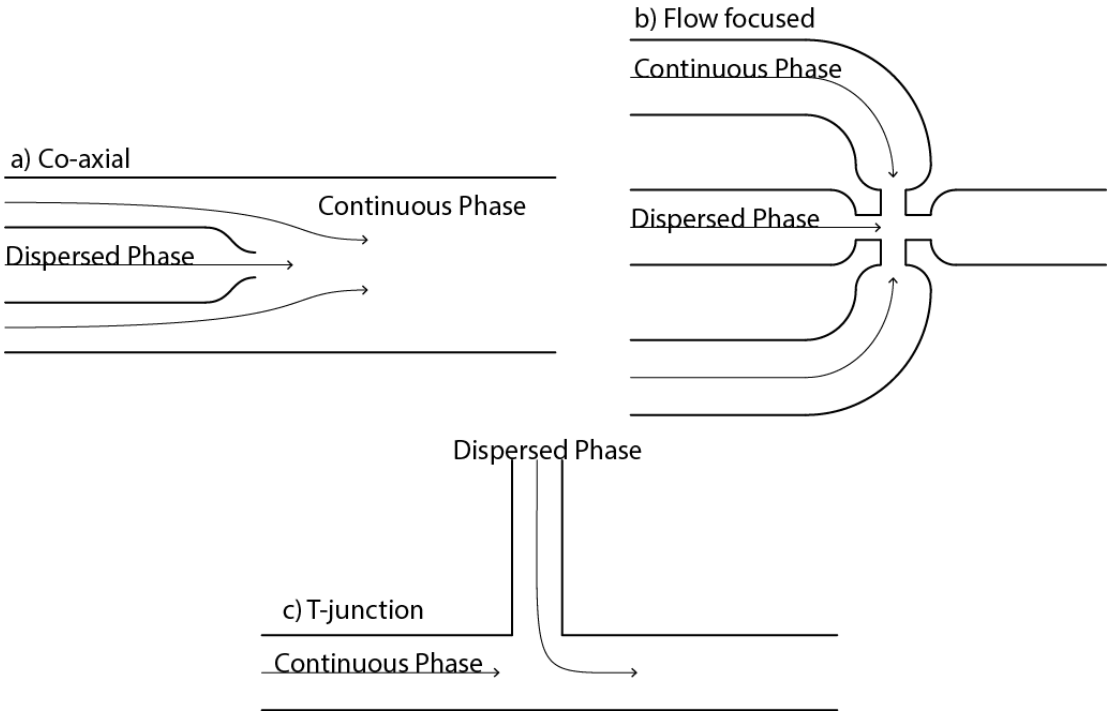

Figure 2.5 – Common microfluidic device geometries for droplet generation, a) co-axial flow, b) flow focused and c) T-junction

The co-axial system typically consists of a central axis-symmetrical capillary channel surrounded by a second outer channel running co-axially. The flow focused arrangement consists of the dispersed phase being introduced perpendicular to two impinging streams of continuous phase with an outlet positioned so that a 'cross' is formed. The outlet is often configured with an annulus, or an expanding width channel. The final geometry is that of a T-junction and, as the name suggests, the dispersed phase is introduced into the continuous phase from a perpendicular channel.

In general, the surface characteristics of the materials which form the walls of the flow channels determine the arrangement of the dispersed phase and continuous phase inlet channels. The material is typically chosen such that the dispersed phase is typically non-wetting relative to the continuous phase. Hydrophilic channels lead to the generation of oil in water arrangements and *vice-versa* for hydrophobic channel walls.

The use of dimensionless numbers can aid in standardisation and cross analysis of the flow dynamics at work in microfluidic channel. The capillary number, Ca_{phase}, for both the continuous (Equation 2.7) and dispersed phases (Equation 2.8) captures the balance of shear stress and capillary pressure. The Weber number, We_{phase}, (Equation 2.9) takes into account the fluid inertia, relevant at high flow rates for certain geometries.

$$Ca_c = \frac{\mu_c U_c}{\gamma} \quad 2.7$$

$$Ca_d = \frac{\mu_d U_d}{\gamma} \quad 2.8$$

$$We_d = \frac{Inertia}{Curvature} = \frac{\rho_d d_d U_d^2}{\gamma} \quad 2.9$$

Where μ is viscosity, U is fluid velocity, γ is interfacial tension, ρ is density and d is diameter. The subscripts c or d refer to continuous and dispersed phase respectively.

A Reynolds number (Re) can be defined for the corresponding phase accordingly.

$$\mathrm{Re} = \frac{We}{Ca} \quad 2.10$$

The balance of the forces described by these dimensionless numbers are useful in describing the mechanisms of droplet formation within these microfluidic junctions. The description of each of the devices and how the balance of the aforementioned forces act to produce different identifiable droplet formation regimes follows. Work attempting to correlate and quantify droplet size to these forces is also included where literature could be found.

2.1.4.1 Co-axial flow

Two droplet forming regimes are identifiable for the co-axial flow configuration, dripping, where the droplets are formed upon exit of the inflowing dispersed phase stream capillary; and jetting where a continuous jet emerges from the dispersed phase capillary followed by downstream break up due to Rayleigh-Plateau instability. A third regime can exist whereby the dispersed phase jet extends along the outlet channel, so that, within the confines of the device, no droplets are formed (Figure 2.5). This is denoted “co-flow”.

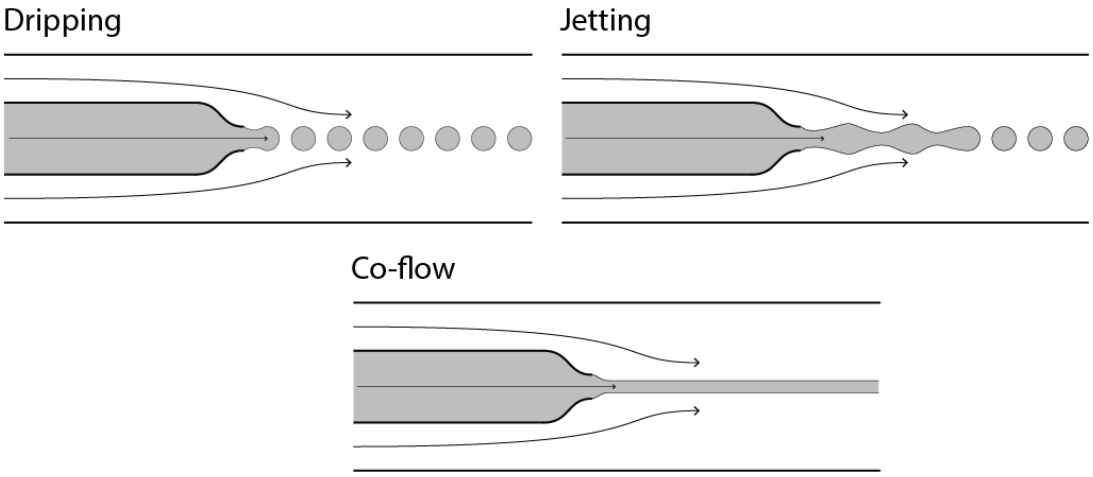

Figure 2.6 - Flow regimes for co-axial geometry. Clockwise from top left: dripping, jetting, co-flow. Not to scale.

The droplet size for the dripping regime can be estimated by the cubic equation, Equation 2.11 (Umbanhowar *et al.*, 1999).

$$\bar{d}^3 - \left(1 + \frac{1}{3Ca_c}\right)\bar{d}^2 - \frac{\varphi}{\alpha}\bar{d} + \frac{\varphi}{\alpha} = 0 \qquad 2.11$$

Where $\bar{d} = d / d_i$, the droplet diameter, d, scaled by the capillary exit internal diameter, d_i; φ is the ratio Q_d / Q_c in which Q is volumetric flow rate and $\alpha = A_d / A_c$ the ratio between cross sectional areas, A, between the dispersed and continuous flow channels.

Equation 2.11 can be simplified to Equation 2.12 as long as the dispersed phase flow rate, Q_d, is low.

$$\bar{d} \approx 1 + \frac{1}{3Ca_c} \qquad 2.12$$

The transition between dripping and jetting relies on relationships between many variables depending on the system under study. Through examination of a range of flow conditions in a recent review (Nunes *et al.*, 2013) it was suggested that the dripping droplet generation regime exists between when capillary numbers have orders of magnitude, $O(10^{-3}) < Ca_c < O(1)$ and Weber numbers, $O(10^{-3}) < We_d < O(1)$, whilst the jetting regime is observed in the ranges $O(10^{-3}) < Ca_c < O(10)$ and $O(10^{-1}) < We_d < O(10^3)$. This suggests quite a large region of overlap where both regimes are achievable, dependent on the exact conditions employed.

In the jetting regime the droplet diameter can be estimated by combining the flow rate into the jet with the pinch-off time for the impinging dispersed phase, according to Equation 2.11.

$$d = 2\left(\frac{15Q_d R_{jet}\mu_c}{\pi\gamma}\right)^{1/3} \qquad 2.13$$

Where R_{jet} is the radius of the jet and all other symbols as defined above.

For the co-axial geometry it is therefore expected that droplet sizes could be predicted in both the dripping and jetting regimes.

2.1.4.2 Flow focused.

Similar to the co-axial arrangement, flow focused devices have been found to exhibit two regimes for droplet generation, dripping and jetting, illustrated in Figure 2.7. For the dripping regime, upon introduction of the dispersed fluid into the perpendicular streams of continuous phase, droplets are immediately formed within a short distance of the inlet. Jetting is so called as a thread or jet of the dispersed phase impinges downstream someway into the outlet channel, followed by break up. When no observable droplets are formed within the confines of the device, so that a continuous stream of 'dispersed' phase passes to the outlet, co-flow results.

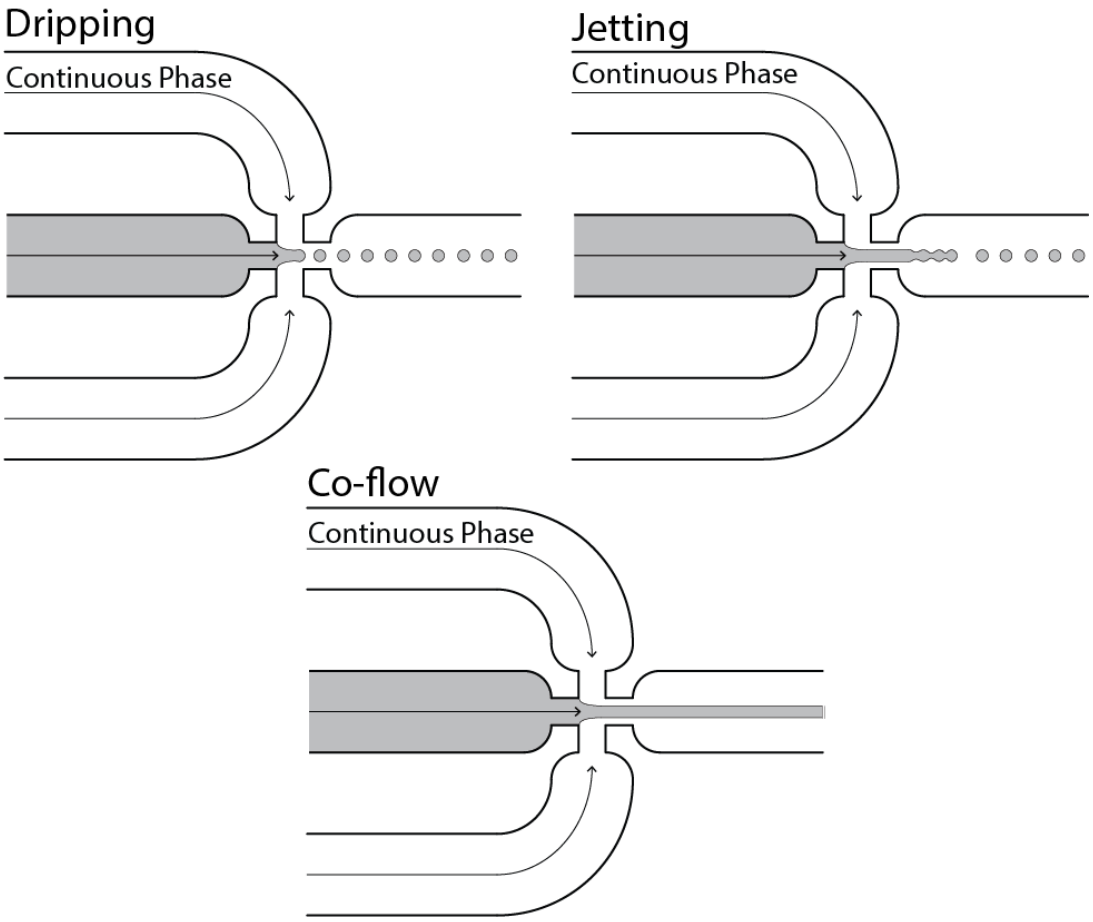

Figure 2.7 - Flow regimes for flow focused geometry. Clockwise from top left: Dripping, Jetting, Co-flow.

Unfortunately, no simple models exist to predict the droplet size for dripping generation (Christopher and Anna, 2007). However experiments into the scaling effects have led to the conclusion that the droplet size is related to a combination of capillary instability (where relationship 2.14 holds true) and the viscous drag forces (where relationship 2.15 holds true).

$$d / w_{or} \sim \varphi^{1/2} \tag{2.14}$$

$$d / w_{or} \sim \frac{\gamma \varphi^{1/2} w_o^{\,2}}{\mu_c Q_c} \sim \frac{\gamma \varphi^{3/2} w_o^{\,2}}{\mu_c Q_d} \tag{2.15}$$

Where d is droplet diameter, w is the channel width where the subscripts or and o signify orifice and outlet respectively; and φ is the volumetric flow rate ratio between the dispersed and continuous phases, Q_d / Q_c. It is important to note that the scaling relationships given above indicate that the droplet size response will be different depending on which flow rate is fixed when investigating changes to the defined flow rate ratio, φ.

Transition into the jetting regime is, in general, thought to occur when the capillary pressures for either the dispersed, or the continuous, phase flows are approximately equal to 1, i.e., $Ca_c \approx 1$ or $Ca_d \approx 1$.

Whilst in the jetting regime the relationship between droplet size and flow parameters can be approximated as for co-axial flow using Equation 2.13.

2.1.4.3 T-Junction geometry

In addition to the two flow regimes seen for the previous two geometries, an additional squeezing regime has been exhibited with T-junction devices. It is important to note that this review will only cover so called confined systems where the dimensions of the two flow channels are roughly equivalent. Information on droplet sizes and flow regimes in unconfined systems can be found in the literature (Gupta and Kumar, 2010, Husny and Cooper-White, 2006). The four possible regimes are illustrated in Figure 2.8. The squeezing regime exists when the dispersed phase enters the main channel and blocks the continuous phase. A pressure gradient is set up across the droplet or plug (since the sides are constrained) squeezing the dispersed phase downstream, deforming and then breaking the connection to the inlet stream. The dripping regime is characterised by droplet detachment immediately downstream of the side channel and the formed droplets need not block the channel. A jetting regime is possible, similar to the flow focused geometry whereby a filament of the dispersed phase extends downstream before droplets are created through flow instability.

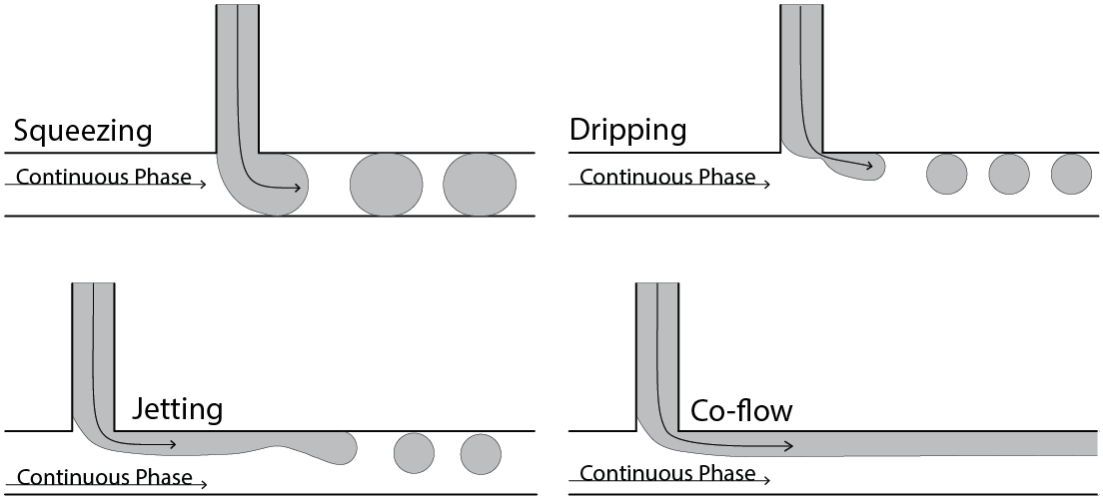

Figure 2.8 - Flow regimes for T-junction geometry. Clockwise from top left: Squeezing, Dripping, Co-flow, Jetting. Not to scale.

In the squeezing regime the droplet size is observed to scale in relation to the flow rates of the incoming streams. Owing to the fact that the dispersed phase droplets are deformed by

confinement in the main channel a droplet volume, *V*, instead of a droplet diameter represented by Equation 2.16,

$$\frac{V}{w_c^3} = 1 + \alpha\varphi \qquad 2.16$$

Where w_c is the continuous phase, main channel width, and α is an experimentally determined constant of the order of 1.

Upon increasing the dispersed phase flow rate, for example, the transition to dripping can occur as the droplet formation becomes increasingly shear dependent. A critical capillary number has been calculated, $Ca_c \simeq 0.015$ for the transition from squeezing to dripping (De Menech *et al.*, 2008, Garstecki *et al.*, 2006). Within the dripping regime the droplet size scales inversely with the capillary number of the continuous phase, and in this regime, the influence of the dispersed phase flow rate on droplet size is almost negligible.

The transition to jetting from dripping can be explained in terms of time scales of the phenomena occurring. For example if the time taken to break the dispersed phase neck is slower than the downstream drop formation then the jetting regime dominates.

2.1.5 Membrane systems

The following section serves as an introduction to the processes and apparatus currently used for emulsification using membranes. The review will be confined to dynamic, where the droplets are formed due to mechanically induced shear as opposed to static systems, where the droplets detach from a pore when buoyant forces overcome surface tensions with the pore. Experimentally defined relationships between droplet creation, size and membrane parameters are explained.

Similar to microfluidics, the use of membrane based systems in the dispersion of immiscible phases has received a lot of attention in recent years (Charcosset *et al.*, 2004, Joscelyne and Trägårdh, 2000, Piacentini *et al.*, 2010). In typical cross flow membrane emulsification, the dispersed phase is permeated through the pores of a cylindrical membrane into a flow of the continuous phase (Figure 2.9). The growing droplets impinge into the flow, where they detach and are carried downstream due to a shearing force imposed across the wall boundary by the continuous phase flow.

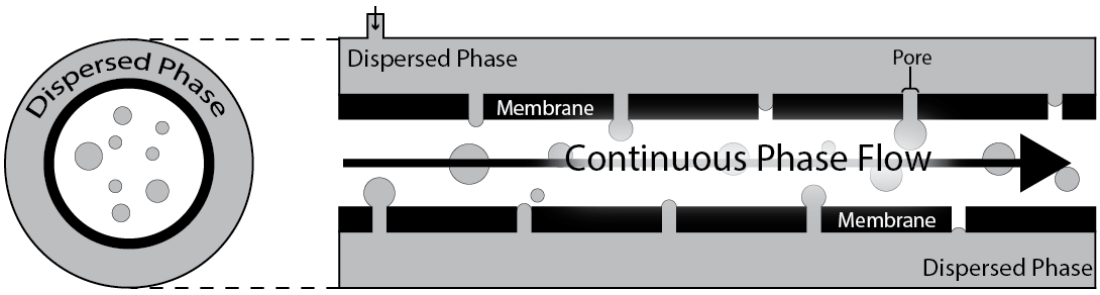

Figure 2.9 – Typical cross flow membrane arrangement. The dispersed phase permeates through the pores perpendicular to the continuous phase flow.

This permeation is pressure driven and as such a transmembrane pressure, ΔP_{tm}, is defined as the difference between the dispersed phase pressure and average continuous phase pressure.

$$\Delta P_{tm} = P_d - \frac{\left(P_{c,in} - P_{c,out}\right)}{2} \qquad 2.17$$

Where P_d is the dispersed phase pressure, P_c is the continuous phase pressure with the subscripts denoting the inlet, in, and outlet, out.

If the membrane pores are approximated as ideal cylindrical channels, the critical pressure, P_{crit}, for permeation can be calculated from the capillary pressure exerted due to interaction of the dispersed phase with the continuous phase wetted pore wall (Equation 2.18).

$$P_{crit} = \frac{4\gamma \cos\theta}{\bar{d}_p} \qquad 2.18$$

Where γ is the interfacial tension between the continuous and dispersed phases, θ is the contact angle between dispersed phase droplet and continuous phase and $\bar{d}_p$ the average pore diameter. The idealities assumed in Equation 2.18 are often not the case in real systems and deviations in pore geometries and surface wettability will often lead to a critical pressure higher than predicted.

To quantify the amount of dispersed phase passed through the membrane, a dispersed phase flux, J_d, can be defined using Darcy's law which relates this to the transmembrane pressure (Equation 2.19).

$$J_d = \frac{L_p \Delta P_{tm}}{\mu_d L} = \frac{M_d}{\rho_d A} \qquad 2.19$$

Where L_p is the membrane permeability, μ_d is the dispersed phase viscosity, L is the membrane thickness, M_d is the mass flow rate of the dispersed phase, ρ_d is the dispersed phase density and A is the membrane surface area.

Typically the material of the membrane is chosen so that it is preferentially wetted by the continuous phase, to encourage dispersed phase droplet formation. For a typically aqueous continuous phase, a hydrophilic material such as glass (microporous or Shirasu Porous Glass, SPG), ceramic or metal is used however hydrophobic polymeric materials such as polypropylene have also been reported. A summary of the various techniques to date used in cross-flow membrane emulsification is given in Table 2.4. The majority of the work conducted in cross-flow emulsification utilise unstructured sintered pore geometries (glass, ceramic). However, slotted type membranes with perpendicular arrays of pores enable very small droplet size distributions when used in conjunction with rotating membranes (Kobayashi *et al.*, 2002, Yuan *et al.*, 2009)

Table 2.4 - Summary of crossflow membrane emulsification experiments from (Spyropoulos et al., 2014)

Material	**Pore Size**	**Droplet Size**	**Emulsion type**	**Flux**	**Reference**
Tubular micro porous glass	0.52 µm	3 × pore size	o/w (o: kerosene)	Not specified	(Nakashima *et al.*, 1992)
Tubular SPG	0.98, 2.7, 4,7 µm	< pore size	w/o (o: toluene oil)	Not specified	(Kandori *et al.*, 1991)
Tubular SPG	0.57, 1.1 and 2.3 µm	5–10 × pore diameter	o/w (o: corn oil)	Flux up to 28 L m^{-2} h^{-1}	(Katoh *et al.*, 1995)
Tubular SPG	2.56 µm	3 × pore diameter	w/o (o: soy bean oil)	Not specified	(Kandori, 1995)
Tubular micro porous glass	0.36, 1.0 and 1.36 µm	3 × pore size	w/o and o/w (o: soy bean oil)	Not specified	(Mine *et al.*, 1996)
Tubular SPG	0.4 and 2.4 µm	1–45 µm	Corn oil in water emulsion	Flux up to 28 L m^{-2} h^{-1}	(Katoh *et al.*, 1996)
Single glass capillaries	5–200 µm	4 × pore diameter	Mineral oil in water	Flux up to ~5000 L m^{-2} h^{-1}	(Peng and Williams, 1998)

			emulsions		
Tubular ceramic	0.2 and 0.8 μm	4 × pore diameter	Mineral oil in water emulsions	Flux up to 8 L m^{-2} h^{-1}	(Williams *et al.*, 1998)
Tubular ceramic	0.2 and 0.8 μm	2–15 μm	Vegetable oil in water emulsion	Flux up to 22 L m^{-2} h^{-1}	(Schröder *et al.*, 1998, Schroder and Schubert, 1999)
Tubular ceramic	0.5 0.2 and 0.1 μm	1–12 μm	Vegetable oil in skimmed milk emulsion	>100 kg m^{-2} h^{-1}	(Joscelyne and Trägårdh, 2000)
Tubular SPG	1–3 μm	3–100 μm	Oil in water emulsion stabilised by Tween20 and milk protein	Not specified	(Christov *et al.*, 2002)
Polypropylene hollow fibre	0.4 μm	0.3–2 μm	Water in oil emulsion stabilised by PGPR	Flux between 0.7–7 L m^{-2} h^{-1} for smallest size distribution span	(Vladisavljević *et al.*, 2002)
Tubular micro-porous glass	5.2 μm	10–45 μm	Oil in water emulsion stabilised with SDS and PVA	Not specified	(Hao *et al.*, 2008)
High porosity micro-engineered silicon wafer	5 μm	10–40 μm	Sunflower oil in water emulsion	Max flux 333 L m^{-2} h^{-1}	(Wagdare *et al.*, 2010)

Tubular ceramic, SPG, polymer and stainless steel	1 and 15 µm	0.8–40 µm	Sunflower oil in water emulsion	Not specified	(Hancocks *et al.*, 2013)

In dynamic membrane emulsification, where the droplets are detached from the pore opening through shearing, a relationship between shear and droplet size has been observed, Figure 2.10.

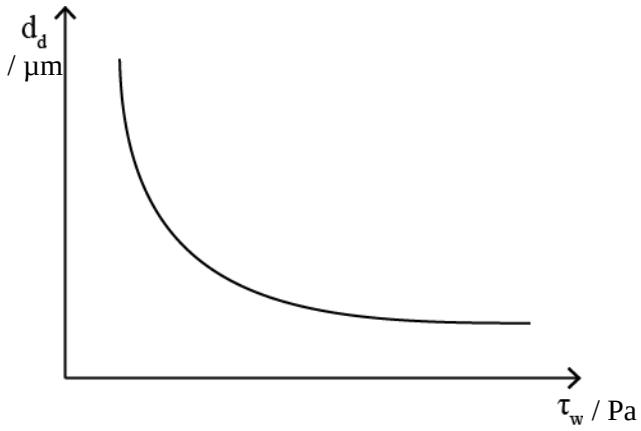

Figure 2.10 – Relationship between shear stress and droplet diameter in membrane emulsification. d_d represents the droplet diameter and τ_w the wall shear stress. Image reproduced from (Joscelyne and Trägårdh, 2000) dinemsion added.

From the above relationship, the change in droplet diameter is more significant at low shear stresses. At higher shear the droplet diameter has been shown to be independent of shear stress. Schröder *et al.* (1998) showed that shear dependence cut off is related to the membrane pore size. For pore sizes 0.1 µm and 0.5 µm in an α-alumina membrane the minimum shear stress was reported to be 2 Pa. For a larger pore diameter of 0.8 µm in a membrane of the same material a shear stress above 20 Pa was required.

In order to attempt prediction of the droplet size the wall shear stress can be calculated from classic fluid dynamics theory. Firstly, the Reynolds number, a measure of the ratio between pressure and shear stress, can be calculated for a tubular membrane, analogous to a pipe:

$$\mathrm{Re} = \frac{\rho_c V_{ax} D}{\mu_c} \qquad 2.20$$

Where ρ_c is the continuous phase density and V_{ax} is the axial velocity of the continuous phase through the membrane tube of diameter D.

The fanning friction factor, f, relationships can relate the flow variables to shear stress, τ_w, at the membrane surface (Peng and Williams, 1998).

$$f = \frac{2\tau_w}{V_{ax}^2 \rho_c} = \begin{cases} 16/\mathrm{Re} & \mathrm{Re} < 500 \\ 0.0792\,\mathrm{Re}^{-0.25} & 500 \le \mathrm{Re} \le 20000 \end{cases} \quad 2.21$$

In addition to the above reported droplet size dependence on wall shear stress, a simple linear relationship between pore size and resultant droplet size has been widely accepted under otherwise identical operating conditions.

$$d_d = x d_p \quad 2.22$$

Where x is the constant of proportionality, or droplet size/pore size ratio. This is system dependent and values from less than 1 up to 75 are common (Charcosset *et al.*, 2004).

2.1.6 Characterisation

The techniques which are used to characterise emulsions can be divided into two broad areas, those that are designed to monitor and investigate the physical properties and those that probe the microstructure. The separation is, however, not clear cut as many bulk physical properties can give insight into the microstructural phenomenon, and observations about structure often elucidate data pertaining to physical characteristics.

Viscosity measurements can routinely be measured with commercially available meters. Examples of where such measurements of a bulk emulsion property can give useful structural information include increasing viscosity as a result of the formation of rod or worm like (reverse) micelles (Yu and Neuman, 1995). Likewise conductivity measurements can differentiate between the possible continuous phases, or allow one to monitor phase inversion (Mehta *et al.*, 1999).

More advanced techniques have been used to probe the inter phase interactions such as the use of pulsed field gradient or diffusion nuclear magnetic resonance spectroscopy (NMR) to monitor the oil or surfactant molecule movement through the emulsion (Regev *et al.*, 1996, Parker Jr *et al.*, 1993). Such techniques also give microstructural and mobility information for the emulsion components. Recently droplet sizing has been achieved by analysis of ^{129}Xe NMR and the results were verified to be consistent with those gained by other spectroscopic methods (Kataoka *et al.*, 2007).

Research into the dynamic nature of dispersed systems has led to the development of a variety of dielectric spectroscopic methods. Amongst these are time domain dielectric spectroscopy (TDDS) which can aid assessment of changing the various polar groups,

associations and aggregates which represent the dipole moments in emulsions. Additionally, relaxation measurements possible with such techniques allow extraction of dimensional data related to cluster formation (Feldman *et al.*, 1997).

Scattering experiments are the most widely used methods for the characterisation and interpretation of emulsion structure. Both dynamic and static light techniques have been used extensively, primarily as a means of measuring particle size distribution (Attwood *et al.*, 1992) and source of diffusivity information (Saint Ruth *et al.*, 1995). Additionally small angle X-ray or neutron scattering (SAXS, SANS respectively) were paramount in the initial investigations into emulsion characterisation, being used to identify transitions between oil-in-water, water in-in-oil and bicontinuous emulsions (Regev *et al.*, 1996). Indeed the bending moduli, noted to be a key variable in the evaluation of emulsion formation and stability, can reportedly be directly measured from a combination of SANS techniques, for example, utilising a neutron spin-echo method (Gradzielski, 2008).

Electron microscopy, frequently considered unsuitable for the investigation of liquid media, has recently proven to be invaluable in probing structural phenomena. The use of cryoscopic methods is crucial when dealing with delicate structures such as those found in emulsions. Indeed by coupling cryoscopy with techniques employing extremely low electron doses, to avoid the scission of intra and inter molecular bonds (<100 $e.nm^2$), detailed electron micrographs have been obtained (Gradzielski, 2008). The sample preparation is arguably the most important aspect of the electron microscopy process, and the invention of a novel 'freeze-fracture direct imaging' technique (FFDI) has been invaluable (Belkoura *et al.*, 2004), allowing direct visualisation of structures, such as in the example shown in Figure 2.11. Despite the apparent advantages of FFDI (given in the associated reference), traditional cryo-transmission electron microscopy (cryo-TEM) has been employed successfully to image O/W emulsions of toluene and water with a didodecyldiphenylether disulfonate (C12-DADS) gemini surfactant (Magdassi *et al.*, 2003). Three dimensional morphological characterisation has been realised through use of cryo-field emission scanning electron microscopy (cryo-FESEM) in the investigation of bicontinuous dispersed systems (Rizwan *et al.*, 2007).

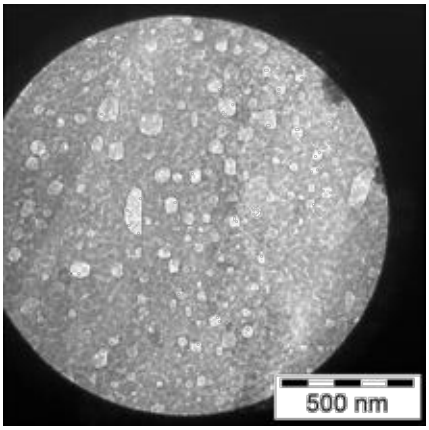

Figure 2.11 - FFDI micrograph of a W/O microemulsion of H_2O/n-octane/$C_{12}E_5$. Reproduced from Belkoura et al. *(2004).*

2.2 Liquid-liquid biphasic reactions

The primary areas of interest in this research are reactions occurring between two mutually immiscible liquid phases.

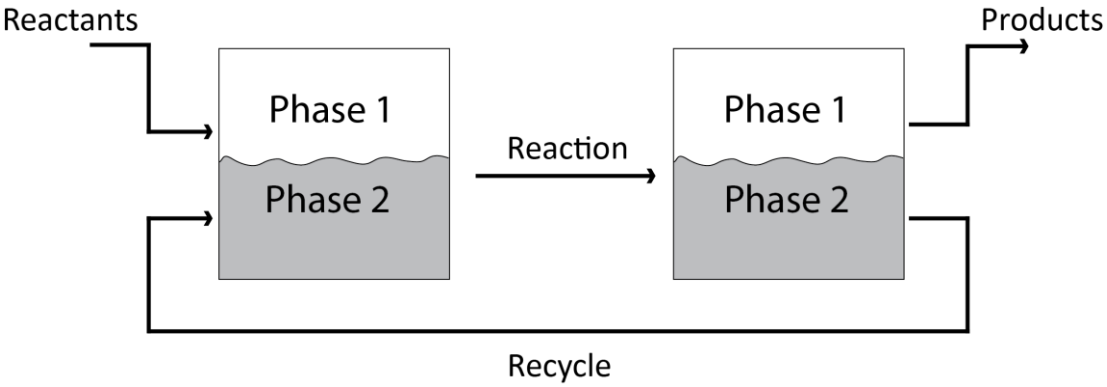

Figure 2.12 – Biphasic reaction block diagram

There are a wide variety of reactions which take part between systems containing two liquid phases. This is predominantly motivated by the notion of enhanced phase separation and potential for reagent recovery, illustrated in Figure 2.12. These reactions primarily take the form of homogeneous catalysis, that is to say the active metal catalyst is soluble typically in only one of the liquid phases. Due to its highly polar nature, water is often used as one of the phases as it is easily separable from non-polar components. Other systems, such as two organic, highly flourous, or ionic liquid phases have all been investigated for use in a biphase (Wiebus and Cornils, 2006). However, although a few examples are included in this section, the main focus is on aqueous-organic systems.

The breadth of the transformations currently undertaken shows is that there is significant interest in the use of these liquid-liquid systems. From a review of the literature it should be noted that a lot of the work in this area relies heavily on the development of novel ligands to alter solubility of complexes containing the active metal species. A brief summary of some of the earlier examples of reactions either inherently biphasic or adapted (through use of immiscible diluents) for use aqueous-organic reactions is given in Table 2.5.

Table 2.5 - Biphasic aqueous-organic reactions. Adapted from (Wiebus and Cornils, 2006)

Reaction	Reference
Aldolization	(Inoue *et al.*, 2002, Manabe and Kobayashi, 2002, Nagayama and Kobayashi, 2000)
Alkylation	(Ooi *et al.*, 2002, Shimizu *et al.*, 2002, Sinou *et al.*, 2003)
Allylation	(Manabe and Kobayashi, 2002, Sigismondi and Sinou,

	1997)
Alternate copolymerisation of CO-ethylene	(Verspui *et al.*, 2000)
Carbonylation	(da Rosa *et al.*, 2000)
Claisen rearrangement	(Wipf and Rodríguez, 2002)
Diels-Alder reaction	(Manabe and Kobayashi, 2002, Itami *et al.*, 2002, Loncaric *et al.*, 2003)
Epoxidation	(Sato *et al.*, 1997)
Friedel-Crafts reaction	(Manabe *et al.*, 2001)
Heck reaction	(Mukhopadhyay *et al.*, 2002)
Hydrogenation	(Yang *et al.*, 2000)
Mannich reaction	(Manabe and Kobayashi, 2002)
Metathesis	(Lynn *et al.*, 1998)
Michael reaction	(Mori *et al.*, 2000)
Oxidation	(Venturello and Gambaro, 1991)
Polymerization/	(Mecking *et al.*, 2002)
Reformatsky reaction	(Chattopadhyay and Salaskar, 2000)
Sharpless dihydroxylation	(Mehltretter *et al.*, 2000)
Ullmann reaction	(Venkatraman *et al.*, 2002)

The use of separation units often come at a high energy cost such as in the use of distillation columns, however the use of biphasic systems allow much lower energy cost units such as simple decanters or separators. As an example the Ruhrchemie-RP process in the manufacture of butanal which adopts such a biphasic system show approximately 10% savings in the cost of manufacture compared to similar rhodium catalysed, non-biphasic processes. This saving is almost entirely due to a reduction in energy costs, attributable to heat recovery and presumably lower unit operation costs. Therefore these are not merely academic endeavours, a few large scale commercialised chemical synthesis adopt the biphasic approach such as those illustrated in Table 2.6

.

Table 2.6 - Biphasic industrial catalytic processes. From (Wiebus and Cornils, 2006)

Process / Catalyst	**Products**	**Capacity / tonnes per annum**
Shell SHOP / Ni-P,O ligand	Olefins	900 000
Ruhrchemie-RP (now Celanese) / Rh-TPPTS	n-Butanal	800 000
Kururay Co Ltd / Pd-TPPMS	n-Octanol, nonadiol	5 000
Clariant AG / Pd-TPPTS	Substituted biphenyls	<1 000
Rhodia (former Rhône-Poulenc)/Rh-TPPTS	Vitamin precursors	*

* Exact production figures not known

The above reported systems have primarily focused on the use of novel stirred tank designs to facilitate phase dispersion, without particular reported quantification of interface area. Alternative dispersion methods such as the use of dedicated emulsification, microfluidic as well as membranes have also been investigated for creation of favourable reaction media. The use of these technologies allow for better characterisation of interface area, due to enhanced droplet lifetimes or more obvious visualisation techniques. For this reason reviews relating to these specific areas follow in the next sections.

2.2.1 Organic reactions in emulsions

The influence of emulsions on reaction rates was first being investigated in the late 1950's studying the fading effects of dye molecules when detergents were added to a reaction mixture (Duynstee and Grunwald, 1959). The work by Letts and Mackay (1975) on metalloporphyrin formation was perhaps the first investigative piece primarily focused on reactions in emulsions. Since then the field has expanded to cover almost all areas of organic chemistry, not to mention polymer chemistry (Athey, 2011) and nanoparticle formation (Shchukin and Sukhorukov, 2004).

Due to the nature of the emulsion structure, reactants of widely differing polarities are subject to contact across potentially huge interface areas. If it assumed that reaction will occur as a result of interaction either at these interfaces, or even in one of the phases, one can see the potential for exploitation of the contact areas to effect mas transfer processes. Indeed several studies have shown work towards this area (Holmberg, 2007). Comparisons have been undertaken comparing a simple biphasic non emulsified biphasic system (with added phase transfer catalyst, a common way to overcome reactant incompatibility) and an emulsion. In some cases the rate of reaction in the emulsion proved to be unmodified

compared to a biphasic non emulsified arrangement (Gutfelt *et al.*, 1997), however in most cases an enhanced rate was observed upon emulsification (Menger and Elrington, 1991, Häger and Holmberg, 2000).

As indicated earlier, metalloporphyrin formation was one of the first reactions to be conducted in emulsions. The same group also studied the reactions of the hydroxide ion on carboxylate esters namely *p*-nitrophenyl stearate, laurate caprylate and acetate esters. It was suggested in the latter case that the reaction proceeded in a W/O emulsion, a relatively unexplored field at that time (Mackay, 1981).

Another early emulsion reaction was the oxidation of half mustard with hypochlorite, Scheme 2.1. Oxidation of mustards are ideal test emulsion reactions as the mustard is insoluble in water while the oxidant chosen to render it less damaging to humans is often delivered as an aqueous solution. In this example emulsification led to a 80 times increase in the rate of oxidation of the mustard, being complete in 15 seconds in the emulsified system, compared to 20 minutes in the two phase system (Menger and Elrington, 1991). Importantly the biphasic, non-emulsified system used as a comparison in this study required a phase transfer catalyst, whereas none was required in the emulsified system.

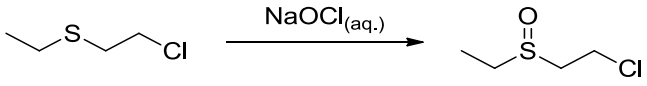

*Scheme 2.1 - Oxidation of 2-chloroethyl ethyl sulfide (*half-mustard*) to 2-chloroethyl ethyl sulfoxide with hypochlorite.*

Nucleophilic substitution of benzyl chloride to benzyl bromide (Scheme 2.2) conducted in an emulsion was achieved with higher rates of reaction than the phase transfer catalysed alternative (Martin *et al.*, 1982). The same group later investigated the borohydride reduction of carbonyl compounds including benzophenone, benzaldehyde, acetophenone, 1-phenyl-1-octadecanone, *trans*-4-phenyl-3-buten-2-one and the diketone, 4-(4'-benzoylphenyl)-2-butanone. In all cases, as before, reaction rates were improved over the phase transfer catalysed equivalents (Jaeger *et al.*, 1984).

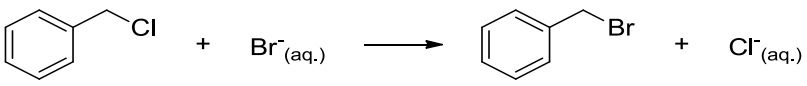

Scheme 2.2 – Benzylic halide substitution

Lactonisation through intramolecular esterification of hydroxyalkanoic acids and the cyclization of brominated alkanoic acids (Scheme 2.3) was achieved in emulsions in both reactions with minimal side product formation (Gonzalez and Holt, 1981). The same group later conducted Diels-Alder condensation of cyclopentadiene and methyl methacrylate in a

water/toluene/2-propanol emulsion. The influence of the surfactant choice on the stereoselectivity was assessed, and found to be partially influenced by surfactant polarity (Gonzalez and Holt, 1982).

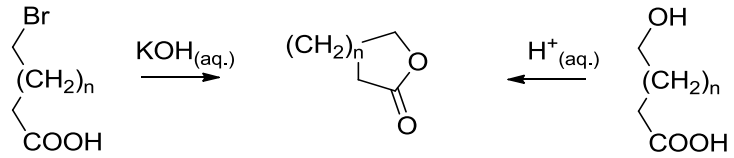

Scheme 2.3 - Lactonisation through esterification of hydroxyalkanoic acids or cyclisation of brominated alkanoic acids

Ring opening of an aliphatic epoxide with sodium hydrogen sulfite to yield long chain hydroxysulfonate was attained with an emulsion based on dodecane/water and a series of surfactants (Anderson *et al.*, 1998). The same system was later used with a chlorinated hydrocarbon in place of the dodecane with added quaternary ammonium hydrogen sulphate to try and marry the aspects of phase transfer catalysis with the use of emulsions (Häger and Holmberg, 2000).

The direct etherification of hexanol and *tert*-butyl alcohol in an emulsion consisting of cyclohexane, water and surfactant was realised. Variation of a range of parameters including surfactant, molar ratios of reactants and reaction temperature was also studied. The reaction proceeded to optimum yields with the use of dodecylbenzene sulfonic acid (DBSA) exhibited a dual purpose as both surfactant to stabilise and increase surface area and as a Brønsted acid to accelerate the reaction (Song *et al.*, 2008).

Regioselective nitration of a range of phenols and anisols was achieved under emulsion conditions, yielding almost exclusively *para* products, in contrast with an equal *ortho*- / *para*- ratios from a standard biphasic system (Scheme 2.4). This directing ability was attributed to the interaction of the electron rich face of the aromatic ring and the cationic surfactants used. Kinetics studies were also performed to confirm the rate enhancement of the nitration in dispersed media, enabling the use of dilute nitric acid in contrast to the concentrated acid required in the biphasic, non-emulsified system (Currie *et al.*, 2001). The same group later reported similar findings with the bromination of the same substrates (Currie *et al.*, 2003). The directional ability of emulsions has also been noted in the photocycloaddition in 9-substituted anthracenes whereby almost exclusively head-to-head photocyclomers were obtained (Wu *et al.*, 2002).

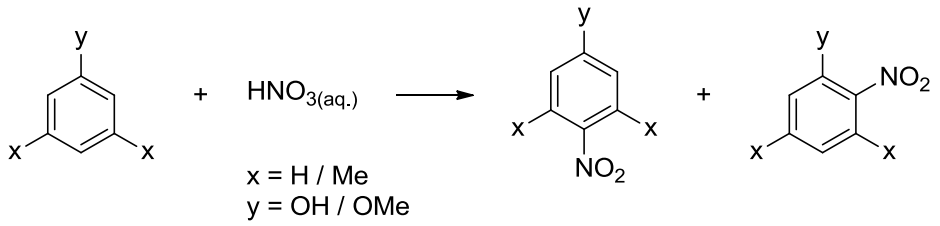

Scheme 2.4 - The nitration of phenols / anisols with nitric acid

A kinetic study on the rate of hydrolysis of acetylsalicylic acid in a variety of emulsions (O/W, W/O) was conducted. A change in reaction rate was seen, attributed to a change in the emulsions structure from O/W through bicontinuous to W/O upon changing the water content of the emulsion (Qian *et al.*, 2001). The structure with the lowest rate was strongly dependent on the surfactant used: anionic showed fastest rate in the O/W, cationic showed the fastest rate in the W/O, non-ionic showed the fastest rate in the discontinuous region. This highlights that the rate limiting step in emulsion reactions can be influenced significantly through structural and electronic considerations.

Electroorganic synthesis in emulsions has been realised for its green credentials. For example, Carrero and co-workers conducted the dimerisation of nitrobenzene as well as selective reduction of naphthalene and biphenyls in O/W emulsions (Carrero *et al.*, 1999). Additionally electrochemical carbon-carbon bond formation has been obtained both through intra-molecular cyclisation and addition of primary alkyl iodides to conjugated cyclohexanones (Gao *et al.*, 1996). Electroorganic synthesis within emulsions is particularly interesting owing to the complex microstructure, affording local and global changes in pH and redox potentials. For this reason, the exact reaction response is reportedly difficult to predict in emulsion media but, in the cases given above, offered significant reaction pathway control.

Hydroformylation, previously seen on a multi-tonne scale in the RCH-RP process, is another area where dedicated emulsion media have been utilised to facilitate reaction. The effective use of rhodium (Haumann *et al.*, 2002) and later cobalt (Haumann *et al.*, 2003) catalysts to hydroformylate 7-tetradecene with high rates of reaction in yielding the aldehyde, 2-hexyl-nonanal, as the primary product in the case of Rh and a combination of terminal aldehydes in the case of cobalt, Scheme 2.5. The use of emulsions enabled simple catalyst recovery through thermally induced emulsion breaking and filtration.

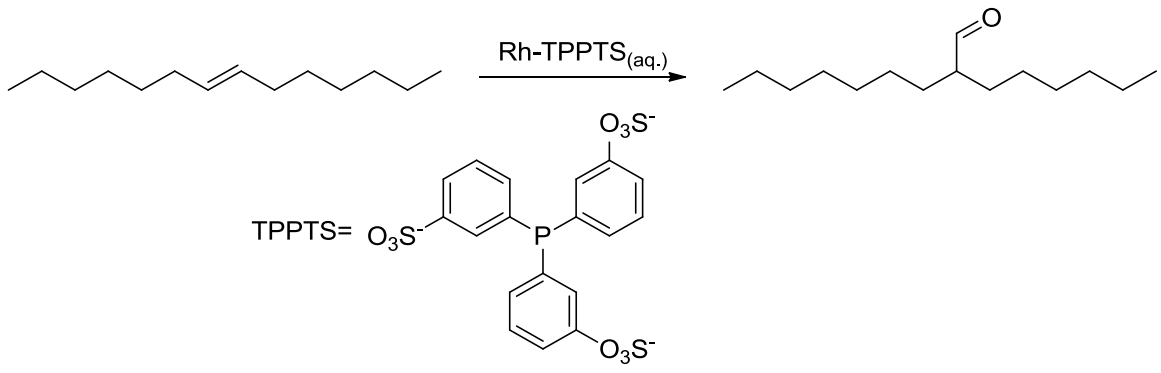

Scheme 2.5 - The rhodium-triphenylphosphinetrisulfonate catalyst hydroformylation of 7-tetradecene into 2-hexyl-nonanal.

An aldol condensation has been performed in an *n*-hexane/water/Cetyltrimethylammonium bromide/ *n*-butanol emulsion. Benzaldehyde was successfully reacted with acetone to yield the cross condensation product. The droplet sizes used in this reaction are of the order of tens of nanometres, corresponding to a huge interface area for even small quantities of dispersed phase. The authors note that there is direct correlation between the reaction rate and the dispersed phase droplet diameter (Shrikhande *et al.*, 2010). Importantly they also show that an increase in surfactant levels has a detrimental effect on the rates of reaction. This has significant connotations in terms of control of mass transfer processes for the use of surfactant stabilised emulsion reactions.

The above review is by no means exhaustive but highlights the diversity of reactions being performed in such media. New examples are being reported almost weekly in a wide ranging number of journals, a testament to the importance of this field. A summary of the discussed and other notable reactions is given in Table 2.7.

Table 2.7 - Organic reactions in emulsions

Reaction	Emulsion Type	Aqueous phase	Oil phase	Surfactants	Type of Reaction	Reference
Metalloporphyrin formation	O/W	water metal salt	benzene porphyrin	sodium cetyl sulfate (SCS) cetylpyridinium bromide (CPB) potassium oleate (PO) co: Cyclohexanol	Metallation/Insertion	**(Letts and Mackay, 1975)**
Surfactant synthesis	W/O Bicontinuous	water sodium sulphite sodium cyanide sodium azide	1-bromodecane dodecane	$C_{12}E_5$ CTAC CTAB CTAAc	Addition	**(Gutfelt *et al.*, 1997)**
Sulphide oxidation	O/W	water hypochlorite	heptane 2-chloroethyl ethyl sulfide	sodium dodecyl sulfate (SDS) CTAB polyoxyethylene 10 oleoyl ether (Brij-96®) AOT co: 1-Butanol/1-pentanol/2-propanol	Oxidation	**(Menger and Elrington, 1991)**
Benzyl halide substitution	O/W	water potassium bromide	hexane benzyl chloride	CTAB co: 1-butanol	Nucleophilic substitution	**(Martin *et al.*, 1982)**

Borohydride reduction of carbonyl compounds	O/W W/O	water KOH $NaBH_4$	hexane(s) mono/di carbonyls	hexadecyltrimethylammonium bromide (HTAB) co: 1-butanol	Reduction	**(Jaeger *et al.*, 1984)**
Lactonisation of hydroxyl and bromo alkanoic acids	Not specified	water *p*-toluenesulfonic acid KOH	toluene hydoxyalkanoic acid bromoalkanoic acid	None	Ring closing esterification	**(Gonzalez and Holt, 1981)**
Epoxide Ring-opening	Not specified	water sodium hydrogen sulfite	dodecane 1,2-epoxyoctane	SDS octa(ethylene glycol)monododecyl ether alcohol ethoxylate	Ring opening substitution	**(Anderson *et al.*, 1998)**
Epoxide Ring-opening	O/W	water sodium hydrogen sulphite	trichloroethane 1,2-epoxyoctane	octyl glucoside dodecyl/hexadecyl glucoside	Ring opening substitution	**(Häger and Holmberg, 2000)**
Direct etherification form alcohols	W/O	water	cyclohexane hexanol *tert*-butanol	DBSA	Etherification	**(Song *et al.*, 2008)**
Regioselective nitration of phenols/anisols	W/O Bicontinuous	water nitric acid	isooctane (3,5-demithyl)phenol (3,5-dimethyl)anisol	dodecyltrimethyl bromide (DTAB) DDAB	Addition	**(Currie *et al.*, 2001)**
Bromination of	Not specified	water	(3,5-demithyl)phenol	DTAB	Addition	**(Currie *et al.*, 2003)**

phenols/anisols		nitric Acid	(3,5-dimethyl)anisol			
Photocycloaddition of substituted anthracenes	W/O	water (9-substituted anthracenes)	dichloromethane (9-substituted anthracenes)	AOT	Photocycloaddition	**(Wu *et al.*, 2002)**
Hydrolysis of acetylsalicylic acid	W/O O/W Bicontinuous	water acetylsalicylic acid	*n*-pentanol, *n*-butanol	CTAB SDS Triton X-100	Hydrolysis	**(Qian *et al.*, 2001)**
Direct electrochemical reduction of nitrobenzene	Not specified	water hydrogen chloride	hexane/dodecane nitrobenzene	DDAB	Electrochemical reduction	**(Carrero *et al.*, 1999)**
Carbon-carbon bond formation in conductive microemulsions	Bicontinuous	water	tetradecane primary alkyl halides 2-cyclohexen-1-one	CTAB SDS Co: 1-pentanol	Eletrochemical catalysis	**(Gao *et al.*, 1996)**

2.2.2 Organic reactions in microfluidic devices

A wide range of chemical transformations between reagents in two immiscible phases have been performed in microfluidic devices. From simple hydrolysis to carbon-carbon bond formation, much attention has been given to the benefits that performing reactions in these devices can offer. To that end, and to complement the previous section on emulsion based reactions, a brief selection of interesting examples is given below.

The use of microfluidic devices to perform reactions was perhaps first demonstrated in the simple isomerisation of allylic alcohols to carbonyls, Scheme 2.6. The use of the microfluidic mixing device in this case was beneficial as the small volumes enabled a rapid screening of reaction variables (de Bellefon *et al.*, 2000).

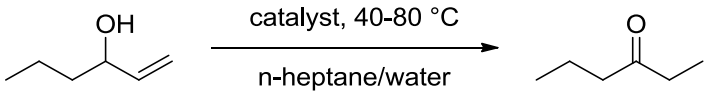

Scheme 2.6 - Isomerisation of 1-hexene-3-ol to 3-hexanone performed in an n*-heptane – water biphase*

Highly fluorinated phases have also been used in combination with organics to form the two immiscible phases. Carbon-carbon bond formation through the Mukaiyama aldol reaction was performed on silyl enol ethers and aldehydes (Scheme 2.7) under such conditions, confining a Lewis acid lanthanide catalyst to the fluorous phase, facilitating separation (Mikami *et al.*, 2003).

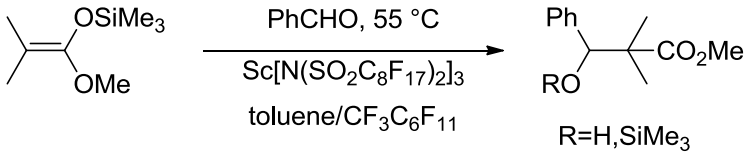

Scheme 2.7– Aldol condensation of silyl enol ether and benzaldehyde in a flourous-toluene biphase

Using the same catalyst under similar conditions, with very low catalyst loadings, resulted in the regioselective Baeyer-Villiger oxidation of *ortho*-substituted cyclohexanones to lactones, Scheme 2.8 (Mikami *et al.*, 2004).

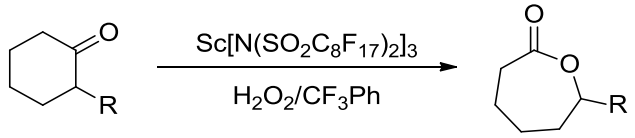

Scheme 2.8 – Baeyer Villiger oxidation of ortho-substituted cyclohexanones in an aqueous-flourous biphase

The dehydration of various carbohydrates to furfural derivatives (Scheme 2.9) was performed in an aqueous-halogenated solvent biphase with high conversions seen over the minute long timescales.

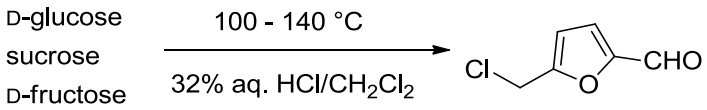

Scheme 2.9 - Dehydration of carbohydrates in an aqueous-halogenated solvent biphasic system

In the two examples above, the scandium based catalysts were complexed to highly fluorinated ligands. Thus, these would partition into the halogenated solvent phase. The addition of separate phase transfer catalysts (PTCs) can have a similar effect for systems where no, or very limited, interphase solubility make reactions prohibitively slow (Starks, 1971). In recent years, the use of PTCs their use in microfluidic based biphasic reactions has received increasing interest. For much more extensive reviews into the area of microfluidic organic reactions see Ahmed-Omer *et al.* (2007), Haswell *et al.* (2001) and Mason *et al.* (2007) including those performed in two phases (Wirth, 2013)

2.2.3 Organic reactions using membrane emulsification

There are two primary modes of operation when attempting to perform chemical reactions in membranes. Enhancements through product separation, or by reactant distribution can be achieved depending on the system under investigation (Li, 2007). The majority of the literature to be found on the reactive dispersion of reactants using membrane is towards particle formation, both polymeric (Rao and Geckeler, 2011, Yanagishita *et al.*, 2009) and inorganic (Supsakulchai *et al.*, 2003, Kakazu *et al.*, 2010). The formation of particles provide a useful guide for the membrane pore size – particle size distribution relationships, due to ease of particle size measurements and allow for interesting separation challenges.

Very few reported studies, are focused on the use of membranes as dispersion methods in liquid-liquid biphasic reaction systems. The most relevant of these combined the investigations of the parameters of membrane emulsification with chemical reaction in the lipase hydrolysis of olive oil (Shiomori *et al.*, 1995). Interestingly their findings suggest an inverse relationship between rate of hydrolysis and surface area. The reason for this, it was suggested, was due a decrease in the interface adsorbed lipase at higher surface areas, i.e. smaller droplets.

The combination of emulsification and reaction using membranes for liquid-liquid systems clearly presents an area requiring further investigation, since, as has been shown in the review of the reactions in emulsions, an increase in interface area can influence the rate of reaction.

2.2.4 Biphasic oxidations

Of the broad range of chemical reaction types covered up to now, oxidative reactions remain the most critical to this research. As such, this section is dedicated to the discussion of these

important reactions conducted in biphasic systems, with the green oxidant, hydrogen peroxide.

The oxidation of organic molecules is a fundamental transformation in a wide range of industrial chemical process (Hudlicky, 1990, Sheldon and Kochi, 1981), including in the formation of value-added intermediates (Sheldon, 1991). However, there is a need to move away from traditional mechanisms for oxidation, which often involve toxic metals (Hill, 1999), or require the use of stoichiometric levels of oxidant such as chromate/sulfuric acid, chromium oxides, permanganates and periodates, which may necessitate complex heat management and produce by-products that are harmful to the environment (Hudlicky, 1990). Increasingly, research is tending towards cleaner selective processes using more benign oxidants such as oxygen from air (Biella and Rossi, 2003, Torrente-Murciano *et al.*, 2013), oxygen (Enache *et al.*, 2006) or hydrogen peroxide (McMorn *et al.*, 1999). Hydrogen peroxide is favourable as a green oxidant (Arends and Sheldon, 2002) as well as an oxidant precursor with a high oxygen content and a singular benign by-product: water.

Many tungsten-based catalytic systems have been reported to be active for the oxidation reaction with aqueous hydrogen peroxide solutions (Ishii *et al.*, 1988, Sato *et al.*, 1997). Any potential mass transfer limitation in the biphasic systems studied were assumed to be easily overcome in the presence of phase transfer agents, as demonstrated in the oxidation (including epoxidation) of alkenes shown in Scheme 2.10.

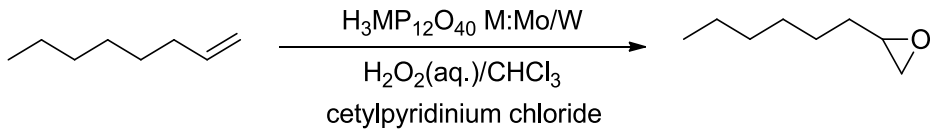

Scheme 2.10 – Heteropoly acid epoxidation of 1-octene under biphasic conditions using a phase transfer catalyst

Much work has been done to investigate and improve on the peroxometallate (POM) structures which are widely reported to be effective oxidation catalysts (Dickman and Pope, 1994, Pope, 1983, Pope and Müller, 2001, Kozhevnikov, 2002). A noteworthy advance in the area combines readily available self-assembling POMs with phosphazenes to provide catalysts for the oxidative desulphurisation (Scheme 2.11) and olefin oxidation (Scheme 2.12) (Craven *et al.*, 2013). The catalyst was reported to self-assemble *in-situ* so that the POM and the phosphazene could be added to the reaction vessel separately, removing the need for additional catalyst pre-synthesis.

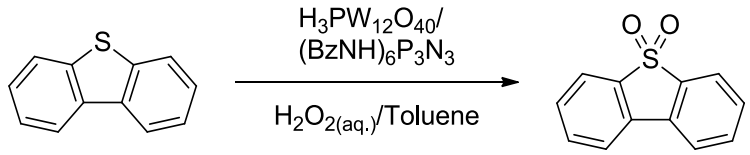

Scheme 2.11 – Heteropoly acid oxidative disulphurisation of dibenzothiophene under biphasic conditions

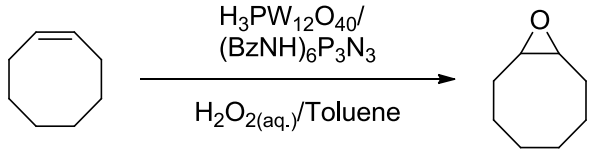

Scheme 2.12 – Heteropoly acid epoxidation of cyclooctene under biphasic conditions

A number of these agents have been used as counterions to the active catalyst species, such as the tertiary ammonium salt in the epoxidation of 3-carene as shown by Nardello *et al.* (2006).

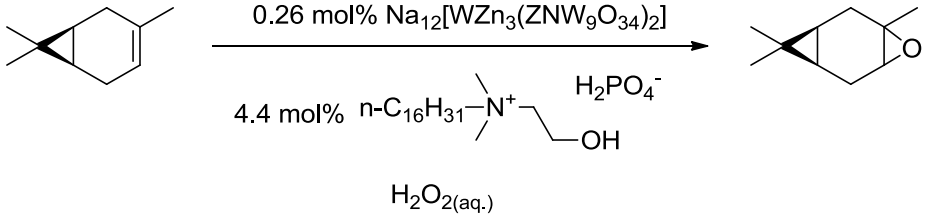

Scheme 2.13 - The hydrogen peroxide epoxidation of 3-carene with a tungsten based catalyst and tertiary ammonium phase transfer catalyst

These phase transfer agents have also been complexed directly to the active metal to create a single catalytic species (Li *et al.*, 2007, Zhu *et al.*, 2008) to ease the transfer between both organic and aqueous phases (Scheme 2.14).

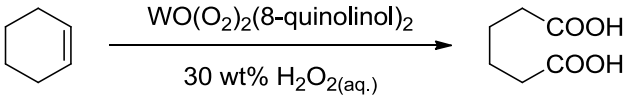

Scheme 2.14 – The synthesis of adipic acid from cyclohexene with an amphiphilic tungsten catalyst and aqueous hydrogen peroxide (Li et al., 2007)

Important progress in this area was achieved by with the development of a combined system of a simple salt, sodium tungstate and a halide-free phase-transfer agent (methyltrioctylammonium hydrogensulfate) which showed high activity towards alcohol and alkene oxidations without the need of organic solvents, or ligands (Noyori *et al.*, 2003). It was this system, applied to the oxidation of cyclohexene through to adipic acid which highlighted (of which the above work by Li *et al.* was presumably based) the possibility of the integration of reaction along with product separation. In this particular case the product

was a solid, allowing for simple filtration, and reuse of the aqueous phase catalyst solution, shown in Figure 2.13.

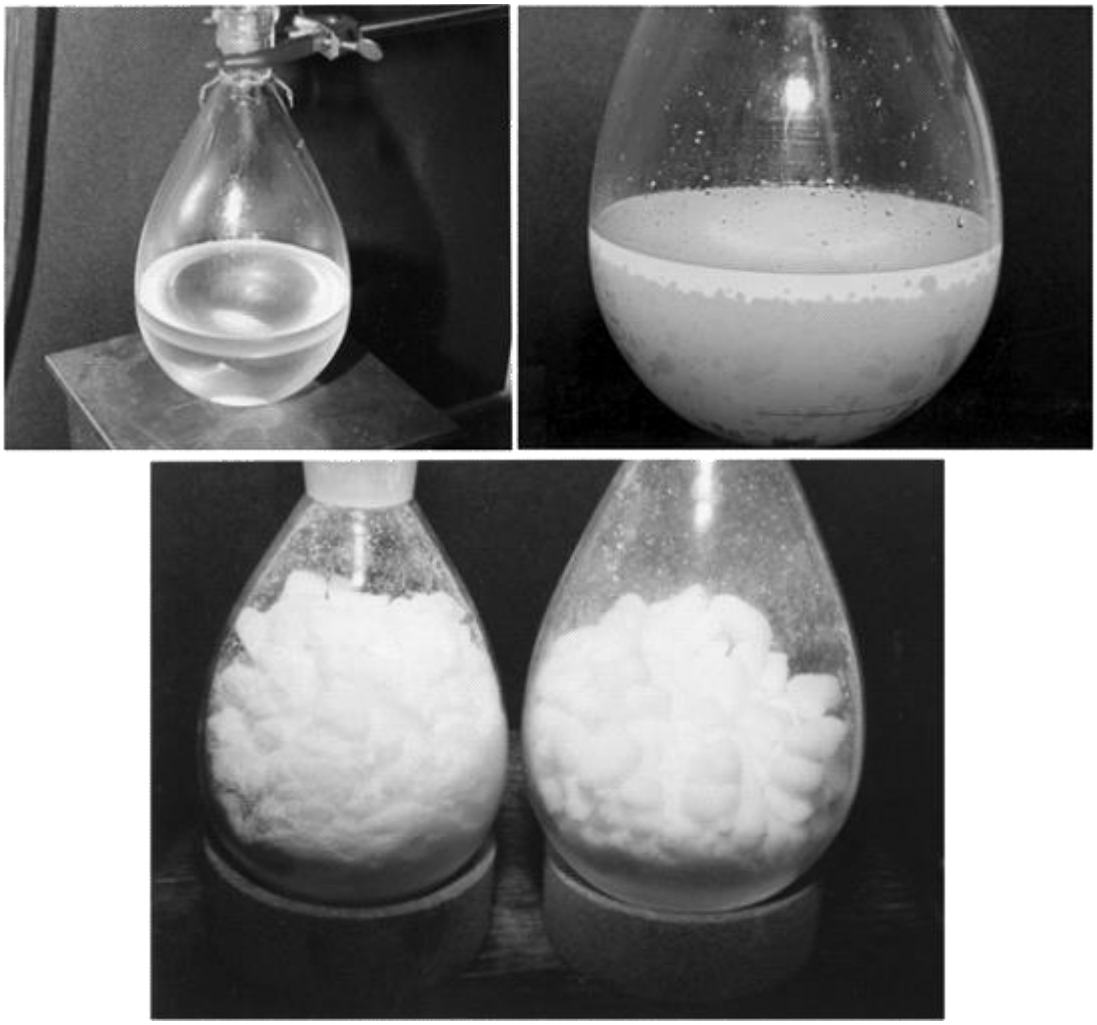

Figure 2.13 – The one pot synthesis of adipic acid. From top left clockwise: starting biphasic reaction mixture with cyclohexene as top phase, post reaction showing precipitated product, filtered and dried product with initial (left) and repeated (right) use of recycled catalyst solution (Noyori et al.*, 2003).*

Whilst the adipic acid synthesis is indeed an elegant, environmentally sound alternative to the previously reported nitric acid based methods, the production of a solid product identifies an important challenge if one wishes to adapt this problem from batch to continuous processing.

The use of POM catalysts have been applied successfully to biphasic primary and secondary alcohol oxidations to the corresponding acids and ketones respectively (Sloboda-Rozner *et al.*, 2003). Interestingly the use of a control reaction containing the oxidant, hydrogen peroxide and sodium tungstate (as an ingredient for the POM formation) yielded less than 1% conversion, in contrast to the observations by Sato who has shown this simple salt to be

effective when combined with a quaternary ammonium phase transfer catalyst (Sato *et al.*, 1999).

The same group as above expanded the scope of this catalytic oxidation system, investigating diols, pyridine derivatives, amines and aniline derivatives (Sloboda-Rozner *et al.*, 2004). In summary; carbon-carbon bond scission was observed with the diol oxidation, the pyridine derivatives were oxidised to the *N*-oxides, amines to the oximes (although significant hydrolysis was observed post reaction) and the aniline derivatives to the azoxy or nitro compounds. This study also addressed the issue of hydrogen peroxide decomposition and concluded that the rate of unproductive decomposition was inversely proportional to the activity of the metal selected for catalyst included in the POM. However this is somewhat unsurprising given that a mere 5 fold excess of hydrogen peroxide was present in the experiments thus competition for the oxidant could easily rate limit the reactions.

All of the reactions above have been liquid-liquid biphasic systems with the catalyst species homogeneous. The use of POMs in a heterogeneous fashion has also been investigated under the reasoning of aiding catalyst reuse and recycle (Vasylyev and Neumann, 2003). The use of tripodal polyammonium salts in combination with a tungsten based POM (Scheme 2.15) produced a mesoporous material which showed sustained catalytic activity over 5 cycles with no loss in activity or observed change in structure, pore size or BET surface area.

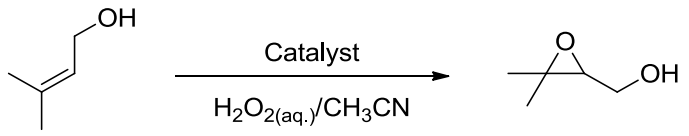

Catalyst: $[ZnWZn_2(H_2O)_2(ZnW_9O_{34})_2]^{12-}$
+ tris[2-(trimethylammonium)ethyl]-1,3,5-benzenetricarboxylate/
1,3,5-tris[4-(N,N,N-trimethylammoniumethylcarboxyl)phenyl]benzene

Scheme 2.15 – The oxidation of primary allylic alcohols, showing preferential selectivity towards the epoxide.

2.3 Kinetic analysis of biphasic systems

With regards to approaching a biphasic reaction optimisation in holistic way authors report the virtues of these systems without significant consideration of mass transfer concerns. However, if one hopes to understand a reaction and decide how best to provide an engineered solution which will maximise the overall desired outcome, be it conversion, yield, selectivity etc., then the influence of each process involved must be determined.

The processes or steps involved can be broadly classified into two main categories.

1. Firstly there are the steps which describe the movement of molecular or ionic species though the reaction space in order to undergo collision.
2. Secondly the steps which describe the chemical interaction, or reaction of the colliding molecules.

Since both of these steps occur simultaneously, it stands to reason that the step which proceeds the slowest will determine the overall observed rate.

It is worth noting that understanding all of these steps is important when, for example, dealing with a complex reaction system with potential side products. A balance between reaction conditions, phase concentrations and product distributions can impact on metrics such as selectivity and yield.

Of course, temperature and concentration changes will affect both of these processes, but the relative values of the rate coefficients for each of the processes enables identification of where the rate limitation lies. In this section the concept of these two classes of coefficients and more importantly, the theory behind determining their importance for liquid-liquid reaction systems is summarised to inform on later discussion.

2.3.1 Reaction rate coefficient

The rate of reaction can often be expressed as a function of temperature and concentration, assuming constant pressure. For example a first order elementary reaction,

$$\begin{aligned} r_i &= f_1(T)\, f_2(C_i) \\ &= k_r\, f_2(C_i) \end{aligned} \qquad 2.23$$

The temperature dependent term is known to practically be represented by the Arrhenius law,

$$k_r = Ae^{-E_a/RT} \qquad 2.24$$

Where A, is a preexponential factor, E_a, is the activation energy, R, is the universal gas constant and T is temperature.

The Arrhenius law tells us that in order to expedite a reaction, with a single mechanism, one can increase temperature. Obviously alteration of the activation energy, for example through use of a catalyst will result in a change in rate but this may have connotations for the mechanism of reaction.

2.3.2 Mass transfer coefficient

According to the classical definition, the rate of transfer of a species across an interface is dependent on both concentration and interface area.

According to Fickian diffusion,

$$Flux = J = \left(\frac{1}{A}\right)\left(\frac{dn_i}{dt}\right) \tag{2.25}$$

Where A is the interface area, over which a number of moles, n, of species i is diffusing over a time t.

In the simplistic situation, that of diffusion across a thin film of thickness l, Equation 2.26 can be re written in terms of concentration,

$$\begin{aligned} J &= -D_i \frac{dc_i}{dx} \\ J &= \frac{D_i}{l}\left(C_{i,1} - C_{i,2}\right) \end{aligned} \tag{2.26}$$

Where D_i is defined as the diffusivity of i across the interface, due to the concentration gradient between points 1 and 2, perpendicular to the plane of an interface

In order to calculate a value for the flux from Equation 2.26 one must know the thickness of the film l. Often this cannot practically be measured, therefore an engineering concept is introduced, the mass transfer coefficient. The mass transfer coefficient can effectively be viewed as the constant of proportionality between the flux and the concentration gradient,

$$\begin{aligned} &Flux \propto concentration\ gradient \\ &J = k_c\left(C_{i,1} - C_{i,2}\right) \end{aligned} \tag{2.27}$$

Where k_c is the mass transfer coefficient based on concentration. Equating Equation 2.26 and Equation 2.27 above we can see that in this case the mass transfer coefficient is equivalent to the diffusivity divided by the film thickness,

$$k_c = \frac{D_i}{l} = \frac{J}{\left(C_{i,1} - C_{i,2}\right)} \tag{2.28}$$

In the case above, the mass transfer coefficient adequately describes the system. For more complex situations, many correlations have been drawn between mass transfer coefficient and parameters relevant to the system at hand.

Often one wishes to calculate absolute quantities of material transferred, a rate of mass transfer, in which case the absolute interface area becomes important. Equation 2.28 can be expanded to remove the area integrated into the flux,

$$rate\ of\ \ mass\ transfer = r_{mass\ transfer} = k_c A\left(C_{i,1} - C_{i,2}\right) \tag{2.29}$$

As mentioned before, the mass transfer coefficient can often be calculated utilising variables inherent to the system under investigation. These relationships take the form of correlations using dimensionless numbers which describe the system parameters. An example of these relationships utilise an analogy which relates heat transfer theory with mass transfer. For the convective heat transfer around a sphere, the heat transfer coefficient can be found from the Nusselt number according to a dimensionless number relationship (Equation 2.30).

$$\mathrm{Nu} = 2 + 0.6\,\mathrm{Re}^{1/2}\,\mathrm{Pr}^{1/3} \begin{cases} \mathrm{Nu} = \dfrac{h d_d}{k_t} \\ \mathrm{Re} = \dfrac{u d_d}{\nu} \\ \mathrm{Pr} = \dfrac{\nu}{k_t} \end{cases} \tag{2.30}$$

Where h is the heat transfer coefficient, d_d is the particle diameter, k_t and ν are the thermal conductivity and kinematic viscosity of the surrounding fluid respectively and u is the surrounding fluid velocity.

The heat transfer/mass transfer analogy states that the relationship (Equation 2.31) holds when the heat transfers terms, namely the heat transfer coefficient and the thermal conductivity are substituted for their mass transfer analogs and hence corresponding dimensionless numbers.

$$h \rightarrow k_c$$
$$k_t \rightarrow D_{AB}$$

$$\mathrm{Sh} = 2 + 0.6\,\mathrm{Re}^{1/2}\,\mathrm{Sc}^{1/3} \begin{cases} \mathrm{Sh} = \dfrac{k_c d_d}{D_{AB}} \\ \mathrm{Re} = \dfrac{u d_d}{\nu} \\ \mathrm{Sc} = \dfrac{\nu}{D_{AB}} \end{cases} \tag{2.31}$$

Where D_{AB} is the diffusivity of A and B through the surrounding fluid.

Rearrangement of the above yields a relationship for the mass transfer coefficient (Equation 2.32) in relation to system parameters, the Frössling correlation.

$$k_c = 0.6\overbrace{\left(\frac{D_{AB}^{2/3}}{\nu^{1/6}}\right)}^{f(T,P)}\left(\frac{u^{1/2}}{d_d^{1/2}}\right) \qquad 2.32$$

The diffusivity and viscosity grouped together in the first term are functions of temperature and pressure for a specific fluid. The second term states that the rate of mass transfer and hence rate of observed reaction is fundamentally linked to the particle size within a mass transfer limited system.

The above is used to describe the mass transfer to and from the surface of a solid sphere. Similar correlations are also known for a range of systems. Relevant correlations for liquid-liquid systems are given in

Table 2.8. Owing to the difficulty in measuring particle diameters in stirred tanks, the use of correlations which relate the accessible stirring parameters such as stirring length and power per volume can be used instead. The relationship between mass transfer coefficient and the droplet diameter can be seen in Equations 2.34 and 2.35, similar to the Frössling correlation in Equation 2.32.

Table 2.8 – A selection of mass transfer correlations for fluid-fluid systems

Physical Situation	**Basic Equation**	**Key variables**	**Equation no.**
Drops in stirred solutions	$\frac{k_c L}{D_{AB}} = 0.13\left(\frac{L^4(P/V)}{\rho\nu^3}\right)^{1/4}\left(\frac{\nu}{D_{AB}}\right)^{1/3}$	L = stirrer length P/V = power per volume	2.33
Large (~0.3 cm) drops in unstirred solutions	$\frac{k_c d_d}{D_{AB}} = 0.42\left(\frac{d_d^3\Delta\rho g}{\rho\nu^2}\right)^{1/3}\left(\frac{\nu}{D_{AB}}\right)^{1/2}$	d_d = droplet diameter $\Delta\rho$ = density difference between droplet and surrounding fluid	2.34
Small drops in unstirred solutions	$\frac{k_c d_d}{D_{AB}} = 1.13\left(\frac{d_d u}{D_{AB}}\right)^{0.8}$	d_d = droplet diameter u = droplet velocity	2.35

Additional theory relating to mass transfer and correlations for the calculation of its coefficient will be covered in more detail in the following section.

2.3.3 The relationship between rate of reaction and mass transfer

In order to illustrate the relationship between the observed rate of reaction, rate of reaction and rate of mass transfer, consider a reaction occurring on the surface of a particle, for example the isomerisation of a single reactant into a single product (Figure 2.14)

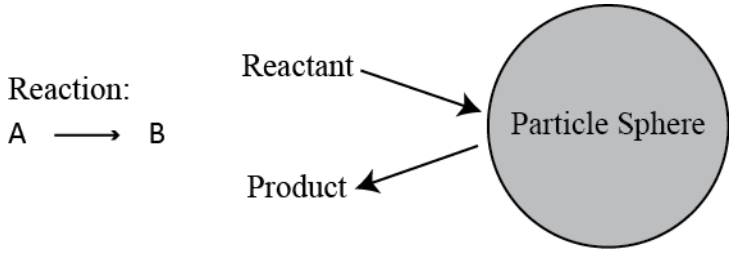

Figure 2.14 - The surface reaction on a particle sphere

In the situation above two phenomena are occurring, firstly the chemical reaction of A isomerising to B and secondly the diffusion of A to and of B from the particle surface. In order to describe the rate of these two phenomena the mass transfer and reaction rate coefficients can be used. Using the information defined for the system above we can write the rate equation (Equation 2.36) for the loss of A at the surface of the particle sphere.

$$-r_{A,\text{surface}} = \frac{k_c k_r}{k_c + k_r} C_A \qquad 2.36$$

For a slow rate of reaction, such that $k_r << k_c$ the rate equation above can be simplified such that we see the observed rate is independent of mass transfer (Equation 2.37).

$$-r_{A,\text{surface}} = \frac{k_c k_r}{k_c + k_r} C_A \cong \frac{k_c k_r}{k_c} C_A = k_r C_A \qquad 2.37$$

Conversely, if the rate of reaction is extremely fast, such that $k_r >> k_c$ then the observed rate is independent of the rate of chemical reaction (Equation 2.38).

$$-r_{A,\text{surface}} = \frac{k_c k_r}{k_c + k_r} C_A \cong \frac{k_c k_r}{k_r} C_A = k_c C_A \qquad 2.38$$

It is evident that the observed rate dependence is really a balance between both mass transfer and reaction rate coefficients. The preceding section introduced various mass transfer

correlations, therefore continuing with the example involving reaction on a particle sphere, the mass transfer coefficient is dependent on the particle size, as shown in

Table 2.8. Therefore, it stands to reason that a particle size will exist where the mass transfer rate is so fast that it can no longer be assumed to be rate limiting i.e the system changes from a mass transfer to reaction limited regime (from Equation 2.38 to Equation 2.37), illustrated in Figure 2.15.

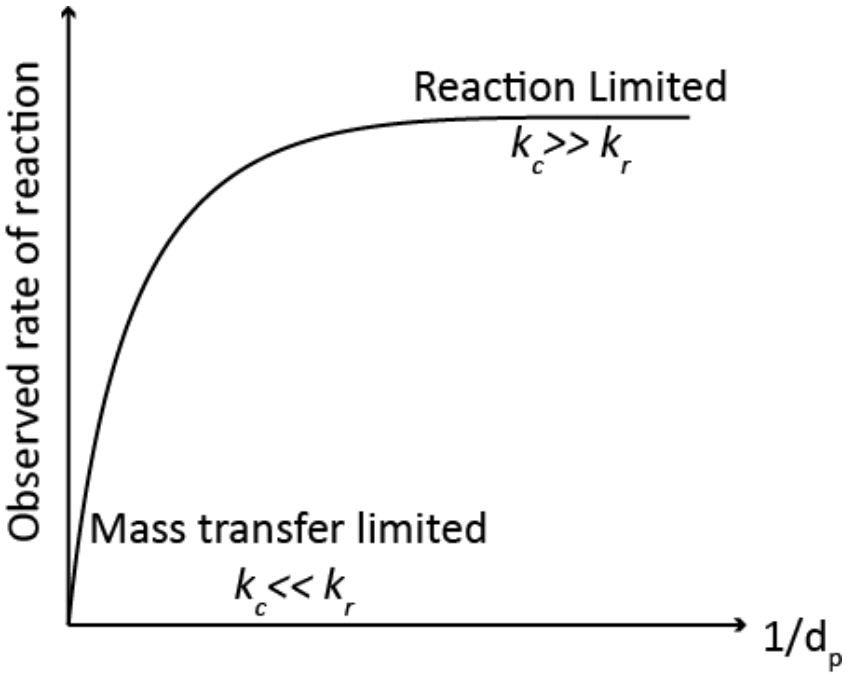

Figure 2.15 - The relationship between particle size and observed reaction rate

Observed changes in reaction rate through a change in mass transfer parameters can indicate where the system is currently limited. In other words it could help suggest where the process should be optimised; towards an increase in mass transfer rate, such as increase area or towards an increase in reaction rate, such as catalyst development.

What is interesting to note about most of the reactions reviewed above is that very few are specifically concerned with quantification of the interface area; indeed few consider the aspects of mass transfer limitation. The aspect of product separation is not specifically dealt with in many cases, and where it was, it was not reported as a main focus of the investigation. Many of the biphasic systems listed indeed use cosolvents to dissolve one of the phases, effectively negating the benefits of low energy separation.

It is clear from reviewing the literature that there is a need to approach liquid-liquid biphasic reaction optimisation and adaptation to a continuous processing method in a holistic way.

As well as reaction specific concerns, the following general challenges need to be addressed:

- Understanding the rate limiting step of the reaction systems, primarily identifying if mass transfer limited
- Careful selection of reagents, utilising neat, liquid components where possible
- Consideration of the downstream separation and work–up for applicability to continuous processing
- Careful consideration of the oxidant decomposition when using hydrogen peroxide

The above could effectively be seen as describing a whole product development route, however, and the reason the above not number listed is that these challenges need to be addressed straight from the bench and not sequentially. In order to address the challenge of liquid-liquid biphasic reaction optimisation one of the primary steps is to determine the surface area sufficient to negate mass transfer limitation.

The techniques reviewed here of high shear homogenisation, microfluidics and membrane based droplet creation offer potential to obtain a wide range of discrete droplet sizes and interface areas. Therefore their application to the oil and aqueous phases under investigation need to be specifically addressed.

The use of such media to perform liquid-liquid biphasic reactions without solvent or phase transfer catalyst offers potential which has not been addressed in many of the reported cases. The applicability to larger scale operation in each of these reported reactions is subject to the requirement of large amounts of complex catalyst, co-solvent or phase transfer aids, a potential barrier to progress. A process without these potential barriers will therefore simplify the forward steps in development.

Finally, a system which allows for the continuous biphasic oxidations with hydrogen peroxide has not been demonstrated which incorporates catalyst recycle, an area which can be exploited to show increased relevance to downstream separation of product and catalyst streams.

3 Experimental Procedures

The general methods and characterisation techniques for the experimental results are outlined in this chapter. The sections given within this chapter roughly follow the order of the result chapters which follow, however general methods which relate to more than one section are combined for conciseness.

The design, construction and operation methods of the continuously operated reactor systems are discussed in Chapter 6.

3.1 Surfactant choice

The selection of an appropriate surfactant for use with sunflower seed oil / water system was qualitatively investigated through the initial formulation of a series of emulsions. The choice of surfactants with regards to appropriateness for use in a reaction system are outlined at the start of Chapter 4. Confining the choice to non-ionic surfactants (to avoid electrostatic interactions) a shortlist of surfactants was investigated at difference weight percentage loadings in an 80:20 aqueous:oil emulsion. The hydrophile lipophile balance (HLB) number required for sunflower seed oil is 7, with that of the surfactant. The emulsions were created using an Ultra Turrax T10 homogeniser at 10750 for 5 minutes. The ability to solubilise all of the oil phase was observed visually upon standing 30 minutes after emulsification, as

listed in Table 3.1. From the table below Brij-S10 was the only surfactant tested which produced a persistent solubilised oil phase at the low surfactant loadings therefore this was the surfactant selected to perform additional formulation investigations. Contrary to what was be expected when comparing the HLB values for the surfactants tested and that required by the sunflower oil, the most equally matched in number did not result in the best option in this case. It can be surmised that the long C18 tail on the Brij-S10 enabled greater compatibility with the carbon chains of the triglyceride in the sunflower oil of a similar length.

Table 3.1 – Initial non-ionic surfactant screen

Surfactant	**Hydrophile lipophile balance (HLB)**	**Oil solubilised at 10 wt% surfactant?**	**Oil solubilised at 1 wt% surfactant?**
Pluronic F-68	24	No	No
Tween-20	16	Yes	No
Tween-80	15	Yes	No
Brij-S10	12	Yes	Yes
Span 20	8.6	No	No

3.1.1 Free fatty acid determination

The free-fatty acid content of the sunflower oil was determined through used of alkaline titration of an average of test samples of the oil using phenolphthalein as indicator(Method according to British Standard BS EN ISO 660:2009). From a series of three titrations the average acid number was 0.32, corresponding to a free fatty acid content of 0.17 wt% in the oil. This value (5.5 mM based on oleic acid as the only fatty acid present in pure oil) would have resulted in a concentration of 0.55 mM for a 10 wt% oil emulsion. This is below the critical micelle concentration reported for oleic acid (0.7-3.5 mM) (Murakami *et al.*, 1986) and significantly below the amount of surfactant shown to be effective to emulsify the oil in the preliminary studies (Table 3.1) therefore this was not taken into account. In addition the presence of phospholipids was not considered.

3.2 Emulsion formulation

Of the conventional methods for emulsification, high shear homogenisation was chosen. This was because of the ease with which the operation can be conducted on small volumes, ideal for a screening experiment such as this. A preliminary study investigating low energy methods, such as the phase inversion technique, or spontaneous microemulsification, indicated that these methods did not produce a reliable, reproducible droplet sizes.

Assuming one has a single, set geometry dispersion unit, the remaining variable is the energy input to a system. Practically this is defined as a function of the power input, controlled by the stirring speed of the homogeniser, and time of operation. The range of homogenisation speeds tested was from 8000 to 13500 rpm, the practical operating limits of the machine. A time period between 1 and 10 minutes was investigated. Mixing times shorter than 1 minute resulted in incomplete dispersion of the oil. At mixing times longer than 10 minutes, no change in oil droplet size, and hence interface area, was seen, as confirmed by laser scattering based particle sizing.

Preliminary investigations showed that the phase volumes of the aqueous phase, oil and surfactant were important in the formation of an emulsion. Of primary interest were O/W emulsions and as such an aqueous phase volume above 60% was used, up to 90%. As discussed in the formulation literature, a majority of aqueous phase does not necessarily determine the type of emulsion (i.e. O/W, W/O), however, in this case, the assumption that a high aqueous phase volume would result in Oil-in-Water emulsions was confirmed to be correct.

The amount of surfactant with respect to oil was the final variable. A preliminary experimental design study confirmed that above 1 % v/v surfactant in oil was required for an emulsion which did not degrade due to oil droplet coalescence. A surfactant level at 0.5 % was insufficient to emulsify the volumes of oil, particularly when the formulation was created at low homogeniser operating speeds and/or short time scales

To summarise, the input variables for the design were:

- homogenisation speed,
- homogenisation duration,
- aqueous phase volume, and
- surfactant:oil ratio.

The outputs were specific surface area (SSA) and the surface area averaged diameter, the D[3,2] or Sauter diameter, used as it gives a useful metric for spherically dispersed liquid droplets.

3.2.1 Design parameters

Since there were relatively few variables, a Resolution V full factorial design was used. This is known as an interaction design and is often used when there is a high likelihood of cross variable interaction. This design enabled the investigation of all the main variables as well as all two way interactions present in the data. Since it was a full design, none of the factors were confounded, i.e. the outputs reflected the true relationships with the input variables.

The design takes the highest and lowest values of the continuous variable ranges, in other words, for each variable two states can exist: high or low. Therefore the number of experiments required to investigate the relationship between the high and the low states of one variable with the high and low states of each of the other variables, is exponentially related to the number of variables.

$$no.\,of\ \ experiments = 2^n \tag{3.1}$$

where *n* is the number of variables.

Therefore the number of experiments for the design was,

$$no.\,of\ \ experiments = 2^4 = 16 \tag{3.2}$$

In addition to this, and to provide robustness and repeatability data for the design, three more identical experiments are added at the mid points of the variable ranges. This brings the total number of experiments to 19. The low, mid and high values for the variables are summarised in Table 3.2.

Table 3.2 - Summary of the DoE design variable ranges

Variable	Low	Mid	High	units
Homogenisation Speed	8000	10750	13500	rpm
Homogenisation Time	1	5.5	10	min
Aqueous phase volume	60	70	80	% (of total volume)
Surfactant: oil	1	5.25	10	% (of oil volume)

The design of experiments investigation into the droplet size using high shear homogenisation utilised an IKA Ultra Turrax T10 homogeniser. The emulsions were created through addition of the required components, given in Table 3.3 and homogenised for the duration at the given speed. The total emulsion volume created was 60 mL.

Table 3.3 - DoE emulsion formulation compositions

Variables						Water	Brij-S10		Oil	
Exp Name	**Surfactant / % oil volume**	**Phase Vol. aqueous phase / % total volume**	**Homogenisation time / min**	**Homogenisation speed / rpm**	**Total Vol. / mL**	**Vol. / mL**	**Vol. / mL**	**Mass / g**	**Vol. / mL**	**Mass / g**
N1	1	60	1	8000	60.00	36.00	0.24	0.23	23.76	21.81
N17	5.25	70	6	10750	60.00	42.00	0.90	0.87	17.10	15.70
N16	10	80	10	13500	60.00	48.00	1.09	1.05	10.91	10.01
N6	10	60	10	8000	60.00	36.00	2.18	2.10	21.82	20.03
N4	10	80	1	8000	60.00	48.00	1.09	1.05	10.91	10.01
N8	10	80	10	8000	60.00	48.00	1.09	1.05	10.91	10.01
N3	1	80	1	8000	60.00	48.00	0.12	0.11	11.88	10.91
N7	1	80	10	8000	60.00	48.00	0.12	0.11	11.88	10.91
N2	10	60	1	8000	60.00	36.00	2.18	2.10	21.82	20.03
N5	1	60	10	8000	60.00	36.00	0.24	0.23	23.76	21.81
N19	5.25	70	6	10750	60.00	42.00	0.90	0.87	17.10	15.70
N12	10	80	1	13500	60.00	48.00	1.09	1.05	10.91	10.01
N11	1	80	1	13500	60.00	48.00	0.12	0.11	11.88	10.91
N15	1	80	10	13500	60.00	48.00	0.12	0.11	11.88	10.91
N10	10	60	1	13500	60.00	36.00	2.18	2.10	21.82	20.03
N18	5.25	70	6	10750	60.00	42.00	0.90	0.87	17.10	15.70
N14	10	60	10	13500	60.00	36.00	2.18	2.10	21.82	20.03
N9	1	60	1	13500	60.00	36.00	0.24	0.23	23.76	21.81
N13	1	60	10	13500	60.00	36.00	0.24	0.23	23.76	21.81

3.3 Microfluidic chip formulation

The formulations were created using a 100 μm hydrophilic glass droplet generation chip purchased from Dolomite Microfluidics. The fittings, fixtures and housing for the chip were also purchased from them and made of PEEK, perfluoroelastomer and stainless steel 316. The tubing used was 1/16" O.D. and made from PTFE, supplied by either Dolomite Microfluidics or Cole Parmer.

The fluids were delivered via 10 mL glass and PTFE syringes utilising luer lock connectors to connect to the PTFE tubing. These were mounted on Fusion-100 syringe pumps obtained from KR Analytical Ltd.

The oil phase contained the 1 wt% Brij S10 supplied by Sigma-Aldrich Co. LLC. The aqueous phase was ultrapure water.

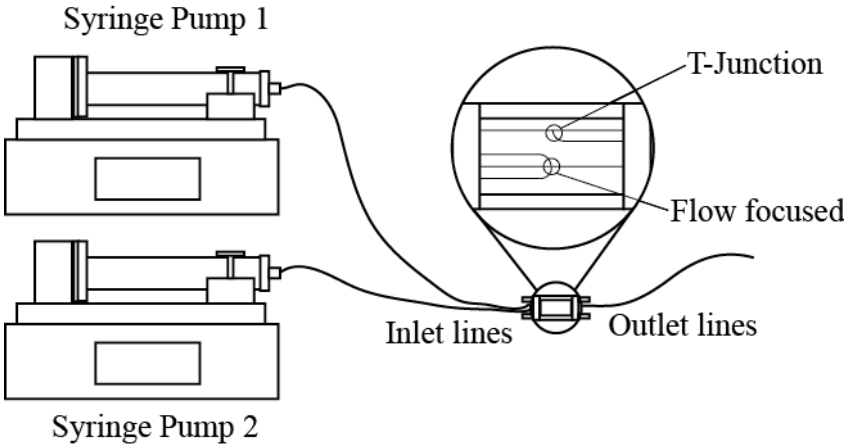

Figure 3.1 – Microfluidic droplet generation apparatus. The T-junction and flow focused channels were on the same chip. As shown, the T-junction flows right to left and the flow focused flows left to right.

In order to form the dispersions the inlets and outlets were connected to the droplet chip, as shown in Figure 3.1. The chip contained both the T-junction and flow focused channels, each requiring different inlet and outlet configurations. The T-junction had one inlet for each the dispersed and continuous phase, whilst the flow focused has to continuous phase inlets and one central dispersed phase inlet. There was one outlet for each geometry. To create the droplets, the filled syringes containing the continuous and dispersed phases were connected to the flow lines which were secured into the droplet chip holder. The outlet line was attached to the other side of the chip holder. The required flow rate was set on the syringe pumps and these were then activated. For the T-Junction and flow focused geometry, the flow rates used in the experiments are given in Table 3.4 and Table 3.3 respectively. The droplets were collected at the outlet. Any air present in the system as a result of assembly was purged.

Table 3.4 - T-Junction geometry formulation flow rates

Surfactant wt% oil phase	**Aqueous phase flow rate (Q_c) / µL.min^{-1}**	**Dispersed phase flow rate (Q_d) / µL.min^{-1}**
1% Brij-S10	10	10
1% Brij-S10	50	10
1% Brij-S10	100	10

1% Brij-S10	200	10

Table 3.5 - Flow focused geometry formulation flow rates

Surfactant wt% oil phase	**Aqueous phase flow rate (Q_c) / µL.min^{-1}**	**Dispersed phase flow rate (Q_d) / µL.min^{-1}**
1% Brij-S10	10	1
1% Brij-S10	50	1
1% Brij-S10	100	1
1% Brij-S10	100	10
1% Brij-S10	200	10

Following the experiments, the tubing, syringes are chip were purged of reagents by flushing with warm soapy water, followed by multiple washes with ultrapure water. An additional wash with acetone was also performed when required. Finally air was pushed through the system to dry and prevent blockage.

3.4 Capillary reactor formulation

The reactor was made from 1mm I.D. borosilicate glass capillary tubing, joined and bent by the in house glass blower at the University of Bath. The tubing used was 1/16" O.D. and made from PTFE, supplied by either Dolomite Microfluidics or Cole Parmer. The reactor was interfaced to the rigid tubing by use of PTFE fittings and 1/4" 28-UNF threaded glass capillary sections supplied by Kinesis Ltd. These threaded sections were appended to the inlets and outlets of the reactor by the in-house glass blower. The chemicals used were the same as those used for the emulsion reactions.

The fluids were delivered via 10 mL glass and PTFE syringes utilising luer lock connectors to connect to the PTFE tubing. These were mounted on Fusion-100 syringe pumps obtained from KR Analytical Ltd.

The oil phase contained the 1 wt% Brij S10 supplied by Sigma-Aldrich Co. LLC. The aqueous phase was ultrapure water.

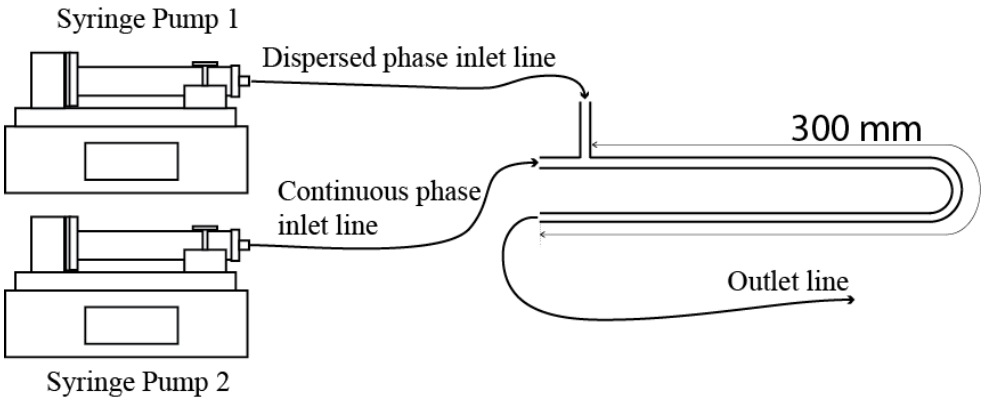

Figure 3.2 – Capillary plug generation apparatus. The dispersed and continuous phase flow lines are connected as shown, there is one outlet line.

To create the plugs the tubing was connected to the filled syringes mounted on the pumps, as shown in Figure 3.2. The required flow rates used in the experiments are given in Table 3.6. These were simply set and the pumps activated to form the plugs. Any air present in the system as a result of assembly was purged.

Table 3.6- Capillary reactor formulation flow rates

Dispersed phase flow rate (Q_d) / µL.min^{-1}	**Aqueous phase flow rate (Q_c) / µL.min^{-1}**
1	100
10	100
25	100
50	100
100	100
100	100
100	100
20	200
50	200
50	200

Following the reaction, the tubing and reactor were purged of reagents by flushing with warm soapy water, followed by multiple washes with ultrapure water. An additional wash with acetone was also performed when required. Finally air was pushed through the system to dry.

3.5 Particle Size analysis

3.5.1 Laser Scattering

The particle size of the formulated emulsions was measured using a Malvern Mastersizer X laser scattering device. The unit utilises Mie theory based upon the refractive index of the analysed dispersion to create a model of the expect diffraction patterns. This is then iterated against the observed pattern to give an indication of the volume distribution of the dispersion. The refractive index of the oil phase used was 1.46 (O'Brien, 2010). The method of operation comprises a laser alignment step, followed by a background scan. After these are conducted the sample is added dropwise to a stirred reservoir connected to a flow cell which is situated in the path of the laser. Upon reaching an indicated obscuration band the measurement sequence is started. Each measurement consisted of 5 sets of 2000 scans.

The measurement reproducibility was found to be excellent, and as such only two measurements were taken for each sample analysed.

The output data supplied by the Malvern Mastersizer are volume distributions displayed as percentage in class at the geometric mean of the class diameter. The size data is outputted as class boundaries requiring simple manipulation to calculate the geometric mean,

$$Geometric\ mean\ diameter = d_i = \sqrt{d_l d_h} \tag{3.3}$$

Where d_l is the lower class boundary and d_h is the upper class boundary

The statistical manipulation that follows assumes spherical particles

The volume distributions can be transformed into number distributions by dividing by the mean droplet volume for a given class. Normalised, this can be expressed,

$$Number\ distribution = n_i = \frac{V_i / d_i^3}{\sum V_i / d_i^3} \tag{3.4}$$

Where V_i is the relative volume in class.

The total surface area and volume for the dispersed phase of the emulsion can calculated using this,

$$Total\ surface\ area = A_t = \sum \pi d_i^2 n_i \tag{3.5}$$

$$Total\ volume = V_t = \sum \frac{\pi d_i^3 n_i}{6} \tag{3.6}$$

The specific surface, or volume averaged surface area for the whole dispersed phase can then be calculated by dividing the total surface area (Equation 3.5) by the total volume (Equation 3.6),

$$Specific\ surface = SS = \frac{A_t}{V_t} \tag{3.7}$$

The specific surface area can be calculated from Equation 3.7 by dividing by the density of the dispersed phase droplet,

$$Specific\ surface\ area = SSA = \frac{A_t}{\rho_d V_t} \tag{3.8}$$

Where ρ_d is the density of the dispersed phase.

A number of measures of droplet diameter can also be calculated. From BS 2955:1993,

$$D[m,n] = \left[\frac{\sum n_i d_i^m}{\sum n_i d_i^n} \right]^{\frac{1}{m-n}},\ when\ m \neq n \tag{3.9}$$

A commonly known diameter is the Sauter mean or *D[3,2]* which is defined as the diameter of a sphere that has the same volume to surface area ratio as a particle or, in this case droplet of interest,

$$D[3,2] = \frac{\sum n_i d_i^3}{\sum n_i d_i^2} \tag{3.10}$$

Comparison between equations 3.8 and 3.10 shows the Sauter mean diameter and specific surface area can be related by,

$$SSA = \frac{6}{\rho D[3,2]} \tag{3.11}$$

3.5.2 Image analysis

Direct image analysis was performed on images for both the capillary and microfluidic systems. The images were acquired using a Canon 40D DSLR camera either tripod mounted with macro lens for the capillary system or attached to the front port of an inverted Nikon

Microscope through use of a lens adapter for the microfluidic chip system. The illumination was via the in-built tungsten lamp in the gas of the microscope or a separate tungsten fibre optic cable light.

For droplet sizing the microfluidic method created droplets, the diameter was calculated by direct measurement of the image using the channel width as calibration. There were three possible measurements since the microfluidic channels were not axisymmetric with a width higher larger than depth. If the measured top down diameter was less than the channel depth and roughly equal in both axial and equatorial directions then this diameter was used. If the measured top down diameter was larger than the channel width then a volume for an oblate spheroid was used (Equation 3.12), which was then used to calculate the diameter of a sphere of the same volume.

$$V_{oblate} = \frac{4}{3}\pi a^2 b \qquad 3.12$$

Where *a* is the length of the major axis and *b* is the length of the minor axis

If there was significant deviation in the axial and equatorial measurement then the volume for an ellipsoid was used (Equation 3.13), which was again used to calculate the diameter of a sphere of the same radius.

$$V_{ellipsoid} = \frac{4}{3}\pi abc \qquad 3.13$$

Where *a*, *b* and *c* are the major axis of the ellipsoid.

The microfluidic chip channel width was 300 μm and depth was 100 μm.

3.6 Contact angle measurements

The contact angle measurements were made by an OCA 15EC goniometer manufactured by Dataphysics operating in a captive bubble mode.

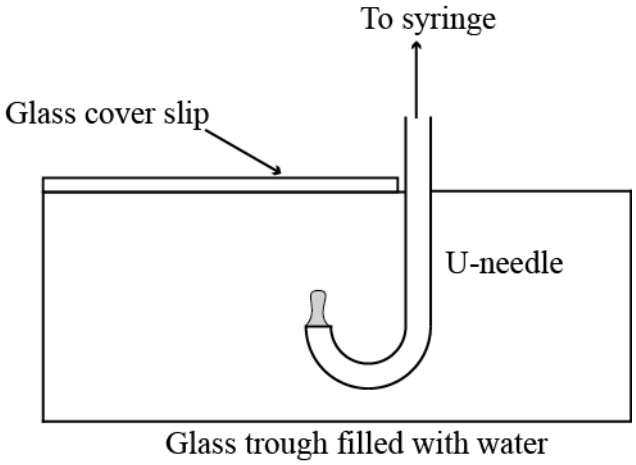

Figure 3.3 – The glass trough for the measurement of the oil-water-glass contact angle using the captive bubble method.

The configuration is shown in Figure 3.3. A quartz trough was filled with ultrapure distilled water and a 1mL glass syringe was filled with the oil or oil-surfactant mixture. This syringe was mounted in the device and a U-shaped needle was attached. The needle was submerged below the water line and positioned under a clean glass slide which was positioned on the top of the trough so that no air was between the glass top-slide and trough. A droplet of oil or oil/surfactant mixture was dispensed through the use of the automated software until a droplet detached from the needle and rose to contact the glass slide. A series of repeat measurements was then taken through the use of image capture, and post processing which used the contrast difference to automatically trace the outline of the interfaces. The image dimensions were calibrated automatically using the known width of the dispensing needle. The contact angle was then computed from the image.

3.7 General method for the batch emulsion reactions

The reactions investigating the observed rate of epoxidation from the effect of catalyst, acid and oxidant were carried out using the general procedure outlines in this section. The materials were purchased from the suppliers listed and used without purification.

Table 3.7 - Materials for the batch emulsion based reactions

Material	Referred to as	Purity	Supplier
Sodium tungstate dihydrate	catalyst	≥99%	Sigma-Aldrich Co. LLC
Acetic acid	acid	>99.7%	Sigma-Aldrich Co.

			LLC
Brij®-S10	surfactant	Not Listed	Sigma-Aldrich Co. LLC
Hydrogen peroxide	oxidant	30 wt%	Sigma-Aldrich Co. LLC
Water	water	Ultrapure (MilliQ filtered, EMD Millipore corporation)	
Sunflower seed oil	oil	Not listed, Characterised in house	Sainsbury's Supermarket Ltd.

The dispersion was created beforehand as described in the emulsion formulation section, namely through homogenisation of a crude mixture of the emulsion components. The formulations were of the composition 80:20 aqueous to oil phase with the oil phase containing 10 wt% Brij-S10. The speed and duration of homogenisation was 13500 rpm and 10 minutes. When diluted at the start of the reaction through addition of the catalyst solution the composition was 90:10

The reactions were performed in glass round bottomed flasks on a multi flask hot plate. Typically 20 mL of the premade emulsions were added to the flasks and heated under reflux to reaction temperature which was 60 °C. This was confirmed via use of thermometers in the reaction flask.

Separately the catalyst solution containing the oxidant, catalyst precursor, acid and diluent water was made up volumetrically to the required concentrations so that the total volume of the solution came to 15 mL. This was heated to reaction temperature. Upon reaching temperature the two solutions were combined to give a total volume of 35 mL emulsion. The reaction was gently stirred using magnetic stirrers. This stirring action was shown previously to have no effect upon the observed rate for emulsion based reactions.

The solution was sampled periodically by extraction of a 100 μL aliquot of reaction mixture. The sample preparation and analysis is covered in the following sections.

3.8 Microfluidic reactions

The reactions performed in microfluidics utilised a 100 μm hydrophilic glass droplet generation chip purchased from Dolomite Microfluidics. The fittings, fixtures and housing for the chip were also purchased from them and made of PEEK, perfluoroelastomer and

stainless steel 316. The tubing used was 1/16” O.D. and made from PTFE, supplied by either Dolomite Microfluidics or Cole Parmer.

The fluids were delivered via 10 mL glass and PTFE syringes utilising luer lock connectors to connect to the PTFE tubing. These were mounted on Fusion-100 syringe pumps obtained from KR Analytical Ltd.

The chemicals used were the same as those for the emulsion reactions

3.8.1 In-situ microfluidic chip reactions

For reactions performed in-situ through the microfluidic device the aqueous phase containing the catalyst solution and oil phase were each supplied in separate syringes. The catalyst solution was prepared through volumetric addition of the catalyst solution, acid, oxidant and diluent water to the concentrations required. This was agitated to aid dissolution.

The oil phase contained the 1 wt% Brij S10 supplied by Sigma-Aldrich Co. LLC. The oil and surfactant were heated to 50 °C with the surfactant and stirred to aid dissolution.

Where heating was required the chip and housing, along with the outlet tubing were submerged within a water bath on a stirrer hot plate. The temperature of reaction was as for the emulsion reactions, 60 °C.

Any air present in the system as a result of assembly was purged. The correct flow rates were set on the syringe pumps and started. Following this the system was deemed primed and ready for operation.

Following the reaction, the tubing, syringes are chip were purged of reagents by flushing with warm soapy water, followed by multiple washes with ultrapure water. An additional wash with acetone was also performed when required. Finally air was pushed through the system to dry.

3.8.2 Reactions with preformed droplets

For reactions using the microfluidic devices as pure droplet generators, the emulsions were preformed following the procedures outlined in the microfluidics formulation section.

Following this the reactions were performed identically to those done in emulsions formed through high-shear homogenisation. The only alteration was that the 20 mL of premade emulsion used was formed through the microfluidic device rather than the high-shear homogeniser.

3.9 Glass capillary reactions

The reactor was made from 1mm I.D. borosilicate glass capillary tubing, joined and bend by the in house glass blower at the University of Bath. The tubing used was 1/16" O.D. and made from PTFE, supplied by either Dolomite Microfluidics or Cole Parmer. As discussed in the relevant chapter, the use of silicone tubing was attempted but this was not compatible with the reagents. The reactor was interfaced to the rigid tubing by use of PTFE fittings and 1/4" 28-UNF threaded glass capillary sections supplied by Kinesis Ltd. These threaded sections were appended to the inlets and outlets of the reactor by the in-house glass blower. At each of the inlets and outlet a PTFE stopcock was attached to contain the fluid within the reactor and stop the flow. The chemicals used were the same as those used for the emulsion reactions.

The fluids were delivered via 10 mL glass and PTFE syringes utilising luer lock connectors to connect to the PTFE tubing. These were mounted on Fusion-100 syringe pumps obtained from KR Analytical Ltd.

For reactions performed in the glass capillary device the aqueous phase containing the catalyst solution and oil phase were each supplied in separate syringes. The catalyst solution was prepared through volumetric addition of the catalyst, acid, oxidant and diluent water to the concentrations required. This was agitated to aid dissolution.

The oil phase contained the 1 wt% Brij S10 supplied by Sigma-Aldrich Co. LLC. The oil and surfactant were heated to 50 °C with the surfactant and stirred to aid dissolution.

To heat, the capillary reactor along with the inlet tubing were submerged within a water bath on a stirrer hot plate, heated to 60 °C.

The system was configured, similar to the formulation, with addition of the water bath and stopcocks, as shown in Figure 3.4.

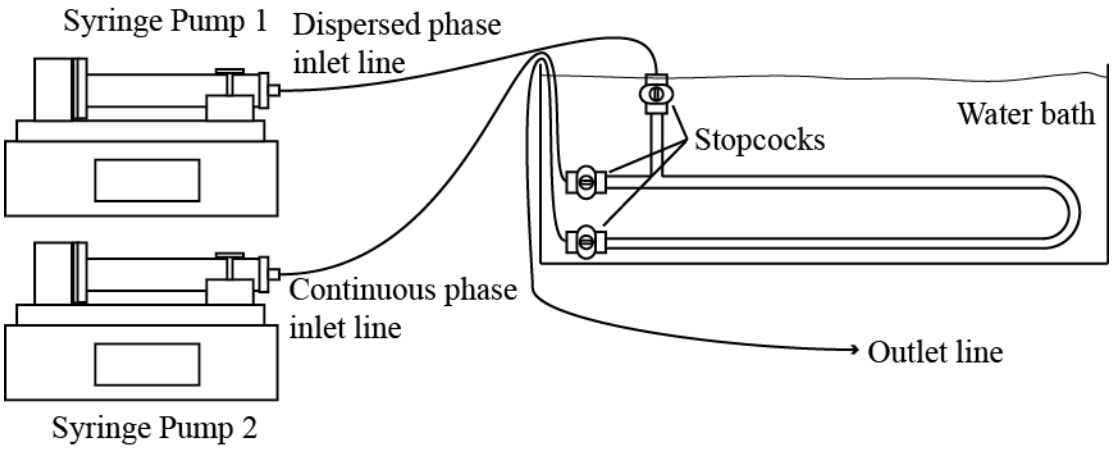

Figure 3.4 – The capillary reactor apparatus used for the stop flow experiments investigating low surface areas.

Any air present in the system as a result of assembly was purged. The correct flow rates were set on the syringe pumps and started. Following this the system was deemed primed and ready for operation. Both phases were pumped through the reactor until it was filled with the required evenly spaced plugs. At this point the inlet and outlet stopcocks were closed, the pumps stopped and the timer started. Following the allotted reaction time the stopcocks were reopened and the flow recommenced. Since the volumes of the outlet tubing as well as the reactor were known, the time for the reactor contents to reach the outlet tube end could be calculated, assuming minimal axial dispersion over such short distances. After this calculated time the sample volume was collected for analysis. The system was allowed to re-equilibrate, determined through visual observation of the plug pattern and spacing. The stopcocks were then re-closed for the next residence time experiment. The residence times investigated were 5, 15, 30, 60 and 120 minutes for each of the surface areas investigated.

Following the reaction, the tubing and reactor were purged of reagents by flushing with warm soapy water, followed by multiple washes with ultrapure water. An additional wash with acetone was also performed when required. Finally air was pushed through the system to dry.

3.10 Rate of epoxidation determination

The sampled reaction mixture/oil/dispersion/emulsions were all analysed in the same way to determine the rate of epoxidation. The sample (100-200 μL) was immediately added to approximately 1 mL deuterated chloroform, sealed in an eppendorf and shaken to extract the oil phase. The chloroform layer was removed and passed through a short plug of magnesium sulfate into tubes for analysis. The removal of oil from the presence of aqueous phase through extraction and drying ensured the reaction was removed from any source of oxidant and hence was effectively quenched.

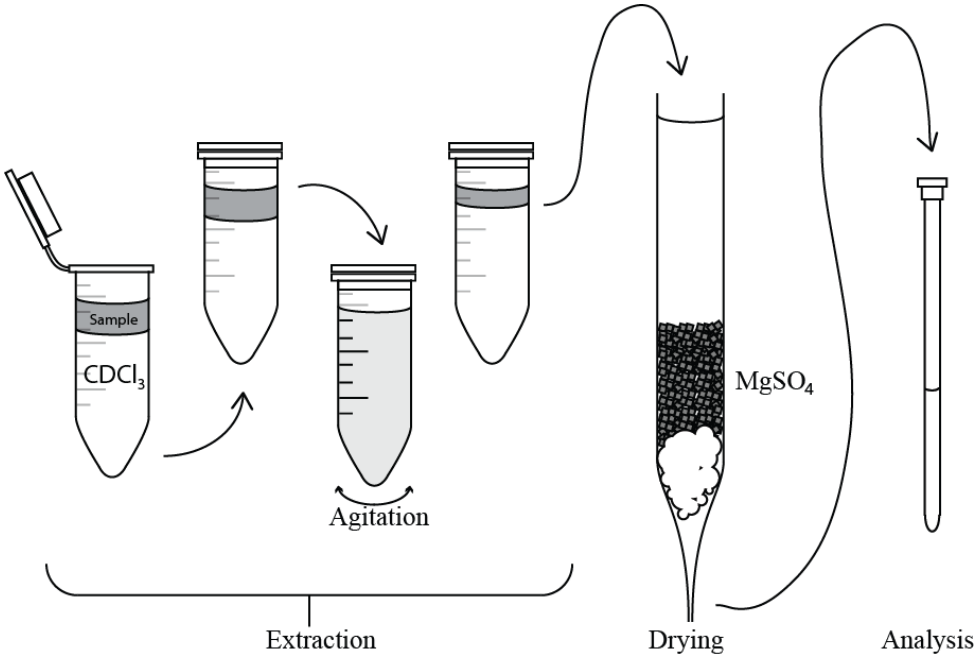

Figure 3.5 - Reaction sample analysis preparation

The extraction method was also investigated. The use of excessive shaking or agitation using sonication or vortex mixer showed no extra extraction over manual shaking for 10 seconds. Multiple extractions of the sample showed that effectively all of the oil was extracted in the first extraction. To ensure no retention of sample within the magnesium sulfate plug, a small amount of deuterated chloroform was passed through after the sample. It was important to note that further addition of the deuterated solvent had the effect of diluting the sample so the total amount used was dependent on the amount of sample, and the observable signals.

The determination of the rates of reaction utilised conversion data determined by nuclear magnetic resonance (NMR) spectroscopy using a 250 MHz Bruker spectrometer and chloroform as the lock signal. Since this method relies on the relative molar ratios of species, the exact volume of sample was not important over ensuring that sufficient integratable signal was observed in the spectra. In order to interpret the spectra obtained from NMR first the oil making up the dispersed phase had to be characterised.

3.10.1 Oil Characterisation

Since the reaction was assumed to occur solely in the oil phase a measure of the concentration of the pure oil had to be calculated. Firstly due to the natural variability in the sunflower oil composition, the molar mass of the sample oil was determined. Firstly the oils fatty acid profile was characterised by analysis of the integrals of relevant peaks in the hydrogen NMR spectrum (Figure 3.6) according to the method by Knothe and Kenar (2004).

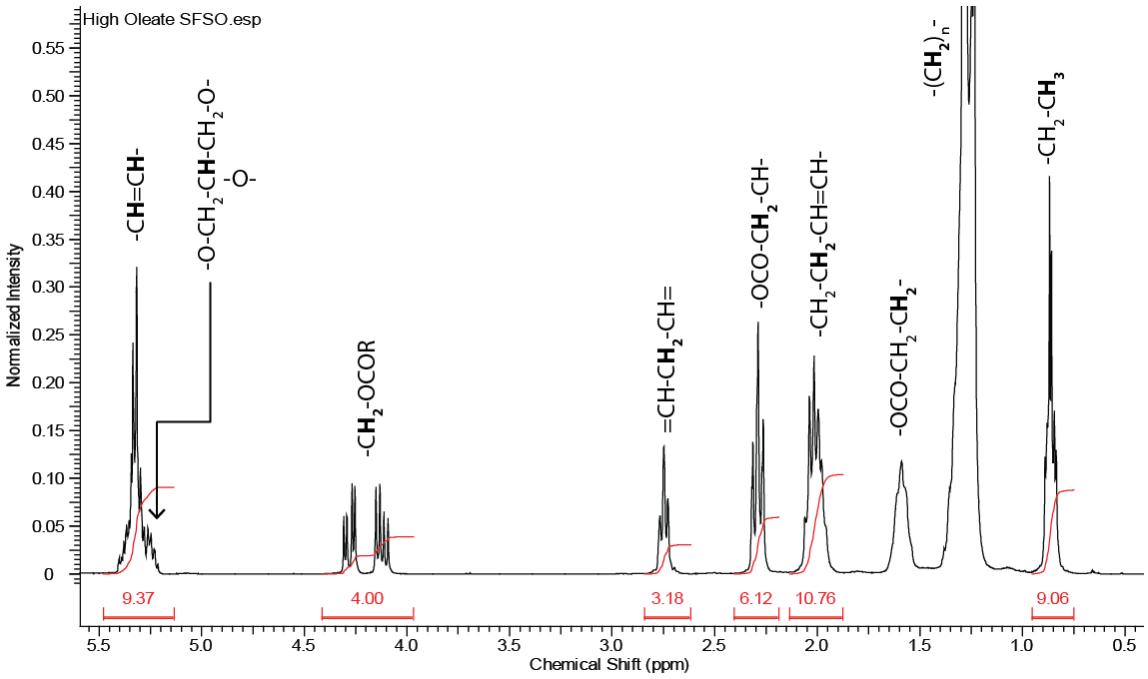

Figure 3.6 – ^{1}H-NMR spectrum of sunflower oil in $CDCl_3$ showing the assignments of the individual signals

According to the aforementioned method, the quantification of the fatty acid profile is performed as follows. The maximum theoretical integrals for the various levels of unsaturation are given in Table 3.8

Table 3.8 –Maximum integral values for unsaturated groups with 1 proton equalling an integration value of 1

Protons (integral range in ppm)	**oleic acid (18:1)**	**linoleic acid (18:2)**	**linolenic acid (18:3)**
olefinic (5.3-5.5)	2	4	6
allylic (1.9-2.1)	4	4	4
***bis*-allylic (2.7-2.9)**	0	2	4

According to the above the experimentally observed integration values for these peak regions are a function of the measured integral area and the maximum theoretical integral values for each of the proton environments:

$$I_{experimental,olefinic} = 2A_{C18:1} + 4A_{C18:2} + 6A_{C18:3} \quad 3.14$$

$$I_{experimental,allylic} = 4A_{C18:1} + 4A_{C18:2} + 4A_{C18:3} \quad 3.15$$

$$I_{experimental,bisallylic} = 2A_{C18:2} + 4A_{C18:3} \quad 3.16$$

Where $I_{experimental}$, corresponds to the measured integral for the relevant proton environment given in the subscript, A corresponds to the molar amount of mono-, di- or triunsaturated fatty acid. Equations 3.14 - 3.16 represent 3 equations with 3 unknowns since the integrals can be determined from the NMR spectrum thus the fatty acid profile cane be determined.

The fatty acid profile for the sunflower oil used for the experiments is displayed in Table 3.9.

Table 3.9 – Sunflower Seed Oil fatty acid profile.

Fatty acid **C n:m where n is the number of carbons in the chain and m the number of double bonds**	**Percentage composition**
C 18:3	0
C 18:2	57.3
C 18:1	35
C 18:0	7.7

Knowing the percentage composition the molar mass can be worked out from the atomic weights of the component atoms. This was found to be 882.43 g/mol.

Using the molar mass, M_r and the density the concentration of the pure oil phase, C_{Oil}, could be calculated as moles of triglyceride per volume,

$$\begin{aligned} C_{Oil} &= \frac{M_r}{\rho_d} \\ &= \frac{882.43}{918} \quad \left(\frac{g.mol^{-1}}{g.L^{-1}} \right) \\ &= 1.03\, mol.L^{-1} \end{aligned} \tag{3.17}$$

Since each molecule of triglyceride contains a random selection of chains knowing the average degree of unsaturated sites per molecule, and hence per mole was useful. This was calculated from the number of unsaturated sites weighted by their mole fractions,

$$\begin{aligned} \frac{n_{alkene}}{n_{triglyceride}} &= x_{C18:1} + 2x_{C18:2} + 3x_{C18:3} \\ &= 0.35 + (2 \times 0.573) + 0 \\ &= 1.496 \end{aligned} \tag{3.18}$$

Therefore the concentrations of alkene or reactive sites of interest, in the pure sunflower oil could be calculated,

$$\begin{aligned} C_{alkene} &= C_{Oil}\left(n_{alkene}/n_{triglyceride}\right) \\ &= 1.03 \times 1.496 \\ &= 1.55\ mol.L^{-1} \end{aligned} \qquad 3.19$$

3.10.2 Conversion

The conversion from alkene to epoxide was calculated through analysis of the ^{1}H-NMR spectra at each time sample. The glycerol signals between 4-4.4 ppm were used as an internal standard, since they were unchanging over the reaction course. These signals represented 4 protons.

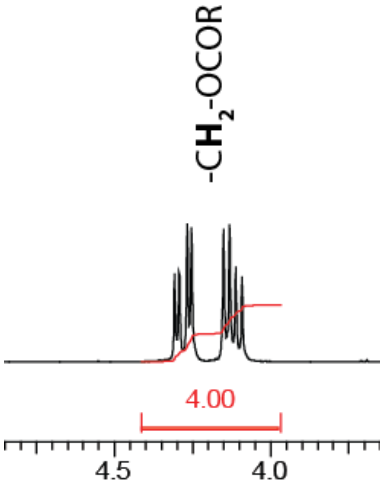

Figure 3.7 – ^{1}H-NMR spectrum of sunflower oil highlighting the glycerol peaks used as internal calibrant

Following this the total observed alkene peaks between 5.2 and 5.5 ppm were integrated, $I_{alkene,\ observed}$. In order to obtain an accurate integration the glycerol methine integral, $I_{methine}$ corresponding to one proton in the calibrated spectrum needed to be subtracted to give the actual alkene integral, $I_{alkene,\ actual}$. In the example spectrum extract given in Figure 3.7the total integral corresponding to the alkene would be,

$$\begin{aligned} I_{alkene,actual} &= I_{alkene,observed} - I_{methine} \\ 8.37 &= 9.37 - 1 \end{aligned} \qquad 3.20$$

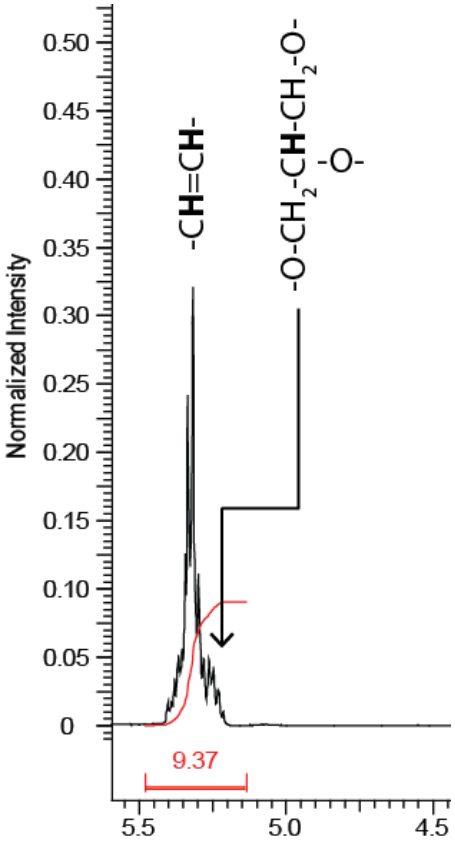

Figure 3.8 – ^{1}H-NMR spectrum of sunflower oil highlighting the alkene region and glycerol methine.

Finally the epoxide signal, I_{epox}, was integrated between 2.8 and 3.1 ppm. This corresponds to the same relative number of protons as the alkene signal. Therefore a simple percentage conversion of alkene to epoxide at time, t, could be calculated

$$Conversion = X_t = \frac{I_{epox,t}}{I_{epox,t} + I_{alkene,actual,t}} \quad 3.21$$

This method assumes a straight conversion of the alkene to the epoxide as the sole product. To validate this assumption the samples were analysed for the presence of further oxidation products, such as the ring opened dialcohol. No signals could be observed, therefore either validating the assumption.

Knowing the starting concentration of alkene, $C_{alkene,0}$, (equal to the concentration calculated for pure oil) the concentration of alkene at a given conversion can be calculated,

$$C_{alkene,t} = C_{alkene,0}\left(1\text{-}X_t\right) \quad 3.22$$

Taking the assumption above of a single product, the concentration of epoxide can be calculated likewise

$$C_{epox,t} = C_{alkene,0} X_t \quad 3.23$$

3.10.3 Reaction rate

Having concentration-time data for both the alkene and formed epoxide, the method of initial rates could be utilised to determine the observed rates of reaction. The method of initial rates analyses the initial linear portions of the concentration-time graphs (e.g. Figure 3.9), during which time there is assumed no significant depletion of reaction components. This was typically at conversions less than 20 %. In order for meaningful analysis it is critical that sufficient data is therefore obtained in this initial region. The reaction was analysed typically every 15 minutes for the first two hours, followed by hourly up to 6 hours, a total of a maximum of 12 samples per experiment. The gradient of the linear portion of the graph (e.g. Figure 3.9) was taken as the rate expressed as the rate of gain of epoxide (and therefore rate of loss of alkene) concentration per time in the oil phase,

$$r_{epox} = -r_{alkene} = \frac{dC_{epox}}{dt} \quad 3.24$$

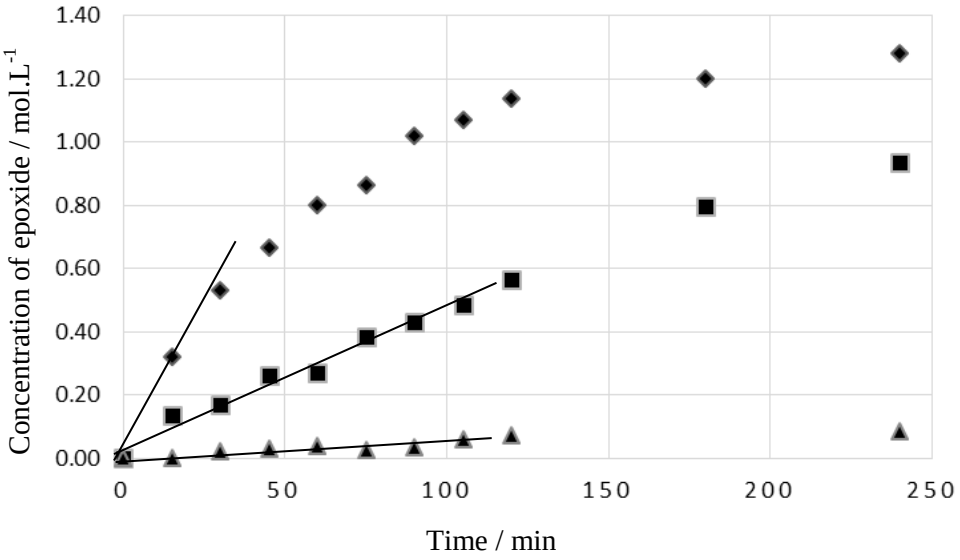

Figure 3.9 – Typical concentration-time data for the epoxidation reactions. Conditions: 60°C, 3 M H_2O_2, AcOH:Na_2WO_4 20:1. Catalyst concentration: ▲0.025 M ■ 0.1 M ♦ 0.15 M

3.10.4 Error analysis

The experimental errors relating to the rate of reaction experimentation as shown in the figures contained in Chapter 5 were determined through analysis of an array of repeated samples at a set times and then multiple analysis of the same samples. The standard deviation of the conversion as determined from integration of the NMR spectra integrals was calculated. This was then used to calculate the percentage error and the average of these taken as the experimental error (Table 3.10).

Table 3.10 – Error analysis for the reaction rate experimental data measured using NMR

	Repeat measurement				
Sample	1	2	3	Standard Deviation	% error
1	40.86	43.16	42.14	0.94	2.24
1	41.86	40.17	43.16	1.23	2.94
1	42.19	41.64	40.79	0.58	1.39
2	10.43	9.41	9.42	0.48	4.90
2	8.96	9.86	9.87	0.43	4.45
2	9.68	10.06	9.55	0.22	2.21
3	14.67	13.68	14.43	0.42	2.96
3	14.05	13.86	14.29	0.17	1.23
3	13.95	14.25	14.62	0.27	1.92
				Average	2.69%

3.11 Oxidant analysis

The decomposition reactions were performed in 100 mL round bottomed flasks on stirrer hotplates with attached reflux condensers.

3.11.1 Effect of catalyst

For investigation into the effect of the concentration of catalyst precursor on the rate of decomposition, a 50 mL solution containing 3 M hydrogen peroxide, 1 M acetic acid was heated to reaction temperature of 60 °C. Once at temperature the required amount of catalyst precursor was added to achieve the desired concentration (Table 3.11) and a timer started. The solution was stirred with magnetic stirrers and sampled hourly according to the sampling protocol given below.

Table 3.11 - Reagent concentration for the catalyst precursor decomposition experiments

Exp No.	**Reaction volume / mL**	**Concentration mol.L^{-1} (M)**		
		Sodium tungstate	Acetic acid	Hydrogen peroxide
D1	50	0.5	1	3
D2	50	0.4	1	3
D3	50	0.3	1	3
D4	50	0.15	1	3
D5	50	0.075	1	3

D6	50	0.05	1	3
D7	50	0.015	1	3

3.11.2 Effect of catalyst precursor at defined acid:catalyst precursor ratio

For investigation into the effect of the concentration of catalyst precursor at a defined catalyst precursor: acid ratio of 0.05 on the rate of decomposition, a 50 mL solution containing 3 M hydrogen peroxide and the required acid concentration (Table 3.12) was heated to reaction temperature of 60 °C. Once at temperature the required amount of catalyst precursor was added to achieve the desired concentration (Table 3.12) and a timer started. The solution was stirred with magnetic stirrers and sampled hourly according to the sampling protocol given below.

Table 3.12 - Reagent concentration for the catalyst precursor decomposition at set catalyst precursor-acid ratios experiments

Exp No.	**Reaction volume / mL**	**Concentration mol.L^{-1} (M)**		
		Sodium tungstate	Acetic acid	Hydrogen peroxide
D8	50	0.155	3.096	3
D9	50	0.1	2.0	3
D6	50	0.050	1.000	3
D10	50	0.025	0.500	3

3.11.3 Effect of acetic acid

For investigation into the effect of the concentration of acetic acid on the rate of decomposition, a 50 mL solution containing 3 M hydrogen peroxide and the required amount of acetic acid (Table 3.13) to give a defined concentration was heated to reaction temperature of 60 °C. Once at temperature the required amount of catalyst precursor (Table 3.13) was added to achieve the desired concentration and a timer started. The solution was stirred with magnetic stirrers and sampled hourly according to the sampling protocol given below.

Table 3.13 - Reagent concentration for the decomposition at set catalyst precursor acid ratios experiments

Exp No.	**Reaction volume / mL**	**Concentration mol.L^{-1} (M)**		
		Sodium tungstate	Acetic acid	Hydrogen peroxide

D11	50	0.1	0.50	3
D12	50	0.1	1.00	3
D9	50	0.1	2.00	3
D13	50	0.1	3.00	3

3.11.4 Effect of hydrogen peroxide

For investigation into the effect of the concentration of acetic acid on the rate of decomposition, a 50 mL solution containing 1 M acetic acid 3 M hydrogen peroxide and the required amount of acetic acid (Table 3.14) to give a defined concentration was heated to reaction temperature of 60 °C. Once at temperature the required amount of catalyst precursor (Table 3.14) was added to achieve the desired concentration and a timer started. The solution was stirred with magnetic stirrers and sampled hourly according to the sampling protocol given below.

Table 3.14 - Reagent concentrations for the decomposition experiments at different starting hydrogen peroxide concentrations

Exp No.	**Reaction volume / mL**	**Concentration mol.L^{-1} (M)**		
		Sodium tungstate	Acetic acid	Hydrogen peroxide
D14	50	0.1	1.0	0.5
D15	50	0.1	1.0	2.0
D12	50	0.1	1.0	3.0
D116	50	0.1	1.0	5.0

3.11.5 Sampling and analysis

Samples of 50 µL were taken in triplicate and diluted in approximately 100 mL water, H_2O and 10 mL sulphuric acid, H_2SO_4 (4 M). These were titrated against 0.2001 M potassium permanganate solution and the titres averaged. The moles of hydrogen peroxide remaining were determined from the titre by molar analysis using the relationship in Scheme 3.1.

$$2KMnO_4 + 3H_2SO_4 + 5H_2O_2 \longrightarrow K_2SO_4 + 2MnSO_4 + 8H_2O + 5O_2$$

Scheme 3.1 - Decomposition of hydrogen peroxide with acidified potassium permanganate

The rates of decomposition were determined by the method of initial rates from the analysis of the gradients of the initial linear regions of the concentration-time plots at low conversion.

4 Controlling the Liquid-Liquid Interface

The overall aim of this research was to develop a methodology to for the optimisation of liquid-liquid reaction systems towards continuous operation including integrated separation. A key objective to achieve this was to develop an understanding of the rate of reaction of a biphasic reaction. The reaction under investigation was the epoxidation of a vegetable oil, being both a liquid-liquid reaction, and commercially relevant, with the product widely used in the polymer industry (Rowland, 1958). In order to understand the rate limiting step in the epoxidation, separation of the variables that control mass transfer and those that control rate of reaction was required.

The interfacial area is a variable unique to mass transfer between the two phases in a liquid-liquid system. Therefore, before analysis of the effect of this variable on observed rate of reaction could be conducted (Chapter 5), a range of stable interfacial areas per mass of oil (specific surface area, or SSA) had to be formulated.

Therefore, this chapter presents the results and discussion of the research conducted to achieve;

1. stable emulsions, through assessment of surfactant use
2. a range of interfacial areas through the use of:
    a. high shear homogenisation,
    b. microfluidic droplet generation, and
    c. capillary plug flow.

The dispersed systems formed, consisted of an aqueous phase, which, for the purpose of the formulation investigations, was ultrapure water and an oil phase. This was unmodified sunflower seed oil, and unless explicitly stated otherwise, the surfactant used in this investigation was Brij-S10, shown below in Figure 4.1.

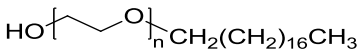

Figure 4.1 - Chemical structure of Brij-S10

A preliminary screening experiment assessed the effectiveness of surfactants to emulsify sunflower oil. The emulsification of vegetable oils is well established, with many surfactant types used, for example those covered in the literature review. However, for use in this reaction system, additional factors had to be considered in the choice of surfactant. In order to avoid ionic interactions, even favourable, between the catalytic species and surfactant, only non-ionic surfactants were investigated. One constraint upon the selection of the surfactant was that it should not be chemically altered when subjected to the oxidation conditions. Many effective surfactants, for example, the unsaturated analogue to Brij-S10, Brij-O10, were discounted due to the presence of functional groups with potential for reaction under the oxidation conditions. Frustratingly, many unsaturated surfactants are not only very effective at emulsifying vegetable oils, but are also both liquid and possess desirable viscosities. The analogous saturated surfactants, with their inherently increased ability to order, are either solid, or of high viscosity.

Since the high shear homogenisation experiments were performed batch-wise on a mixture of the formulation components, the aspect of viscosity and the state of the surfactant proved not to be an issue. This however, became extremely important when flow processes were used, such as in the microfluidic and capillary methods and as such will be discussed further in the relevant section.

4.1 Emulsion formulation using Design of Experiments (DoE)

The formulation of emulsions can often appear much as an art rather than a rigorous scientific endeavour. This is due to the complex interactions that exist on the molecular level, often confounded by addition of a temporal factor. The number of variables input into a formulation, from the method of emulsification to the choice, and relative ratios, of individual phase components, can often not be adequately explored by traditional scientific methods. Observing the outcome of a stepwise change in a single variable, in addition to being time consuming, can critically miss any interactions, be these synergistic or antagonistic, between combinations of inputs.

In order to overcome these pitfalls a Design of Experiments (DoE) approach was used. This technique is used to define the minimum number of experiments required to satisfy a design space. By this one means a region of investigation covering the whole range of a set of continuous variables.

4.1.1 Design of Experiments Results

For each experiment 60 mL of the formulations was created by addition of the various components to a vessel followed by homogenisation for the required duration, at the specified speed. The experiments were conducted in the random order given in the table to minimise the effect of day to day experimental bias. The results are summarised in Table 4.1. Since the droplet size (D[3,2]) and specific surface area are mathematically related by the dispersed phase density, only the surface area is reported.

Table 4.1 - Summary of the DoE input variables and resultant surface areas. Displayed in the order of formulation, randomised to reduce day to day experimental errors.

Exp Name	Surfactant / % oil volume	Phase Vol. aqueous phase / % total volume	Homogenisation time / min	Homogenisation speed / rpm	Day 1 Surface Area / $m^2.g^{-1}$	Day 1 Standard deviation	Day 2 Surface Area / $m^2.g^{-1}$	Day 2 Standard Deviation
NL1	1	60	1	8000	0.37	0.009	0.35	0.010
N17	5.25	70	5.5	10750	2.04	0.031	2.17	0.081
N16	10	80	10	13500	3.14	0.031	3.13	0.095
N6	10	60	10	8000	1.44	0.037	1.65	0.088
N4	10	80	1	8000	0.84	0.029	0.72	0.001
N8	10	80	10	8000	1.78	0.100	1.63	0.025
NL3	1	80	1	8000	0.67	0.013	0.59	0.83

NL7	1	80	10	8000	0.44	0.040	0.50	0.071
N2	10	60	1	8000	0.91	0.003	0.92	0.016
NL5	1	60	10	8000	0.86	0.070	0.79	0.027
N19	5.25	70	5.5	10750	2.52	0.087	2.25	0.038
N12	10	80	1	13500	2.49	0.067	2.35	0.037
NL11	1	80	1	13500	1.17	0.071	0.78	0.013
NL15	1	80	10	13500	0.91	0.032	1.02	0.035
N10	10	60	1	13500	2.27	0.116	1.95	0.066
N18	5.25	70	5.5	10750	2.08	0.066	2.31	0.010
N14	10	60	10	13500	3.78	0.089	3.59	0.056
NL9	1	60	1	13500	1.13	0.039	1.19	0.001
NL13	1	60	10	13500	0.99	0.009	1.07	0.025

The results of the DoE array were analysed using Umetrics MODDE design software to provide statistical information. The software effectively creates a model which attempts to describe the relationship of the resulting outputs and inputs of the system under analysis. A range of statistical metrics are used to validate the model and give confidence to any future predictions, specifically:

- 'R^2' indicates the model fit to the input data, < 0.5 indicates a model with low significance;
- 'Q^2' indicates an estimate of future prediction precision, >0.5 indicates a good model;
- 'Model validity' is a catch all phrase for a range of model problems, <0.25 indicates significant model problems; and
- 'Reproducibility' indicates the variation of the repeat runs when compared to the overall variability, >0.5 indicates good reproducibility.

At R^2 of greater than 95% the factors in the obtained model express most of the variation in the results for the surface area. A Q^2 value of over 90% is very good and indicates the potential to allow prediction of optimal conditions with some confidence in obtain a required droplet surface area.

The remaining summary model statistics for the design, shown in Figure 4.2, indicate an extremely strong model based on the guidelines given above.

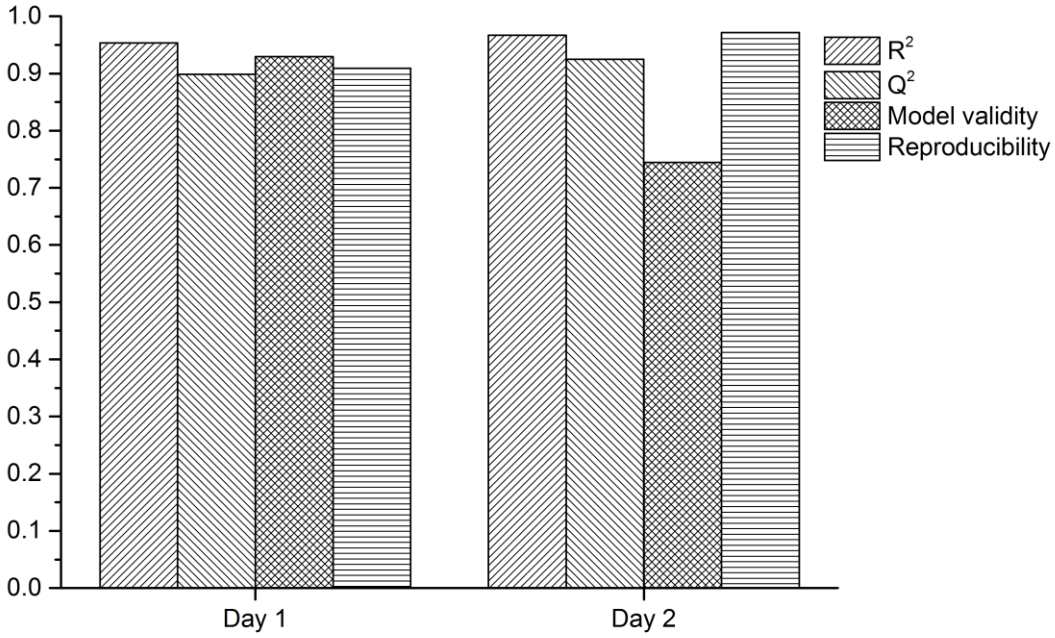

Figure 4.2 – The summary statistics for the DoE model. D1 and D2 signify day 1 and day 2 results respectively.

The determination of an input variable's statistical significance to the resultant change in the outputs can be determined through analysis of plots of regression coefficients with associated confidence intervals. The variables are said to be significant, i.e. outside experimental error, when the confidence intervals do not cross zero.

From analysis of the model, the variables that significantly influenced the surface area were: the oil:surfactant ratio, homogenisation speed and, to a lesser extent, the duration of homogenisation (Figure 4.3). The phase volume of the aqueous phase had no significant effect.

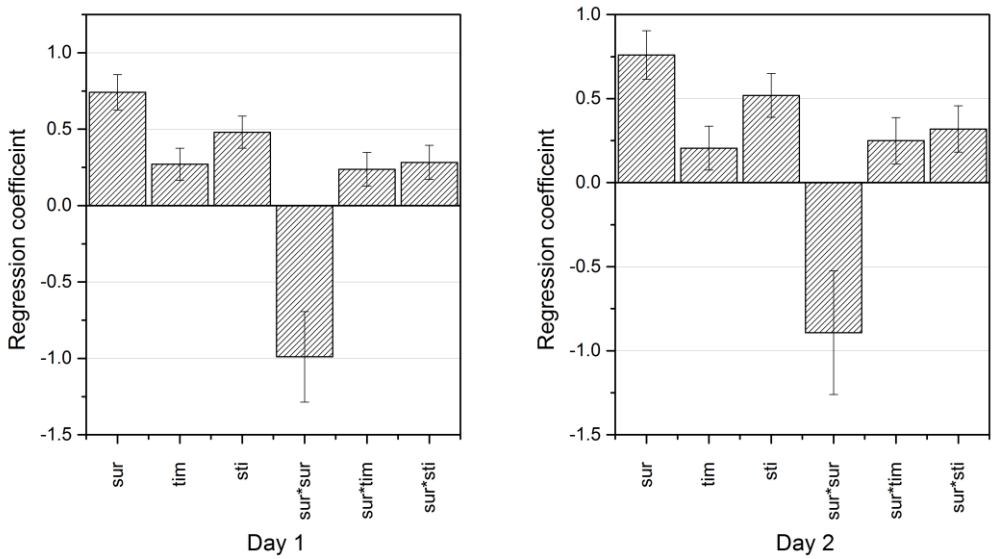

*Figure 4.3 – Coefficient plots showing surfactant (sur), stirring time (tim), stirring speed (sti) variables as well as the interactions between surfactant levels and time (sur*tim) and between surfactant levels and stirring speed (sur*sti) for the revised DoE. D1, and D2 indicate day 1 and day 2 respectively.*

A more in depth analysis of the interactions indicated in the coefficient plots was performed. The plots display predicted change in the response (in this case surface area) when one variable is changed, and the second variable is set at both its low and high level. The remaining variables are all set at their mid-point values.

The surfactant level – stirring time interaction showed an increasing surface area when high levels of surfactant were used with an increased stirring time (Figure 4.4). When the levels of surfactant were low, increasing the stirring time had a much less pronounced effect.

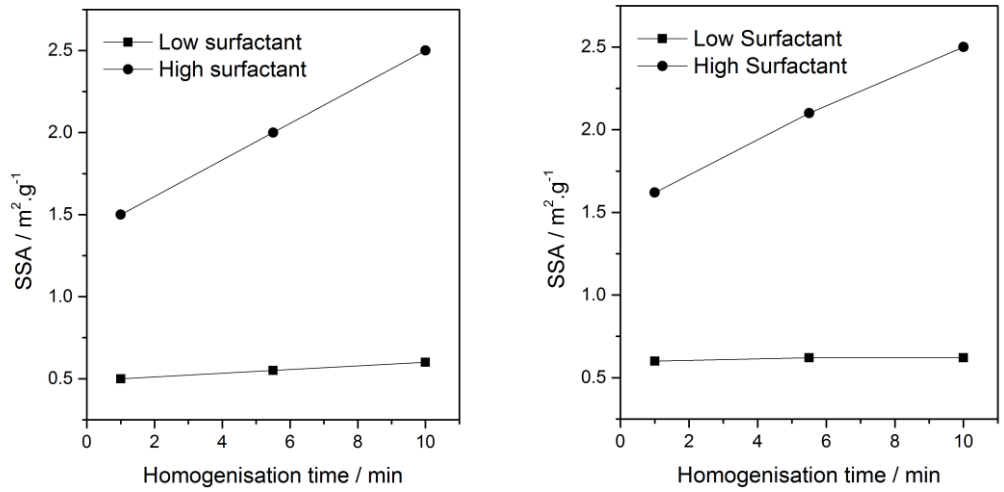

Figure 4.4 – Surfactant level and stirring duration interaction plots for the revised DoE. Left to right, Day 1 Day 2.

The interaction plots between surfactant level and stirring speed is shown in Figure 4.5. The increase in stirring speed clearly shows a larger increase in surface area at high levels of surfactant when compared to lower levels of surfactant.

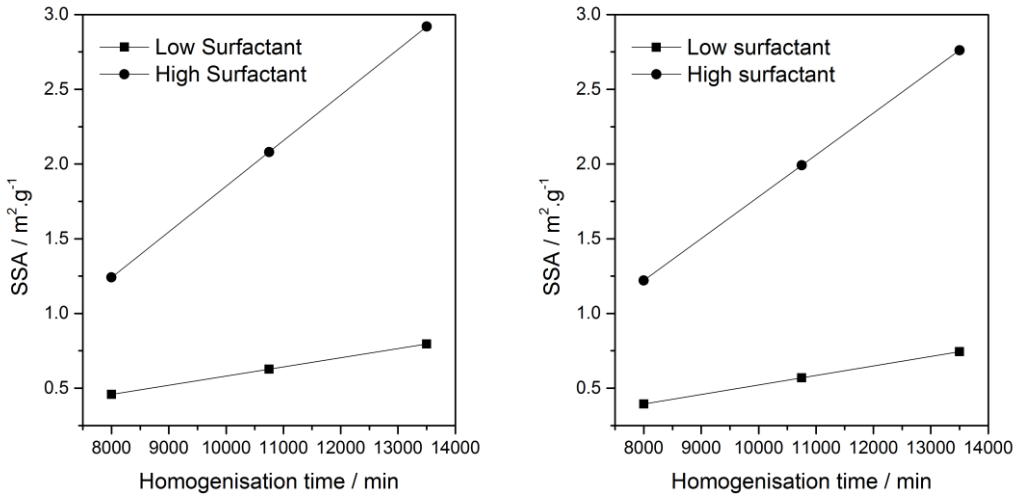

Figure 4.5 – Surfactant level and stirring speed interaction plots for the revised DoE. Left, Day1 and right, Day 2.

Both of the interactions above indicate that the longer the homogenisation time and the faster homogenisation speed applied to the emulsions, with higher levels of surfactant, the larger the increase in surface area compared to the low levels of surfactant. These results reinforce the idea that the input of more power to achieve a larger surface area (smaller droplet size) is only fruitful when there is sufficient surfactant present to be able to stabilise the created interface.

The relationship between the significant variables of homogenisation speed, homogenisation time and surfactant levels with respect to the outcome of surface area can be illustrated through contour plots (Figure 4.6 - Figure 4.7). The plots below show clearly that the most significant variables to adjust to increase the surface area are stirring speed and surfactant levels. Increasing the stirring time shows an effect, but it is less significant when compared to the other two. The model responses for day 1 and day 2 show very little change.

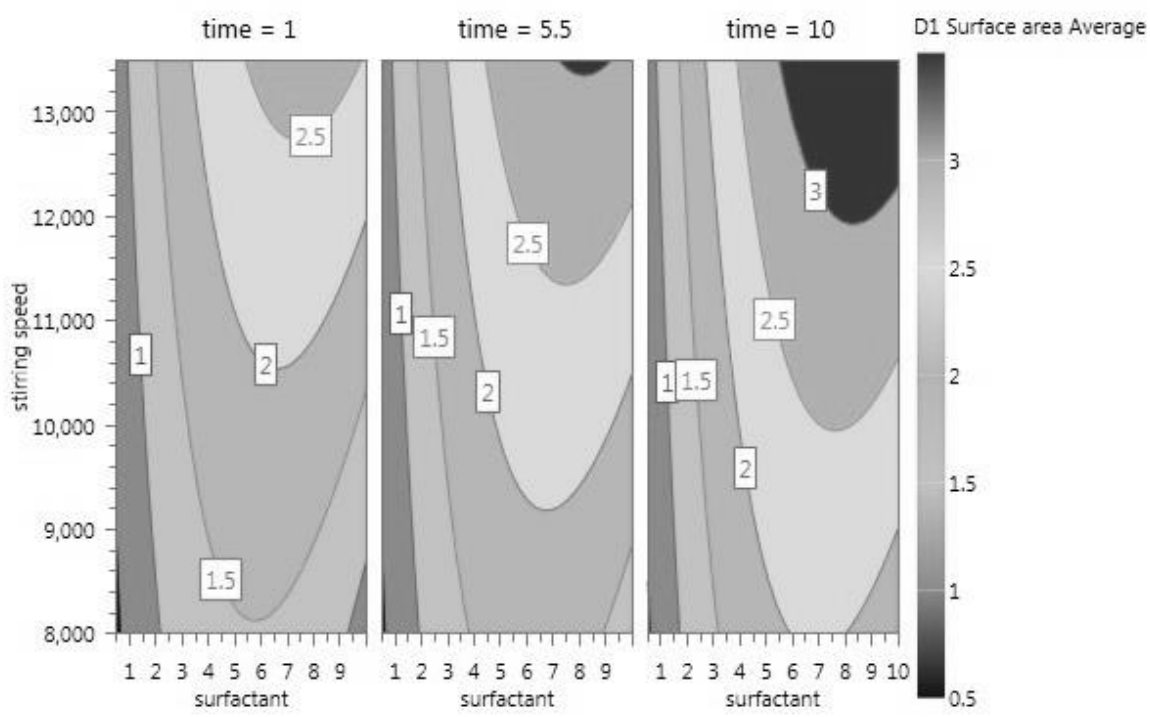

Figure 4.6 – Contour plot showing surface area as a function of surfactant level and stirring speed and time for Day 1 results of the revised DoE model

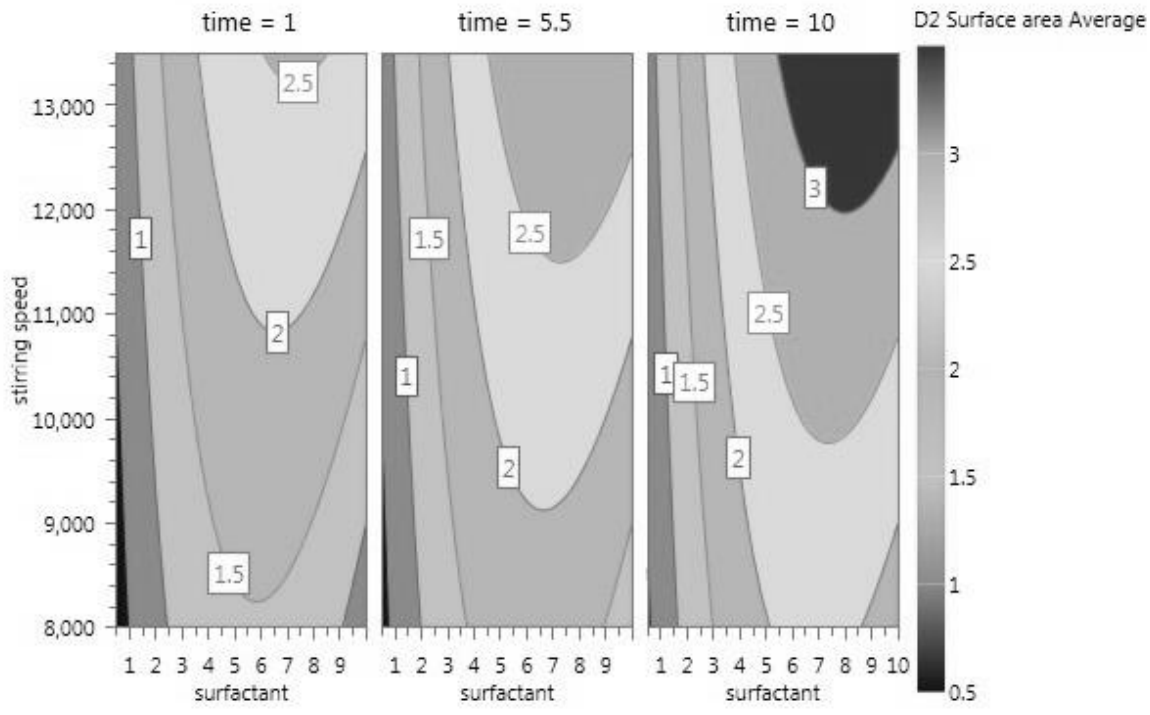

Figure 4.7 – Contour plot showing surface area as a function of surfactant level and stirring speed and time for Day 2 results of the DoE model

From the results of the DoE investigations a robust, accurate system model was able to be produced. The Q^2 values calculated for the model shows that confident predictions for the surface area can be made from specifications of the surfactant level, stirring speed and time.

The effect of stirring speed is well known for rotor-stator homogenisation and the results observed here correspond to previous reported systems (Maa and Hsu, 1996)

After analysis of all the results the following conclusions can be drawn:

- the range of surface areas obtainable from these formulations was 0.27 to 3.78 $m^2.g^{-1}$;
- both measurement of surface area and droplet size in the individual formulations were reproducible; and
- the average percentage change in surface area over one day was less than 10%.

The variables which showed the biggest increase in surface area were:

- the oil:surfactant ratio;and
- homogenisation speed.

Interestingly, the results show that higher homogenisation durations and speeds are only productive towards increased surface area when sufficient surfactant is available. The lack of surface area increase for a given surfactant concentration despite harsher processing can give useful insight into the surfactant use. Since the surfactant weight percentage at this maximum surface area is known and if it as assumed that, at this maximum area, the surfactant is present at a monolayer, metrics such as the maximum surface area able to be stabilised per gram surfactant present in the oil phase can be calculated. In this instance the maximum surface area can only be determined as corresponding to a range (due to the slight gradient of the lower lines in Figure 4.5) between approximately 0.5-0.75 m^2 per gram of oil phase containing 1 wt% surfactant. For 1 gram of oil containing 0.01 g of surfactant (molar mass = 711 g/mol, 1.4 x 10^{-5} moles) the area per molecule based on single monolayer coverage can be calculated from Avogadro's constant (6.022 x 10^{23}) is approximately between 6 and 9 square angstroms. This is low when compared to the literature value of 53 Å (Broze, 1999) however this data is for the air water interface and not the air-oil interface. One could suggest increased penetration of the surfactant molecule into the oil phase compared to the air, resulting in an elongation of the molecule and hence a smaller surfactant area as was observed experimentally.

Whilst not the primary goal of this section of the research (that was to achieve a range of interface areas) knowledge of the factors likely to be limiting allows for the optimum use of materials. The use of the multivariable analysis using the design of experiment approach enabled these relationships to be extracted from a minimal number of experiments.

4.2 Microfluidic devices

The DoE experiments using high shear-homogenisation produced a range of large surface areas. To complement this and extend the lower end of the range of surface areas accessible, microfluidic devices were investigated. Microfluidic devices offer an attractive method for emulsion formation due to the defined channel geometries and typically serial nature of droplet formation (Christopher and Anna, 2007). This reportedly leads to a much narrow droplet size distribution (Steegmans *et al.*, 2009) compared with the high shear homogenisation method used previously.

Two geometries of glass microfluidic chip were initially chosen to create droplets, the T-Junction, and the flow focused. Each of the chips had junction dimensions of 100 μm. Similar to the previous section, oil-in-water emulsions were created in these devices. Therefore, the devices used were hydrophilic, unmodified glass. This is important to ensure that the dispersed phase (in this case oil, known to be hydrophobic) would preferentially not wet the walls, facilitating oil droplet formation (Li *et al.*, 2007, Xu *et al.*, 2006).

It is worth noting that, due to the microscopic length scales encountered in microfluidic devices, the choice of equipment and reagents were critical. More specifically, as suggested in the introduction to this chapter, the choice of surfactants imposed additional constraints when applied in a flow process.

Unlike the batch-wise methods used in the high shear homogenisation formulations, the surfactant had to be dissolved within one of the phases. Since the surfactant used for previous studies, Brij-S10, had a reported melting point of approximately 38 °C, this had to be heated to achieve a homogeneous solution or dispersion within one of the phases. Very limited aqueous phase solubility was observed for the surfactant even upon heating. Whereas, upon heating the surfactant in the oil phase to 45 °C, a transparent solution was obtained. However, upon cooling again to room temperature at oil phase surfactant concentrations higher than 1 wt% the entire mixture solidified, forming a gel. Attempts to combine continuous heating of the oil phase lines, so that oil containing higher surfactant quantities could be effectively pumped, proved unsuccessful. Whilst the high fluid surface area to volume ratio present in flow line facilitated rapid heat transfer, this was also an issue as certain fixtures and fittings were unable to be heated effectively. It was surmised that these created blockage points, increasing the line pressure drop to a point which resulting in pump failure. An effective heating solution could no doubt be constructed, but this was not pursued since the previous studies showed that surfactant levels of 1 wt% were sufficient to produce emulsions.

Complete solubilisation of the Brij-S10 even at the 1 wt% level was important since small levels of solid crystallites were observed to accumulate and block the channels, as shown in Figure 4.8.

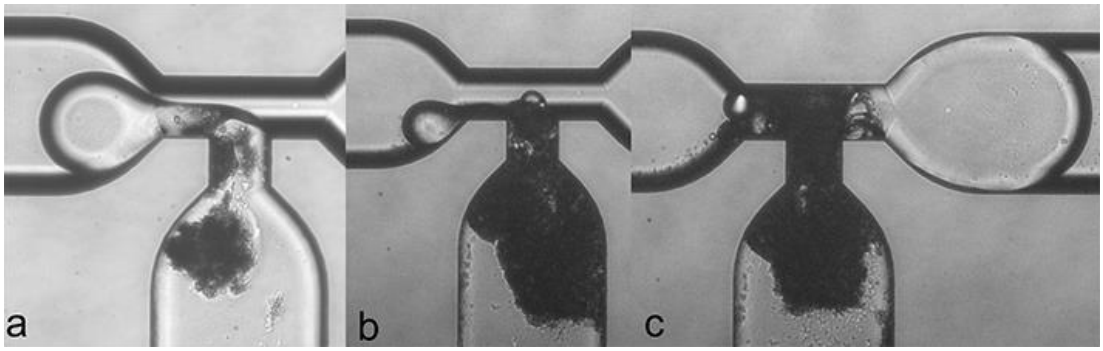

Figure 4.8 – Progressive blockage of the flow channel by accumulation of undissolved Brij-S10 in a microfluidic T-junction. Oil phase containing surfactant is flowing up from the bottom in each case and the aqueous continuous phase flowing right to left.

4.2.1 T-junction Chip Geometry

The ability to alter the droplet size and hence surface area was investigated firstly using the T-junction geometry chip. The oil and surfactant phase was pumped in perpendicular to the aqueous phase, resulting in droplet formation over a range of flow rate ratios, φ. The results and conditions, along with assignment to the reported droplet formation regime are summarised in Table 4.2.

Table 4.2 – Result of the droplet formation in 100 μm T-junction geometry chip. (sample size approx. 50 droplets)

Surfactant wt% oil phase	**Aqueous phase flow rate (Q_c) / μL.min^{-1}**	**Dispersed phase flow rate (Q_d) / μL.min^{-1}**	$\varphi = Q_d / Q_c$	**Droplet diameter / μm (±1 S.D)**	**Flow regime**
1% Brij-S10	10	10	1	104 (±15)	Dripping
1% Brij-S10	50	10	0.2	108 (±12)	Dripping
1% Brij-S10	100	10	0.1	169 (±8)	Jetting/Dripping
1% Brij-S10	200	10	0.05	117 (±12)	Jetting

No clear trend could be observed over the range of flow rate ratios investigated, although a range of droplet formation regimes was observed. Curiously no squeezing regime was observed.

The Jetting/Dripping listed in Table 4.2 is exhibited in b) and d) of Figure 4.9 was hard to classify. It was neither classical dripping as seen in c) nor, possessing a long jet as in a). The

classification of dripping/jetting was used as it could be viewed as an intermediate regime between the two.

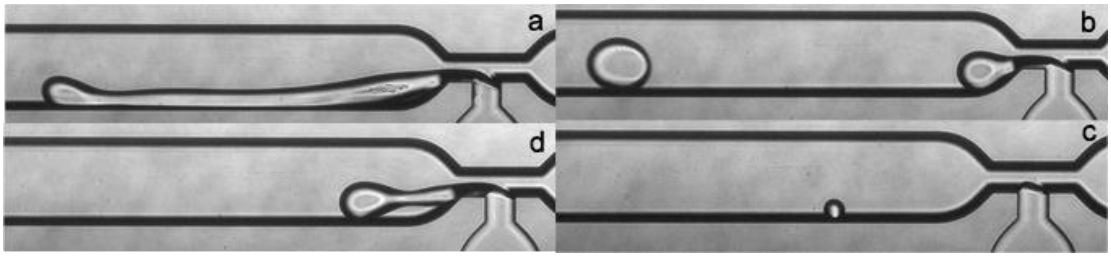

Figure 4.9 – Droplet formation regimes using 1% Brij-S10 in sunflower oil. a) Jetting, b) dripping/jetting, c) dripping, d) dripping/jetting

Upon comparison with the T-junction geometries reported in other microfluidic devices (De Menech *et al.*, 2008, Garstecki *et al.*, 2006, Gupta and Kumar, 2010, van der Graaf *et al.*, 2005), the explanation for the lack of squeezing regime becomes apparent. The immediate enlargement of the downstream flow path, effectively removes the channel constriction which is critical in the formation of a squeezing regime. This geometry allows for a 'by-pass' for the continuous phase, minimising the effective shear exerted on the oil stream (Figure 4.10).

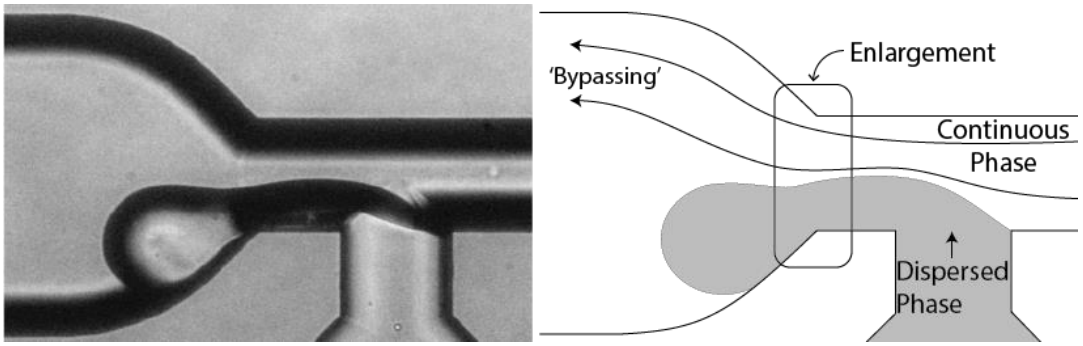

Figure 4.10 – Proposed continuous (aqueous) phase by-passing within the T-Junction geometry.

This has an effect on the ability of the device to exhibit a squeezing regime. This also has implications for the formation of other regimes, which are also dependent on the shear exerted by the continuous phase. The extra phase observed somewhere between dripping and jetting could be explained by this geometry. If the neck of the drip, detaching from the junction, was long enough so that the forming droplet protruded into the enlargement, the shear rate would be decreased due to continuous phase by-passing allowing for an extended period of drop growth within the opening. This would lead to enlarged droplets, as shown in the series of droplet generation photographs given in Figure 4.11.

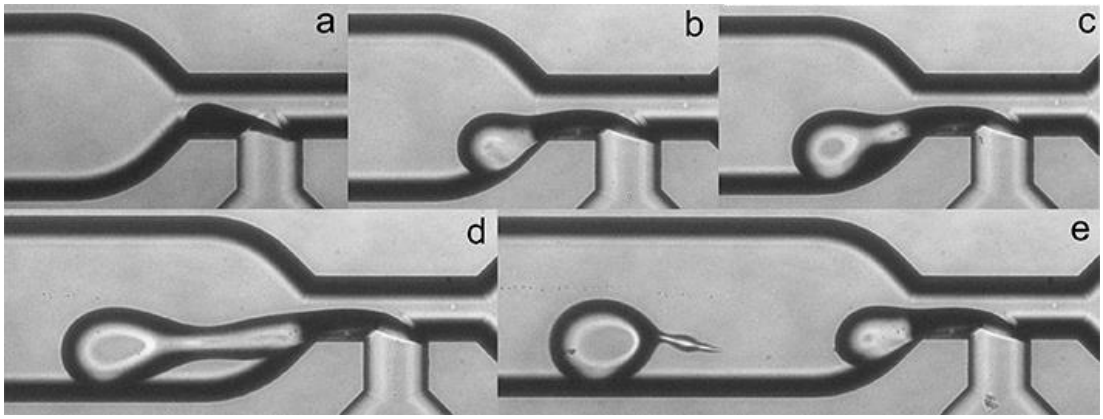

Figure 4.11 – Transition from dripping to dripping/jetting with droplet neck elongation into outlet (a-b) enlargement followed by droplet growth (c-d) and subsequent detachment (e)

Droplet sizes between approximately 100 and 200 μm could be created using this configuration of device over the range of flow rates.

4.2.2 Flow Focused Chip Geometry

For the flow focused geometry chip, the oil and surfactant phase was pumped in as for the T-junction chip, however this chip geometry required that two continuous, aqueous streams were introduced perpendicular to a single central dispersed phase. Again, the relative flow rates were characterised by a ratio, φ. The results and conditions, along with assignment to the reported droplet formation regime, are summarised in Table 4.3.

Table 4.3 - Droplet formation in 100 micron flow focused geometry chip (sample size approx. 50 droplets)

Surfactant wt% oil phase	**Aqueous phase flow rate (Q_c) / μL.min^{-1}**	**Dispersed phase flow rate (Q_d) / μL.min^{-1}**	$\varphi = Q_d / Q_c$	**Droplet diameter / μm (± 1 S.D)**	**Flow regime**
1% Brij-S10	10	1	0.1	179 (±4)	Jetting
1% Brij-S10	50	1	0.02	98 (±17)	Jetting
1% Brij-S10	100	1	0.01	101 (±8)	Jetting
1% Brij-S10	100	10	0.1	110 (±4)	Jetting
1% Brij-S10	200	10	0.05	114 (±10)	Jetting

The only observable droplet forming regime was that of jetting flow. Within the jetting regime Rayleigh-Plateau instability could clearly be observed, indicating that this was the method of droplet break up. Indeed this method of droplet formation leads to a variation in the droplet diameter as illustrated in Figure 4.12 (a-b). This resulted in a degree of polydispersity of the droplets created under fixed flow rates. Despite this, the results seen here do not fit with the scaling relationships previously reported solely for capillary instability induced break-up. This would imply that a combination of both capillary

instability and viscous drag forces could potentially be influencing the break-up, as reported in the literature (Christopher and Anna, 2007). Since no universal droplet size prediction model for flow focused geometries could be found, the main theory available to offer comparison is the approximation offered by Utada *et al.* (2005),

$$R_d = \left(\frac{15 Q_d}{\pi} \frac{R_{jet} \mu_c}{\gamma} \right)^{1/3} \quad 4.1$$

Where R_d is the droplet radius, Q_d, is the dispersed phase volumetric flowrate, R_{jet}, is the radius of the impinging jet, μ_c, is the continuous phase viscosity and γ, is the interfacial surface tension between the continuous and dispersed phases.

The practical use, however, of Equation 4.1 relies on the determination of the radius of the impinging jet. As can be visualised in Figure 4.12, this was not straight forward as the jet varies quite significantly owing to the instability effects discussed previously. Taking the jet radius to be approximately 100 µm, slightly smaller than the junction width, the droplet radius was calculated to be between 5 and 10 µm. As is apparent from the results in Table 4.3 and Figure 4.12 c this is not representative of the true droplet size, with an under estimation of about ten times, indicating that perhaps this is not true jetting flow.

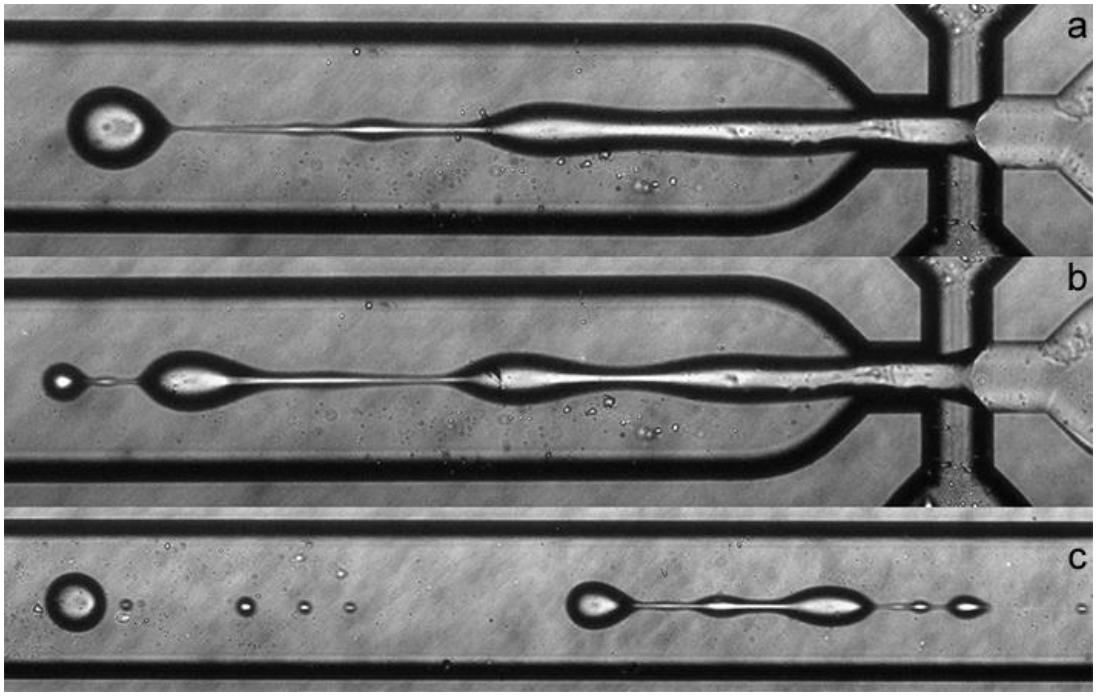

Figure 4.12 – Droplet formation within the jetting flow regime. Droplet formation of different sizes (a-b) due to Rayleigh-Plateau instability. Detached droplets/ droplet chain downstream after and before break up (c).

Curiously, no dripping regime was observed over the range of flow rates measured. The reason for this could, again be due to the enlargement after the cross joint, similar to the explanation for T-junction bypassing as previously discussed.

Droplet sizes between approximately 100 and 200 μm could be created using this flow focused configuration of device over the range of flow rates examined (Table 4.3).

Overall the achieving monodisperse droplet formation in these microfluidics systems was not straightforward. The small variation in produced droplets sizes across both devices and across the range of flow rate ratios investigated, suggest that the unchanging variables, such as, for example, surfactant concentration and channel width at the junction, may be the defining factors. The work by Garstecki *et al.* (2006) confirms such a hypothesis that interfacial factors, such as those influenced by surfactant dominate over shear factors in systems with capillary numbers, Ca_c, greater than ~ 10^{-2}. For comparison the capillary numbers of the fluids flows in the research conducted herein were orders of magnitude smaller, approximately 10^{-7}.

For both microfluidic devices the range of droplet sizes created was between approximately 100 and 200 μm. This corresponds to a surface area range of 0.06 - 0.03 $m^2.g^{-1}$, an order of magnitude smaller than that produced by high shear homogenisation. Development of exact droplet size relationships for the flow and system parameters, after this initial study, was outside the scope of this project.

4.3 Glass T-junction capillary device

A glass capillary reactor was constructed, based upon the principle of segmented flow (Tice *et al.*, 2003). The creation of defined plugs of dispersed phase constrained within a capillary promised defined and measurable interfacial areas. This section contains the results for the studies of the influence of the different flow rates upon the formation of a defined series of interface areas. The mathematical derivation of the defined surface areas for each plug based on simple geometry rules is also discussed. As with the microfluidic chip devices, in order to achieve definable plugs of confined dispersed phase, hydrophilic glass was used to avoid wall wetting by dispersed phase. This is demonstrated later in the discussion regarding glass-oil-water phase contact angle.

The interphase contact surface area of a plug within a capillary will depend on:

1. The diameter of the capillary
2. The shape of the interface

The wettability of the capillary wall surface with the plug material plays a role in defining the shape of the interface between the two phases. It was assumed that the sides of the plug did not contribute towards the liquid-liquid surface area. This assumption was based on the fact that the end goal was to perform reactions utilising these systems. Any reaction components present in the thin film of continuous phase between the plug and the walls were assumed to be bulk diffusion limited and therefore not significantly able to influence the rate of reaction. Indeed the same assumption, that the wall sides were unavailable for mass transfer, based on visual observation of no thin film was reported by a neutralisation experiment conducted by Burns and Ramshaw (2001). Visual confirmation of a thin film was reported for a hydrophobic wall surface by Kashid *et al.* (2005) although a comparison of the two systems above by Dessimoz *et al.* (2008) report comparable mass transfer coefficients (~0.5 s^{-1}). For these reasons a thin film approach was not considered.

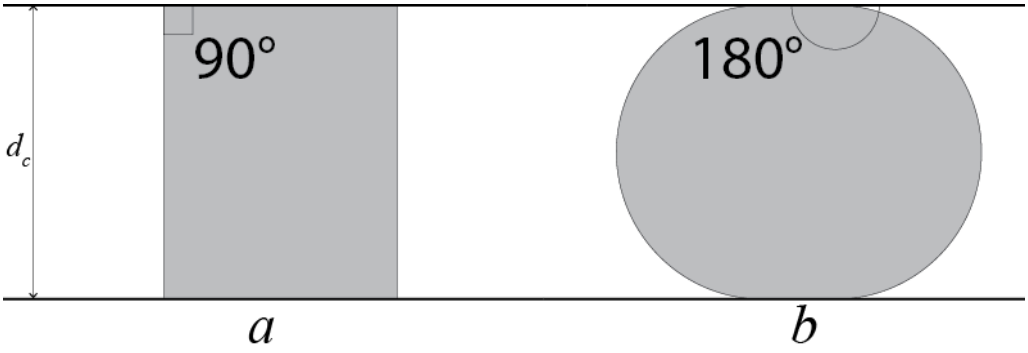

Figure 4.13 – Theoretical cross section of plug shapes with a contact angle of 90° and 180° within a flow channel. Cylindrical plug (a) and hemispherically capped plug (b).

Assuming a cylindrical channel then the minimum surface area a given plug of set volume has, excluding the area touching the walls, would be twice the area of a circle of diameter equal to the channel width,

$$Area\ of\ cylindrical\ plug = \frac{\pi d_c^2}{2} \qquad 4.2$$

Whereby d_c is the channel diameter as indicated in Figure 4.13.

Therefore the maximum area would be twice this, the surface area of a sphere,

$$Area\ of\ hemispherically\ capped\ plug = \pi d_c^2 \qquad 4.3$$

In reality the value must be somewhere in between these two extremes. In fact the area of a single cap can be calculated:

$$Area\ of\ cap = 2\pi rh \tag{4.4}$$

Where *h* is the height of the cap, and *r* is the radius of a theoretical spherical droplet of the same curvature as the cap. To calculate the height of this cap the contact angle needs to be known. When the height of the cap is the same as radius of the channel the surface area reduces to the area of a sphere as in. The height of the cap can be calculated from the triple phase contact angle between the plug phase, the continuous phase and the capillary wall. This was measured using the captive bubble method for the system and the contact angle was determined to be 121° (Figure 4.14).

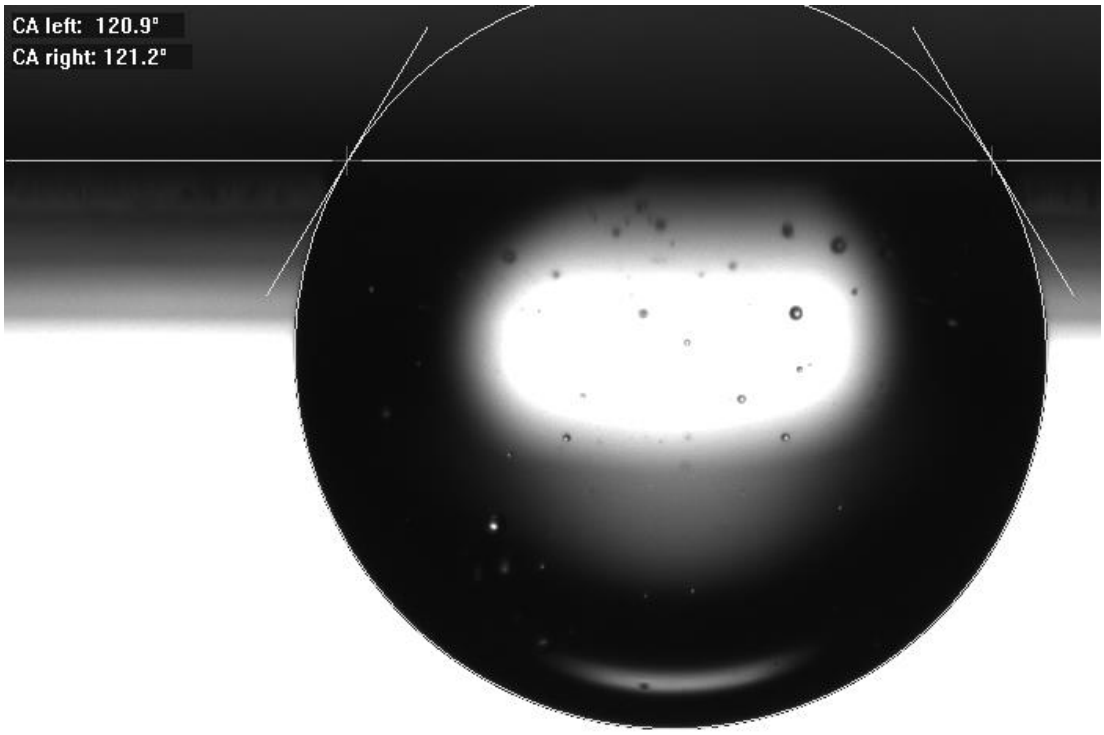

Figure 4.14 – Captive bubble contact angle measurement for a sunflower seed oil droplet in water against borosilicate glass.

The main assumption in using this method is that the confined plug will possess the same contact angle as the free droplet.

Knowing the contact angle, the height of the cap could be calculated from the relationship shown in Figure 4.15 and the derivation that follows.

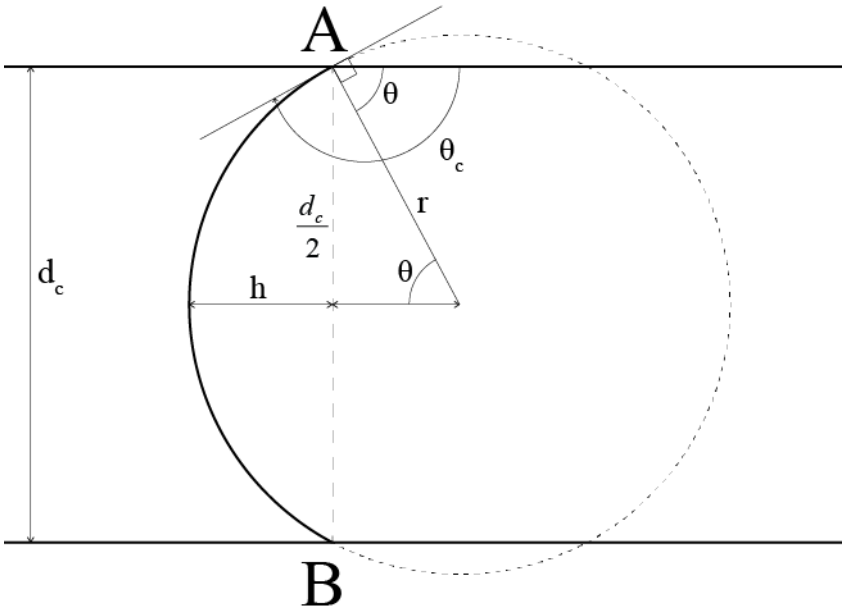

Figure 4.15 – Calculation of arc AB height from chord AB (cap height in an axisymmetric channel) of a bounded circle.

The height can thus be calculated:

$$\theta = \theta_c - 90° \tag{4.5}$$

where θ_c is the contact angle.

$$r = \frac{2\sin\theta}{d_c} \tag{4.6}$$

$$h = r - \frac{d_c}{2\tan\theta} \tag{4.7}$$

Thus Equations 4.5 - 4.7 can be substituted into Equation 4.4 to yield and expression for the area of a cap based upon the contact angle and the diameter of the channel,

$$Area\ of\ cap = 2\pi\left[\left(\frac{2\sin(\theta_c - 90)}{d_c}\right)\left(\frac{2\sin(\theta_c - 90)}{d_c} - \frac{d_c}{2\tan(\theta_c - 90)}\right)\right] \tag{4.8}$$

The surface area per plug is twice this, assuming that the bounded sides to not count towards the interface area,

$$SA_p = 4\pi\left[\left(\frac{2\sin(\theta_c - 90)}{d_c}\right)\left(\frac{2\sin(\theta_c - 90)}{d_c} - \frac{d_c}{2\tan(\theta_c - 90)}\right)\right] \tag{4.9}$$

Therefore the surface area per plug, SA_p, assuming no contribution from the plug sides could be calculated as 1.68 μm^2 for a contact angle of 121°.

Knowing the volume of the dispersed phase within a defined length of capillary, the number of plugs and the dispersed phase density, the specific surface area, SSA could be calculated,

$$Specific\ Surface\ Area,\ SSA = \frac{SA_p \times n}{\rho_d v_d} \qquad 4.10$$

Where SA_p is the surface area per plug, n the number of plugs, ρ_d the dispersed phase density and v_d the dispersed phase volume in the reactor.

Table 4.4 – Surface area per gram attainable from different flow rates

Dispersed phase flow rate (Q_d) / µL.min^{-1}	**Aqueous phase flow rate (Q_c) / µL.min^{-1}**	$\varphi = Q_d / Q_c$	**SSA @ 121° contact angle / m^2.g^{-1}**
1	100	0.01	5.57 x 10^{-3}
10	100	0.1	1.42 x 10^{-3}
25	100	0.25	1.23 x 10^{-3}
50	100	0.5	1.05 x 10^{-3}
100	100	1	7.90 x 10^{-4}
20	200	0.1	1.48 x 10^{-3}
50	200	0.25	1.38 x 10^{-3}
100	200	0.5	1.14 x 10^{-3}
200	200	1	9.60 x 10^{-4}

The resultant SSA for dispersed flow rates between 1 and 200 µL.min^{-1} and aqueous flow rates of 100 or 200 µL.min^{-1} are reported in Table 4.4. The results above show an inverse relationship with an increase in flow rate ratio resulting in a decrease in the SSA. In all cases the number of plugs observed increased with increasing flow rate ratio. The largest attainable SSA of dispersed phase was 5.57 x 10^{-3} m^2.g^{-1} obtained with the lowest flow rate ratio, φ = 0.01. This was because, whilst the total surface area formed at flow rate ratio was small, the mass of the dispersed phase was very low hence resulting in the largest area per gram. The error was calculated, from repeated runs under identical conditions, to be less than 5%. The use of identical volumetric flow rate ratios at different absolute flow rates were roughly comparable, although a higher set aqueous phase flow rate (200 µL.min^{-1}) resulted in a slightly larger SSA in every case. The small variation observed between the same flow rate ratios can only be attributed to a slight difference in the number of plugs obtained, resulting in a slight difference in plug length (since identical volumes were in the capillary). However, the defining factor was clearly was the flow rate ratio with the absolute flow rates predominantly resulting in a decrease in residence time within the capillary.

The range of surface areas obtainable with this technique was between 9.6 x 10^4 and 5.57 x 10^3 $m^2.g^{-1}$ (equivalent approximate spherical droplet size 1-2 mm). This represented an order of magnitude decrease from the surface areas obtain via the microfluidic methods and two orders of magnitude decrease from the high shear homogenisation investigations.

4.4 Conclusion

The experimental outcomes reported in this chapter show that a series of techniques (high shear homogenisation, microfluidics and glass capillaries) enabled the reproducible formulation of oil in water dispersions possessing a range of interfacial areas, summarised in Table 4.5.

Table 4.5 – Comparison of the different specific surface areas obtainable using different dispersion techniques

Technique	**Specific Surface area**	**Approximate equivalent droplet size**
High Shear Homogenisation	0.27 - 3.8 $m^2.g^{-1}$	~ 1-10 μm
Microfluidics – Glass droplet generator chip	3.0 x 10^{-2} – 6.0 x 10^{-2} $m^2.g^{-1}$	~ 100-200 μm
Glass capillary reactor	9.6 x 10^{-4} - 5.6 x 10^{-3} $m^2.g^{-1}$	~ 1000-2000 μm

The formulation of large interface areas (0.27 - 3.8 $m^2.g^{-1}$) is possible through use of high shear homogenisation. The stirring speed and oil to surfactant ratio are the most critical factors in determining the interface area obtainable. Interestingly the DoE approach showed potential for additional insights into the emulsions system. The approximate maximum surface area when using 1 wt% (based on oil phase) Brij-S10 as surfactant was observed to be between 0.5 - 0.75 m^2 per gram of oil phase. For the high shear homogenisation the design of experiments method enabled a four variable system to be modelled with sufficient statistical confidence to allow for surface area predictions.

The use of microfluidic devices allowed for the creation of an intermediate range of droplet sizes and hence interface areas (0.06 - 0.03 $m^2.g^{-1}$). The geometry of T-junction chips with an immediate enlargement downstream, whilst reducing pressure drop, resulted in a complicated flow pattern and as a result only the dripping and jetting droplet generation

regimes were observed. An intermediate transitional regime which portrayed characteristics of both was also observed for a dispersed phase/ aqueous phase flow rate ratio of 0.1.

The use of a flow focused geometry resulted in droplet generation in the jetting regime. This is characterised by a droplet break up method attributable to Rayleigh plateau instability as evidenced by the images captured using high speed photography. This break up method lead to polydispersity in the droplet sizes obtained for set flow conditions.

The use of a capillary T-junction was able to form a range of stable, very low interface areas (9.6×10^4 and 5.6×10^3 $m^2.g^{-1}$. The size of the interface was dependent on the flow rate ratio, with the lowest flow rate ratio (0.01) resulting in the highest specific surface area (5.6×10^3 $m^2.g^{-1}$).

5 Analysis of a Liquid-Liquid Chemical Process

Within the overall framework of this project, to develop a procedure for liquid-liquid biphasic reaction optimisation whilst integrating separation, this chapter contains the results and discussion from the study of the chemical steps taking place. To understand each of these steps, one must know how the reaction conditions affect the observed rate of reaction. In this way, the rate limiting step of the overall reaction system can be determined over a range of conditions. Obtaining such knowledge then enables focus of the optimisation process, for example, towards increasing the rate of inter phase mass transfer or perhaps towards increasing the rate of chemical reaction.

In order to conduct these investigations the reaction system had to be a biphasic liquid-liquid system. Following a review of the literature, the epoxidation of sunflower seed oil (Scheme 5.1) using an aqueous solution of sodium tungstate as catalyst and hydrogen peroxide as oxidant was selected. Acetic acid was also used and its role as a promoter is discussed. It was important that the reaction product, epoxidised sunflower oil was also oily, and hence immiscible with the aqueous phase. This would allow simple downstream separation and recovery of the product.

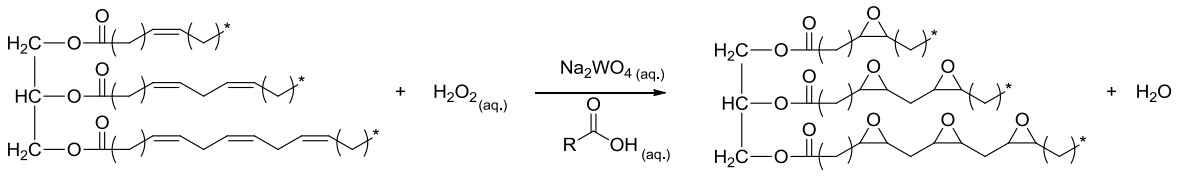

Scheme 5.1 – The epoxidation of sunflower seed oil by a sodium tungstate catalyst, hydrogen peroxide oxidant and acetic acid promoter.

The catalyst chosen for this model reaction was that used in previously reported investigations into biphasic systems (Sato *et al.*, 1998, Sato *et al.*, 1996, Sato *et al.*, 1997). This catalyst was shown to be highly effective for the conversion of alkenes to epoxides under mild conditions when used in conjunction with hydrogen peroxide as an oxygen source. The use of hydrogen peroxide as a green oxidant is well known, with a 47 % atom efficiency and water as the only by-product (Noyori *et al.*, 2003, Goti and Cardona, 2008, Jones, 1999).

A reaction temperature of 60 °C was selected as, at this temperature, both phases remained liquid, and the reaction proceeded at a reasonable rate. No solvents were used, specifically no chlorinated solvents which are traditionally used for the dissolution of triglycerides.

Contrary to what is widely reported for biphasic reactions, dedicated phase transfer agents such as quaternary alkyl ammonium salts were not used in this investigation. Such phase transfer catalysts (PTCs) are used to alter the partitioning of species between phases and, as such, have the potential to alter the rate limiting step. Since detecting whether or not interphase transfer was limiting was one of the major aims of this research, added PTCs were not used.

There are four stages which must occur in this biphasic oxidation reaction (Figure 5.1):

1. aqueous phase formation of active catalyst species from the reaction of sodium tungstate, hydrogen peroxide and acetic acid;
2. transfer of the active catalyst species from the aqueous phase to the oil phase;
3. reaction of the active catalyst species with the unsaturated sites in the triglyceride to form epoxide product; and
4. transfer of the spent catalyst back from the oil phase to the aqueous phase to be reoxidised.

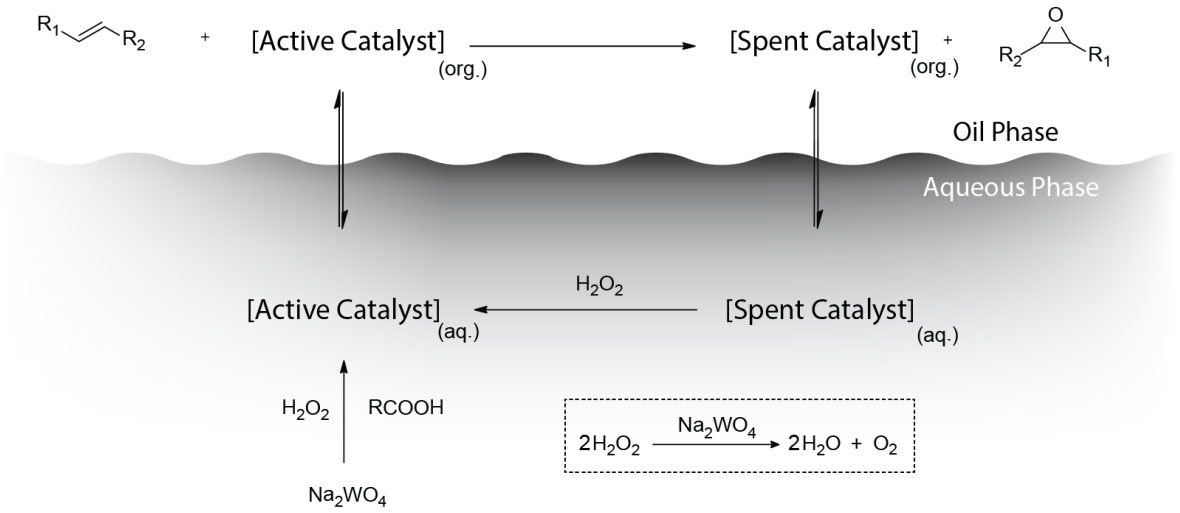

Figure 5.1 – Reaction stages for the catalysed biphasic epoxidation of sunflower seed oil. The oil phase is pure sunflower oil however only the unsaturated sites on the triglyceride are assumed to take part in the oxidation.

Each of the four stages proposed above for the epoxidation was investigated to determine the rate limiting step of the epoxidation. The dependence of the observed rate of epoxidation on the variation of:-

- the interface area, enabled the investigation of the interface transfer steps, steps 2 and 4;
- the concentrations of the aqueous phase components (sodium tungstate, hydrogen peroxide, acetic acid) allowed for investigation of the catalyst formation step, step 1; and
- the starting concentrations of alkene groups allowed for investigation of the oil phase epoxidation step, step 3.

The differential method of analysis, based on initial rates of reaction, was used to determine reaction progress. The initial rates of reaction were extracted from the gradient of the plot of epoxide concentration against time at low conversion (<20%). The epoxide concentration was determined by comparing the well-defined integrated signals assigned to the alkene and epoxide groups in the triglyceride molecule in the ^{1}H–NMR (nuclear magnetic resonance spectroscopy) spectra for each time sample using the glycerolic signals as an internal standard. All other concentrations were fixed unless stated otherwise. Algebraically this method can be expressed as pseudo first order (rate constant = *k'*) for the component under analysis, *I*, setting all other components as constant:

$$r_{epox.} = \frac{dC_{epox.}}{dt} = -\frac{dC_{alkene}}{dt} = k'\mathrm{C}_{i,\mathrm{species}}{}^{n} \qquad 4.11$$

The order of reaction, n, could be calculated by plotting the logarithm of the initial rate against the logarithm of the initial concentration of the species under investigation, $C_{i,species}$, (Equation 4.12) .

$$\log r_{epox.} = \log k' + n \log C_{i,species} \qquad 4.12$$

5.1 Effect of the inter-phase surface area

The resulting dispersions with a range of interfacial areas reported in Chapter 4 were used in the reaction system described above to determine the importance of the interphase mass transfer step with relation to the observed rate of reaction.

Table 5.1 - Range of inter-phase droplet surface areas

Technique	**Specific Surface area / $m^2.g^{-1}$**	**Equivalent droplet size / µm**
High shear homogenisation	0.27 - 3.8	~ 1-10
Microfluidics – glass droplet generator chip	$3.0 \times 10^{-2} – 6.0 \times 10^{-2}$	~ 100-200
Glass capillary reactor	$9.6 \times 10^{-4} - 5.6 \times 10^{-3}$	~ 1000-2000

An initial set of scoping reactions were carried out at 60 °C, using a stirrer hotplate and magnetic stirrer to ascertain a crude understanding of the effect of interface area on a biphasic non-emulsified system without surfactant. A set of control emulsification experiments with added surfactant, were also performed to investigate any stirring effects if any, as well as to provide a useful comparison.

The emulsions for this comparison were formed using high shear homogenisation with the oil phase containing 10 wt% of surfactant, Brij-S10, which was preheated, followed by addition of preheated aqueous phase containing sodium tungstate, hydrogen peroxide and acetic acid. The final aqueous phase volume was 90% in all cases.

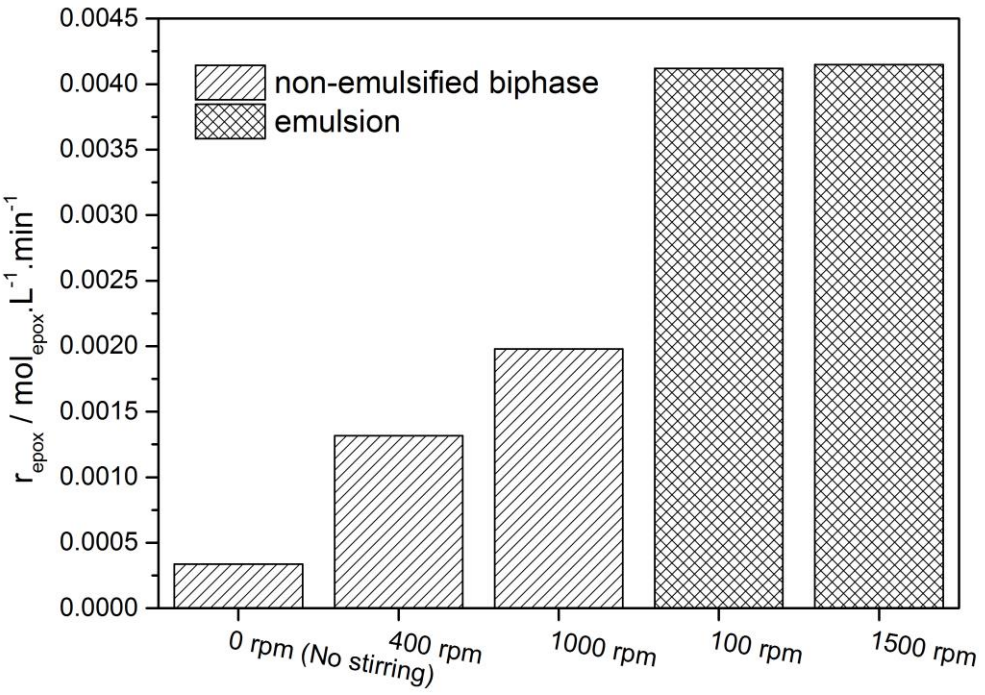

Figure 5.2 – Comparison between the observed rates of epoxidation with different stirring speeds under both emulsified (10 wt% Surfactant in oil) and non-emulsified biphasic conditions. Conditions: 60 °C. aqueous phase concentrations: 2 M AcOH, 0.1 M Na_2WO_4, 3 M H_2O_2 (18 fold molar excess).

From the results presented in Figure 5.2 it is clear that an increase is observed in the rate of epoxidation with increased stirring speed under the non-emulsified biphasic conditions. This is indicative of the influence of surface area, which is assumed to increase with increased agitation. In other words, the system was mass transfer limited. A small degree of conversion of alkene to epoxide (5% in 24 h) was detected even with no stirring at all, meaning that no actual agitation was required for successful reaction. The rate in this case however was extremely low so as to not be practically useful.

Stirring speed had no effect on the rate of conversion to product in emulsions, indicating that there is no bulk mass transfer limitation when the oil and aqueous phases are emulsified. The rates of reaction are much higher for the emulsified reaction, over double those for even the high stirring speed.

Further comparison across a range of interfacial surface areas was conducted by two different methods. The dispersions obtaining high and intermediate areas ($0.27 – 6.0 \times 10^{-2}$ $m^2.g^{-1}$), produced by both high shear homogenisation and microfluidics, were reacted in batch. This involved preformation and preheating of an emulsion of oil in water supported by surfactant, by the particular method chosen, followed by addition of preheated aqueous

solution of sodium tungstate, hydrogen peroxide and acetic acid at the selected concentrations. Very low interface areas ($9.6 \times 10^{-4} - 5.6 \times 10^{-3}$ $m^2.g^{-1}$), achieved using the plug flow approach in the capillary reactors, were investigated by charging both the oil (containing 1 wt% Brij S10) and aqueous catalyst phase into the preheated reactor followed by closure of inlets and outlets in a stop flow arrangement.

The confined use of hydrogen peroxide was challenging for the low interfacial surface area experiments in the capillary reactor. Due to the very small volumes of the reactor (300 μL) even very low levels of hydrogen peroxide decomposition, below measurable amounts, created problems due to bubble formation. This was mitigated through careful selection of construction materials to avoid formation of gases.

The comparison drawn in Figure 5.3 across the four order of magnitude range of interface areas tested shows that increasing interfacial area results in an increase in the rate of epoxidation. Analysis of Figure 5.3 suggest an inflection at around 0.25 $m^2.g^{-1}$ where there is a shift in observed rate response to surface area. Above this value a smaller interrelationship is observed, below which a much larger mass transfer dependence is observed. The response from the surface area is similar to that seen for the Frössling correlation for rate of a surface reaction on a solid particle, indicating that the observed rate of reaction is shifting dependencies between reaction limitation for high surface areas and mass transfer limitation for low surface areas. A plateau was not reached for larger surface areas, however it is clear from Figure 5.3 that increasing the surface area yet further, will have an increasingly minimal effect on the observed rate, i.e. there will be a diminishing return, until finally the rate is independent of the interfacial surface area.

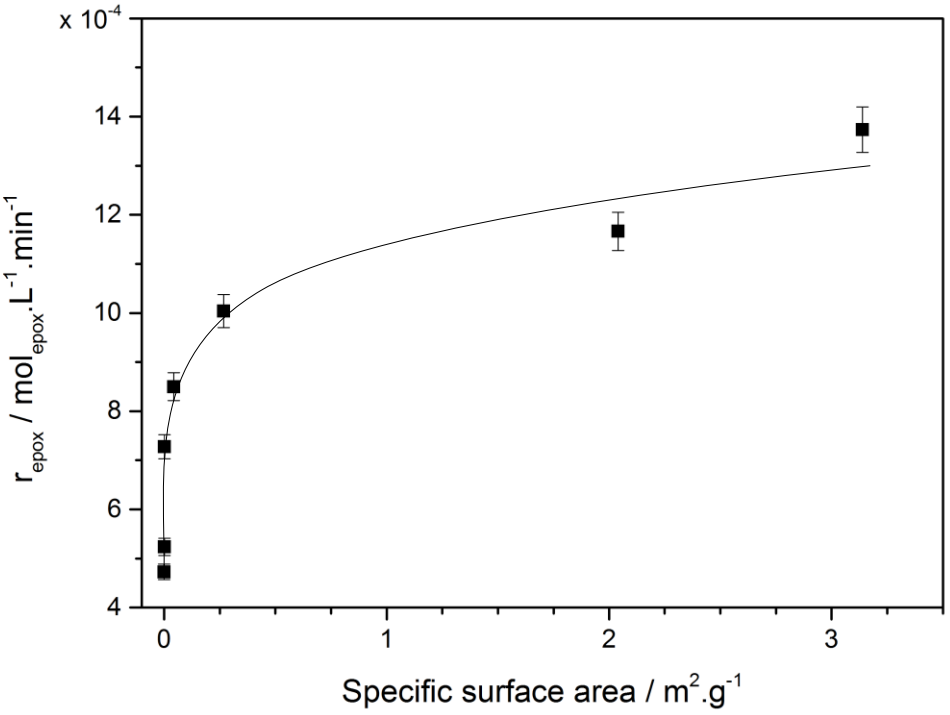

Figure 5.3 – Comparison between the rates of observed epoxidation over the whole range of surface areas achievable from the different surface area creation techniques. Conditions - 60 °C, aqueous phase concentrations = 1 M AcOH, 0.1 M Na_2WO_4, 3 M H_2O_2.

To try and understand the increase in observed rate in the region of high surface area, a more detailed examination of the mass transfer process was considered. The lack of response to stirring speed shown for the reactions indicates that bulk diffusion in the aqueous phase is not a limiting step under these conditions. Any mass transfer limitation must therefore either be due to a hindrance of penetration of the interface, or diffusion from the interface internally within the oil droplet.

Focussing on the internal diffusion within the oil droplet, from mass transfer theory, this must occur within a thin film inside of the droplet surface. For smaller droplets the volume percentage occupied by the internal film of given thickness will be larger than for larger droplets. At a certain droplet size the volume occupied by the film will equal the volume of the droplet, indeed it may even exceed it that is to say that the thin film thickness is greater than the radius of the droplet. Under such a condition, due to the reduced diffusion path and hence diffusion time (Mcclements and Decker, 2000) the concentration of any diffusing compound will be higher at the centre than for a larger droplet. As the driving force to mass transfer is the concentration gradient of the transferred component, a higher minimum internal concentration with an assumed uniform 'external' concentration will result in a smaller rate of mass transfer. This effect could be small, and it is postulated that a process

such as this could be responsible for the continued increase in observed rate above the 0.25 $m^2.g^{-1}$ turning point.

From the results from this investigation one can conclude that reactions with interfacial surface areas above 0.25 $m^2.g^{-1}$ will not be significantly mass transfer limited.

5.2 Formation of active catalyst species

It is reported that the catalyst species responsible for oxidation is a combination of the sodium tungstate with the hydrogen peroxide oxidant, to form a peroxometallate species (Pope, 1983, Pope and Müller, 2001). There is also literature precedent suggesting that oxidation reactions using the peroxometallate can be promoted through complexation of an acid (Noyori *et al.*, 2003, Maheswari *et al.*, 2006). Since this system is catalytic, a reoxidation process of the active species must occur at steady state. In this section the variables involved in both the initial creation of the active catalytic species as well as the reoxidation will be investigated, these will be treated as a single step, namely the formation of the active catalyst species. The observed rate dependence of the concentration of sodium tungstate, hydrogen peroxide and acetic acid was investigated. Extra attention was given to the use of acid since its role in promotion of this reaction is still yet to be fully elucidated.

To avoid any mass transfer limitations, the reactions were operated with the oil phase dispersed as an emulsion. The emulsions were made prior to reaction through high shear homogenisation with 80% aqueous phase, 20% oil phase (with 10 wt% Brij S10) at 13500 rpm for 10 minutes. Droplets with specific surface areas of 3.8 $m^2.g^{-1}$ were used for all experiments, far in excess of the 0.25$m^2.g^{-1}$ which was previously found to correspond to a mass transfer limited regime in Section 5.1. The emulsion and aqueous catalyst phase (the latter containing hydrogen peroxide, acid and sodium tungstate at the required amounts), were preheated to reaction temperature of 60 °C prior to combination. The final aqueous and oil phase volumes were 90% and 10% respectively.

5.2.1 Effect of the concentration of sodium tungstate

Perhaps the most logical starting point in the analysis of the rate dependence of this aqueous phase step was to determine the effect of the sodium tungstate concentration. The concentration of sodium tungstate was varied between 0.01 and 0.5 M whilst the concentrations of acetic acid and hydrogen peroxide were fixed at 3 M and 1 M respectively.

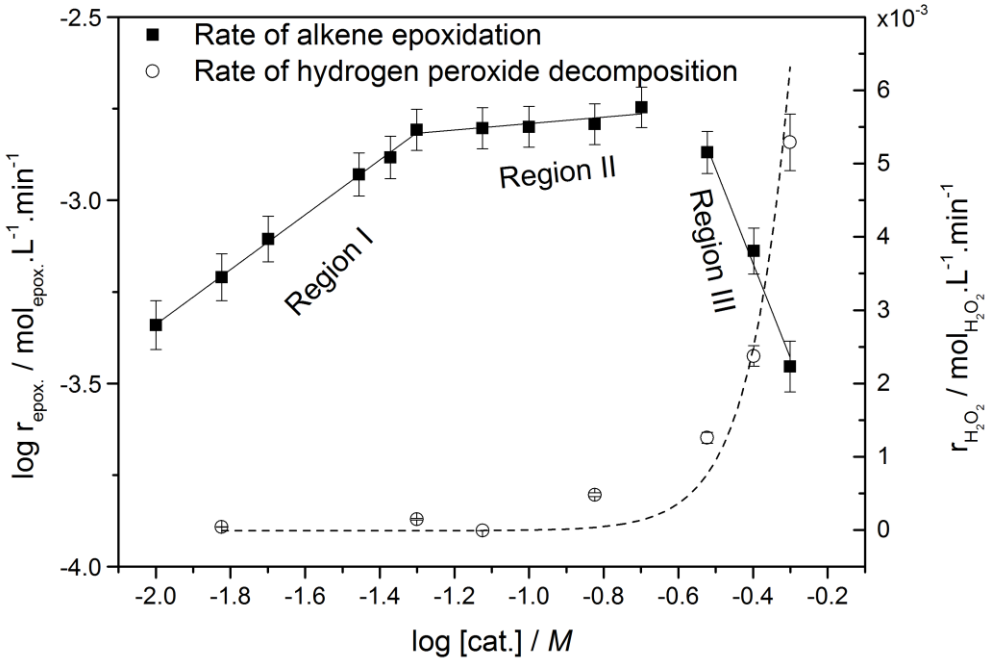

Figure 5.4 - Comparison of sodium tungstate concentrations on epoxidation rate (primary axis) and hydrogen peroxide decomposition rate (secondary axis). Conditions: 60°C, 1 M AcOH, 3 M H_2O_2

An increase in the loadings of sodium tungstate resulted in a complicated response in reaction rate when the log of rate of epoxidation against the log of sodium tungstate concentration was plotted (Figure 5.4)Three different regions can clearly be observed in Table 5.2.

Table 5.2 – Orders of reaction for the three observed regions of sodium tungstate concentration

Region	**[Na_2WO_4] / M**	**Apparent order of reaction with respect to Na_2WO_4**
I	0.01-0.05	0.75
II	0.05-0.2	0.09
III	0.3-0.5	-2.58

From 0.01 up to 0.05 M a linear relationship between sodium tungstate concentration and rate of epoxidation was observed, resulting in an apparent order of reaction of 0.75 with

respect to this catalyst. At concentrations above this (Region II, from 0.05 up to 0.2 M) an apparent order of reaction of 0.09 was observed, which, as shown in Table 5.2, is unchanging within the error defined by the experimental uncertainty in the analysis method. It was therefore justified in approximating this to 0 order. At the highest concentration range (Region III, from 0.3 up to 0.5 *M*) a strong negative correlation is observed with an apparent order of reaction of -2.58 with respect to sodium tungstate. From these results it suggests that the higher concentration of catalyst has a detrimental effect on the overall rate.

However, plotting the rate of decomposition of hydrogen peroxide at the various sodium tungstate concentrations reveals why adding more catalyst does not monotonously increase the rate of production of epoxide. Many metal complexes that are hydrogen peroxide activation catalysts are also hydrogen peroxide decomposition catalysts (Haber and Weiss, 1934) and so a study of the effect of aqueous phase composition on oxidant decomposition was conducted. Specifically, the rate of hydrogen peroxide decomposition was measured over the same range of sodium tungstate concentrations, Figure 5.4. A sharp increase in the decomposition rate is observed corresponding approximately to the region II/II boundary. Thus, the apparent rapid decrease in rate of conversion of alkene to epoxide is due to the decomposition of the oxidant and not to any change in the mechanism of the epoxidation reaction at elevated catalyst concentrations. It should be noted that the spontaneous decomposition of hydrogen peroxide under basic conditions is well known, with the instability attributable to the perhydroxyl anion under high pH conditions (Jones, 1999). However, under neutral or weakly acid conditions, such as those in this investigation (pH 4-5) decomposition is largely catalytically induced by inorganic agents.

This was an intriguing result as many authors (Noyori *et al.*, 2003, Deng *et al.*, 1999, Hoegaerts *et al.*, 2000, Li *et al.*, 2007) extol the virtues of sodium tungstate as non-active towards the unproductive decomposition of hydrogen peroxide, and hence its attractiveness for use in conditions such as these.

To try and understand the increase in decomposition, in light of the catalyst precursors commonly reported inactivity, a careful reanalysis of the results was required. As a result of fixing the acetic acid concentration at 1 M throughout these experiments, the ratios of the catalyst to acid were inadvertently changed.

Indeed one can substitute the x-axis in Figure 5.4 with catalyst: acetic acid molar ratios, as shown in Figure 5.5.

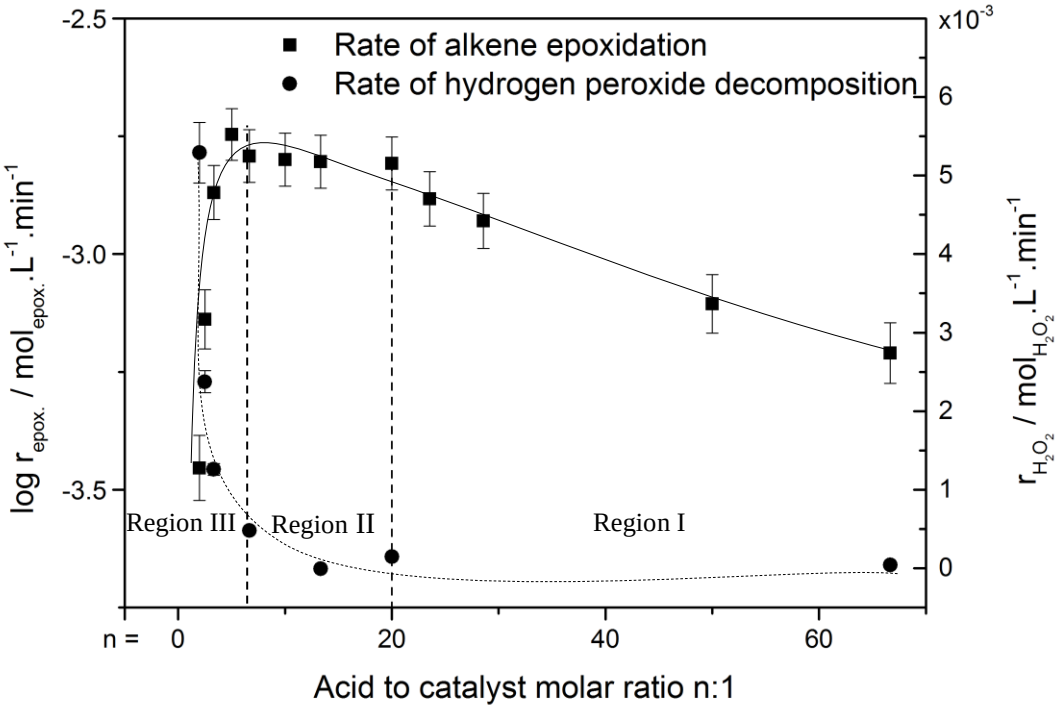

Figure 5.5 - Comparison of sodium tungstate concentrations on epoxidation rate (primary axis) and hydrogen peroxide decomposition rate (secondary axis). The x-axis shows the acetic acid to sodium tungstate ratio in the form n:1. The drop line indicates a ratio of 20:1, the inflection between Region I and Region II. Conditions: 60°C, 1 M AcOH, 3 M H_2O_2

Now the inflection points between the catalyst concentration regions can be determined as occurring at a defined ratio between sodium tungstate and acetic acid. Notably the carboxylic acid: catalyst molar ratios of 20:1 and the range 10:1-6.67:1 correspond to the transition from region I to II and II to III respectively.

In light of this, it can be hypothesised that the ratio between the catalyst and carboxylic acid was critical to avoid unproductive decomposition of the hydrogen peroxide. This can be tested by fixing the carboxylic acid to catalyst ratio to that of the first step change in reaction order where no decomposition was observed: 20:1. An experiment was performed changing the catalyst concentration over the accessible range 0.16 to 0.25 M, keeping the aforementioned ratio and fixing the hydrogen peroxide concentration at 3 M, as before. A linear relationship between the catalyst precursor concentration and rate of epoxidation was observed, Figure 5.6. The apparent order of reaction, whilst it could be calculated, could not be assigned owing to the fact that the change in observed rate was a result of a change in both the catalyst precursor and acetic acid concentrations. However a negligible rate of hydrogen peroxide decomposition was observed, confirming the hypothesis that it is the

ratio between acetic acid and sodium tungstate that is critical to controlling the unproductive decomposition of hydrogen peroxide.

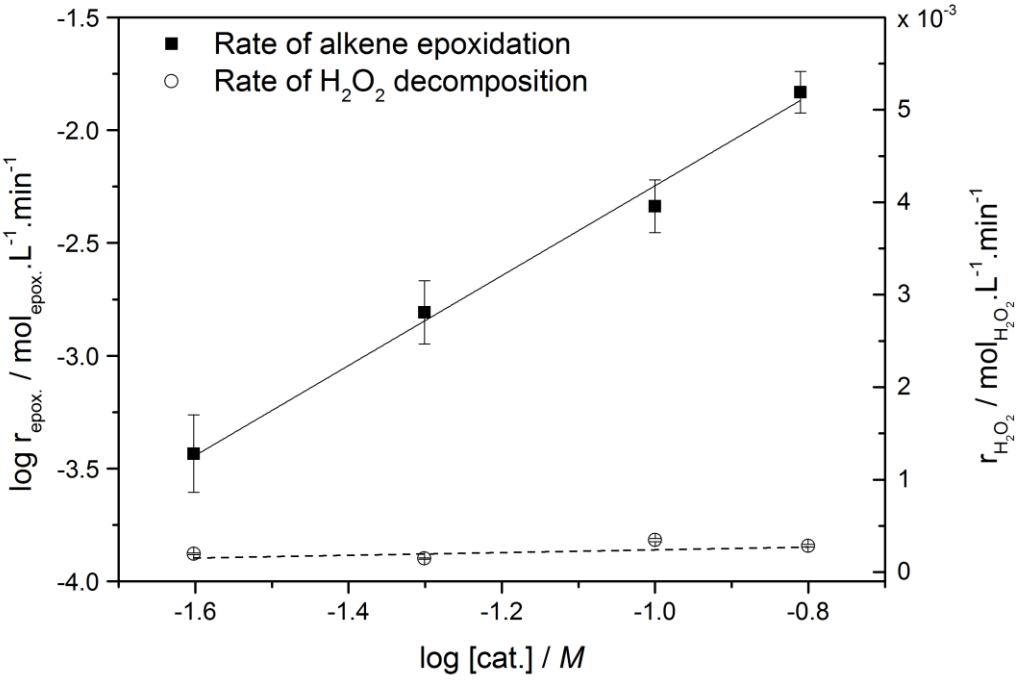

Figure 5.6 - Comparison of catalyst precursor concentrations on epoxidation rate (primary axis) and hydrogen peroxide decomposition rate (secondary axis) with a fixed catalyst precursor: carboxylic acid ratio. Conditions: 60°C, 3 M H_2O_2, AcOH:Na_2WO_4 20:1.

The combined (due to fixing the catalyst precursor and carboxylic acid ratio) order of reaction was calculated through determining the gradient of the linear regression in Figure 5.6 and found to be 2. The previously calculated order for catalyst precursor alone from the linear section of region I exhibited in

Figure 5.4 was 0.75. In order to deconvolute these orders of reaction, analysis of the effect of carboxylic acid alone was undertaken (Section 5.2.2).

To summarise, the dependence of the rate of epoxidation on concentration of catalyst precursor is linear, and approaches first order, but only when the decomposition of hydrogen peroxide is halted. The decomposition of hydrogen peroxide is high when insufficient acid is present.

5.2.2 Effect of the concentration and type of acid

As described in the previous section addition of acetic acid to the reaction mixture enhanced the rate of the epoxidation. In this section the role of an acid as a reaction promoter and hydrogen peroxide stabiliser will be considered.

Whilst the majority of the experimentation involves the use of a carboxylic acid, brief consideration is also given to the use of other acids. In the well-known work by Noyori *et al.* (2003) on the biphasic oxidation of alkenes, the use of phosphoric and phosphonic acids as promoters was described although their role was not described in detail. Complexation to the tungsten metal centre was suggested in this study, increasing the electrophilicity of the peroxo group for attack on the unsaturated sites although this was not probed in detail.

The use of phosphoric acid as a promoter was investigated spanning the range of the previous cited work (Table 5.3). There was no epoxide product observed, despite the longer reaction time and a tenfold increase in the amount of catalyst compared to alkene. The difference between this work and Noyori's is the lack of phase transfer catalyst (trioctylmethylammonium hydrogensulfate) and the lower reaction temperature of 60 °C compared to 90 °C in the published work.

Table 5.3 - Comparison between the reaction conditions for the use of phosphoric/phosphonic acids for the epoxidation of sunflower seed oil.

	Relative molar ratios standardised to moles of tungsten.				
Reaction	**Tungsten**	**Hydrogen Peroxide**	**Phosphoric/ phosphonic acid**	**Alkene**	**Yield / %, Time / h, Temp. / °C**
1	1	68	1.52	10	0, 6, 60
2	1	68	0.76	10	0, 6, 60
3	1	68	2.27	10	0, 6, 60
(Noyori *et al.*, 2003)	1	150	1 (0.60)*	100	87, 2, 90

*The acid used was a phosphonic acid but this was assumed to be largely decomposed (approx. 60% to phosphoric)

The only other likely source of acid in this reported system is the hydrogen sulfate anion of the phase transfer catalyst, which it was suggested is likely to be deprotonated under the reaction conditions. The use of sulfuric acid was investigated, under similar conditions as for the phosphoric acid tests. Since sulfuric acid is a relatively strong acid and hence can be assumed fully deprotonated in solution, the tungstate to acid ratios were 0.25, 0.50 and 0.75. Regardless, no epoxide was observed after 6 hours. Therefore it must be assumed that a phase transfer catalyst is required when used in combination with the mineral acids, showing a benefit in the use of carboxylic acids instead.

A detailed study by Maheswari *et al.* (2006) investigated the effect of a range of carboxylic acids on the epoxidation of alkenes. They also concluded that the promotion of the reaction rate was due to binding of acid to the tungstate centre. Additionally they proposed chlorinated carboxylic acids as offering the best rate enhancement for alkene epoxidation, due to the resultant increase in electrophilicity of the peroxo moiety on the active catalyst species due to enhanced electron donation from these ligands.

As shown in the previous section, the use of a carboxylic acid has both a beneficial effect on the rate of epoxidation, when used in conjunction with the sodium tungstate catalyst, and hinders the decomposition of hydrogen peroxide. The effect of changing the acetic acid concentration was investigated. The order of reaction with respect to the concentration of acetic acid on the epoxidation of sunflower oil was determined to be 1.24 through linear regression analysis of the data presented in Figure 5.7. This is in keeping with the previous results, namely being equal to the measured combined order of reaction seen when fixing acid and catalyst ratio (1.99) minus the order of reaction with respect to sodium tungstate alone (0.75).

The oxidation of acetic acid in-situ by the hydrogen peroxide was considered owing to the fact that the oxidation product, peracetic acid is a well-known oxidant for alkene epoxidation. The formation of peracetic acid was shown to proceed slowly with 30 wt% hydrogen peroxide and glacial acetic acid, with a maximum equilibrium concentration of 8.6 wt% after 80-90 hours (Greenspan, 1946). In comparison to the system used in this thesis, the concentration of reagents used in the cited work is much higher as well as utilising a sulfuric acid catalyst. This would indicate that the wt% of peracetic acid in the present system would be much lower over the course of the 6 hour typical reaction. In addition, the use of a higher reaction temperature (this work: 60ºC, cited: 23ºC) has actually been shown to be detrimental to the peracetic acid equilibrium concentration, whilst obviously expediting equilibrium (Zhao *et al.*, 2008, Zhao *et al.*, 2008, Zhao *et al.*, 2007). A control reaction performed under the typical conditions (6 h, 60ºC) and concentrations of 1 M AcOH, 3 M H_2O_2 yielded no observable epoxide without the use of sodium tungstate, confirming that a spontaneously forming peracid is unlikely to be the primary oxidant in this reaction. Despite the evidence in the work in this thesis the of peracid oxidants cannot be excluded since the exact mechanism of epoxidation has yet to be elucidated.

The rate of hydrogen peroxide decomposition was again confirmed to be negligible over the range of conditions tested, Figure 5.7.

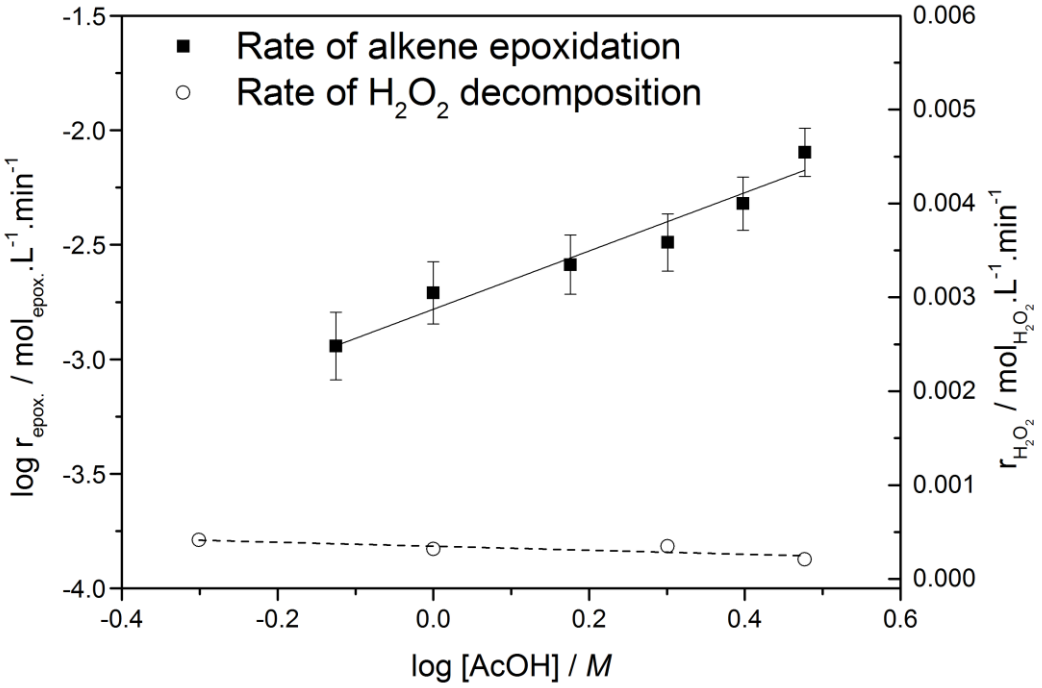

Figure 5.7 – Effect of the concentration of acetic acid on the rate of epoxidation of sunflower oil. Conditions: 60°C, 3 M H_2O_2, 0.1 M Na_2WO_4.

Since no phase transfer catalyst was required, unlike for both phosphonic and presumably sulfuric acids it seems that the carboxylic acid, if bound to the tungstate, could be increasing the solubility of the active catalyst in the oil phase. To test this, a range of linear carboxylic acids with varying hydrophobicity indicated by octanol/water partition coefficients, Table 5.4.

Table 5.4 - Carboxylic acid pKa, logP and pK_a, logP and solubility data from the CRC Handbook of Chemistry and Physics 94th Ed.

Acid	**pK_a**	**logP**	**Solubility / g.kg^{-1} H_2O, 25 °C**
Ethanoic (acetic)	4.79	-0.17	Miscible
Propanoic (propionic)	4.87	0.33	Miscible
Butanoic (butyric)	4.82	0.79	Miscible
Pentanoic (valeric)	4.83	1.39	45
Hexanoic (caproic)	4.85	1.92	11

The rate of epoxidation increased as the carboxylic acid chain length increased from two to four, however at higher chain lengths (> 4 carbon atoms) the rate of reaction was dramatically reduced. These results can be explained by considering both the partition

coefficient and aqueous solubility data of the acids (Table 5.4). The increase in partition coefficient with acid carbon chain lengths indicate that the rate of epoxidation is strongly influenced by the relative quantity of the acid in the oil phase. This however is counterbalanced by the solubility of acid in the aqueous phase. So long as the acid remains entirely miscible with the aqueous phase, the observed pattern of rate increase with partition coefficient is held. As the solubility drops to a finite amount, a severe retardation is observed in the rate of epoxidation. Further to this when the carbon chain length on the acid is increased from 5 (pentanoic acid) to 6 (hexanoic acid) the aqueous solubility decreases and as a result the rate of epoxidation decreases.

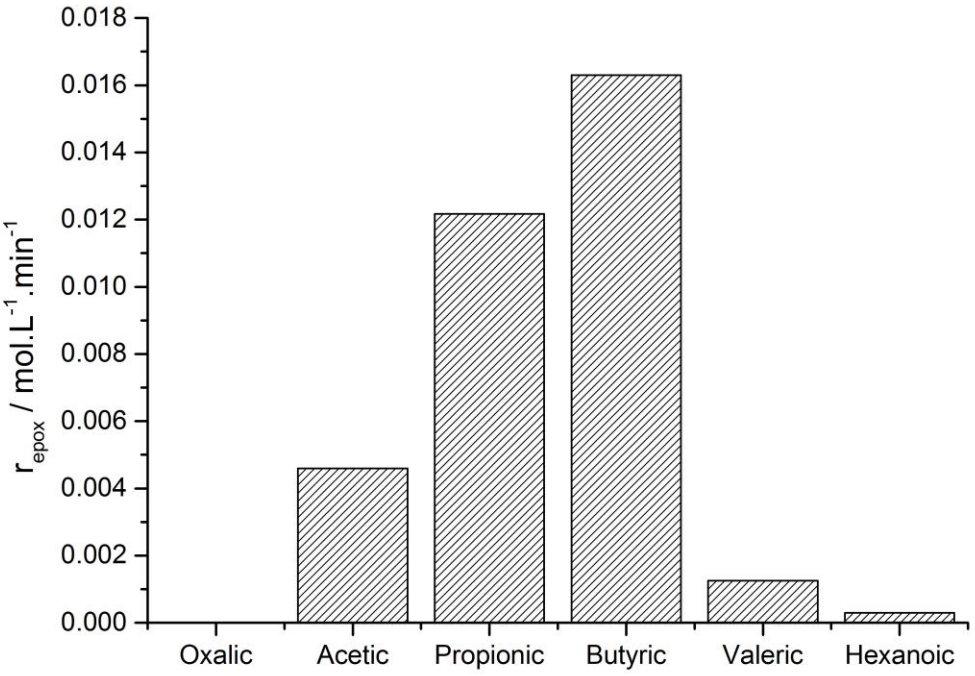

Figure 5.8 – Effect of the carboxylic acid carbon chain length on the rate of epoxidation of sunflower oil. Conditions: 60°C, 3 M H_2O_2, 0.1 M Na_2WO_4, 2 M R_nCO_2H (n=1-5). The diacid, oxalic acid (2 M), was also investigated under the same conditions

The above results indicate that the acid does indeed play an important role in the transfer of oxygenated catalytic species from aqueous to oil phases. This fits with the postulated ligand binding of acid to tungstate and hence acting to influence the relative inter phase equilibrium of the catalyst.

Interestingly the use of a diacid, namely oxalic acid, showed no activity towards the epoxidation of sunflower oil, although its use in alcohol oxidation with the same catalyst and oxidant is known (Wei *et al.*, 2002). However, the oxalic acid was shown to chelate due to the presence of the second acid group (Dickman and Pope, 1994, Wei *et al.*, 2002), perhaps suggesting a difference in activity towards epoxidation between mono- and bi- dentate ligands. The same reasoning was postulated by Maheswari *et al.* (2006) when justifying an observed reduction in the rate of alkene epoxidation when salicylic acids were used in a similar system. It has been noted that oxalic acid can be oxidised by hydrogen peroxide solution through to carbon dioxide but only when the concentrations are in excess of 6 wt% (Walton and Graham, 1928). However, the decomposition of the hydrogen peroxide during the reaction course was measured and shown not to decrease appreciably, thus not likely to be reaction rate limiting.

The concentration of protons in the aqueous phase is suggested to be of key importance in the formation of the active catalytic species, illustrated in Figure 5.9.

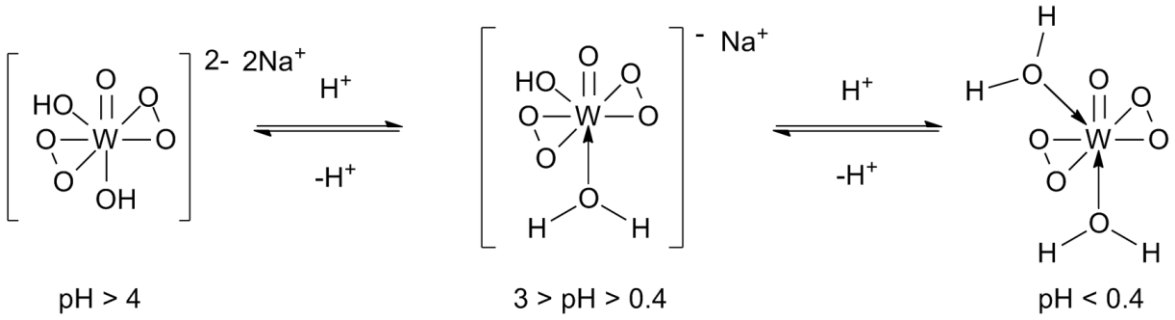

Figure 5.9 - The proposed structures of the peroxotungstate active catalyst under different pH ranges. From Noyori et al. (2003)

An investigation into the different levels of protonation was undertaken. Initial investigations, changing the solution pH using mineral acids, i.e. phosphoric or sulfuric acid showed no conversion to epoxide, as discussed previously. The use of mineral acids in conjunction with carboxylic was considered however this may have convoluted any result since, sulfuric acid catalyses the formation of peracetic acid (a good oxidant) from acetic acid and hydrogen peroxide(Chou and Chang, 1986)

Instead a more elegant solution was found by altering the molar ratios of sodium tungstate/tungstic acid as the tungstate source. Adjusting the ratio of sodium tungstate/tungstic acid and allowed adjustment of the pH whilst maintaining a constant dissolved tungstate concentrations. There was no significant correlation between pH and rate of epoxidation (Figure 5.10) over the range of accessible pH values. Higher pHs could not be tested due to hydrogen peroxide decomposition observed at elevated pH. Likewise lower

pH levels were not accessible, using this method, due to poor tungstic acid aqueous solubility. Using this catalytic system, it seems likely that the mono protonated species (central structure in Figure 5.9) is likely to be dominant.

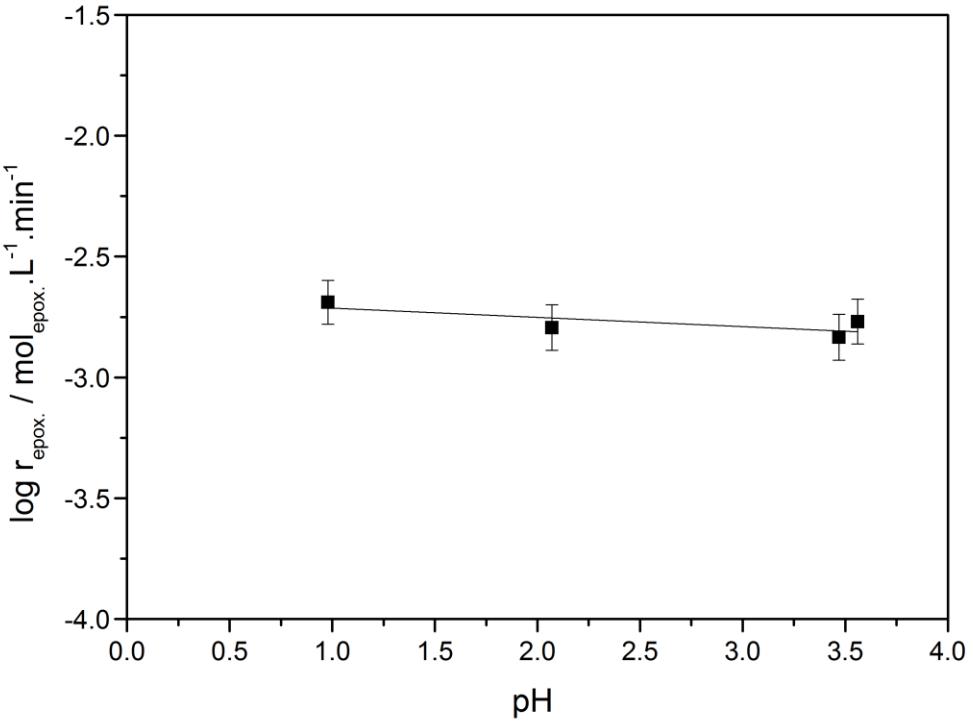

Figure 5.10 – Effect of pH on the rate of epoxidation of sunflower oil. Conditions: 60°C, 3 M H_2O_2, 0.1 M WO_4^{2-}, 1 M AcOH.

To summarise the acid appears to have two main roles in this tungstate catalyst biphasic epoxidation system. Firstly it acts as a hydrogen peroxide decomposition inhibiter. Secondly it promotes the epoxidation, potentially by enhancing the catalyst solubility in the oil phase. The carboxylic acid system is preferable to the mineral acid system, as it does not require additional phase transfer agents.

5.2.3 Effect of the concentration of hydrogen peroxide oxidant.

The oxidant is a key component necessary in providing the oxygen atoms for the epoxidation. A combination of the hydrogen peroxide and the sodium tungstate yields a peroxotungstate species, thought to be the active catalyst in this reaction system (Sato *et al.*, 1997). The effect of the initial concentration of hydrogen peroxide upon the rate of epoxidation was investigated. An order of reaction of 0.74 with respect to initial concentration of hydrogen peroxide was calculated from the slope of a linear regression, as

shown in Figure 5.11. This indicates that the initial concentration of hydrogen peroxide has a strong influence on the rate of epoxidation

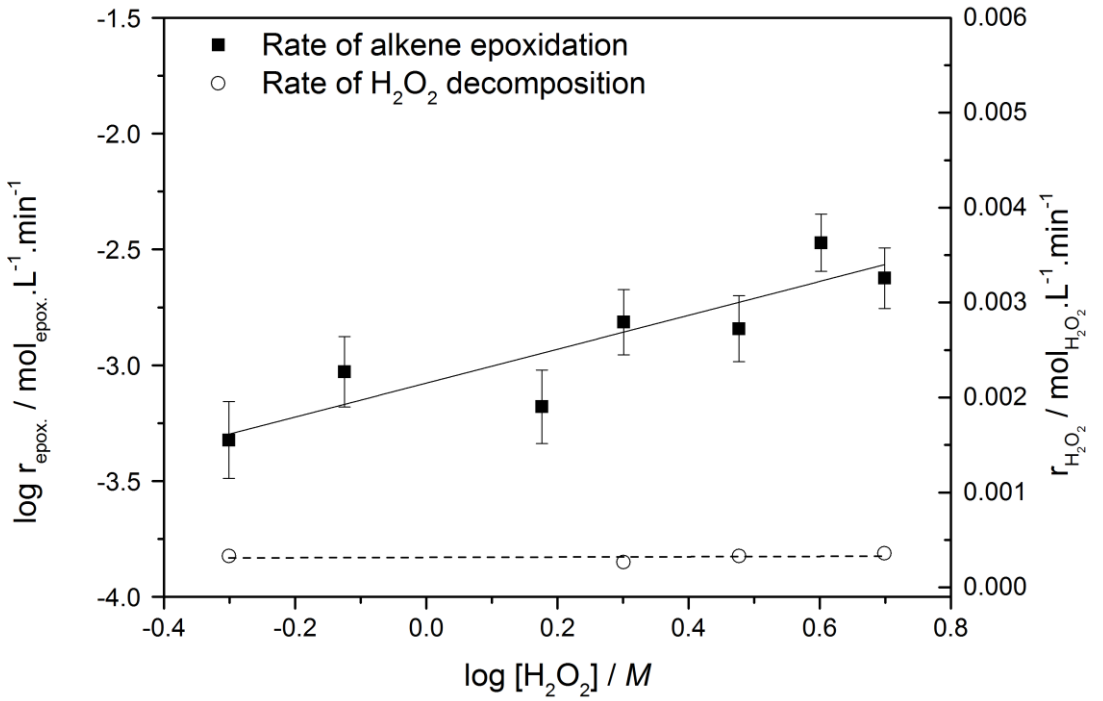

Figure 5.11 – Primary axis: Effect of the initial concentration of H_2O_2 on the rate of sunflower seed oil epoxidation. Secondary axis: Rate of hydrogen peroxide decomposition in the aqueous phase alone under reaction conditions. Conditions: 60°C, 3 M H_2O_2, 0.1 M Na_2WO_4, 1 M AcOH.

The rate of decomposition of hydrogen peroxide, in the presence of the aqueous phase catalytic solution, over this concentration range, were negligible, Figure 5.11.

As alluded to earlier, control of the decomposition of hydrogen peroxide under the reaction conditions was critical for successful epoxidation. When the catalyst precursor, sodium tungstate, is dissolved in water, the resultant solution is alkaline, with a pH of approximately 9. If hydrogen peroxide is then added, and the solution heated to the reaction temperature of 60 °C, there is rapid decomposition of the hydrogen peroxide according to the reaction scheme below. Indeed, owing to the exothermic nature ($-\Delta H_r = -94.6\ kJ.mol^{-1}$, (Marzzacco, 1999)) of the decomposition, the reaction self-perpetuates, leading to a potential "run-away" scenario unless the system is suitably quenched.

Scheme 5.2 – The decomposition of hydrogen peroxide

The literature commonly extols the virtue of tungstate as a catalyst, explicitly indicating the lack of activity towards the decomposition of hydrogen peroxide (Noyori *et al.*, 2003, Deng *et al.*, 1999, Hoegaerts *et al.*, 2000, Li *et al.*, 2007). However, even at relatively low loadings, such as those used by Noyori *et al.* (2003) of 3.3 mM, hydrogen peroxide is completely decomposed within 15 minutes in the absence of acid of PTC, trioctylmethyl ammonium hydrogensulfate. The reported stability of the oxidant in the previous work was due to the presence of the phase transfer catalyst, Figure 5.12. Moreover, it was only due to the inclusion of the anion of phase transfer catalyst, HSO_4^-, which gave rise to the stability, as the corresponding chloride was tested and afforded no decrease in the rate of decomposition. Interestingly, Maheswari *et al.* (2006) used this chloride phase transfer catalyst (trioctylmethylammonium hydrogensulfate) successfully for alkene epoxidation but only in combination with a carboxylic acid, which presumably stabilises the decomposition.

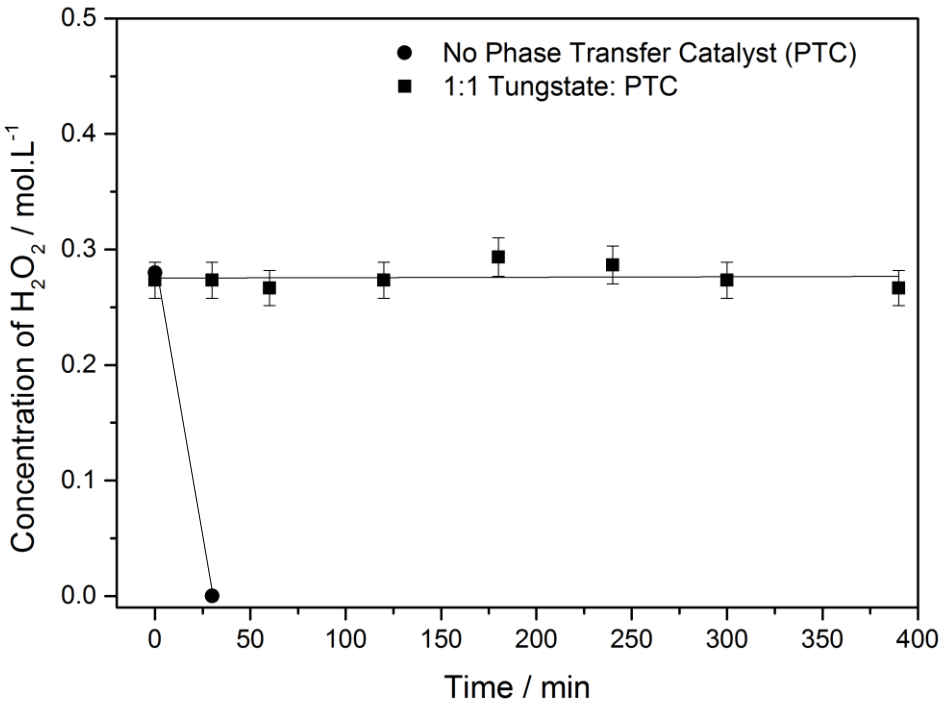

Figure 5.12 – Comparison between the decomposition of hydrogen peroxide with and without the phase transfer catalyst, trioctylmethyl ammonium hydrogen sulfate. Conditions: 60°C. 0.25 M H_2O_2, 3.3 mM Na_2WO_4, 1 M AcOH (Concentrations used were those based upon the molar ratios reported by Noyori et al. (2003)).

5.3 The effect of reactant concentration

The step which must take part in the oil phase, (due to insolubility of oil in water) is the oxidation of the alkene groups of the sunflower oil triglyceride molecules. It seems likely from the result discussed prior to this that the rate limiting step is most likely to be the aqueous phase catalyst formation. To confirm this, the reaction rate order with respect to the average degree of triglyceride unsaturation in the oil phase was investigated. Since the oil phase is neat triglyceride, in order to conduct this investigation a method to vary the unsaturation was devised through blending the sunflower oil with other more saturated oils.

All plant based oils and fats have characteristic compositions which vary from species to species and, indeed, from plant to plant, depending on growth conditions. Table 5.5 lists common saturation information for a range of known and harvested natural oil bearing plants for use in food and consumer care products. As is evident, coconut oil is highly saturated, therefore this oil was selected to act as a "diluent" to adjust the overall average unsaturation of the oil phase.

Table 5.5 - Common natural oil compositions (Gunstone, 2011)

Oil Name	**Weight % saturated/unsaturated as a % total fats**		
	Saturated	Mono unsaturated	Poly unsaturated
Rapeseed	7.4	63.3	28.1
Coconut	91.0	6.0	3.0
Olive	14.0	72.0	14.0
Palm Kernel	49.3	37.0	9.3
Sunflower Seed	9.9	83.7	3.8
Soybean	15.6	22.8	57.7

A series of blends were created with a coconut oil percentage of 0, 25, 50 and 75 % by mass with the remaining mass comprised entirely of sunflower seed oil. The fatty acid profiles were analysed using NMR spectroscopy: the ratio of the integrated areas of signals due to mono, di and tri unsaturated moieties were compared.

The order of reaction with respect to this variable was 0.021 as determined by a linear regression analysis of the data set. As this is within error of the data this suggests that there is no rate dependence on the initial degree of unsaturation (concentration of alkene groups) of the oil phase.

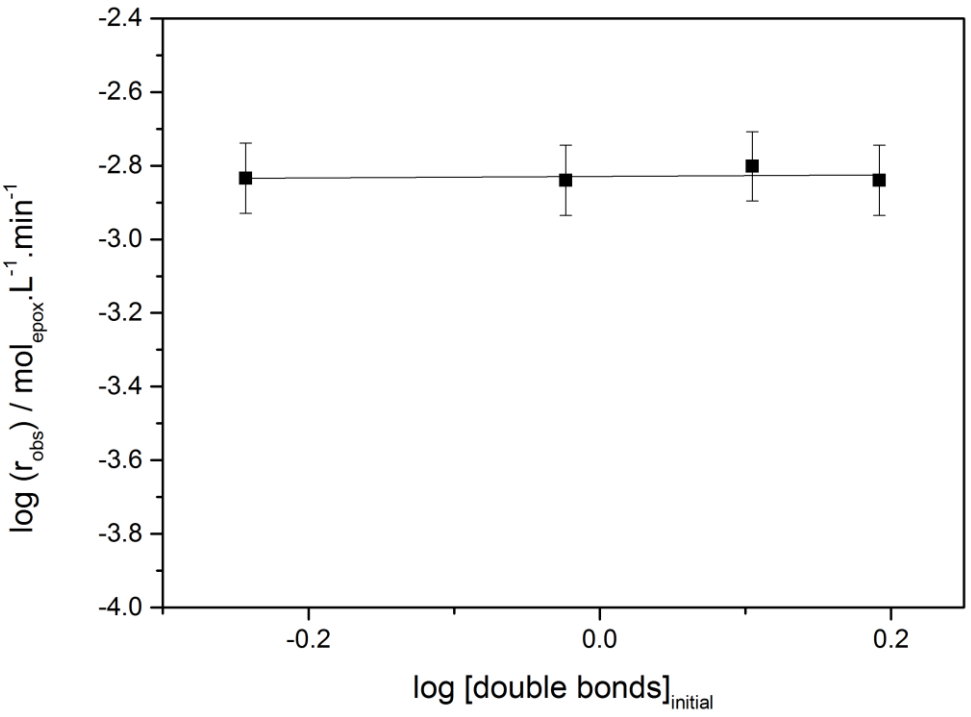

Figure 5.13 - The effect on epoxidation rate with starting concentrations of double bonds present in oil phase. Conditions: 60°C, 1 M AcOH, 3 M H_2O_2, 0.1 M Na_2WO_4

From the results obtained during these unsaturation studies it was concluded that this reaction step, the oil phase epoxidation of alkene, was not rate limiting under the conditions analysed. The remaining component in this proposed reaction step was the oil phase concentration of the peroxometallate catalyst species. From the work investigating the effect of carboxylic acid partition coefficient, it suggests that the availability of the active catalyst in the oil phase is a limiting factor.

5.4 Conclusions

The results presented in this chapter show the rate limiting step of a liquid-liquid biphasic epoxidation system catalysed by sodium tungstate, with hydrogen peroxide as oxidant and acetic acid as promoter. Each of the 4 reaction stages were examined individually, namely: the aqueous phase formation of the active peroxotungstate catalyst, the interphase transfer of this active catalyst species (and the post reaction reduced form) between aqueous and oil phases, and the oil phase epoxidation of the unsaturated sites in the neat triglyceride comprising the oil phase.

The results suggest that the reaction system is mass transfer limited at interfacial areas below 0.25 $m^2.g^{-1}$. At interfacial areas above this the rate limiting step is likely to be a combination of:

- Formation of the active catalyst species – assumed to take place in the aqueous phase
- The concentration of the active catalyst in the oil phase.

There is a strong dependence, approximately first order, of the rate of epoxidation on the amount of sodium tungstate catalyst, acetic acid and hydrogen peroxide. It was also found that an increasing carbon chain length (from acetic to butyric acid and hence oil phase solubility of the carboxylic acid increased the observed rate of epoxidation but only when the acid retained aqueous miscibility. The pH of the aqueous phase suggests that the mono protonated peroxometallate species is likely to be dominant in this reaction system.

It was found that hydrogen peroxide, whilst a useful green oxidant, has to be stabilised for use in this catalytic system. An acetic acid to catalyst ratio of 20:1 or higher was shown to effectively negate hydrogen peroxide decomposition. It was determined that previously reported systems tungstate catalyst hydrogen peroxide epoxidation systems, whilst not explicitly mentioned, must rely on the acidity of additives such as the phase transfer catalyst to negate hydrogen peroxide decomposition.

Interestingly the difference in rate seen with the different carboxylic acids (acetic to hexanoic acid) does indicate that the partition equilibrium of the active catalyst species, and hence oil phase concentration of active catalyst is also likely to be a limiting factor.

In context to the overall aim of this research the results reported in this chapter confirm a minimum interfacial area required to negate mass transfer limitation. In addition, controlling factors of hydrogen peroxide decomposition were established and the rate dependence of the sodium tungstate, acetic acid and hydrogen peroxide determined. This combination of data was required so that the system could be engineered from a batch to a continuous system, the focus of the following chapter, Chapter 6.

6 Process Integration: Reaction and Separation

Continuing the overall theme within this research, the results contained in this chapter build on those presented in the previous two chapters (Chapter 4 and 5). To briefly summarise, Chapter 4 contained the results of the investigation into the formation of dispersed systems, concluding that a range of oil-aqueous dispersions could be created with interfacial surface areas spanning from 3.8 $m^2.g^{-1}$, using high shear homogenisation down to 9.6 x 10^{-4} $m^2.g^{-1}$, through use of a capillary T-junction device. Chapter 5 presented the results of the investigation into determining the rate limiting step for the sunflower seed oil epoxidation catalysed by sodium tungstate with hydrogen peroxide oxidant and acetic acid acting as a promoter. The main conclusion from the rate determining step investigations, relevant in this chapter, was that operating with an interfacial surface area in excess of 0.25 $m^2.g^{-1}$ resulted in the system not being mass transfer limited. Above this, the rate of reaction was determined to be limited by the formation of active catalyst, reported to be a peroxotungstate species (Noyori *et al.*, 2003).

The focus of the results and discussion presented in this chapter is the integration of the reaction of the previously investigated alkene epoxidation, along with a downstream

separation process. This was towards an end goal of continuous operation involving the recycle of both oil and aqueous catalyst streams. Critically, and where the approach taken in this chapter differs significantly from the results reported thus far, no interfacial stabilising agents, i.e. surfactants, were used. This was necessary to maintain the inherent separation seen between the two immiscible (oil and aqueous) phases. Attempting to 'break' surfactant stabilised emulsions often requires the input of significant energy, i.e. heating or centrifugation or additional additives (Schuster, 1985), both of which wished to be avoided. The idea that an unstabilised dispersion, with the required interface area (>0.25$m^2.g^{-1}$), could be created through an engineering solution would allow for both reaction outside of mass transfer limitation as well as maintaining the inherent separation downstream.

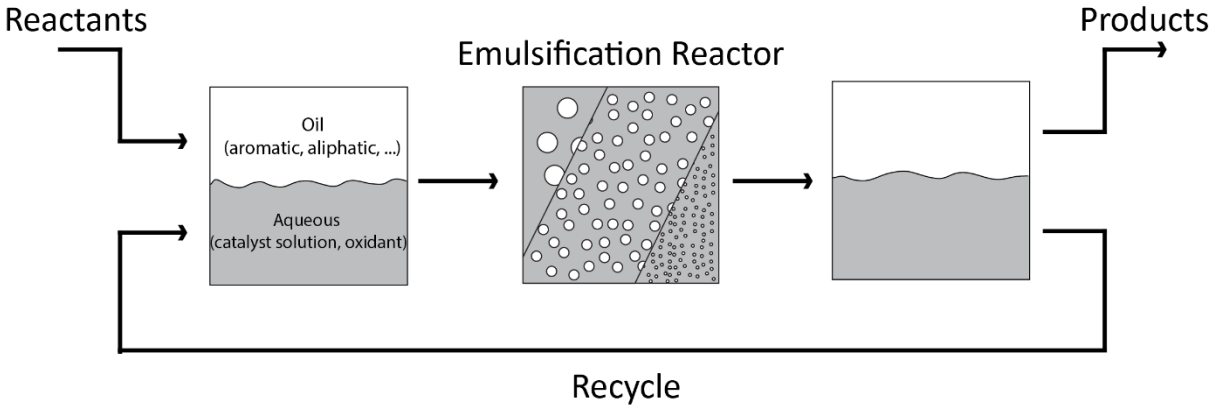

Figure 6.1 – Reaction of a biphasic system through transient dispersion with integrated separation and recycle streams

To achieve this process, illustrated in Figure 6.1 above, the use of the previously investigated technique of microfluidic based droplet generation used in Chapter 4 was revisited with a focus on its use as a reactor. The use of the capillary device use in Chapter 4 was not investigated as the interfacial surface areas produced by this technique resulted in the reaction system being mass transfer limited, as discussed in Chapter 5

To complement the previous method, cross flow membrane emulsification was investigated due to its attractiveness in controlling droplet size distribution. In addition to the size control offered it operates continuously, being an ideal candidate for the integration of continuous reaction and separation.

The design considerations taken into account in the process integration of each of these techniques (microfluidic, and membrane) are discussed, culminating in the presentation of the results of the successful continuous epoxidation. Critically the integration of reaction and separation was proven using membrane emulsification for the generation of the transient dispersion, as illustrated in Figure 6.1.

6.1 Process integration in microfluidic devices

The use of the microfluidic device as a reactor was considered. The parameters of residence time, and heating requirements were investigated along with the ability of the techniques to produce non-stabilised surfactantless dispersions.

6.1.1 Formation of non-surfactant stabilised dispersions in microfluidic devices

The use of the microfluidic chip devices were investigated for the suitability in forming droplets without the use of surfactants. As reported in Chapter 4, two geometries of device were employed, the flow focused and the T-junction, with the inlet streams fed via independently metered syringe pumps. The critical difference between the investigations here and those reported in Chapter 4 conducted here was that the lack of surfactant. This was characterised by an increase in surface tension, between the oil and aqueous phases, from 1.06 $mN.m^{-1}$ with 1% Brij-S10 to 15.8 $mN.m^{-1}$ without, as measured through use of a pendent drop goniometer.

The use of a flow focused geometry arrangement was successful in forming non-stabilised emulsions, but only at an oil to aqueous flow rate ratio of 0.03 or smaller. This suggests that the increased interfacial tension due to lack of surfactant can be counteracted through an increase in the flow velocity of the individual streams. This result can be rationalised through analysis of the capillary numbers, a dimensionless number relating to the relationship between shear stress and capillary pressure, for the continuous and dispersed phases (Equation 4.13 and 4.14 respectively).

$$Ca_c = \frac{\mu_c U_c}{\gamma} \qquad 4.13$$

$$Ca_d = \frac{\mu_d U_d}{\gamma} \qquad 4.14$$

Where μ is viscosity, U is fluid velocity, γ is interfacial tension. The subscripts c or d refer to continuous and dispersed phase respectively.

The detachment of a droplet from the outlet of the dispersed phase channel is a balance between the interfacial forces and the shear forces, indicated by the capillary number. Hence if the interfacial force is increased (from 1.06 $mN.m^{-1}$ to 15.8 $mN.m^{-1}$), in order to detach a droplet successfully the shear forces must also be increased. Due to the arrangement of a flow focused channel, the main shear stress is applied to a growing droplet through the impinging continuous phase; ergo an increase in this flow rate is required. At a fixed dispersed phase flow rate this increase in shear stress can be summarised by a decrease in flow rate ratio, φ, defined as the ratio between dispersed and aqueous phase flow rates. The

precise mechanism of droplet detachment is outside the scope of this study, and still very much a topic under investigation (Fu *et al.*, 2012), but is dependent on the specific geometry of the device, the flow regime as well as the capillary numbers of the fluids, discussed here.

Experiments into using the T-junction chip for the formation of non-stabilised dispersions were unsuccessful, even at very low flow rate ratios (<0.01) with only a co-flowing situation existing. This failure was assessed to be function of the capillary number, i.e. the ratio between interfacial tension and shear stress. Due to the peculiarities of the geometry, discussed in Chapter 4, it is surmised that an insufficient increase in shear stress could be obtained, due to fluid bypassing in the downstream enlargement, to overcome the increase in surface tension forces, due to lack of surfactant. The characteristic squeezing regime which has been reported (De Menech *et al.*, 2008) was again not observed as discussed in Chapter 4.

The droplets which were created through the flow focused geometry device were able to be collected and remained stable to coalescence for several days (>7) at room temperature (19-23 °C). The average droplet diameter was measured to be approximately 100 μm, as determined by visual measurement and laser scattering experiments, similar to those reported in Chapter 4.

6.1.2 Residence time in the microfluidic device

In the consideration of a continuous operation, some thought had to be given to the design and ability to control residence time of the fluid in the reactor. In order to achieve successful reaction, and observable levels of conversion, as determined from the results presented in Chapter 5, the fluid-fluid interfacial area had to be maintained at a quantifiable area for a defined period of time. In the ideal situation the interfacial area is both able to be defined and constant within the reactor, i.e. no change in droplet size, this was the assumption made here. To clarify, the reactor was initially defined as the point at which the fluids first interface the junction within the chip up to a measured length of outlet tubing downstream. This definition was later modified, due to the complications in heating the chip to reaction temperature, discussed in the following sections.

The diameter of the outlet tubing was 250 μm and as such the typical residence times for the reactor was seconds at the flow rates investigated (total flow <400 $\mu L.min^{-1}$). As discussed in the previous section, the selection of the flow rates was linked to the flow rate ratio necessary to achieve droplet formation (<0.03). In addition it was found that this flow rate ratio was only valid above a minimum total flow, below which it can be theorised that insufficient shear was created. Again, the exact mechanism for the droplet break detachment is not well defined; therefore this theory cannot be verified. Suffice to say that below a

minimum total flow rate, of approximately 103 uL.min^{-1}, a co-flowing regime was observed. The requirement of droplet creation placed significant constraint on the ability to adjust residence times via alteration of flow rates. Another solution was to increase the length of outlet tubing and hence increase the volume of the reactor, for a given volumetric flow. Attempting to increase this presented challenges since for laminar flow (Re of this system <<2000) a well-known parabolic flow profile exists across the cross sections of the flow path, due to viscous drag forces imposed by the wall (Coulson and Richardson, 1999). As a result, droplets existing in this channel were observed to experience a range of velocities, resulting in collision, and eventual coalescence at elongated path lengths. This again placed a limit on the residence time obtainable whilst maintain a given oil-water interfacial area. Considering both the approaches taken to adjust residence time, the maximum achievable time, without observable coalescence whilst maintaining droplet generation was of the order of <10 seconds.

6.1.3 Temperature control in the microfluidic device

The careful control of temperature was critical when conducting the alkene epoxidation reactions under investigation, since this affects both reaction rate and mas transfer.

Electrical heating of the microfluidic device using insulated resistance wire was investigated as a means to bring the reactor to the reaction temperature of 60 °C. A test apparatus was created consisting of a glass syringe, filled with oil, connected to a length of tubing. At either ends of the tubing thermocouple junctions were mounted into female-female NPT connectors to provide inline temperature monitoring, illustrated in Figure 6.2.

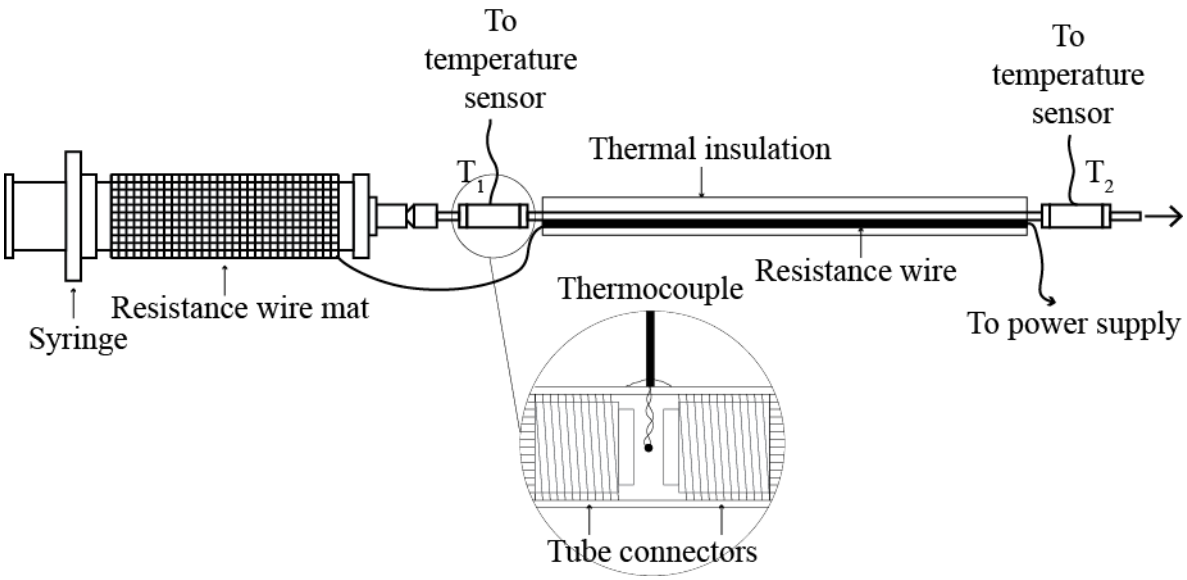

Figure 6.2 – Details of the heating system for the microfluidic integrated reaction system.

Upon supplying a current to the electric wiring the syringe contents was heated successfully, measured using a separate thermocouple mounted inside the syringe in a separate experiment. Upon connection to the tubing and activation of the flow, there was no perceptible increase over ambient temperature of the fluid detected at the junction between the syringes and tubing (T_1 on Figure 6.2) and after the heated tubing section (T_2 on Figure 6.2). It was surmised that due to the small volumes and relatively large surface areas exhibited in these microfluidic devices, heat loss was rapid enough that the small distances of unheated sections, before the inline thermocouples, were sufficient to decrease the temperature of the fluid in the lines to ambient. This method was therefore not carried forward, since small lengths of unheated regions were unavoidable due to the necessity of fixtures and fittings, such as the syringe/tube interface, which were unable to be effectively heated.

An alternative method involving the complete submersion of the chip and outlet tubing in a water bath set to 60 °C was investigated. The chip was found to be unsuitable for this as significant dislocation of the chip from the holder was observed, likely due to the difference in the thermal expansion between the borosilicate glass chip and the aluminium holder. This method of direct heating, via submersion in the preheated water bath was successful when the outlet tubing alone was heated. This of course mandated a change in the definition of the reactor since now only the outlet tubing was effectively at the reaction temperature.

6.1.4 Reaction and separation in the microfluidic device

The epoxidation of sunflower oil was performed in the microfluidic devices, taking into account the residence time and heating considerations discussed above. The aqueous stream contained 0.1 M sodium tungstate, 2 M acetic acid and 3 M hydrogen peroxide. The oil phase was pure sunflower oil. The residence time for a length of outlet tubing of length 300 mm and internal diameter 250 μm was calculated to be 9 s at a total flow rate of 103 $\mu L.min^{-1}$. As for the experiments conducted in Chapter 5, the reaction analysis was carried out using NMR spectroscopy, analysing the well-defined signals for the alkene and the epoxide.

At these reaction timescales no observable conversion to epoxide could be discerned from the baseline noise of the NMR spectra. This was no doubt due to the extremely short timescales available for reaction.

Additional experiments to elongate the reaction timescales were undertaken. These were conducted by flowing the outlet of the reactor into vials, preheated to 60 °C. However, under the same reaction conditions as above, upon standing in the vials, the reaction dispersion exhibited rapid coalescence. This rendered the assumption of a single interfacial area invalid since the droplets no longer existed. However, despite the failure of this brief experiment in

elongating the reaction time, it did highlight the potential for downstream separation with this reaction system.

Continuous regeneration of the dispersed phase interfacial area was required in order to elongate the effective residence time i.e. time at a given interfacial area at reaction temperature. The observation of the downstream separation showed potential for exploitation. By removing both phases and returning them to pass through the microfluidic device a number of times the effective residence time could be accumulated, each pass providing an additional 9 seconds (under identical conditions to above) residence time. Since the fluids were injected into the device via syringe pumps it was found that under the low flow rate constraints imposed by having to form droplets, the device was unable to produce practically separable volumes. For example, 180 μL of dispersed phase was only reacted after 10 hours of operation (at 0.03 flow rate ratio of a total flow rate of 103 $\mu L.min^{-1}$). Therefore to approach detectable conversions (~5%) under the conditions investigated previously in Chapter 5, a typical residence time of 15 minutes requires a total run time of around 1000 hours. This equates to approximate 3.5 hours per microliter. For this method of recycle to be effective, much larger scale operation was implemented, using continuous pumps adopting parallel drop formation using a porous membrane.

6.2 Process design for an integrated membrane system

As discussed in the previous section on the use of microfluidic devices, the ability to continually re-form a transiently stable dispersion was critical in obtaining reactor residence times which result in observable conversion for the sunflower oil epoxidation reaction system. The results and discussion contained in this section describe the design, construction and operation of a membrane reactor with the integration of separation and recycle of both aqueous and dispersed phases. The successful epoxidation of sunflower seed oil with an aqueous sodium tungstate catalyst, acetic acid and hydrogen peroxide was performed.

A membrane can be seen as analogous to a parallel array of the single capillary T-junction channels. The droplets of dispersed phase are detached from the pores as they protrude into the continuously flowing stream due to the shear stress imposed by the fluid (Figure 6.3).

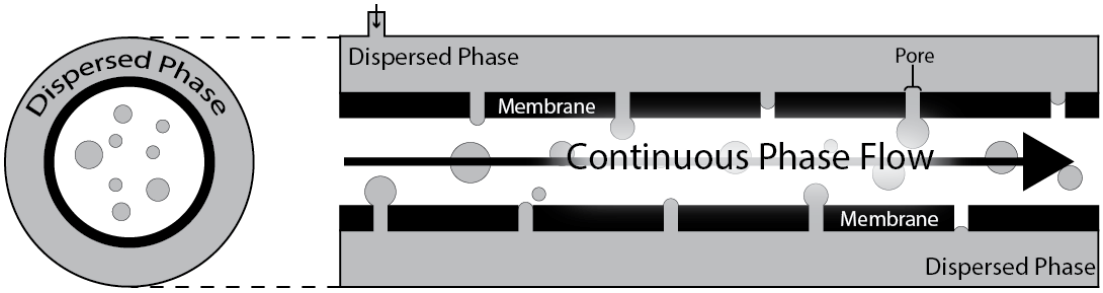

Figure 6.3 - Schematic of a cross section of a tubular membrane operating in a cross flow emulsification arrangement.

Equating this to the above microfluidic devices, despite using the flow focused geometry devices for the investigations above, it becomes apparent that the use of a membrane device results in a significant increase in the permeation of dispersed phase, shown to be a limitation in the integration of separation and recycle of the microfluidic system.

A schematic of the designed reaction system is given in Figure 6.4. The design considerations for each of the marked sections are considered separately.

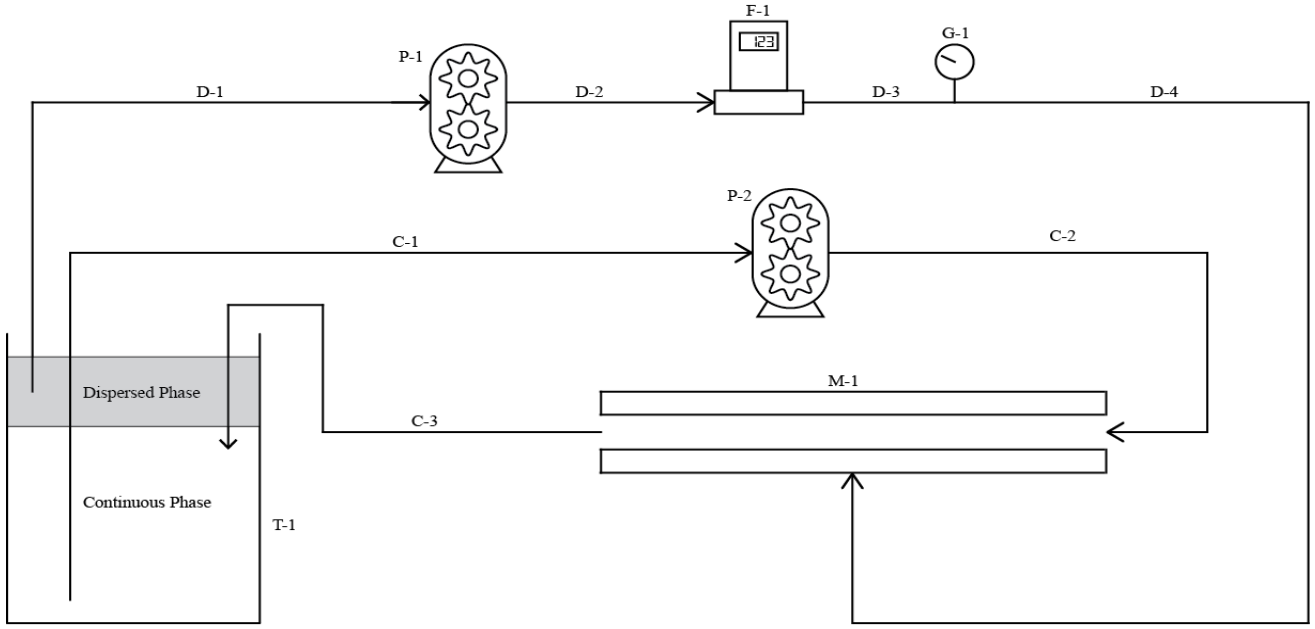

Item	Description	Dimensions/capacity	Range	Materials
D-1	Dispersed phase line - tank, T-1 to pump, P-1	400 mm L x 1/4" O.D. x 3/16" ID		PTFE, (Stainless Steel 316 fittings)
D-2	Dispersed phase line - pump, P-1 to flow meter, F-1	200 mm L x 1/4" O.D. x 3/16" ID		PTFE, (Stainless Steel 316 fittings)
D-3	Dispersed phase line - flow meter, F-1 to pressure gauge, G-1	400 mm L x 1/4" O.D. x 3/16" ID		PTFE, (Stainless Steel 316 fittings)
D-4	Dispersed phase line - pressure gauge, G-1 to membrane module, M-1	400 mm L x 1/4" O.D. x 3/16" ID		PTFE, (Stainless Steel 316 fittings)
C-1	Continuous phase line - tank, T-1 to pump, P-2	1000 mm L x 3/8" O.D. x 1/4" ID		PTFE, (Stainless Steel 316 fittings)
C-2	Continuous phase line - pump, P-2 to membrane module, M-1	1000 mm L x 3/8" O.D. x 1/4" ID		PTFE, (Stainless Steel 316 fittings)
C-3	Continuous phase line - membrane module, M-1 to tank, T-1	950 mm L x 3/8" O.D. x 1/4" ID		PTFE, (Stainless Steel 316 fittings)
P-1	Dispersed phase gear pump	-		Stainless Steel 316
P-2	Continuous phase gear pump	-		Stainless Steel 316, Viton, PPS
F-1	Dispersed phase line digital flow meter	-		-
G-1	Dispersed phase line pressure gauge	-	0-4 bar	Stainless Steel 316
T-1	Main tank	5 L		Borosilicate glass
M-1	Membrane module	250 mm		Stainless Steel 316

Figure 6.4 – Process diagram for the continuous integrated membrane reaction system.

The design consisted of a main tank, containing the two phases. From this, both the aqueous and dispersed phases were recirculated via gear pumps. The phase to be dispersed, the oil, was extracted from the top of the main tank and pumped to a cross flow membrane module. The oil phase was allowed to permeate inwards towards the central axis of a tubular membrane. The flow rate was set and pressure of the line was monitored. The aqueous phase was extracted from the bottom of the main tank and passed through the centre of the membrane, with flow perpendicular to the direction of permeation, providing a shear by which the oil was dispersed. The now combined continuous aqueous phase with dispersed oil phase was allowed to return to the main tank, passing into an intermediate vessel to reduce the flow velocity and assist dispersion coalescence. The epoxidation reaction between the sunflower oil and the aqueous catalyst phases was assumed to predominantly take place from the moment of dispersion, thus creation of greatly increased interphase surface area, to the moment of coalescence.

6.2.1 Materials of constructions

The materials of construction were important, firstly to ensure the safe running of the apparatus there should be no degradation of the internal surfaces subjected to the reaction media. Arguably more important was the reagent susceptibility to degradation due to adverse reaction with the internal materials. A preliminary indication of suitability can be inferred from chemical compatibility databases published online. Whilst these databases only offer information typically under ambient temperatures and pressures, the knowledge gained from the small scale operations under reaction conditions was able to inform on the likely best choice of construction material. The major materials used were stainless steel 316 and polytetraflouroethene (PTFE). These materials were primarily used for the unit interconnections, fittings and tubing. The compatibility of each with the two major reagents at levels approximate to those used are given in Table 6.1.

Table 6.1 – Ratings for major materials of construction for fittings and tubing for the continuous epoxidation equipment. Based on a 48 hour exposure, A = Excellent, no observable effect, B = Good, mild discolouration (Cole Parmer Chemical Compatibility Guide)

	Stainless Steel 316	**PTFE**
Hydrogen peroxide (30 wt%)	B	A
Acetic acid (20 %)	A	A

PTFE was listed as having excellent resistance to the major reactive compounds. Stainless steel 316 was listed has having excellent compatibility with dilute acetic acid however was

only listed as having a lower, B rating with hydrogen peroxide 30 wt%. This suggested minor corrosion or discolouration was likely, indicating perhaps a reaction with hydrogen peroxide. Since the total contact area of fluid with stainless steel was confined to small sections within fittings, this rating was expected to be acceptable, avoiding the use of a more expensive but more resistant alloys, or polymers. To justify this, in light of the issues encountered with hydrogen peroxide decomposition in the previous sections of the project, a stainless steel 316 fitting was subjected reaction temperatures (60°C) submersed in an aqueous phase of 3 M hydrogen peroxide, 2 M acetic acid (the reaction conditions) determined from the investigations conducted in Chapter 5. Over the course of 18 hours there was no observable decomposition of the hydrogen peroxide (Figure 6.5).

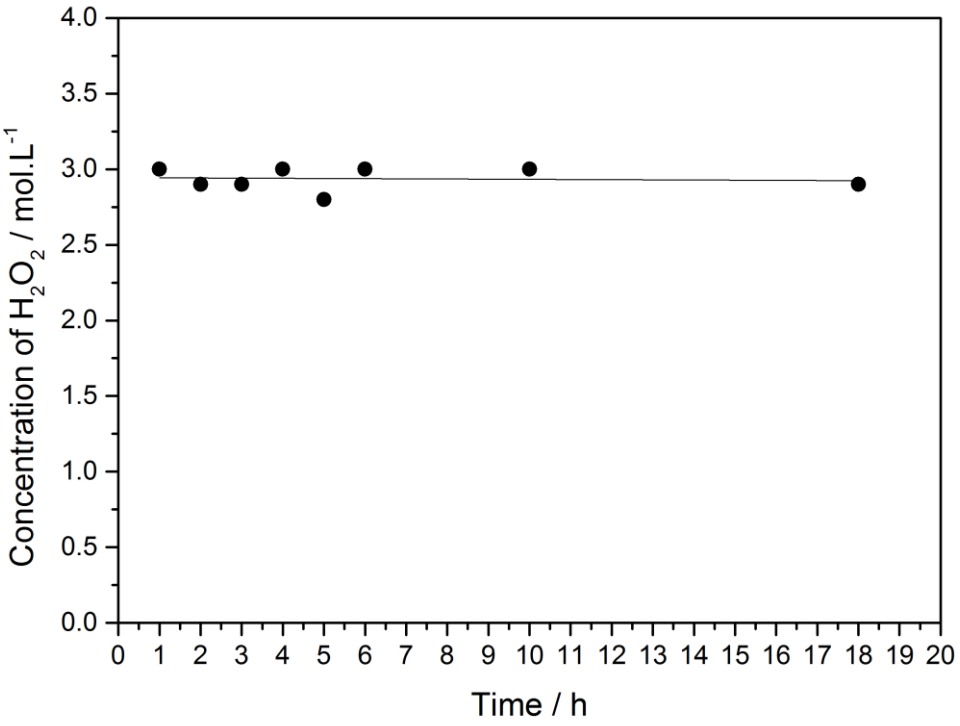

Figure 6.5 – Hydrogen peroxide decomposition in the presence of a stainless steel ferrule. Conditions: 60 °C, 3.0 M H_2O_2, 2.0 M AcOH.

Materials not covered here are discussed in the relevant sub section for each unit.

6.2.2 Selection of membrane

The main criteria in the selection of the suitable α-alumina membrane, with pore size of 80 μm were:

1. Ability to form droplets of an interfacial area greater than 0.25 $m^2.g^{-1}$ to ensure the epoxidation reaction is not mass transfer limited
2. Hydrophilic, so that it was not wetted by the dispersed phase, important to encourage the formation of discrete oil droplets.
3. Chemically compatible with respect to the reagents, i.e. no degradation of the membrane or unproductive decomposition of the hydrogen peroxide oxidant.

The creation of a certain droplet size, d_d, is commonly accepted as being proportional to the pore diameter, d_p, for given flow conditions (Joscelyne and Trägårdh, 2000).

$$d_d = x d_p \tag{4.15}$$

From review of the literature, the constant of proportionality, x, does not typically exceed 50 for ceramic membranes. Therefore the minimum theoretical pore diameter to achieve > 0.25 $m^2.g^{-1}$ surface area (26 μm droplet size) can be calculated,

$$d_p = \frac{d_d}{x}$$
$$d_p = \frac{26}{50} \approx 500\ nm \tag{4.16}$$

Considering the above, an 80 nm membrane was used, theoretically allowing for a much larger surface area, assuming a constant of proportionality of 50 as in Equation 6.4.

A common material for use in the formation of ceramic membranes is α-Al_2O_3. These are known to be hydrophilic, therefore lipophobic and appropriate for the creation of oil in water dispersions

The compatibility of α-alumina with the key reagents is listed as A, Excellent for both 100 % acetic acid and 100 % hydrogen peroxide. This suggested that at the weaker concentrations of those used in the reaction there would be no degradation, and hence pore size change in the membrane.

The membranes and housing were available in the group, for an alternative application, purchased from atech innovations (Innovationspark Wiesenbusch Am Wiesenbusch 26 D-45966 Gladbeck, info@atech-innovations.com). Details of the membrane dimensions are summarised in Table 6.2.

Table 6.2 – Ceramic membrane dimensions and material summary from the information supplied with the membranes from atech innovation

Material	**α-Al_2O_3**
Pore size	80 nm
Length	250 mm
Outside diameter (O.D)	10 mm
Inside diameter (I.D)	6 mm

6.2.3 Surface area determination for membrane emulsification

In order to determine the surface area of the dispersed phase within the reactor the droplet size obtainable with the membrane was measured. Preliminary investigations involved installation of a laser scattering particle sizer connected inline downstream from the membrane to provide a real time output of the droplet size. However, insufficient signal was detected in the particle sizer, which required a minimum obscuration of the laser in order to obtain a reliable output. Under the reaction conditions there was insufficient volume of dispersed phase in the continuous phase as a result of low oil phase flux.

In order to utilise this method of particle sizing, the concentration of droplets was built up in the main tank. This resulted in the detectable levels being reached. Upon continued recycling in this fashion the detected droplet size decreased.

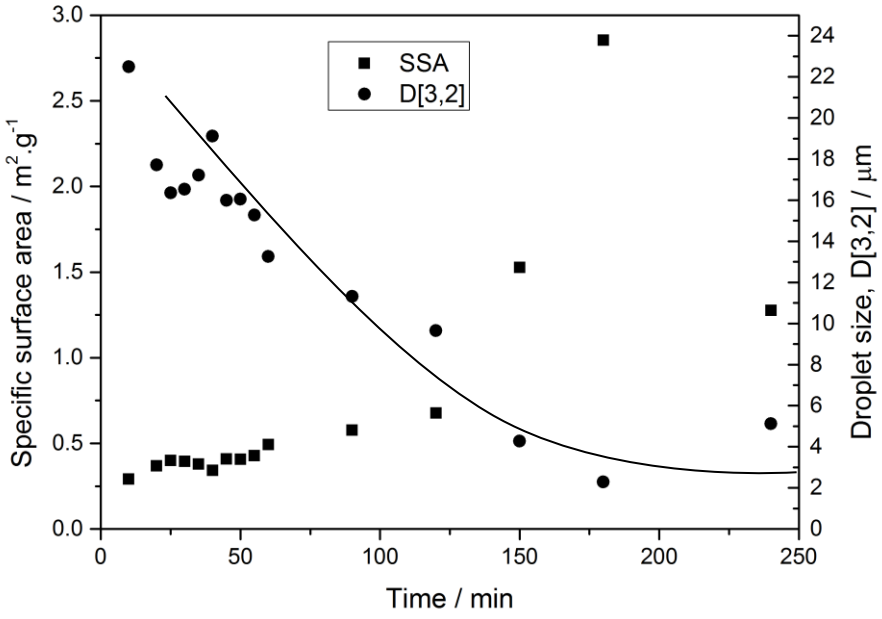

Figure 6.6 – Observed surface area and D[3,2] with time online using α-Al_2O_3 membrane (80 nm pore size). Transmembrane pressure 2 bar, wall shear 2 Pa (continuous phase flow rate 1.1 L.min^{-1}).

When operated for longer than 240 min, the concentration was no longer high enough to provide accurate readings. At face value, the results indicated in Figure 6.6 would appear that progressively smaller droplets are being created. This seems counter to what might be expected when operating under steady state conditions. The key variables which have been reported to alter droplet size such as wall shear (2 Pa), transmembrane pressure (2 bar) and membrane pore size (80 nm), for example, were unchanging. Another explanation of the trends seen is that the droplets dispersed in the aqueous phase were coalescing at different rates. One might expect the larger droplets to coalesce first, due to their increased buoyant force therefore progressively lowering the average droplet size still present in the bulk aqueous phase. Coalescence was observed through a phase separation in the main tank, since in this case, the dispersed phase was heated and charged into the system. What this explanation highlights is that there was indeed a distribution of droplet sizes. This is potentially an indication of a degree of pore size distribution within the membrane, although this was not measured, or perhaps the effect of attempting to maintain a dispersion of two immiscible liquids without the aid of stabilising agents.

A combination of the two is also possible and seems likely as the initial larger droplets were not 'replaced' which would have been expected should the same sized droplets be being created. The observation of the droplet sizes between 150 and 240 minutes suggest that a minimum value has reached corresponding to approximately 3-4 μm.

Comparison can be drawn from the results here against the previously reported droplet size relationships for certain pore sizes with ceramic membranes. The constant of proportionality, or droplet size/pore size ratio for this system (pore size 80 nm, droplet size 4 μm) was calculated as approximately 50, in line with the highest reported values (Joscelyne and Trägårdh, 2000). This large ratio was no doubt the result of using no stabilising agents, the use of which would have resulted in lower interfacial surface tensions between the phases and hence more rapid droplet detachment, arresting the droplet growth at the pore.

Peng and Williams (1998) suggest a method for the prediction of droplet size through a force balance on the droplet exiting a single pore. The proposed model was tested in the range of cross flow velocities 0.1-0.4 $m.s^{-1}$ which is smaller than the crossflow velocity used in these experiments of 0.65 $m.s^{-1}$. Despite this, the model assuming non-deformed droplets predicts a value of 3.4 μm, in keeping with the experimentally observed results (3-4 μm). The calculations are given in Appendix 2. For the sake of comparison the adjusted model which allows for a deformation of droplets predicts droplets of the size 21 μm. This might suggest that, accordingly to the parameters assumed in the model, the droplets are not deformed during growth.

Whilst the exact value is difficult to judge, due to the sensitivity of the surface area per gram to droplet size, all the surface areas measured even with the largest droplet sizes are above 0.25 $m^2.g^{-1}$. This was the value measured in Chapter 5 to signify an observed rate change response to surface area, above which indicating the system was not mass transfer limited. Therefore, from the aspect of increasing reaction rate it was important to simply be not mass transfer limited as a further increase in surface area will have an insignificant impact on the observed rate of reaction.

6.2.4 Reaction area

The membrane was enclosed in a 18 mm O.D. stainless steel housing with one quick disconnect inlet from the 1/4" O.D. dispersed side oil stream tubing. The membrane was enclosed in the middle of the module with rubber o-rings sealing the oil phase from the ends of the membrane to prevent bypassing into the continuous stream. The membrane module was connected to the continuous stream with a series of fittings from the 18 mm module down to 3/8" tubing.

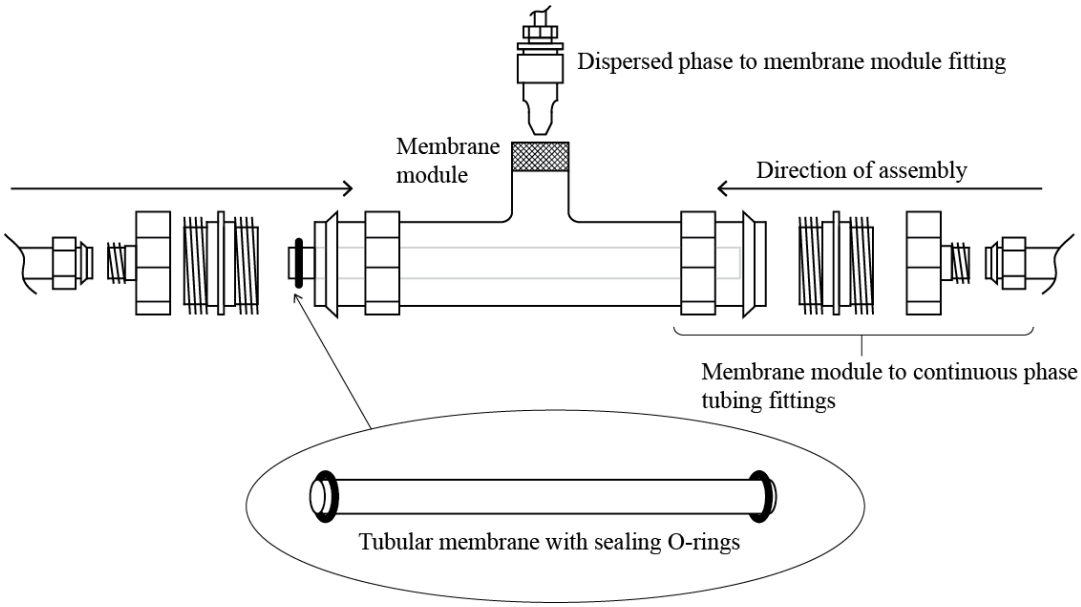

Figure 6.7 – Expanded diagram of membrane module showing key fittings and assembly

The use of 3/8" O.D. tubing for the continuous phase flow lines allowed for an I.D of approximately 1/4" or more specifically 6.37 mm. In order for the least perturbation of flow within the membrane module, as close a match between the internal diameters of the tubing and the membrane (6 mm) was required. Control of the flow pattern within the module was needed to ensure uniform wall shear rate could be assumed, with minimum entry effects imposed through step changes in flow path diameter (Coulson and Richardson, 1999).

The main parameter which describes the permeation of dispersed phase through the membrane is the transmembrane pressure (Equation 4.17). In order to calculate this the

difference between the dispersed phase side and the continuous phase side was measured. To determine the pressure drop across the continuous stream side of the module pressure gauges were mounted at the inlet, ($P_{c,in}$), and outlet, ($P_{c,out}$). There was no detectable pressure (gauge) in the lines over the range of flow rates used, therefore the average continuous stream pressure was assumed ambient. The transmembrane pressure (P_{tm}) was thus defined as the gauge pressure of the dispersed phase (P_d).

$$\begin{aligned} P_{tm} &= P_d - \frac{\left(P_{c,in} - P_{c,out}\right)}{2} \\ P_{c,in} &\approx P_{c,out} \approx 0 \\ P_{tm} &= P_d \end{aligned} \qquad 4.17$$

The reactor was defined similarly to that of the microfluidic device, which is from the point of first contact between the two fluids to the point of separation, assumed to be the outlet of the tube into the storage vessel. Essentially the reactor was the total volume in which a defined surface area of dispersed phase was assumed.

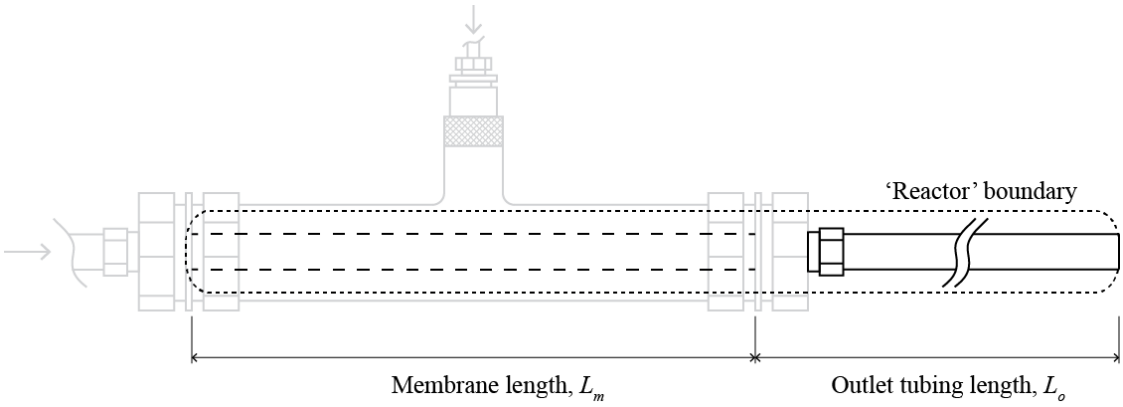

Figure 6.8 – Reactor boundary definition for the continuous epoxidation rig

The total volume of the reactor was therefore defined as the a combination of half the cylindrical membrane tube with volume of the outlet tube (Equation 4.18)

$$Total\ Reactor\ Volume = V_r = \frac{L_m \pi d_m^2}{2} + \frac{L_o \pi d_o^2}{4} \qquad 4.18$$

Where L denotes length and d, tube diameter of the membrane, m, or outlet tubing, o, respectively.

6.2.5 Main tank design: Storage, heating and separation

Both continuous and dispersed phases were stored in a single glass 5L vessel. The natural difference in density resulted in a bi-phase, with oil situated above aqueous. This vessel was placed upon a stirrer hot plate to allow for heating to reaction temperature (60 °C). The tank outlets for the aqueous and dispersed streams were at the bottom and top of the layers, respectively, illustrated in Figure 6.9.

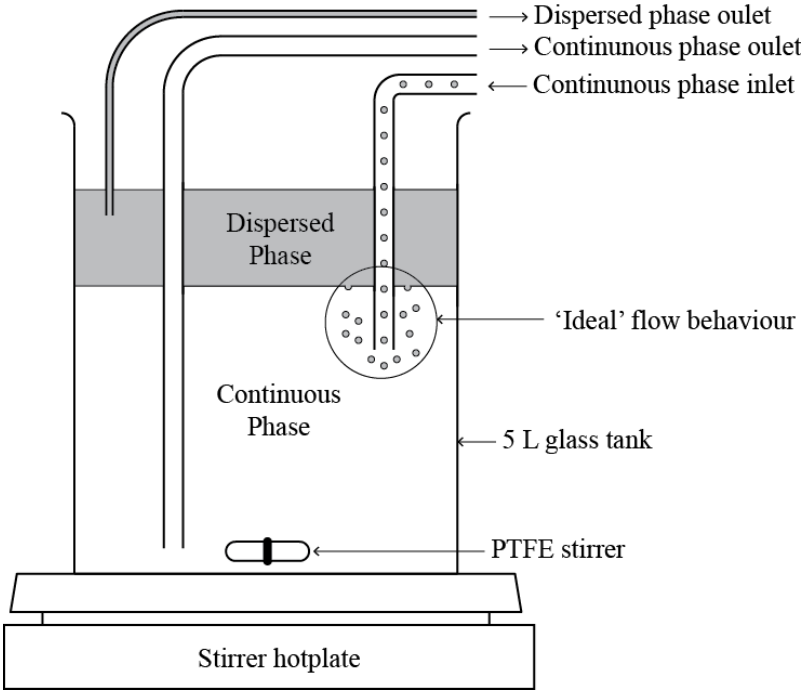

Figure 6.9 – Main storage tank showing location of inlets and outlets

Gentle agitation was encouraged to facilitate heat transfer, however this was kept to a minimum so as not to disrupt the oil-aqueous interface and hence prematurely increase surface area. Preliminary heating studies across volume of the tank showed an approximately uniform temperature upon heating with a maximum measured variation of 2 °C measured at a set point of 60 °C

A critical aspect in the design of the storage vessel was the ability to separate the dispersion upon return to the main tank. Preliminary experiments with outlet directly into the main tank allowed for a gradual increase in entrained dispersed phase. Observation showed bypassing of the entrained dispersed phase directly into the aqueous phase inlet (Figure 6.10).

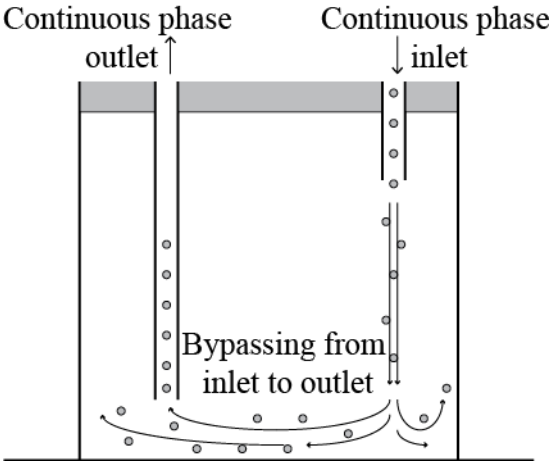

Figure 6.10 – Main storage tank with observed droplet bypassing

This was problematic since natural coalescence was undefinably delayed and therefore a quantifiable volume of dispersed phase was unknown. Indeed the continual recycle could potentially alter the size of the dispersed phase when passed through the pumps. This was best avoided for the acquisition of comparable reaction data.

To avoid bypassing, baffling of the main tank was investigated. The most effective baffling was to effectively direct the outlet flow upwards away from the aqueous phase inlet. In fact moderately coalesced dispersed phase droplets allowed for easy observation of the flow pattern, useful in the assessment of effectiveness of baffling. A preliminary modification involved the use of an additional vessel submerged in the aqueous phase layer into which the outlet could be flowed. Assessment of a range of vessel geometries led to the selection of one with a spherical lower section, which allowed the outlet flow to circulate and calm significantly (Figure 6.11). Importantly the intermediate vessel was wide enough neck so as not to reintroduce a constriction to reaccelerate the outlet flow.

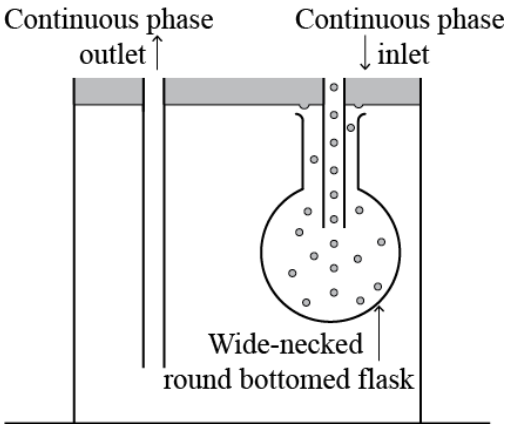

Figure 6.11 – Main storage tank with intermediate flow calming vessel

Optimisation of the design was made by installation of additional flow dissipation within the intermediate vessel. This was performed by filling the inlet vessel with glass ballast in the form of beads of sufficient weight so as they were not moved by the outlet flow. Observation of the modified design showed large drops of oil were rising from the vessel to reintegrate with the above bulk phase (Figure 6.12), indicative of increased coalescence and decrease flow turbulence.

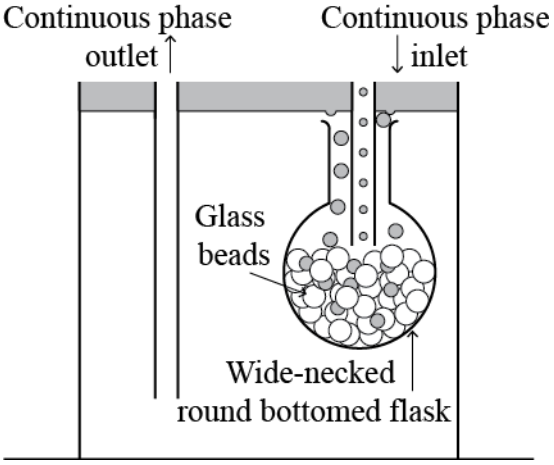

Figure 6.12 – Main storage tank with intermediate flow calming vessel filled with glass beads

6.2.6 Continuous phase stream design consideration

The continuous phase streams were all delivered via 3/8" O.D. 1/4" I.D. PTFE tubing. The fluid was pumped via a Micropump gear pump. The materials of the construction of the pump gear were PPS, the seals Viton and the main base material Stainless steel 316.

The pump was calibrated using timed collection, shown in Figure 6.13 along with the associated Reynolds number for a fluid with the same viscosity and density of water. The pump setting was designated as the frequency of the gear rotation, n, out of a maximum of 60

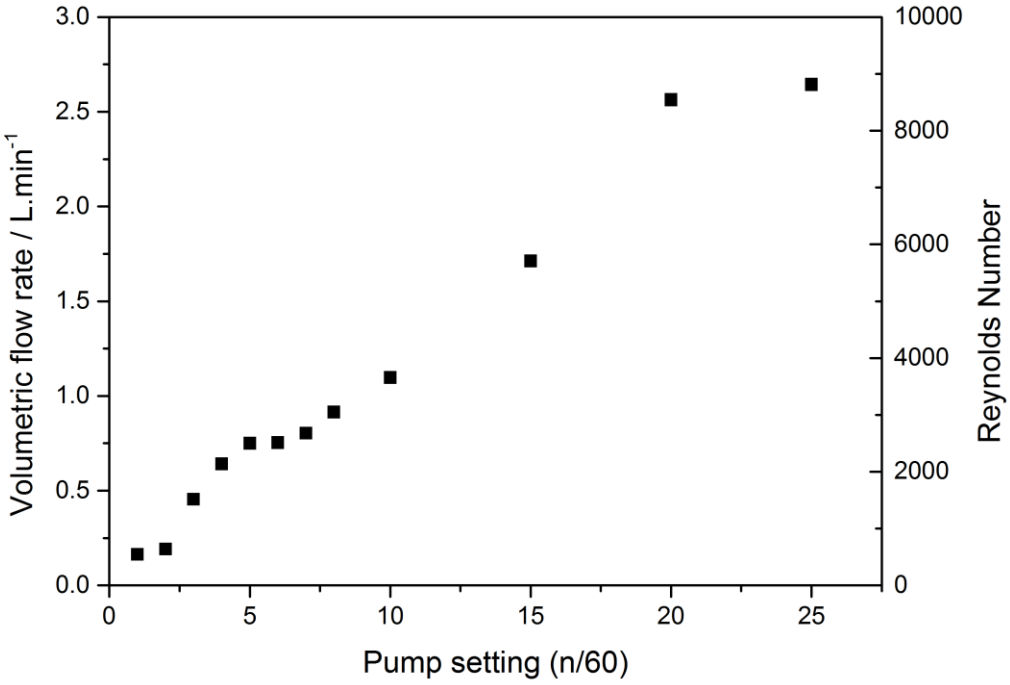

Figure 6.13 – Continuous phase pump calibration graph. Associated Reynolds number is plotted on the secondary axis.

An important parameter shown to influence the droplet size was the wall shear stress applied across the membrane surface (Schröder *et al.*, 1998). This varies with flow rate, and hence Reynolds number (Equation 4.19). In addition the shear rate is a dependent on the friction factor (Equation 4.20), which displays a relationship with flow parameters which varies depending on the flow regime (Peng and Williams, 1998).

$$\mathrm{Re} = \frac{\rho_c V_{ax} D}{\mu_c} \qquad 4.19$$

Where D is the membrane tube diameter and μ_c is the continuous phase viscosity, V_{ax}, is the continuous phase axial velocity and ρ_c is the continuous phase density, assumed to be that of water.

$$f = \frac{2\tau_w}{V_{ax}^2 \rho_c} = \begin{cases} 16/\mathrm{Re} & \mathrm{Re} < 500 \\ 0.0792\,\mathrm{Re}^{-0.25} & 500 \le \mathrm{Re} \le 20000 \end{cases} \qquad 4.20$$

Where f denotes the fanning friction factor and τ_w, denotes the wall shear stress.

Using the relationships given above for a 6 mm diameter tubular membrane the shear stress at the wall was calculated (Figure 6.14) over the range of accessible flow rates. An

assumption was made the tube was smooth, which defines the fanning friction factor relationships indicated in Equation 4.20, although no attempt was made to quantify the roughness.

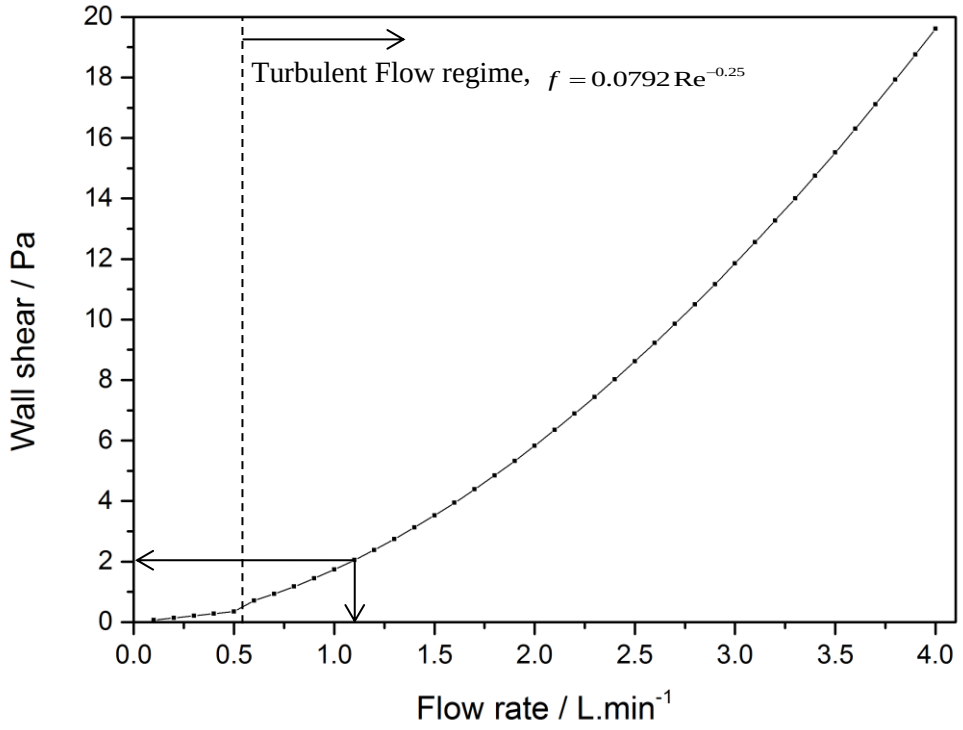

Figure 6.14 – Calculated plot of the wall shear resulting from a given flow rate for the 6 mm smooth membrane tube.

Since the droplet size is reported to only be dependent on the shear stress only up until a finite value, above this the droplet size was assumed to be at the minimum. For a given pore size the shear rate at which the droplet size can assumed to be at its minimum has been suggested as > 2 Pa for a 0.1-0.5 μm pore size, and > 20 Pa for 0.8 μm (Joscelyne and Trägårdh, 2000).

The selected pump setting was ten, which corresponded to an operating flow rate of approximately 1.1 L.min^{-1}. The calculated wall shear was thus 2 Pa (indicated by the drop arrows on Figure 6.14) indicated by the above report to result in shear stress independent droplet generation for membranes of 0.1 μm. From the above reported relationships one can reason that membranes with pore sizes much lower than this, such as the 80 nm device used in these experiments will hence also be operating in a shear independent droplet regime. In addition, in order to keep the flow regime out of the transitional region, this flow rate of 1.1 L.min^{-1} corresponded approximately to the lower limit of Reynolds number which describes

turbulent flow (Figure 6.14). The maximum flow rate lower than this, with Reynolds number not indicating the transitional regime, i.e. the laminar regime, would result in a wall shear less than 0.5 Pa, and therefore potentially not operating at minimum droplet size.

6.2.7 Dispersed phase stream design considerations

The dispersed phase lines were similarly all PTFE with a smaller bore tubing of O.D. 1/4", ample for the much reduced flow rate in these lines (< 10 $mL.min^{-1}$). The streams flow rate was adjusted using a gear pump to a certain pressure (typically 2 bar), metered downstream with the flow rate measured on line. A digital flow meter was used which was calibrated for aqueous flows therefore this had to be adjusted for oil. The difference in indicated to actual flow rates was the ratio between the viscosities of the process fluid compared to water. This was confirmed via timed volumetric collection.

The Reynolds numbers for the operating flow rates (<10 $mL.min^{-1}$) were calculated to be < 1 which would signify laminar or creeping flow regimes.

6.2.8 Start-up

The start-up procedure focused on two key aspects,

1. removing any entrained air within the system and
2. heating the phases and main tank to reaction temperature.

The main tank was filled with the continuous phase and set the hot plate set to heat to reaction temperature of 60°C. The air was purged, and the tubing heated of the continuous phase line by flowing the continuous phase through the line. The dispersed phase was heated separately to temperature and then the pump started to fill the dispersed line, which was disconnected so as to avoid pushing air into the module. The line was then connected to the module and the module repositioned so that the oil inlet pointed down and the continuous side outlet was raised, to encourage air to collect in this upper position on the outside of the membrane in the module. The pressure was monitored during this purging phase and was observed to steadily increase during this period with a degree of fluctuation which was attributed to the compression of the air pocket. The oil phase was run in this manner until the fluctuation ceased, and the pressure reached a steady value, suggesting that the entrapped air had permeated through the membrane. The continuous phase flow was restarted and a measured volume was then run out to a separate vessel to flush the inside of the module along with the permeated oil which would have coalesced on the inside due to no shear stress being applied during the air flush. The continuous phase was flushed through until the line had been completely filled and no air could be observed. The flow of all phases was ceased and the dispersed phase, having been heated separately, was gently poured onto the

top of the continuous in the main tank. The continuous outlet was returned to the main tank and at this point the system designated as primed, heated and ready for operation. Operation was commenced through restarting all flows at the operating conditions along with activation of the run timer.

6.3 Process integration of reaction and separation using the membrane system

The system as a whole is a batch reactor with the membrane acting as an integrated dispersion unit. A series of simplifying assumptions are made:

1. The reaction in the bulk reservoir is mass transfer limited, and as such the observed rate (the rate of diffusion of catalyst species between oil and aqueous phase) is very low approximately 0.01 $mmol_{epox}.L^{-1}.min^{-1}$. This is based on preliminary biphasic experiments and the rate normalised for the surface area and volume changes.
2. The kinetic reaction regime takes place when the oil phase is dispersed as droplets, as proved by the experiments contained in Chapter 5.
3. Droplets are formed along the length of the membrane. Assuming that porosity is homogeneous, for modelling purposes, the average residence time of a droplet inside the membrane module will be equal to that of a droplet formed at the longitudinal centre. As such, the overall reaction residence time can be calculated as shown in Equation 4.18.
4. The unsaturated sites are situated on the oil molecules therefore the epoxidation must occur within the oil phase each of the dispersed droplets.
5. There is complete coalescence of all oil droplets upon contact with the coalescer.

The rate of reaction in the bulk reservoir system was determined from previous smaller scale batch reactions, and normalised according to the interfacial area (since mass transfer limited) and volume of oil phase used.

Owing to the recycle of both phases the reactor is the equivalent to a single batch reactor with the membrane acting to disperse the oil phase, akin to an impeller mounted in a batch vessel.

In order to provide useful measures of the effectiveness of the reactor, various parameters had to be calculated. The critical parameter was the reactor residence time, this can be defined as the total time the fluid has spent within the reactor, i.e. the time spent at an increased surface area. The reaction was assumed to occur during this time period only. The residence time of the reactor was calculated from reactor volume (V_r) and the combined flow rate of the dispersed (Q_d) and continuous (Q_c) phases,

$$Residence\ time\ per\ pass = \tau_p = \frac{V_r}{(Q_c + Q_d)} \quad 4.21$$

The time per pass, or recycle times for both phases was also be calculated,

$$Dispersed\ phase\ recycle\ time = t_{r,d} = \frac{V_d}{Q_d}$$
$$Continuous\ phase\ recycle\ time = t_{r,c} = \frac{V_c}{Q_c} \quad 4.22$$

Where V is the volume of the dispersed, d, or continuous phase, c.

The dispersed phase recycle time was taken to be the time that the total volume of dispersed phase had run through the reactor once. In other words, the total volume of dispersed phase had been in the reactor i.e. dispersed to a definable surface area for a time equal to the residence time.

Therefore the total residence time could be calculated from the total run time, t_t,

$$Total\ accumulated\ residence\ time = \tau = \frac{\tau_p t_t}{t_{r,d}} = \frac{V_r Q_d}{(Q_c + Q_d)V_d} \quad 4.23$$

The assumption was made that $t_{r,d}$ corresponded to the time at which the volume V_d had spent the residence time, τ, as a dispersion.

A progressive reduction in the observed rate of epoxidation, taken to be gradients of tangents of the concentration time graph in Figure 6.15, with increasing residence time was observed. To validate the assumption above, namely that the majority of the reaction takes place whilst the oil phase is dispersed, the normalised bulk reaction rate is plotted for comparison, along with the corrected concentration data excluding any mass transfer limited bulk reaction. From Figure 6.15 the initial rate of reaction appears to be largely unaffected by the bulk phase reaction.

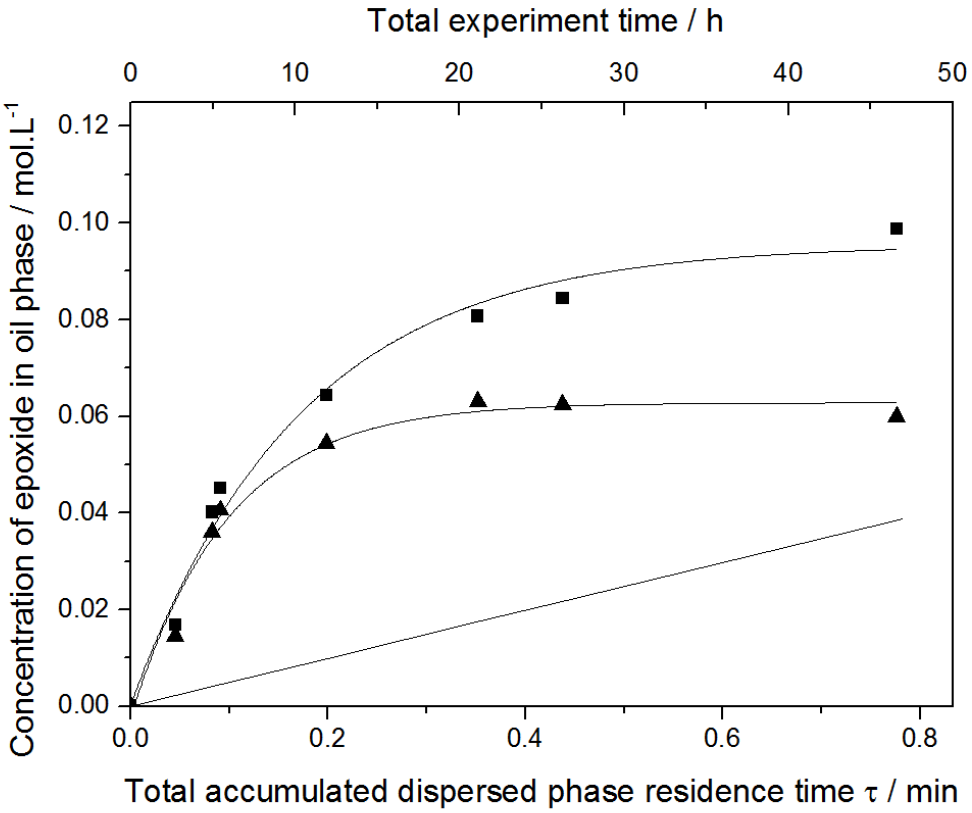

Figure 6.15 – Observed concentration increase of epoxide with residence time in the membrane reactor (■). The line represents the surface area normalised, mass transfer limited, rate of reaction which exists in the bulk reservoir. The lower curve represents the observed results corrected for any bulk reservoir reaction (▲). Conditions: 60°C Aqueous phase concentrations: 0.1 M Na_2WO_4, 2 M AcOH, 3 M H_2O_2.

Initially, the concentration of the epoxide product increases linearly as the reaction time increase, and plateaus after about 10 h of experiment run time (equivalent to 0.2 min oil dispersed residence time). This observed loss of reaction rate was attributable to aqueous phase hydrogen peroxide concentration which was found to be 0.1 M after 20 h total run time, a significant reduction from the initial 3 M starting concentration. To encourage further reaction more hydrogen peroxide was added at this point, to bring the aqueous phase concentration to 1 M. This additional oxidant probably accounts for the additional slight increase in the epoxide concentration in the remainder of the reaction time. At 48 h total run time the hydrogen peroxide was again depleted. Since the rate of decomposition for the aqueous phase conditions and major materials of construction was tested previously and shown to be negligent the decomposition was determined to be due to an outside contaminating influence, probably an iron species dissolved from a support clamp.

Inspection of the flow lines showed no traces of pitting or contamination. The likely source of contamination was found to be from the clamps situated above the main storage vessel which were used for guiding the inlet and outlet lines to the main tank. Observation of the clamp screw showed significant discolouration and corrosion. For easy access of flow lines

to the main tank it was open topped. It was assumed that the relatively non-volatile sunflower oil phase sitting above the aqueous would mitigate any evaporation likely to occur over the course of operation. However it was reasoned that this assumption was likely to be wrong as the most likely explanation for the decomposition is that that there must have been some evaporation of the aqueous phase resulting in the vapours contacting that clamp. This then resulted in the condensation and subsequent return of a solution contaminated with trace amounts of metal ions, for example iron, the clamp material of construction. This is a known to be very active towards the decomposition of the oxidant (Haber and Weiss, 1934). An attempt was made to mitigate this at the 24 h mark by enclosing the clamping arms above the tank within non-reactive polymer coverings. However this proved to be ineffective, confirming that the source of decomposition was contamination now already in the system.

Despite the lack of long term reaction stability of the system due to this contamination, the initial linear region of the concentration-residence time graph suggests that within this region the concentration of hydrogen peroxide were not limiting. Therefore the initial observed rate could be calculated. The initial rates of reaction in a surfactant-less biphasic, emulsion (Chapter 5) and the membrane reaction system reported in this chapter are compared in Figure 6.16.

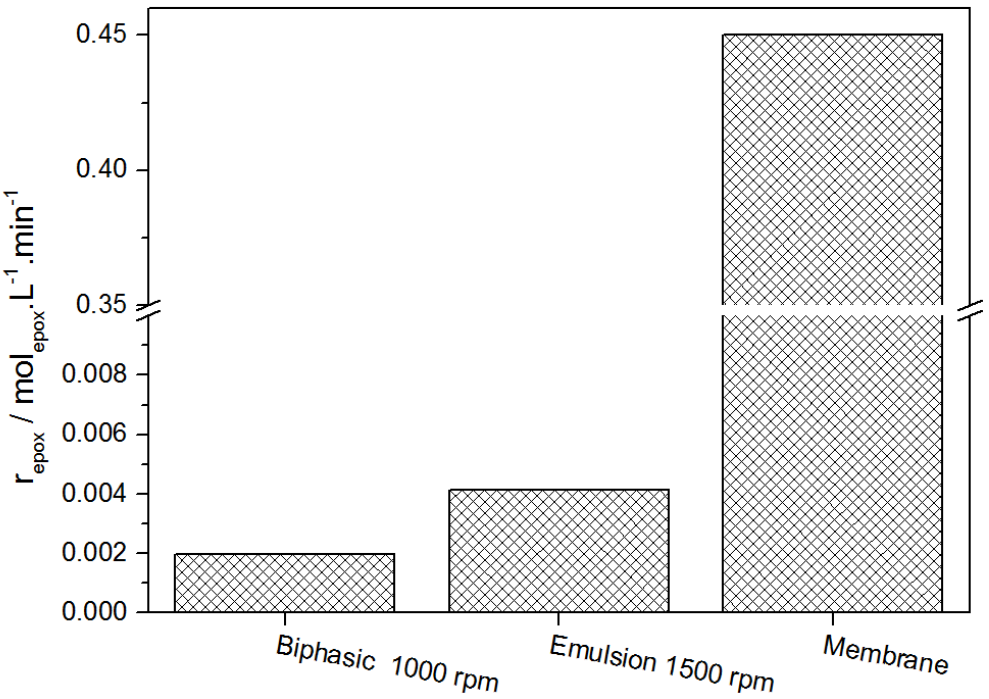

Figure 6.16 – The observed rate of epoxidation with different techniques. Conditions: 60°C Aqueous phase concentrations: 0.1 M Na_2WO_4, 2 M AcOH, 3 M H_2O_2. Aqueous:oil phase volumes are the same, 90:10. No surfactant was used in the Biphasic and membrane operations. 10 wt% Brij-S10 was used in the emulsion reaction.

When compared to all previous methods of reaction the membrane reactor resulted in a two orders of magnitude increase in reaction rate. In addition this reaction was performed on a twenty fold increase in total reaction volume. One possible explanation for the observable differences seen between the reaction systems may be due to the use, or not, of surfactant. Considering that the surfactant molecule will populate the oil-aqueous interface one can imagine that these molecules may be imposing a steric effect, effectively slowing the inter phase transfer (Chen and Lee, 2000). Another possible situation which could result in the high rate of reaction is that the smallest entrained oil droplets are not completely coalesced upon entering the main vessel, and persist in the aqueous phase, being drawn round and recycled. In this situation the assumed accumulated residence time would be a large under estimation, resulting in an apparent rapid rate.

6.4 Conclusions

Process integration in a microfluidic device was investigated to attempt to marry the epoxidation of sunflower seed oil with a downstream separation to enable a continuous operation. Various methods to control the reaction variables of residence time and temperature were investigated, with the conclusion that the use of such a microfluidic system actually inhibited the integration of reaction and separation. The reaction temperature was maintained by immersion of the reactor in a heated bath, after the use of electrical heating proved ineffective. Various methods to control the residence time were investigated, namely elongation of the flow path and variation of the flow rates, however the lack of stabilising agents meant that coalescence was observed at high path lengths or slow flow rates, giving an upper limit of 9 seconds residence time. Multiple passes of each phase were envisaged to accumulate residence time however, this proved impractical since the volumes of reaction media required to successfully separate required extremely long total run times.

The hindrance of small volumes in the separation of the aqueous and the oil phase in the microfluidic system was circumvented by operating on a much larger scale. The design and construction of a membrane reactor was carried out, culminating in the successful epoxidation of sunflower seed oil on a multi litre scale with the integration of separation of both aqueous and oil phase. An α-alumina membrane was used with pores of the order of 0.08 μm which resulted in an average droplet size of 3-4 μm, resulting in a pore size-droplet size ratio of around 50, in keeping with the upper values reported in the literature. Indeed much high rates of reaction were observed for the membrane systems with continuous operation and recycle when compared to the stirred, surfactantless biphasic and the surfactant mediated emulsion systems. The explanation of this behaviour was attributable to a combination of a large interfacial surface area and the lack of a barrier surfactant layer, which has been shown to hinder inter-phase transfer across an interface, and slow or prevent separation.

7 Overall Conclusions

The results and the approach shown in this thesis present a multidisciplinary method for the adaptation of liquid-liquid biphasic reactions towards continuous processing and downstream separation of product streams. To summarise the main findings paramount for the development of this method:

A detailed investigation into the biphasic epoxidation of sunflower seed oil enabled determination of the rate limiting step. At interfacial areas between the oil and aqueous biphase of approximately less than 0.25 $m^2.g^{-1}$ the system was mass transfer limited, indicating the observed rate was dependent on diffusion between the phases. At interfacial surface areas higher than this the rate limiting step was found to most likely be the presence of the active catalyst species in the oil phase.

Understanding the rate limiting step and the minimum surface area needed to avoid mass transfer limitation the biphasic epoxidation reaction was integrated into continuous process. The use of an α-Al_2O_3 hydrophilic membrane enabled oil-in-water dispersions at surface areas in excess of 0.25 $m^2.g^{-1}$. Importantly these dispersions were not stabilised by use of surfactant, allowing for a transiently interface, facilitating reaction, before inherent downstream separation through phase immiscibility. Phase separation was enhanced through use of a flow calming,

coalescence unit installed in the membrane system. High rates of reaction were observed considering the very short residence time (seconds) the droplets existed for. This reactor was operated in a continuous recycle type arrangement to allow for multiple passes of the separated oil and aqueous phases to increase conversion to epoxide. In addition to operation in a continuous manner, the epoxidation was performed on 400 mL, a scale up factor of over 100 compared to the previous batch emulsion reactions.

Additional to the above a range of interfacial areas of the oil-aqueous biphasic system were formed to test the mass transfer limitation via the use of three techniques.

1. A design of experiments approach for the use of high shear homogenisation was able to produce interfacial areas between approximate 0.3 and 3.9 $m^2.g^{-1}$. The variables which showed the most significant change in the interface area were the speed and duration of homogenisation and the oil phase surfactant concentration. Interestingly there was a limit to the effectiveness of an increase the power input (homogenisation speed and duration) upon surface area increase. Only high levels of surfactant showed an increase in surface area when subjected to an increase in power, enabling information regarding the minimum surfactant requirement per volume of oil to be calculated.
2. The use of glass microfluidic devices with channels 100 - 300 μm enabled droplet generation in the approximate interfacial area range 3.0×10^{-2} – 6.0×10^{-2} $m^2.g^{-1}$. Changing the flow rate ratio, between 0.01 and 1 (dispersed to continuous phases) did not show a large change in the droplet size generated. From visual observations using high speed photography, it was concluded that the geometry and the surfactant concentrations were most likely defining factors. The limited surface area range was likely due to the ability to form one (in the case of the flow focused) and two (in the case of then T-junction) droplet generating regimes. Attempting to alter surfactant levels, in keeping with the homogenisation approach, was not feasible due to high viscosities of oil phase surfactant levels in excess of 1 wt%, creating prohibitively large pressure drops across the microchannel chips.
3. A glass T-junction capillary device was used for the creation of interfacial areas between 9.6×10^{-4} and 5.6×10^{-3} $m^2.g^{-1}$. This was conducted by changing the dispersed to aqueous flow rate ratio. The interfacial area was defined by the approaching hemispherical cap area of the oil phase segments within the capillary. This cap area could be calculated by measuring the oil-water-glass contact angle (121°), using the captive bubble technique, followed by mathematical manipulation.

Further detailed studies into at high oil-aqueous interfacial areas found the rate limiting step to be dependent on two factors:

1. The formation of the active catalyst species, which occurs in the aqueous phase, found to be dependent on the aqueous phase concentrations of sodium tungstate, acetic acid, and hydrogen peroxide.
2. The partitioning of the active catalyst species into the oil phase. This was shown to be a function of the relative solubility of the carboxylic acid promoter, bound to the tungstate. The use of longer carbon chain acids with a higher oil solubility exhibited a fast rate, but only when still aqueously miscible.

7.1 Comparison with research aims

To assess the progress of this research against the conclusions present here the aims set out for the project are summarised below, along with how each were achieved:

- *Develop a suitable model system for both emulsification and reactivity;*

  The epoxidation of sunflower seed oil using sodium tungstate as catalyst, hydrogen peroxide as oxidant and acetic acid as promoter was found to be suitable as the product was easily identifiable form starting materials. The dispersion of a vegetable oil – aqueous system is well studied in the literature allowing for development from a strong literature precedent
- *Understand the phase space relationship between surfactant, oil and aqueous phase for an appropriate model system;*

  Preliminary investigations into the relative volumetric ratios between the components of the dispersions sunflower oil, aqueous, Brij-S10 system identified that high aqueous low oil and relatively low surfactant were suitable to form the oil in water emulsions needed in this investigation
- *Be able to reliably and reproducibly achieve a range of droplet sizes with oil-surfactant-water emulsions;*

  The use of experimental design in conjunction with high-shear homogenisation enabled a range of relatively high interfacial area dispersions. The techniques of microfluidic and capillary based reactors were further able to produced relatively intermediate and low interfacial areas respectively. These results are contained in Chapter 4.
- *Develop rigorous analytical methods for droplet sizing and extent of reaction;*

The use of laser scattering and light microscopic techniques allowed for the reproducible measurement of the droplet size distributions of the emulsions formed. The extent of the epoxidation reactions were able to be followed through the well-defined integrals of the ^{1}H – NMR spectra of the extracted oil phase.

- *Obtain comprehensive kinetic data assessing the effect of the reaction variables and droplet sizing;*

  The relative orders of reaction for each of the oxidant, catalyst and promoter were investigated as well as the influence on droplet size. These results are reported in Chapter 5.

- *Implement the kinetic data in the design and construction of a microfluidic reactor*

  The implementation of the microfluidic reactor was attempted but was found to be unsuitable owing to the low residence times and the inability to recycle at such low reaction volumes. These results are reported in Chapter 6

- *Consider scale up in the form of design and construction of a novel membrane reactor; and*
- *Ultimately, upon achieving the above to integrate reaction and separation in non-surfactant stabilised systems*

  The culmination of the project involved the development of the continuous membrane reactor which was implemented and the epoxidation of sunflower seed oil achieved in a continuous fashion

Considering the conclusions given above the aims of this project were predominantly met.

7.2 Further study

The limitations to the work contained herein along with proposed areas of research to strengthen the topic are given in this section, divided broadly into the research areas of formulation, reaction, microfluidic and membrane although overlap between two or more groupings is inevitable.

7.2.1 Formulation

The main limitation of the formulation work contained within this thesis is that only a single surfactant has been investigated to any significant depth. The use of TWEEN type non-ionic surfactants in the emulsification of sunflower seed oil was also investigated in some detail but did not lead to any significant difference so was omitted from this report. An experimental design approach could have been used to more systematically assess the

effectiveness of the surfactants, enabling potential discovery of new formulations. Further to this the inclusion of ionic (anionic/cationic) surfactants could have been assessed, as there is literature precedent to suggest an enhancement of rate of reaction when ionic homogeneous catalysts are used. As the scope of this project was confined to liquid-liquid systems, the aspect of Pickering emulsions was not considered. However, the use of nanoparticulate polyoxometallate (POM) catalysts in this sense could combined the surface stabilising effect and catalysis specifically for liquid-liquid systems whereby the reaction can be assumed to be at the boundary of the two liquids.

For reactions which involve the penetration of one species into another, a quantification of the boundary effects of stabilising agents would enable evaluation of any mass transfer limitations which may be occurring. The use of SANS along with deuterated or labelled compounds would allow this to be undertaken, although admittedly at a significant cost.

7.2.2 Chemical reaction

Specifically related to the polyoxometallate/peroxotungstate catalysed reactions investigated in this thesis, the determination of the actual active catalytic species still requires much work. Initial investigations were conducted during this research using mass spectrometry to attempt to clarify the existence of metallate cluster. The preliminary results suggest multinuclear species do exist and are heavily dependent on the pH of the solution in which they are formed, although this is known for other POMs. Additionally the presence or absence of hydrogen peroxide showed a marked difference in the ability to form clusters. Inclusion of the peroxide limited the ability of the system to form clusters, although, again this is not new.

Since the reaction under investigation is clearly multiphasic an immediate concern is the local concentration of catalyst species existing in each phase. Knowledge of this would not only help elucidate the mechanism but facilitate kinetic analysis through knowledge of the equilibrium constants. In addition the direct influence on the partitioning of the catalyst centre through carboxylic acid chain length or use of phase transfer agents could be directly measured. Techniques such as ^{183}W-NMR and/or ICP-MS would allow analysis of the presence of the tungsten amounts in each phase although this would require separation of the phases, still not elucidating the *in-situ* concentrations. Tungsten NMR shows promise to elucidate the actively oxygenated species since a difference in chemical shifts would no doubt result.

An expansion in the scope of the substrates would obviously help show relevance for this system in the wider context. Initial studies with cyclooctene as substrate were carried out and although reaction was successful, the failure to emulsify as simply as sunflower oil

result in it being dropped. That being said, some success was made with TWEEN and SPAN combinations to emulsify cyclooctene so persistence down this route would be fruitful. In hindsight, and although not a major issue, the use of a chemically, more simple molecule as model substrate would probably have been successful, despite the vast literature on sunflower oil emulsification. Immediate choices such as 1-octene, although terminal alkenes can be difficult to epoxidise or hexadecene would perhaps have simplified the system, although with a complex system it is obviously hard to predict.

The investigation of other liquid-liquid reactions, many of which listed in the literature review, could also have been selected and would be a productive area of investigation specifically if improvements can be made to industrially relevant processes, such as oxidation

7.2.3 Microfluidics

The microfluidics devices used in the research have a very large potential and would likely have been the primary method of investigation if this work or similar were to be repeated. The primary benefit is in the monodisperse and fine control afforded to the creation of dispersed systems. This is well known, with the examples given in the literature review along with the models created to offer predictions from flow parameters. Where this work failed was in the inability of the system to offer stable flow conditions, related to the high viscosity of the fluids being used. Higher pressure, pulseless delivery systems exist and their use along with measurement of the line pressures is critical. Coupled with high speed video capture these would facilitate the use of such devices as well as providing data with which to compare and update literature models, for the various junction geometries investigated. An additional limitation which was realised during this research was the use of hydrogen peroxide in confined systems. As mentioned throughout this thesis, low levels of decomposition exist and make flow behaviour difficult to predict and hence modelling quite challenging. Despite its green credentials the decomposition of hydrogen peroxide in closed systems remains a significant barrier, therefore in these systems, other oxidants must be advised. Obviously the selection of a different reaction would negate these problems. The exciting aspect of microfluidics is the ability to use computation fluid dynamics to predict flow behaviour since the experimental length scales are not so large as to be computationally prohibitive.

7.2.4 Membrane technologies

The research into the use of the membrane in this thesis can only really be taken as a preliminary guide and an example to show that successful reaction can be achieved. There are many more experiments to carry out to gain real insight into this process.

The selection of the type of membrane should be addressed with regards to porosity, pore spacing and pore size distribution. For example the selection of slotted or microporous glass devices with notably defined pore sizes would be advantageous.

A detailed emulsification study with regards to the flow parameters and subsequent droplet sizes would facilitate understanding the emulsification process specific to fluids being used. Models have been proposed and indeed are compared in this thesis; however they are limited in their validity to a narrow range of parameters. Therefore a study exploring new fluid combinations and a wider range of flow parameters would add to the wider understanding.

Repeated experimentation with regards to the oxidation reaction as the primary focus of the work, would obtain a much broader range of reaction data. This would enable a much more complete assessment of the system and allow reactor comparison. Sampling at different points in the reactor would allow for a baseline assessment of reaction progress in the bulk phase compared to the dispersed region. Additionally the prevention of hydrogen peroxide decomposition is of immediate concern due to its exothermic nature. A more controlled environment with a bespoke heating and separation vessel is envisaged.

With regards to the processing aspect the recycle of both phases requires a better understanding of the coalescence rate of the oil. This would also act to confirm, or not, the assumptions made within the relevant chapter of immediate phase separation

8 References

AHMED-OMER, B., BRANDT, J. C. & WIRTH, T. 2007. Advanced organic synthesis using microreactor technology. *Organic & biomolecular chemistry,* 5**,** 733-740.

ANASTAS, P. T. & WARNER, J. C. 2000. Green chemistry : theory and practice. xi, 135 p.

ANDERSON, K., KIZLING, J., HOLMBERG, K. & BYSTROOM, S. 1998. A ring-opening reaction performed in microemulsions. *Colloids and Surfaces A: Physicochemical and Engineering Aspects,* 144**,** 259-266.

ARENDS, I. & SHELDON, R. A. 2002. Recent developments in selective catalytic epoxidations with H2O2. *Topics in Catalysis,* 19**,** 133-141.

ASERIN, A. 2008. *Multiple Emulsion: Technology and Applications*, Wiley.

ATHEY, R. D. 2011. *Emulsion Polymer Technology*, Taylor & Francis.

ATTWOOD, D., MALLON, C., KTISTIS, G. & TAYLOR, C. J. 1992. A study on factors influencing the droplet size in nonionic oil-in-water microemulsions. *International Journal of Pharmaceutics,* 88**,** 417-422.

ATTWOOD, D., MALLON, C. & TAYLOR, C. J. 1992. Phase studies on oil-in-water phospholipid microemulsions. *International Journal of Pharmaceutics,* 84**,** R5-R8.

BECHER, P. 1983. *Encyclopedia of Emulsion Technology: Basic Theory*, Taylor & Francis.

BELKOURA, L., STUBENRAUCH, C. & STREY, R. 2004. Freeze Fracture Direct Imaging: A New Freeze Fracture Method for Specimen Preparation in Cryo-Transmission Electron Microscopy. *Langmuir,* 20**,** 4391-4399.

BIELLA, S. & ROSSI, M. 2003. Gas phase oxidation of alcohols to aldehydes or ketones catalysed by supported gold. *Chemical Communications***,** 378-379.

BINKS, B. P. (ed.) 1998. *Modern aspects of emulsion science,* Cambridge: Cambridge Royal Society of Chemistry.

BISHOPP, S. D., SCOTT, J. L. & TORRENTE-MURCIANO, L. 2014. Insights into biphasic oxidations with hydrogen peroxide; towards scaling up. *Green Chemistry,* 16**,** 3281-3285.

BROZE, G. 1999. *Handbook of Detergents: Properties*, Taylor & Francis.

BURNS, J. R. & RAMSHAW, C. 2001. The intensification of rapid reactions in multiphase systems using slug flow in capillaries. *Lab on a Chip,* 1**,** 10-15.

CARRERO, H., GAO, J., RUSLING, J. F., LEE, C.-W. & FRY, A. J. 1999. Direct and catalyzed electrochemical syntheses in microemulsions. *Electrochimica Acta,* 45**,** 503-512.

CHAN, E. M., ALIVISATOS, A. P. & MATHIES, R. A. 2005. High-Temperature Microfluidic Synthesis of CdSe Nanocrystals in Nanoliter Droplets. *Journal of the American Chemical Society,* 127**,** 13854-13861.

CHARCOSSET, C., LIMAYEM, I. & FESSI, H. 2004. The membrane emulsification process—a review. *Journal of Chemical Technology & Biotechnology,* 79**,** 209-218.

CHATTOPADHYAY, A. & SALASKAR, A. 2000. A Practical Method for the Reformatsky Reaction of Aldehydes. *Synthesis,* 2000**,** 561-564.

CHEN, L.-H. & LEE, Y.-L. 2000. Adsorption behavior of surfactants and mass transfer in single-drop extraction. *AIChE Journal,* 46**,** 160-168.

CHOU, T.-C. & CHANG, J.-Y. 1986. ACETIC ACID AS AN OXYGEN CARRIER BETWEEN TWO PHASES FOR EPOXIDATION OF OLEIC ACID. *Chemical Engineering Communications,* 41**,** 253-266.

CHRISTOPHER, G. F. & ANNA, S. L. 2007. Microfluidic methods for generating continuous droplet streams. *Journal of Physics D: Applied Physics,* 40**,** R319.

CHRISTOV, N. C., GANCHEV, D. N., VASSILEVA, N. D., DENKOV, N. D., DANOV, K. D. & KRALCHEVSKY, P. A. 2002. Capillary mechanisms in membrane emulsification: oil-in-water emulsions stabilized by Tween 20 and milk proteins. *Colloids and Surfaces a-Physicochemical and Engineering Aspects,* 209**,** 83-104.

CLAYTON, W. 1943. The theory of emulsions and their technical treatment. vii, 492 p.

COULSON, J. M. & RICHARDSON, J. F. 1999. *Coulson & Richardson's Chemical Engineering: Fluid flow, heat transfer and mass transfer. Solutions. Volume 1,* Butterworth-Heinemann.

CRAVEN, M., YAHYA, R., KOZHEVNIKOVA, E., BOOMISHANKAR, R., ROBERTSON, C. M., STEINER, A. & KOZHEVNIKOV, I. 2013. Novel polyoxometalate-phosphazene aggregates and their use as catalysts for biphasic oxidations with hydrogen peroxide. *Chemical Communications,* 49**,** 349-351.

CURRIE, F., HOLMBERG, K. & WESTMAN, G. 2001. Regioselective nitration of phenols and anisols in microemulsion. *Colloids and Surfaces A: Physicochemical and Engineering Aspects,* 182**,** 321-327.

CURRIE, F., HOLMBERG, K. & WESTMAN, G. 2003. Bromination in microemulsion. *Colloids and Surfaces A: Physicochemical and Engineering Aspects,* 215**,** 51-54.

DA ROSA, R. G., DE CAMPOS, J. D. R. & BUFFON, R. 2000. The effect of water on the rhodium-catalyzed carbonylation of isopropylallylamine. *Journal of Molecular Catalysis A: Chemical,* 153**,** 19-24.

DE MENECH, M., GARSTECKI, P., JOUSSE, F. & STONE, H. A. 2008. Transition from squeezing to dripping in a microfluidic T-shaped junction. *Journal of Fluid Mechanics,* 595**,** 141-161.

DE BELLEFON, C., TANCHOUX, N., CARAVIEILHES, S., GRENOUILLET, P. & HESSEL, V. 2000. Microreactors for Dynamic, High Throughput Screening of Fluid/Liquid Molecular Catalysis. *Angewandte Chemie International Edition,* 39**,** 3442-3445.

DENG, Y. Q., MA, Z. F., WANG, K. & CHEN, J. 1999. Clean synthesis of adipic acid by direct oxidation of cyclohexene with H2O2 over peroxytungstate-organic complex catalysts. *Green Chemistry,* 1**,** 275-276.

DESSIMOZ, A.-L., CAVIN, L., RENKEN, A. & KIWI-MINSKER, L. 2008. Liquid–liquid two-phase flow patterns and mass transfer characteristics in rectangular glass microreactors. *Chemical Engineering Science,* 63**,** 4035-4044.

DICKMAN, M. H. & POPE, M. T. 1994. Peroxo and Superoxo Complexes of Chromium, Molybdenum, and Tungsten. *Chemical Reviews,* 94**,** 569-584.

DUYNSTEE, E. F. J. & GRUNWALD, E. 1959. Organic Reactions Occurring in or on Micelles. I. Reaction Rate Studies of the Alkaline Fading of Triphenylmethane Dyes and Sulfonphthalein Indicators in the Presence of Detergent Salts1. *Journal of the American Chemical Society,* 81**,** 4540-4542.

ENACHE, D. I., EDWARDS, J. K., LANDON, P., SOLSONA-ESPRIU, B., CARLEY, A. F., HERZING, A. A., WATANABE, M., KIELY, C. J., KNIGHT, D. W. & HUTCHINGS, G. J. 2006. Solvent-free oxidation of primary alcohols to aldehydes using Au-Pd/TiO2 catalysts. *Science,* 311**,** 362-365.

FAUSTINO, C. M. C., CALADO, A. R. T. & GARCIA-RIO, L. 2010. Dimeric and monomeric surfactants derived from sulfur-containing amino acids. *Journal of Colloid and Interface Science,* 351**,** 472-477.

FELDMAN, Y., KOZLOVICH, N., NIR, I. & GARTI, N. 1997. Dielectric spectroscopy of microemulsions. *Colloids and Surfaces A: Physicochemical and Engineering Aspects,* 128**,** 47-61.

FU, T., WU, Y., MA, Y. & LI, H. Z. 2012. Droplet formation and breakup dynamics in microfluidic flow-focusing devices: From dripping to jetting. *Chemical Engineering Science,* 84**,** 207-217.

GAO, J., RUSLING, J. F. & ZHOU, D.-L. 1996. Carbon−Carbon Bond Formation by Electrochemical Catalysis in Conductive Microemulsions. *The Journal of Organic Chemistry,* 61**,** 5972-5977.

GARSTECKI, P., FUERSTMAN, M. J., STONE, H. A. & WHITESIDES, G. M. 2006. Formation of droplets and bubbles in a microfluidic T-junction-scaling and mechanism of break-up. *Lab on a Chip,* 6**,** 437-446.

GONZALEZ, A. & HOLT, S. L. 1981. Formation of macrocyclic lactones in microemulsions. *The Journal of Organic Chemistry,* 46**,** 2594-2596.

GONZALEZ, A. & HOLT, S. L. 1982. Effect of microemulsions on the Diels-Alder reaction: endo/exo ratios in the reaction of cyclopentadiene and methyl methacrylate. *The Journal of Organic Chemistry,* 47**,** 3186-3188.

GOTI, A. & CARDONA, F. 2008. Hydrogen Peroxide in Green Oxidation Reactions: Recent Catalytic Processes. *Green Chemical Reactions,* 191-212.

GOUIN, S. 2004. Microencapsulation: industrial appraisal of existing technologies and trends. *Trends in Food Science & Technology,* 15**,** 330-347.

GRADZIELSKI, M. 2008. Recent developments in the characterisation of microemulsions. *Current Opinion in Colloid & Interface Science,* 13**,** 263-269.

GREENSPAN, F. P. 1946. The Convenient Preparation of Per-acids. *Journal of the American Chemical Society,* 68**,** 907-907.

GUNSTONE, F. 2011. *Vegetable Oils in Food Technology: Composition, Properties and Uses,* Wiley.

GUPTA, A. & KUMAR, R. 2010. Flow regime transition at high capillary numbers in a microfluidic T-junction: Viscosity contrast and geometry effect. *Physics of Fluids,* 22**,** 122001-11.

GUTFELT, S., KIZLING, J. & HOLMBERG, K. 1997. Microemulsions as reaction medium for surfactant synthesis. *Colloids and Surfaces A: Physicochemical and Engineering Aspects,* 128**,** 265-271.

HABER, F. & WEISS, J. 1934. The Catalytic Decomposition of Hydrogen Peroxide by Iron Salts. *Proceedings of the Royal Society of London. Series A, Mathematical and Physical Sciences,* 147**,** 332-351.

HABER, F. & WEISS, J. 1934. The Catalytic Decomposition of Hydrogen Peroxide by Iron Salts. *Proceedings of the Royal Society of London. Series A - Mathematical and Physical Sciences,* 147**,** 332-351.

HÄGER, M. & HOLMBERG, K. 2000. A substitution reaction in an oil-in-water microemulsion catalyzed by a phase transfer catalyst. *Tetrahedron Letters,* 41**,** 1245-1248.

HANCOCKS, R. D., SPYROPOULOS, F. & NORTON, I. T. 2013. Comparisons between membranes for use in cross flow membrane emulsification. *Journal of Food Engineering,* 116**,** 382-389.

HAO, D. X., GONG, F. L., HU, G. H., ZHAO, Y. J., LIAN, G. P., MA, G. H. & SU, Z. G. 2008. Controlling factors on droplets uniformity in membrane emulsification: Experiment and modeling analysis. *Industrial & Engineering Chemistry Research,* 47**,** 6418-6425.

HASWELL, S. J., MIDDLETON, R. J., O'SULLIVAN, B., SKELTON, V., WATTS, P. & STYRING, P. 2001. The application of micro reactors to synthetic chemistry. *Chemical Communications***,** 391-398.

HAUMANN, M., KOCH, H. & SCHOMÄCKER, R. 2003. Hydroformylation in microemulsions: conversion of an internal long chain alkene into a linear aldehyde using a water soluble cobalt catalyst. *Catalysis Today,* 79-80**,** 43-49.

HAUMANN, M., YILDIZ, H., KOCH, H. & SCHOMÄCKER, R. 2002. Hydroformylation of 7-tetradecene using Rh-TPPTS in a microemulsion. *Applied Catalysis A: General,* 236**,** 173-178.

HILL, C. L. 1999. Controlled green oxidation. *Nature,* 401**,** 436-7.

HOAR, T. P. S., J. H 1943. Transparent Water-in-Oil Dispersions: the Oleopathic Hydro-Micelle. *Nature,* 152**,** 102-103.

HOEGAERTS, D., SELS, B. F., DE VOS, D. E., VERPOORT, F. & JACOBS, P. A. 2000. Heterogeneous tungsten-based catalysts for the epoxidation of bulky olefins. *Catalysis Today,* 60**,** 209-218.

HOLMBERG, K. 2007. Organic reactions in microemulsions. *European Journal of Organic Chemistry***,** 731-742.

HUDLICKY, M. 1990. *Oxidations in organic chemistry,* Washington DC, American Chemical Society.

HUNG, L.-H., CHOI, K. M., TSENG, W.-Y., TAN, Y.-C., SHEA, K. J. & LEE, A. P. 2006. Alternating droplet generation and controlled dynamic droplet fusion in microfluidic device for CdS nanoparticle synthesis. *Lab on a Chip,* 6**,** 174-178.

HUSNY, J. & COOPER-WHITE, J. J. 2006. The effect of elasticity on drop creation in T-shaped microchannels. *Journal of Non-Newtonian Fluid Mechanics,* 137**,** 121-136.

INOUE, K., ISHIDA, T., SHIBATA, I. & BABA, A. 2002. Remarkable Dependence of Diastereoselectivity on Anhydrous or Aqueous Solvent in the Indium Hydride Promoted Reductive Aldol Reaction of α,β-Unsaturated Ketones. *Advanced Synthesis & Catalysis,* 344**,** 283-287.

ISHII, Y., YAMAWAKI, K., URA, T., YAMADA, H., YOSHIDA, T. & OGAWA, M. 1988. Hydrogen peroxide oxidation catalyzed by heteropoly acids combined with cetylpyridinium chloride. Epoxidation of olefins and allylic alcohols, ketonization of alcohols and diols, and oxidative cleavage of 1,2-diols and olefins. *The Journal of Organic Chemistry,* 53**,** 3587-3593.

ISRAELACHVILI, J. N., MITCHELL, D. J. & NINHAM, B. W. 1976. Theory of self-assembly of hydrocarbon amphiphiles into micelles and bilayers. *Journal of the Chemical Society, Faraday Transactions 2: Molecular and Chemical Physics,* 72**,** 1525-1568.

ITAMI, K., NOKAMI, T. & YOSHIDA, J.-I. 2002. 2-Pyridyldimethylsilyl Group as a Removable Hydrophilic Group in Aqueous Organic Reactions: Formation of Molecular Aggregates and Dramatic Rate Enhancement in Diels–Alder Reactions. *Advanced Synthesis & Catalysis,* 344**,** 441-451.

JAEGER, D. A., DARLENE WARD, M. & MARTIN, C. A. 1984. Reactions in microemulsion media. Borohydride reduction of mono- and dicarbonyl compounds. *Tetrahedron,* 40**,** 2691-2698.

JONES, C. W. 1999. Application of hydrogen peroxide for the synthesis of fine chemicals. *Applications of Hydrogen Peroxide and Derivatives.* The Royal Society of Chemistry.

JONES, C. W. 1999. *Applications of Hydrogen Peroxide and Derivatives*, Royal Society of Chemistry.

JOSCELYNE, S. M. & TRÄGÅRDH, G. 2000. Membrane emulsification — a literature review. *Journal of Membrane Science,* 169**,** 107-117.

KAKAZU, E., MURAKAMI, T., AKAMATSU, K., SUGAWARA, T., KIKUCHI, R. & NAKAO, S.-I. 2010. Preparation of silver nanoparticles using the SPG membrane emulsification technique. *Journal of Membrane Science,* 354**,** 1-5.

KANDORI, K. 1995. Chapter 7 - Applications of microporous glass membranes: Membrane emulsification. *In:* GAONKAR, A. G. (ed.) *Food Processing.* Amsterdam: Elsevier Science B.V.

KANDORI, K., KISHI, K. & ISHIKAWA, T. 1991. Preparation of monodispersed W/O emulsions by Shirasu-porous-glass filter emulsification technique. *Colloids and Surfaces,* 55**,** 73-78.

KASHID, M. N., GERLACH, I., GOETZ, S., FRANZKE, J., ACKER, J. F., PLATTE, F., AGAR, D. W. & TUREK, S. 2005. Internal Circulation within the Liquid Slugs of a Liquid−Liquid Slug-Flow Capillary Microreactor. *Industrial & Engineering Chemistry Research,* 44**,** 5003-5010.

KATAOKA, H., UEDA, T., ICHIMEI, D., MIYAKUBO, K., EGUCHI, T., TAKEICHI, N. & KAGEYAMA, H. 2007. Evaluation of nanometer-scale droplets in a ternary o/w microemulsion using SAXS and 129Xe NMR. *Chemical Physics Letters,* 441**,** 109-114.

KATOH, R., ASANO, Y., FURUYA, A., SOTOYAMA, K. & TOMITA, M. 1996. Preparation of food emulsions using a membrane emulsification system. *Journal of Membrane Science,* 113**,** 131-135.

KATOH, R., ASANO, Y., FURUYA, A. & TOMITA, M. 1995. Conditions For Preparation of O/W Food Emulsions Using a Membrane Emulsification System. *NIPPON SHOKUHIN KAGAKU KOGAKU KAISHI,* 42**,** 548-555.

KISSA, E. 1999. *Dispersions: Characterization, Testing, and Measurement*, Taylor & Francis.

KNOTHE, G. & KENAR, J. A. 2004. Determination of the fatty acid profile by1H-NMR spectroscopy. *European Journal of Lipid Science and Technology,* 106**,** 88-96.

KOBAYASHI, I., NAKAJIMA, M., CHUN, K., KIKUCHI, Y. & FUKITA, H. 2002. Silicon array of elongated through-holes for monodisperse emulsion droplets. *Aiche Journal,* 48**,** 1639-1644.

KOZHEVNIKOV, I. V. 2002. Catalysts for fine chemical synthesis. *Catalysis by Polyoxometalates,* 2.

LAWRENCE, M. J. & REES, G. D. 2000. Microemulsion-based media as novel drug delivery systems. *Advanced Drug Delivery Reviews,* 45**,** 89-121.

LAWRENCE, M. J. & REES, G. D. 2000. Microemulsion-based media as novel drug delivery systems. *Advanced Drug Delivery Reviews,* 45**,** 89-121.

LETTS, K. & MACKAY, R. A. 1975. Reactions in microemulsions. I. Metal ion incorporation by tetraphenylporphine. *Inorganic Chemistry,* 14**,** 2990-2993.

LI, H., ZHU, W. S., HE, X. Y., ZHANG, Q., PAN, J. M. & YAN, Y. S. 2007. Oxodiperoxo tungsten complex-catalyzed synthesis of adipic acid with hydrogen peroxide. *Reaction Kinetics and Catalysis Letters,* 92**,** 319-327.

LI, H., ZHU, W. S., HE, X. Y., ZHANG, Q., PAN, J. M. & YAN, Y. S. 2007. Oxodiperoxo tungsten complex-catalyzed synthesis of adipic acid with hydrogen peroxide. *Reaction Kinetics and Catalysis Letters,* 92**,** 319-327.

LI, K. 2007. *Ceramic membranes for separation and reaction*, Wiley. com.

LI, W., NIE, Z., ZHANG, H., PAQUET, C., SEO, M., GARSTECKI, P. & KUMACHEVA, E. 2007. Screening of the Effect of Surface Energy of Microchannels on Microfluidic Emulsification. *Langmuir,* 23**,** 8010-8014.

LINK, D. R., ANNA, S. L., WEITZ, D. A. & STONE, H. A. 2004. Geometrically Mediated Breakup of Drops in Microfluidic Devices. *Physical Review Letters,* 92**,** 054503.

LONCARIC, C., MANABE, K. & KOBAYASHI, S. 2003. AgOTf-Catalyzed Aza-Diels–Alder Reactions of Danishefsky's Diene with Imines in Water. *Advanced Synthesis & Catalysis,* 345**,** 475-477.

LYNN, D. M., MOHR, B. & GRUBBS, R. H. 1998. Living Ring-Opening Metathesis Polymerization in Water. *Journal of the American Chemical Society,* 120**,** 1627-1628.

MAA, Y.-F. & HSU, C. 1996. Liquid-liquid emulsification by rotor/stator homogenization. *Journal of Controlled Release,* 38**,** 219-228.

MACKAY, R. A. 1981. Chemical reaction in microemulsions. *Advances in Colloid and Interface Science,* 15**,** 131-156.

MAGDASSI, S., BEN MOSHE, M., TALMON, Y. & DANINO, D. 2003. Microemulsions based on anionic gemini surfactant. *Colloids and Surfaces A: Physicochemical and Engineering Aspects,* 212**,** 1-7.

MAHESWARI, P. U., TANG, X., HAGE, R., GAMEZ, P. & REEDIJK, J. 2006. The role of carboxylic acids on a Na2WO4/H2WO4-based biphasic homogeneous alkene epoxidation, using H2O2 as oxidant. *Journal of Molecular Catalysis A: Chemical,* 258**,** 295-301.

MANABE, K., AOYAMA, N. & KOBAYASHI, S. 2001. Friedel–Crafts-Type Conjugate Addition of Indoles Using a Lewis Acid–Surfactant-Combined Catalyst in Water. *Advanced Synthesis & Catalysis,* 343**,** 174-176.

MANABE, K. & KOBAYASHI, S. 2002. Catalytic Asymmetric Carbon–Carbon Bond-Forming Reactions in Aqueous Media. *Chemistry – A European Journal,* 8**,** 4094-4101.

MARTIN, C. A., MGCRANN, P. M., ANGELOS, G. H. & JAEGER, D. A. 1982. Reactions in microemulsion media. Nucleophilic displacement reaction of benzyl chloride with bromide ion. *Tetrahedron Letters,* 23**,** 4651-4654.

MARZZACCO, C. J. 1999. The Enthalpy of Decomposition of Hydrogen Peroxide: A General Chemistry Calorimetry Experiment. *Journal of Chemical Education,* 76**,** 1517.

MASON, B. P., PRICE, K. E., STEINBACHER, J. L., BOGDAN, A. R. & MCQUADE, D. T. 2007. Greener approaches to organic synthesis using microreactor technology. *Chemical reviews,* 107**,** 2300-2318.

MCCLEMENTS, D. J. & DECKER, E. A. 2000. Lipid Oxidation in Oil-in-Water Emulsions: Impact of Molecular Environment on Chemical Reactions in Heterogeneous Food Systems. *Journal of Food Science,* 65**,** 1270-1282.

MCMORN, P., ROBERTS, G. & HUTCHINGS, G. J. 1999. Oxidation of glycerol with hydrogen peroxide using silicalite and aluminophosphate catalysts. *Catalysis Letters,* 63**,** 193-197.

MECKING, S., HELD, A. & BAUERS, F. M. 2002. Aqueous Catalytic Polymerization of Olefins. *Angewandte Chemie International Edition,* 41**,** 544-561.

MEHLTRETTER, G. M., DÖBLER, C., SUNDERMEIER, U. & BELLER, M. 2000. An improved version of the Sharpless asymmetric dihydroxylation. *Tetrahedron Letters,* 41**,** 8083-8087.

MEHTA, S. K., KAWALJIT & BALA, K. 1999. Phase behavior, structural effects, and volumetric and transport properties in nonaqueous microemulsions. *Physical Review E,* 59**,** 4317.

MENGER, F. M. & ELRINGTON, A. R. 1991. Organic reactivity in microemulsion systems. *Journal of the American Chemical Society,* 113**,** 9621-9624.

MIKAMI, K., ISLAM, M. N., YAMANAKA, M., ITOH, Y., SHINODA, M. & KUDO, K. 2004. Nanoflow system for perfect regiocontrol in the Baeyer–Villiger oxidation by aqueous hydrogen peroxide using lowest concentration of a fluorous lanthanide catalyst. *Tetrahedron Letters,* 45**,** 3681-3683.

MIKAMI, K., YAMANAKA, M., ISLAM, M. N., KUDO, K., SEINO, N. & SHINODA, M. 2003. 'Fluorous nanoflow' system for the Mukaiyama aldol reaction catalyzed by

the lowest concentration of the lanthanide complex with bis(perfluorooctanesulfonyl)amide ponytail. *Tetrahedron,* 59**,** 10593-10597.

MINE, Y., SHIMIZU, M. & NAKASHIMA, T. 1996. Preparation and stabilization of simple and multiple emulsions using a microporous glass membrane. *Colloids and Surfaces B: Biointerfaces,* 6**,** 261-268.

MITTAL, K. L. & KUMAR, P. 1999. *Handbook of microemulsion science and technology,* New York, Marcel Dekker.

MORI, Y., KAKUMOTO, K., MANABE, K. & KOBAYASHI, S. 2000. Michael reactions in water using Lewis acid–surfactant-combined catalysts. *Tetrahedron Letters,* 41**,** 3107-3111.

MUKHOPADHYAY, S., ROTHENBERG, G., JOSHI, A., BAIDOSSI, M. & SASSON, Y. 2002. Heterogeneous Palladium-Catalysed Heck Reaction of Aryl Chlorides and Styrene in Water Under Mild Conditions. *Advanced Synthesis & Catalysis,* 344**,** 348-354.

MURAKAMI, K., CHAN, S. Y. & ROUTTENBERG, A. 1986. Protein kinase C activation by cis-fatty acid in the absence of Ca2+ and phospholipids. *Journal of Biological Chemistry,* 261**,** 15424-9.

NAGAYAMA, S. & KOBAYASHI, S. 2000. A Novel Polymer-Supported Scandium Catalyst Which Shows High Activity in Water. *Angewandte Chemie International Edition,* 39**,** 567-569.

NAKASHIMA, T., SHIMIZU, M. & KUKIZAKI, M. 1992. Membrane emulsification by microporous glass. *Key Engineering Materials,* 61**,** 513-516.

NARDELLO, V., AUBRY, J.-M., DE VOS, D. E., NEUMANN, R., ADAM, W., ZHANG, R., TEN ELSHOF, J. E., WITTE, P. T. & ALSTERS, P. L. 2006. Inorganic compounds and materials as catalysts for oxidations with aqueous hydrogen peroxide. *Journal of Molecular Catalysis A: Chemical,* 251**,** 185-193.

NOYORI, R., AOKI, M. & SATO, K. 2003. Green oxidation with aqueous hydrogen peroxide. *Chemical Communications***,** 1977-1986.

NUNES, J. K., TSAI, S. S. H., WAN, J. & STONE, H. A. 2013. Dripping and jetting in microfluidic multiphase flows applied to particle and fibre synthesis. *Journal of Physics D-Applied Physics,* 46**,** 20.

O'BRIEN, R. D. 2010. *Fats and Oils: Formulating and Processing for Applications, Third Edition,* Taylor & Francis.

OOI, T., UEMATSU, Y. & MARUOKA, K. 2002. Evaluation of the Efficiency of the Chiral Quaternary Ammonium Salt β-Np-NAS-Br in the Organic-Aqueous Phase-Transfer Alkylation of a Protected Glycine Derivative. *Advanced Synthesis & Catalysis,* 344**,** 288-291.

PARDEIKE, J., HOMMOSS, A. & MÜLLER, R. H. 2009. Lipid nanoparticles (SLN, NLC) in cosmetic and pharmaceutical dermal products. *International Journal of Pharmaceutics,* 366**,** 170-184.

PARKER JR, W. O., GENOVA, C. & CARIGNANO, G. 1993. Study of micellar solutions and microemulsions of an alkyl oligoglucoside via NMR spectroscopy. *Colloids and Surfaces A: Physicochemical and Engineering Aspects,* 72**,** 275-284.

PENG, S. J. & WILLIAMS, R. A. 1998. Controlled Production of Emulsions Using a Crossflow Membrane: Part I: Droplet Formation from a Single Pore. *Chemical Engineering Research and Design,* 76**,** 894-901.

PERRY, R. H. & GREEN, D. W. 2008. *Perry's Chemical Engineers' Handbook, Eighth Edition,* McGraw-Hill.

PIACENTINI, E., FIGOLI, A., GIORNO, L. & DRIOLI, E. 2010. 4.03 - Membrane Emulsification. *In:* EDITOR-IN-CHIEF: ENRICO, D. & LIDIETTA, G. (eds.) *Comprehensive Membrane Science and Engineering.* Oxford: Elsevier.

PICKERING, S. U. 1907. Emulsions. *Journal of the Chemical Society, Transactions,* 91**,** 2001-2021.

POPE, M. T. 1983. *Heteropoly and isopoly oxometalates,* Berlin ; New York, Springer-Verlag.

POPE, M. T. & MÜLLER, A. 2001. *Polyoxometalate chemistry : from topology via self-assembly to applications,* Dordrecht ; Boston, Kluwer Academic Publishers.
PRINCE, L. M. 1977. *Microemulsions : theory and practice,* New York, Academic Press.
PRINCE, L. M. 1977. Microemulsions : theory and practice. xii, 179 p.
QIAN, J., GUO, R. & ZOU, A. 2001. Effect of Microemulsion Structures on the Hydrolysis of Acetylsalicylic Acid. *Journal of Dispersion Science and Technology,* 22**,** 541 - 549.
RAO, J. P. & GECKELER, K. E. 2011. Polymer nanoparticles: preparation techniques and size-control parameters. *Progress in Polymer Science,* 36**,** 887-913.
REGEV, O., EZRAHI, S., ASERIN, A., GARTI, N., WACHTEL, E., KALER, E. W., KHAN, A. & TALMON, Y. 1996. A Study of the Microstructure of a Four-Component Nonionic Microemulsion by Cryo-TEM, NMR, SAXS, and SANS. *Langmuir,* 12**,** 668-674.
RIZWAN, S. B., DONG, Y. D., BOYD, B. J., RADES, T. & HOOK, S. 2007. Characterisation of bicontinuous cubic liquid crystalline systems of phytantriol and water using cryo field emission scanning electron microscopy (cryo FESEM). *Micron,* 38**,** 478-485.
ROWLAND, S. P. 1958. Epoxidized vegetable oils. Google Patents.
SAINT RUTH, H., ATTWOOD, D., KTISTIS, G. & TAYLOR, C. J. 1995. Phase studies and particle size analysis of oil-in-water phospholipid microemulsions. *International Journal of Pharmaceutics,* 116**,** 253-261.
SATO, K., AOKI, M. & NOYORI, R. 1998. A "green" route to adipic acid: Direct oxidation of cyclohexenes with 30 percent hydrogen peroxide. *Science,* 281**,** 1646-1647.
SATO, K., AOKI, M., OGAWA, M., HASHIMOTO, T. & NOYORI, R. 1996. A Practical Method for Epoxidation of Terminal Olefins with 30 Hydrogen Peroxide under Halide-Free Conditions. *The Journal of organic chemistry,* 61**,** 8310-8311.
SATO, K., AOKI, M., OGAWA, M., HASHIMOTO, T., PANYELLA, D. & NOYORI, R. 1997. A Halide-Free Method for Olefin Epoxidation with 30% Hydrogen Peroxide. *Bulletin of the Chemical Society of Japan,* 70**,** 905-915.
SATO, K., AOKI, M., TAKAGI, J., ZIMMERMANN, K. & NOYORI, R. 1999. A practical method for alcohol oxidation with aqueous hydrogen peroxide under organic solvent- and halide-free conditions. *Bulletin of the Chemical Society of Japan,* 72**,** 2287-2306.
SCHRÖDER, V., BEHREND, O. & SCHUBERT, H. 1998. Effect of dynamic interfacial tension on the emulsification process using microporous, ceramic membranes. *Journal of Colloid and Interface ...,* 202**,** 334-340.
SCHRODER, V. & SCHUBERT, H. 1999. Production of emulsions using microporous, ceramic membranes. *Colloids and Surfaces a-Physicochemical and Engineering Aspects,* 152**,** 103-109.
SCHULMAN, J. H., STOECKENIUS, W. & PRINCE, L. M. 1959. Mechanism of Formation and Structure of Micro Emulsions by Electron Microscopy. *Journal of Physical Chemistry,* 63**,** 1677-1680.
SCHUSTER, D. 1985. *Encyclopedia of Emulsion Technology: Applications*, Taylor & Francis.
SHCHUKIN, D. G. & SUKHORUKOV, G. B. 2004. Nanoparticle Synthesis in Engineered Organic Nanoscale Reactors. *Advanced Materials,* 16**,** 671-682.
SHELDON, R. 1991. Industrial Catalytic Oxidations: An Overview. *Studies in Surface Science and Catalysis.*
SHELDON, R. A. & KOCHI, J. K. 1981. *Metal-catalyzed oxidations of organic compounds : mechanistic principles and synthetic methodology including biochemical processes,* New York, Academic Press.
SHERMAN, P. 1968. *Emulsion science,* Academic Press.
SHESTOPALOV, I., TICE, J. D. & ISMAGILOV, R. F. 2004. Multi-step synthesis of nanoparticles performed on millisecond time scale in a microfluidic droplet-based system. *Lab on a Chip,* 4**,** 316-321.

SHIMIZU, S., SUZUKI, T., SHIRAKAWA, S., SASAKI, Y. & HIRAI, C. 2002. Water-Soluble Calixarenes as New Inverse Phase-Transfer Catalysts. Their Scope in Aqueous Biphasic Alkylations and Mechanistic Implications. *Advanced Synthesis & Catalysis,* 344**,** 370-378.

SHIOMORI, K., HAYASHI, T., BABA, Y., KAWANO, Y. & HANO, T. 1995. Hydrolysis rates of olive oil by lipase in a monodispersed OW emulsion system using membrane emulsification. *Journal of Fermentation and Bioengineering,* 80**,** 552-558.

SHRIKHANDE, J. J., HASSAN, P. A. & JAYARAM, R. V. 2010. Condensation reaction of benzaldehyde and acetone in o/w microemulsions: Effect of microemulsion compositions. *Colloids and Surfaces A: Physicochemical and Engineering Aspects,* 370**,** 64-71.

SIGISMONDI, S. & SINOU, D. 1997. Palladium(0)-catalyzed substitution of allylic substrates in an aqueous-organic medium. Influence of various parameters on the selectivity of the reaction. *Journal of Molecular Catalysis A: Chemical,* 116**,** 289-296.

SINOU, D., RABEYRIN, C. & NGUEFACK, C. 2003. Catalytic Asymmetric Alkylation in Water in the Presence of Surfactants. *Advanced Synthesis & Catalysis,* 345**,** 357-363.

SLOBODA-ROZNER, D., ALSTERS, P. L. & NEUMANN, R. 2003. A Water-Soluble and "Self-Assembled" Polyoxometalate as a Recyclable Catalyst for Oxidation of Alcohols in Water with Hydrogen Peroxide. *Journal of the American Chemical Society,* 125**,** 5280-5281.

SLOBODA-ROZNER, D., WITTE, P., ALSTERS, P. L. & NEUMANN, R. 2004. Aqueous Biphasic Oxidation: A Water-Soluble Polyoxometalate Catalyst for Selective Oxidation of Various Functional Groups with Hydrogen Peroxide. *Advanced Synthesis & Catalysis,* 346**,** 339-345.

SONG, H., CHEN, D. L. & ISMAGILOV, R. F. 2006. Reactions in Droplets in Microfluidic Channels. *Angewandte Chemie International Edition,* 45**,** 7336-7356.

SONG, K., CHU, Y., DONG, L., SONG, J. & WANG, D. 2008. Etherification in cyclohexane/DBSA/water microemulsion system. *Journal of Molecular Catalysis A: Chemical,* 282**,** 144-148.

SPYROPOULOS, F., LLOYD, D. M., HANCOCKS, R. D. & PAWLIK, A. K. 2014. Advances in membrane emulsification. Part A: recent developments in processing aspects and microstructural design approaches. *Journal of the Science of Food and Agriculture,* 94**,** 613-627.

STARKS, C. M. 1971. Phase-transfer catalysis. I. Heterogeneous reactions involving anion transfer by quaternary ammonium and phosphonium salts. *Journal of the American Chemical Society***,** 195-199.

STEEGMANS, M. L. J., SCHROËN, C. G. P. H. & BOOM, R. M. 2009. Generalised insights in droplet formation at T-junctions through statistical analysis. *Chemical Engineering Science,* 64**,** 3042-3050.

STUBENRAUCH, C. 2009. Microemulsions : background, new concepts, applications, perspectives. xxiii, 375 p.

STUBENRAUCH, C. 2009. *Microemulsions : background, new concepts, applications, perspectives,* Chichester, West Sussex, U.K. ; Ames, Iowa, Wiley.

SUPSAKULCHAI, A., MA, G., NAGAI, M. & OMI, S. 2003. Preparation of uniform titanium dioxide (TiO2) polystyrene-based composite particles using the glass membrane emulsification process with a subsequent suspension polymerization. *Journal of microencapsulation,* 20**,** 1-18.

TADROS, T., IZQUIERDO, P., ESQUENA, J. & SOLANS, C. 2004. Formation and stability of nano-emulsions. *Advances in Colloid and Interface Science,* 108-109**,** 303-318.

TICE, J. D., SONG, H., LYON, A. D. & ISMAGILOV, R. F. 2003. Formation of Droplets and Mixing in Multiphase Microfluidics at Low Values of the Reynolds and the Capillary Numbers. *Langmuir,* 19**,** 9127-9133.

TORCHILIN, V. P. 2006. *Nanoparticulates as drug carriers,* London, Hackensack, N.J., Imperial College Press; Distributed by World Scientific Pub.

TORRENTE-MURCIANO, L., GILBANK, A., PUERTOLAS, B., GARCIA, T., SOLSONA, B. & CHADWICK, D. 2013. Shape-dependency activity of nanostructured CeO2 in the total oxidation of polycyclic aromatic hydrocarbons. *Applied Catalysis B: Environmental,* 132–133**,** 116-122.

UMBANHOWAR, P. B., PRASAD, V. & WEITZ, D. A. 1999. Monodisperse Emulsion Generation via Drop Break Off in a Coflowing Stream. *Langmuir,* 16**,** 347-351.

UTADA, A. S., LORENCEAU, E., LINK, D. R., KAPLAN, P. D., STONE, H. A. & WEITZ, D. A. 2005. Monodisperse Double Emulsions Generated from a Microcapillary Device. *Science,* 308**,** 537-541.

VAN DER GRAAF, S., STEEGMANS, M. L. J., VAN DER SMAN, R. G. M., SCHROËN, C. G. P. H. & BOOM, R. M. 2005. Droplet formation in a T-shaped microchannel junction: A model system for membrane emulsification. *Colloids and Surfaces A: Physicochemical and Engineering Aspects,* 266**,** 106-116.

VASYLYEV, M. V. & NEUMANN, R. 2003. New Heterogeneous Polyoxometalate Based Mesoporous Catalysts for Hydrogen Peroxide Mediated Oxidation Reactions. *Journal of the American Chemical Society,* 126**,** 884-890.

VENKATRAMAN, S., HUANG, T. & LI, C.-J. 2002. Carbon-Carbon Bond Formation via Palladium-Catalyzed Reductive Coupling of Aryl Halides in Air and Water. *Advanced Synthesis & Catalysis,* 344**,** 399-405.

VENTURELLO, C. & GAMBARO, M. 1991. Selective oxidation of alcohols and aldehydes with hydrogen peroxide catalyzed by methyltrioctylammonium tetrakis(oxodiperoxotungsto)phosphate(3-) under two-phase conditions. *The Journal of Organic Chemistry,* 56**,** 5924-5931.

VERSPUI, G., SCHANSSEMA, F. & SHELDON, R. A. 2000. A Stable, Conspicuously Active, Water-Soluble Pd Catalyst for the Alternating Copolymerization of Ethene and CO in Water. *Angewandte Chemie International Edition,* 39**,** 804-806.

VLADISAVLJEVIĆ, G. T., TESCH, S. & SCHUBERT, H. 2002. Preparation of water-in-oil emulsions using microporous polypropylene hollow fibers: influence of some operating parameters on droplet size distribution. *Chemical Engineering and Processing: Process Intensification,* 41**,** 231-238.

WAGDARE, N. A., MARCELIS, A. T. M., HO, O. B., BOOM, R. M. & VAN RIJN, C. J. M. 2010. High throughput vegetable oil-in-water emulsification with a high porosity micro-engineered membrane. *Journal of Membrane Science,* 347**,** 1-7.

WALTON, J. H. & GRAHAM, D. P. 1928. A STUDY OF THE OXIDATION OF SOME DICARBOXYLIC ACIDS BY HYDROGEN PEROXIDE IN THE PRESENCE OF CERTAIN CATALYSTS1. *Journal of the American Chemical Society,* 50**,** 1641-1648.

WEI, J., SHI, X., HE, D. & ZHANG, M. 2002. Organic solvent- and phase transfer catalyst-free oxidation of cyclohexanol to cyclohexanone with dilute H2O2. *Chinese Science Bulletin,* 47**,** 2060-2062.

WHITESIDES, G. M. 2006. The origins and the future of microfluidics. *Nature,* 442**,** 368-373.

WIEBUS, E. & CORNILS, B. 2006. Biphasic Systems: Water — Organic. *In:* COLE-HAMILTON, D. & TOOZE, R. (eds.) *Catalyst Separation, Recovery and Recycling.* Springer Netherlands.

WILLIAMS, R. A., PENG, S. J., WHEELER, D. A., MORLEY, N. C., TAYLOR, D., WHALLEY, M. & HOULDSWORTH, D. W. 1998. Controlled Production of Emulsions Using a Crossflow Membrane: Part II: Industrial Scale Manufacture. *Chemical Engineering Research and Design,* 76**,** 902-910.

WINSOR, P. A. 1954. *Solvent properties of amphiphilic compounds,* London,, Butterworths Scientific Publications.

WIPF, P. & RODRÍGUEZ, S. 2002. Water-Accelerated Claisen Rearrangements. *Advanced Synthesis & Catalysis,* 344**,** 434-440.

WIRTH, T. 2013. *Microreactors in Organic Chemistry and Catalysis*, Wiley. com.

WU, D.-Y., ZHANG, L.-P., WU, L.-Z., WANG, B.-J. & TUNG, C.-H. 2002. Water-in-oil microemulsions as microreactors to control the regioselectivity in the photocycloaddition of 9-substituted anthracenes. *Tetrahedron Letters,* 43**,** 1281-1283.

XU, J. H., LI, S. W., TAN, J., WANG, Y. J. & LUO, G. S. 2006. Controllable Preparation of Monodisperse O/W and W/O Emulsions in the Same Microfluidic Device. *Langmuir,* 22**,** 7943-7946.

YANAGISHITA, T., FUJIMURA, R., NISHIO, K. & MASUDA, H. 2009. Fabrication of monodisperse polymer nanoparticles by membrane emulsification using ordered anodic porous alumina. *Langmuir,* 26**,** 1516-1519.

YANG, Z., EBIHARA, M. & KAWAMURA, T. 2000. Homogeneous hydrogenation of olefins catalyzed by a novel tetrarhodium(II) complex as precursor in aqueous solution. *Journal of Molecular Catalysis A: Chemical,* 158**,** 509-514.

YU, Z.-J. & NEUMAN, R. D. 1995. Reversed Micellar Solution-to-Bicontinuous Microemulsion Transition in Sodium Bis(2-Ethylhexyl) Phosphate/n-Heptane/Water System. *Langmuir,* 11**,** 1081-1086.

YUAN, Q. C., ARYANTI, N., HOU, R. Z. & WILLIAMS, R. A. 2009. Performance of slotted pores in particle manufacture using rotating membrane emulsification. *Particuology,* 7**,** 114-120.

ZHAO, X.-B., ZHANG, T., ZHOU, Y.-J. & LIU, D.-H. 2008. Preparation of peracetic acid from acetic acid and hydrogen peroxide: Experimentation and modeling. *过程工程学报,* 8.

ZHAO, X., CHENG, K., HAO, J. & LIU, D. 2008. Preparation of peracetic acid from hydrogen peroxide, part II: kinetics for spontaneous decomposition of peracetic acid in the liquid phase. *Journal of Molecular Catalysis A: Chemical,* 284**,** 58-68.

ZHAO, X., ZHANG, T., ZHOU, Y. & LIU, D. 2007. Preparation of peracetic acid from hydrogen peroxide: Part I: Kinetics for peracetic acid synthesis and hydrolysis. *Journal of Molecular Catalysis A: Chemical,* 271**,** 246-252.

ZHU, W. S., LI, H. M., HE, X. Y., ZHANG, Q., SHU, H. M. & YAN, Y. S. 2008. Synthesis of adipic acid catalyzed by surfactant-type peroxotungstates and peroxomolybdates. *Catalysis Communications,* 9**,** 551-555.

9 Appendix 1: Rate of reaction calculation from concentration-time data

This appendix contains a typical example of the worked reaction rate data. This is representative of the method used throughout the thesis.

9.1 Initial integral data from NMR

The integrals were read directly from the NMR spectra calibrating the spectra to the glycerol signals which represent 4 protons

Table 9.1 - NMR integrals for a series of typical reactions. The missing point was due to a sample on which the analysis failed.

Reaction ID	Compound	Time										
		0	15	30	45	60	75	90	105	120	180	240
	alkene	10.3	7.41	5.45	4.8	3.66	3.66	2.87	2.68	2.38	2.15	1.79
130222-SB-1	epoxide	0	1.84	2.59	3.25	3.32	3.93	4.45	4.77	5.06	5.67	6.2
	glycerol	4	4	4	4	4	4	4	4	4	4	4
	alkene	10.1	8.7	8.45	7.42	8.79	6.43	6.04	5.62	5.15	3.66	3.1
130222-SB-2	epoxide	0	0.8	0.99	1.43	1.79	1.96	2.15	2.32	2.66	3.26	3.83
	glycerol	4	4	4	4	4	4	4	4	4		4
	alkene	9.9	10	9.83	9.69	9.84	9.45	9.55	9.43	9.36		7.69
130222-SB-3	epoxide	0	0	0.14	0.18	0.24	0.15	0.21	0.36	0.43		0.41
	glycerol	4	4	4	4	4	4	4	4	4		4

9.2 Calculation of conversion, $X_{epoxide}$

The conversion can be calculated based on the ratio of integrals of epoxide and alkene signals since this was the only product. From the fatty acid profile the initial concentration of double bonds can be calculated as described in the experimental section. This can then be multiplied by the conversion to give concentration of epoxide. The typical data for this worked example is given in Table 9.2.

Table 9.2 - Conversion and concentration time data from the raw integral data for a typical reaction set

		Time / min										
	Reaction ID	0	15	30	45	60	75	90	105	120	180	240
$X_{epoxide}$	130222-SB-1	0.00	22.30	36.79	46.10	55.52	59.64	70.41	73.95	78.57	83.14	88.70
	130222-SB-2	0.00	9.41	11.73	18.22	18.68	26.52	29.90	33.43	39.06	55.07	64.59
	130222-SB-3	0.00	0.00	1.56	2.03	2.64	1.74	2.40	4.10	4.89		5.77
$C_{epoxide}$	130222-SB-1	0.00	0.32	0.53	0.67	0.80	0.86	1.02	1.07	1.14	1.20	1.28
	130222-SB-2	0.00	0.14	0.17	0.26	0.27	0.38	0.43	0.48	0.56	0.80	0.93
	130222-SB-3	0.00	0.00	0.02	0.03	0.04	0.03	0.03	0.06	0.07		0.08

9.3 Creation of the Concentration-Time graph

A graph can be plotted (Figure 9.1) using the concentration time data and the gradients of the initial portion of the curves can be measured. Each of the tangents was assessed by eye and linear regression analysis to test for fit to data.

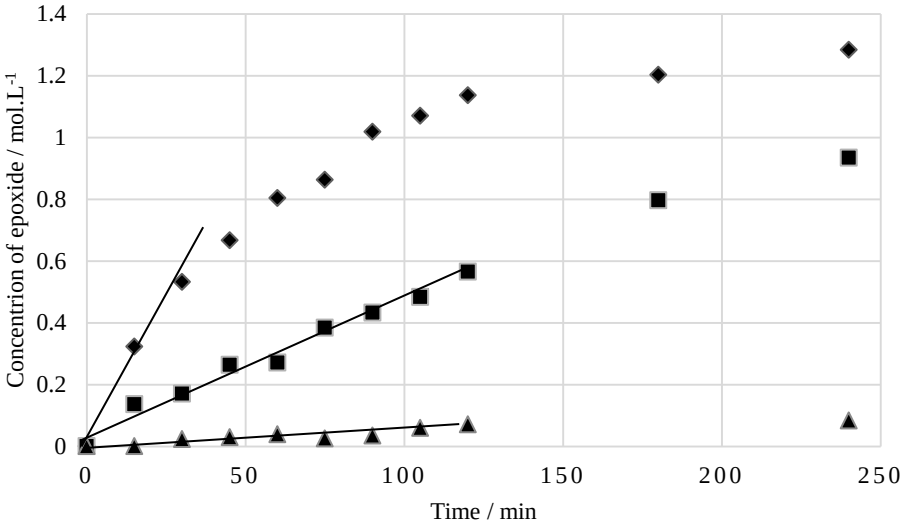

Figure 9.1 – Typical concentration-time data for the epoxidation reactions. Conditions: 60°C, 3 M H_2O_2, AcOH:Na_2WO_4 20:1. Catalyst concentration: ▲0.025 M ■ 0.1 M ♦ 0.15 M

The rate of reaction was calculated from the tangents represented above using the SLOPE function in Microsoft EXCEL. This data along with the relevant catalyst data which was used to plot the graphs contained within this thesis. Specifically this data relates to 3 of the 4 points in Figure 5.6 relating to the catalyst concentration at fixed acid: catalyst concentrations.

Table 9.3 - Conversion and concentration time data from the raw integral data for a typical reaction set

Reaction ID	Rate	Log rate	Catalyst Concentration	Log Catalyst Concentration
130222-SB-1	1.47E-02	-1.83	0.15	-0.81
130222-SB-2	4.60E-03	-2.34	0.10	-1.00
130222-SB-3	3.68E-04	-3.43	0.03	-1.60

10 Appendix 2: Droplet size prediction

This section contains the calculations in the determination of the droplet size based on the Peng & Williams (1998) force balance approach for a single droplet detaching from a single pore.

The force balance involves three dominant forces, the shear stress exerted by the fluid flowing perpendicular to the pore, the interfacial tension drawing the dispersed phase back into the pore and the buoyant force resulting from the density difference in the droplets. These are represented by the equations given in Table 10.1

Table 10.1 - Peng & Williams (1998) force balance equations for a single droplet leaving a single pore into a crossflowing fluid flow

Force	Symbol	Equation	
Shearing force	F_1	$F_1 = 3\pi f k_x \rho V_w^{\ 2} R_d^2$	10.1
		$f = \begin{cases} 16/\mathrm{Re} & \mathrm{Re} < 500 \\ 0.0792\,\mathrm{Re}^{-0.25} & 500 \le \mathrm{Re} \le 20000 \end{cases}$	

Buoyant force	F_3	$F_3 = \frac{4}{3}\pi R_d^3(\rho - \rho_o)g$	10.2
Interfacial tension	F_2	$F_2 = 2\pi\gamma R_p$	10.3

Where the symbols of the above are given below:

Symbol	Meaning	Unit
k_x	the wall correction factor given as 1.7 for a single sphere touching an impermeable wall within simple shear	
V_w	average flow velocity of continuous phase	$m.s^{-1}$
μ_c	continuous phase viscosity	$kg.m^{-1}.s^{-1}$
D	inner diameter of membrane tube	m
ρ	density of continuous phase	$kg.m^{-3}$
ρ_o	density of dispersed phase	$kg.m^{-3}$
g	gravitational constant	$m.s^{-2}$
γ	interfacial tension	$N.m^{-1}$
R_p	pore radius	m
R_d	droplet radius	m
Re	Reynolds number	

The above equations can be used to predict the growth size of a droplet. After this growth stage, the droplet is still attached to the pore via a small 'neck' of dispersed phase. The final droplet size will therefore be dependent on the rate of flow of dispersed phase through this neck and the time during which the droplet remains attached. In reality the rate of dispersed phase flow and the time before detachment can be neglected since they are often very low. Therefore solving a force balance of the above equations can give a prediction for the droplet size and the operating conditions.

For a droplet which can be approximated as spherical before detachment the force balance can be represented by,

$$(F_1 + F_3)R_d = F_2 R_p \qquad 10.4$$

If there is deformation then the force balance is simply,

$$F_1 + F_3 = F_2 \qquad 10.5$$

An iterative approach was used to solve for the droplet radius under the conditions in Chapter 6, equating the balance to zero and iterating until an 18 decimal point condition was satisfied using SOLVER in Microsoft EXCEL.

Table 10.2 - Droplet size prediction based on the parameters in the membrane emulsification plant used in Chapter 6

	Term	Value	Units	Symbol	Value	Units
Droplet Size	R_d	3.35E-06	m	k_x	1.7	
		3.351002	μm	μ_c	0.00089	$kg.m^{-1}.s^{-1}$
Fluid Flow	V_w	0.65	$m.s^{-1}$	D	0.006	m
		1102.699	$mL.min^{-1}$	ρ	1000	$kg.m^{-3}$
Flow characteristics	Reynolds	4382.022		ρ_o	846	$kg.m^{-3}$
	f	0.009734		g	9.806	$m.s^{-2}$
Acting Forces	F_1	7.4E-10	N	γ	0.06	$N.m^{-1}$
	F_2	3.02E-08	N	D_p	8.00E-08	m
	F_3	2.38E-13	N			
Spherical Droplet	$(F_2*R_p)-((F_1+F_3)R_d)$	-6.8E-17				
Droplet Size	R_d	2.14E-05	m			
		21.37169	μm			
Fluid Flow	V_w	0.65	$m.s^{-1}$			
		1102.699	$mL.min^{-1}$			
Flow characteristics	Reynolds	4382.022				
	f	0.009734				
Acting Forces	F_1	3.01E-08	N			
	F_2	3.02E-08	N			
	F_3	6.17E-11	N			
Deformed drop	F2-F1-F3	-2.6E-17				

11 Appendix 3: Publications

The manuscript is attached for the work published in the RSC journal Green Chemistry.

BISHOPP, S. D., SCOTT, J. L. & TORRENTE-MURCIANO, L. 2014. Insights into biphasic oxidations with hydrogen peroxide; towards scaling up. *Green Chemistry,* 16**,** 3281-3285.